**A thesis submitted in fulfilment of the requirements for the degree of**

**Doctor of Philosophy at University College London**

# Changes in endocytosis and trafficking during proliferative quiescence

Claudia Hinze

2018


Department of Structural and Molecular Biology

University College London

Gower Street, London, WC1E 6BT

# Declaration

I, Claudia Hinze, confirm that the work presented in this thesis is my own. Where information has been derived from other sources, I confirm that this has been indicated in the thesis.

Signed. . . . . .

# Abstract

A significant proportion of cells in the adult human body, including naïve lymphocytes, hepatocytes, stem cells and cancer stem cells, reside in an actively maintained state of proliferative quiescence (G0). Quiescent cells exit the cell cycle under certain conditions and resume proliferation upon appropriate stimuli, which distinguishes them from senescent or terminally differentiated cells. Little is known about how molecular processes, such as endocytosis, are regulated upon cell cycle exit. The aim of this study was to measure endocytic pathways during quiescence and study how their regulation contributes to quiescence maintenance. A quiescence induction protocol was optimised for hTERT-immortalised RPE1 (retina pigmented epithelial) cells to compare endocytosis between quiescent and proliferating RPE1 cells. A SILAC mass spectrometry screen comparing proteome and phosphoproteome between G0 and G1 RPE1 cells revealed changes in total protein levels and phosphorylation of endocytic proteins during G0. Confocal microscopy, Western blotting, flow cytometry and high throughput imaging techniques were used to measure clathrin-mediated (CME) and -independent endocytosis in quiescent and continuously proliferating RPE1 cells. Total levels of core proteins of the clathrin machinery were increased during G0, but uptake of the classical CME cargoes transferrin, EGF and LDL were decreased. CME activity during quiescence is cargo-specific, as could be shown for elevated Lamp1 endocytosis. Endocytosis of clathrin-independent cargoes such as oxidised LDL and Cholera toxin was highly active in quiescent cells, as was uptake of the macropinocytosis cargoes dextran and BSA. Elevated BSA uptake, however, did not promote mTORC1-mediated survival in a nutrient-(amino acid-) deprived environment. Moreover, BSA endocytosis was mediated by AP2. Finally, quiescence survival signalling via integrins was found to be dependent on endocytosis and recycling. Together, this study identified differentially regulated endocytic pathways and suggestd a role for integrin trafficking to maintain proliferative quiescence.

# Impact

Endocytosis is a process ubiquitously present in cells and required for vital cellular functions such as nutrient uptake, cell signalling regulation and migration (Barbieri *et al.*, 2016). Genetic mutations resulting in impaired endocytosis cause diseases ranging from cancer to neurodegeneration, atherosclerosis or lysosomal storage diseases (Doherty & McMahon, 2009). It is also hijacked by pathogens such as bacteria and viruses (Gruenberg & Van Der Goot, 2006). Thus, understanding the molecular mechanism and activity of endocytic pathways is important for prevention and treatment of heredetary diseases or infections. The majority of research on endocytosis has been performed in *in vitro* cell line models, often cancer cells, which are continuously dividing. The majority of cells in the adult human body, however, have reversibly or irreversibly exited the cell cycle and reside in a quiescent, terminally differentiated or senescent state.

In this study, endocytosis in quiescent cells, which can re-enter the cell cycle upon stimuli such as wounds or mitogen stimulation, was investigated. Among quiescent cells in the adult human body are hepatocytes, endothelial cells, naive lymphocytes, dormant stem cells and dormant cancer stem cells. An *in vitro* cell line model was established to induce quiescence in non-transformed human telomerase reverse transcriptase (hTERT)-immortalised retina pigmented epithelial cells (RPE1). To date, studies of quiescent cells have been limited to primary cells such as fibroblasts, naive lymphocytes or dormant cancer stem cells (Cheng *et al.*, 2000a; Orford & Scadden, 2008; Malumbres & Barbacid, 2001). A quiescence cell line model is advantageous in that passage numbers do not affect gene expression or survival, allowing for high reproducibility of experiments and for complex studies requiring large numbers of cells.

It was discovered that endocytic pathways are differentially regulated in quiescent RPE1 cells compared to continuously dividing RPE1 cells. Endocytosis of the classical cargoes of clathrin-mediated endocytosis, transferrin, low-density lipoprotein and epithelial

growth factor, was decreased while uptake of the lysosomal protein Lamp1 or albumin was elevated in quiescent cells. Studying differences of endocytosis in quiescent and proliferating cells of the same cell type is not only suited to discover molecular mechanisms regulating endocytic activity. This allows for a better understanding of endocytosis during quiescence, in which many cells of the adult human body reside. Differentially regulated endocytosis supports the hypothesis that quiescence is not a passive state, but actively maintained (Coller *et al.*, 2006). It furthermore allows for optimisation of targeted drug delivery, as drugs might be internalised with different efficiency in dividing cells, such as hyperproliferative cancer cells, and quiescent tissue cells or dormant cancer stem cells.

Finally, a high-throughput screening approach based on high-content fluorescence microscopy or confocal microscopy in conjunction with automated image analysis adapted to specific analyses, such as protein expression level quantification, measurement of endocytosed cargo or colocalisation studies was employed in this study. This allowed for analysis of high numbers of cells, resulting in robust population statistics and was superior to flow cytometry by increasing signal-to-noise ratios. Using this approach, inhibitor- and knockdown screens identified endocytosis and recycling as processes critical for quiescence entry, proposing a role for endocytosis and endosomal trafficking in reversible cell cycle exit.

# Publications

Hinze C, McGourty K and Boucrot E. Dedicated endocytosis supports long-term survival of quiescent cells. *In preparation*

McGourty K, Yu C, Hinze C, Soueid-Baumgarten S, Cryar A, Bain C, Mendes AP, Ooi S, Cosgrove B, Thalassinos KT and Boucrot E. Biased ERK signalling mediates long-term survival of quiescent cells. *In preparation*

Hinze C & Boucrot E (2018). Endocytosis in proliferating, quiescent, senescent or terminally-differentiated cells. Journal of Cell Science. *In Press*.

Hinze C & Boucrot E (2018). Local actin polymerization during endocytic carrier formation. Biochemical Society Transactions, 46(3), 565-576.

# Acknowledgments

My biggest thanks go to my supervisor Emmanuel Boucrot, who gave me the possibility to do my master's project in his lab five years ago. A small six-month project then turned into a PhD. For this, I had the best supervisor I can imagine, giving me the freedom to take my project where I wanted but also reminding me of the final goal when my creativity threatened to carry me away, with an always open door when advice was needed. It is unbelievable how much I have learned during the past four years and I want to thank you for all the possibilities you gave me to develop as a scientist.

I cannot express my gratitude to my parents, who always have my back, and without whom I would not be where I am right now. You supported all of my decisions despite not knowing what I was actually doing since my second semester at university. You suffered my long absences from home and accepted my temporary AWOL periods from social media in times of pressure without any complains. I love you dearly and cannot wait for the day the three of us will roam the city of London again together.

I would particularly like to thank Kieran, who took me by the hand as a master's student and later on was a constant source of inspiration.

A big thank you goes out to the members of the Boucrot lab, past and present, particularly to the *incredibly sage* Shaan, whose *magical* use of the English vocabulary and grammar was *indispensible* to transform the contents of the fifth chapter into legible sentences. Alessandra, thank you for demonstrating what perseverance can achieve (I remembered you often in the final days of despair while writing this book) and for always being up for discussions of work, Sicily/Italy and god knows what. Behzad, thank you for all your encouragements, advice and sharing of your mass spec wisdom. I would also like to thank Ana, who taught me how important it is to read labels and who, until today, always has an open ear and advice for my questions. And last but not least Antonio, who, as the most senior PhD student of the Boucrot lab, was the person to go to for

formal issues and who was, typical for the Boucrot lab, not just a colleague but also a dear friend.

Nathanael, the Tuesdays in the office were unforgettable since you joined!

Finally, I am grateful for all the friends I have back in Germany, here in London and spread all over the world. You inspire me, support me, distract me when needed and push me when needed. I am a happy person to know so many amazing people.

Thank you, thank you, thank you

# Contents

# Nomenclature

| | |
|---|---|
| 2n genome | Diploid genome |
| 4E-BP1 | Eukaryotic translation initiation factor 4E-binding protein 1 |
| µHD | Adaptor protein 2 µ-homology domain |
| AJs | Adherens Junctions |
| AP2 | Adaptor protein complex 2 |
| APPL1 | Adaptor protein, phosphotyrosine interacting with PH domain and leucine zipper 1 |
| ASCs | Adult stem cells |
| BAD | Bcl2-associated agonist of cell death |
| BAR domain | Bin–Amphiphysin–Rvs domain |
| BSA | Bovine serum albumin |
| C-terminal | Carboxy-terminal |
| CCP | Clathrin-coated pit |
| CCV | Clathrin-coated vesicle |
| CDK2 | Cyclin-dependent kinase 2 |
| CHC | Clathrin heavy chain |
| CLC | Clathrin light chain |
| CLIC/GEEC | Clathrin-independent tubovesicular carrier/glycosylphosphatidylinositol-anchored proteins enriched carriers |
| CME | Clathrin-mediated endocytosis |
| CSCs | Cancer stem cells |
| CtxB | Cholera toxin subunit B |
| Dab2 | Disabled homolog 2 |
| DABCO | 1,4-diazabicyclo[2.2.2]octane |
| DAPI | 4’,6-diamidino-2-phenylindole |
| DMEM | Dulbecco’s Modified Eagle Medium |
| DQBSA | Self-quenched BSA |
| ECM | Extracellular matrix |
| EEA1 | Early endosomal antigen 1 |
| EFC domain | Extended Fes/Cip4 homology domain |
| EGFR | Epithelial growth factor receptor |
| EIPA | 5-(N-Ethyl-N-isopropyl)amiloride |
| EPS15 | Epithelial growth factor receptor pathway substrate 15 |
| ERK | Extracellular signal-regulated kinases |

| | |
|---|---|
| F-BAR | Fes and CIP4 homology Bin/Amphiphysin/Rvs |
| FAK | Focal adhesion kinase |
| FBS | Foetal bovine serum |
| FCHo protein | Fer/Cip4 homology domain only protein |
| FEME | Fast Endophilin-mediated endocytosis |
| G0 | G0 cell cycle phase |
| G1 phase | G1 cycle phase |
| G2/M phase | G2 or Mitosis cell cycle phase |
| GAPDH | Glyceraldehyde-3-phosphate dehydrogenase |
| GJs | Gap Junctions |
| HDL | High density lipoprotein |
| HRP | Horseradish peroxidase |
| hTERT | Human telomerase reverse transcriptase |
| IF | Immunofluorescence |
| KD | Knockdown |
| Lamp1 | Lysosomal-associated membrane protein 1 |
| LDLR | Low-density lipoprotein receptor |
| mAb | Monoclonal antibody |
| mTOR | Mammalian target of rapamycin |
| N-terminal | Amino-terminal |
| oxLDL | Oxidised LDL |
| PBS | Phosphate-buffered saline |
| PBS++ | Phosphate-buffered saline with 0.9 mM calcium chloride and 0.5 mM magnesium chloride |
| PCNA | Proliferating nuclear antigen |
| PCR | Polymerase chain reaction |
| PFA | Paraformaldehyde |
| PQ | Primaquine |
| pRb | Phosphorylated Retinoblastoma protein |
| PY | Pyronin Y |
| Rb | Retinoblastoma protein |
| RPE1 cells | Retinal pigmented epithelial cells immortalised with hTERT |
| S phase | DNA synthesis cell cycle phase |
| SDS-PAGE | Sodium dodecyl sulfate polyacrylamide gel electrophoresis |
| SH3 domain | Src homology 3 domain |
| SILAC | Stable isotope labeling by amino acids in culture |
| siRNA | Small interfering RNA |
| SNX9 | Sorting-nexin 9 |
| StxB | Shiga toxin subunit B |
| TfR | Transferrin receptor |
| TGN | Trans-Golgi network |
| TJs | Tight Junctions |
| VPS35 | Vacuolar protein sorting-associated protein 35 |

# List of Figures

# List of Tables

# 1 Introduction

In this project, endocytic pathways were studied in quiescent cells and the requirement of integrin endocytosis and recycling was tested for quiescence entry and maintenance. This introduction will therefore review mechanisms of endocytosis and proliferative quiescence and briefly describe integrin trafficking pathways.

## 1.1 Endocytosis

Endocytosis is a ubiquitous mechanism enabling cells to interact with their environment. It describes the mechanism mediating the internalisation of nutrients and signals from the extracellular space and regulation of plasma membrane receptors levels or plasma membrane turnover. Cargo is internalised by formation of membrane invaginations, which are eventually budding from the plasma membrane as vesicles. Endocytic cargo is defined as extracellular molecules, transmembrane proteins or ligand-receptor complexes: transmembrane proteins, like receptors which, upon ligand binding, traffic to the lysosome (such as epithelial growth factor receptor) or ligands binding to receptors which are recycled (such as transferrin receptor). Internalised cargo is then either sent to the lysosomal compartment for degradation or back to the plasma membrane for recycling of their cargo (reviewed in Robinson, 2004; Naslavsky & Caplan, 2018). Different forms of endocytosis, namely receptor-mediated and -independent endocytosis, exist. Receptor-mediated endocytosis is an efficient and highly controlled endocytic pathway relying on membrane-embedded proteins cycling from one intracellular organelle to another, allowing for distinct trafficking pathways of internalised cargoes (Goldstein *et al.*, 1979).

### 1.1.1 Clathrin-mediated endocytosis (CME)

**Clathrin-mediated endocytos** Clathrin was first observed in electron microscopy images in 1964, and later described as required for intracellular transport, forming a coat around budding membrane vesicles (Roth & Porter 1964; Pearse 1976, see Fig. 1.1.1). To date, Clathrin-mediated endocytosis (CME) is the best characterised endocytic has been described in many excellent reviews (Robinson, 2015; Kaksonen & Roux, 2018; Mettlen *et al.*, 2018): Upon formation of a nucleation module at PI(4,5)P2 lipid-containing plasma membrane regions by BAR domain-containing proteins, AP2 is recruited and recruits itself Clathrin heavy and light chain, which assemble in a coat of pentagons and hexagons around the nascent vesicle. CME occurs over a timecourse of minutes, is constitutive and, constituting the major endocytic pathway in eukaryotic cells, is involved in maintenance of many house-keeping functions (Schmid, 1997; Bitsikas *et al.*, 2014; Loerke *et al.*, 2009). It contributes to at least 50% of total endocytic activity; and can turn over membrane areas equivalent to the entire surface of the cell within one hour (Boucrot & Kirchhausen, 2007; Bitsikas *et al.*, 2014). Characteristic cargoes of CME are transferrin receptor (TfR), LDL receptor (LDLR) and EGF receptor (EGFR) and their cognate ligands (Anderson *et al.*, 1977; Pearse, 1982; Hanover *et al.*, 1984; Jing *et al.*, 1990). This busy endocytic pathway regulates a whole range of different functions important for cellular survival and interaction with the environment: nutrient uptake, cell signalling and growth promotion, which will be described in more detail in this section.

#### 1.1.1.1 Molecular mechanism of CME

CME has been extensively studied over decades and its mechanism has been described in both mammalian cells (reviewed in Doherty & McMahon, 2009; Taylor *et al.*, 2011) and yeast (reviewed in Payne, 1990; Boettner *et al.*, 2012; Kaksonen & Roux, 2018). Rather than being a sequential process, it is facilitated by of a network of interacting proteins. The mechanism of CME was defined by McMahon & Boucrot, 2011 in a five step process:

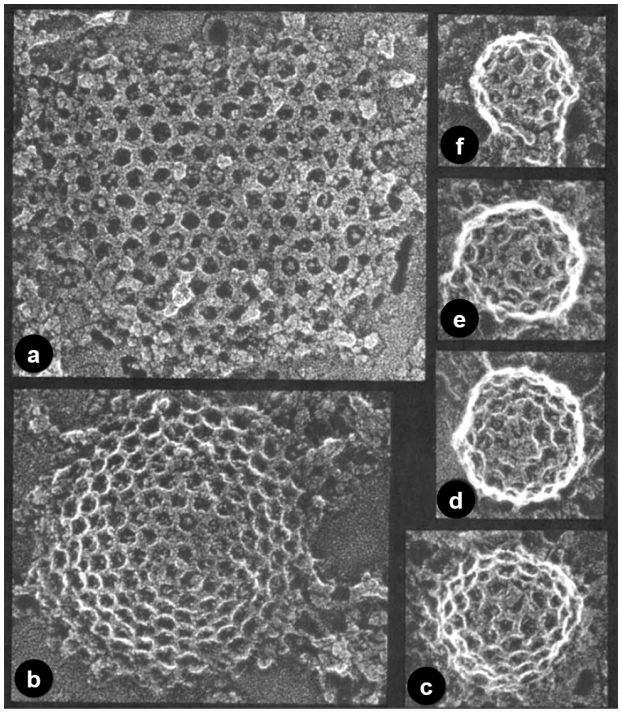


**Figure 1.1.1:** Electron microscopy images of Clathrin-coated membranes and pits
Clathrin polymerisation occurs at multiple stages of membrane bending, ranging from polymerisation on almost flat plasma membrane (a) and ending with Clathrin-coated pits (f). Adapted and modified from Heuser (1980).

**Formation of a nucleation module** In a first step, a putative nucleation module is formed by membrane-binding proteins, among others Fer/Cip4 homology domain only 1 and 2 (FCHo1 and FCHo2) in mammals, Syp1 and Ede1 in yeast (Stimpson *et al.*, 2009; Henne *et al.*, 2010). The F-BAR (FCH-Bin/Amphiphysin/Rvs) domain of FCHo2 has a high affinity for low membrane curvatures, EGFR pathway substrate 15 (EPS15) and intersectins as scaffolding and clustering components (Reider *et al.*, 2009). FCHo1/2, EPS15 and intersectins assemble at the plasma membrane and mark the site to which further proteins of the Clathrin machinery will be recruited to form Clathrin-coated pits (CCPs) (Stimpson *et al.*, 2009; Reider *et al.*, 2009; Henne *et al.*, 2010). It is proposed that this occurs by pre-complex formation of FCHo2 and EPS15, which recruits the adaptor protein complex 2 (AP2) (Ma *et al.*, 2016).

**Cargo selection by adaptor proteins and CCP stabilisation** Many cargo adaptors exist to mediate trafficking of Clathrin coated pits, of which the adaptor protein complex 2 (AP2) mediates endocytosis (Robinson, 2004). The affinity of AP2 for the plasma membrane lipid PI(4,5)P2 ensures that the endocytic process takes place at the cell surface (Beck & Keen, 1991; West *et al.*, 1997; Jost *et al.*, 1998). Plasma membrane binding

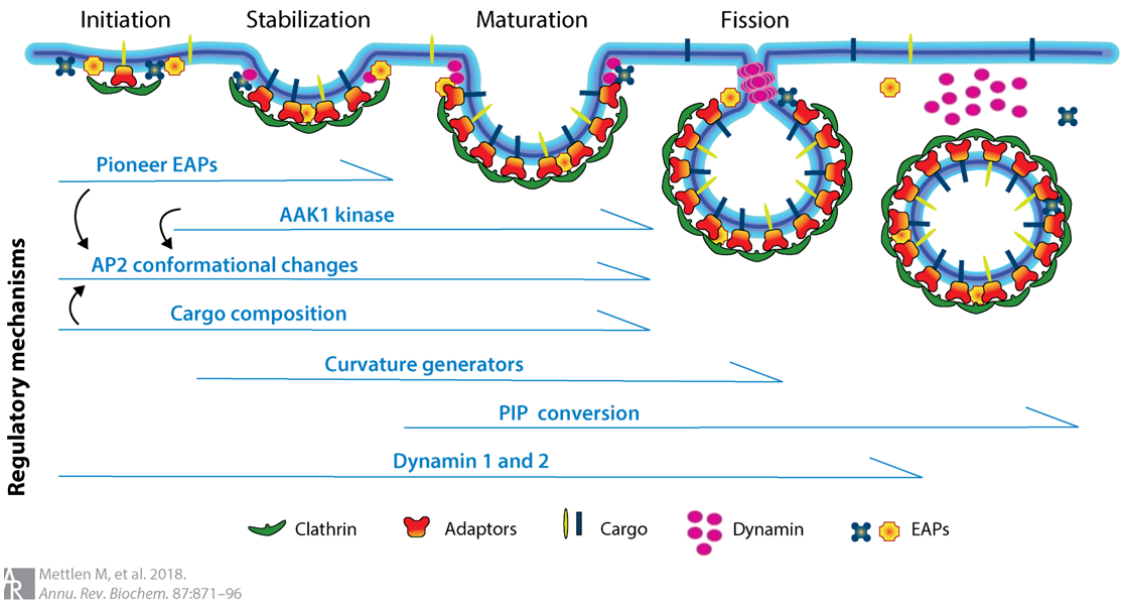


**Figure 1.1.2:** Multiple stages of CME
EAPs - Early arriving proteins. From Mettlen *et al.* (2018).

of AP2 is stabilised by its interaction with FCHo1/2 or the vertebrate ortholog SH3-containing GRB2-like protein 3-interacting protein (SGIP), which activate it by phosphorylation at the µ2 subunit, triggering an extended conformation (Hollopeter *et al.*, 2014; Umasankar *et al.*, 2014). It is an essential component in CME for CME of transferrin and partakes in EGF and LDL uptake (Motley *et al.*, 2003; Boucrot *et al.*, 2010). Serving as major hub at the heart of the Clathrin coated pit it links the plasma membrane to accessory proteins, cargo-binding proteins and Clathrin (Boucrot *et al.*, 2010; Kelly *et al.*, 2014).

AP2 is a heterotetrameric complex. It consists of a trunk region containing one µ2 and one σ2 subunit and two flexible “hinge” regions connecting one large α-adaptin trunk and one large β2 trunk (“appendage ears”) with the small µ2 and σ2 subunits (Zaremba & Keen, 1985; Kirchhausen *et al.*, 1989). Plasma membrane-binding is mediated by the α and µ2 domain (Gaidarov *et al.*, 1996; Rohde *et al.*, 2002) and the functions of α and µ2 subunit appear to be partially redundant (Motley *et al.*, 2006). In addition to membrane-binding, the µ2 subunit interacts with a hydrophobic tyrosine-based translocation motif of integral membrane proteins (Ohno *et al.*, 1995; Owen & Evans, 1998), such as EGFR and TfR (Nesterov *et al.*, 1999). In early endocytic stages, the µ2 subunit can interact with FCHo1/2 proteins, which allosterically trigger an open AP2 conformation (Hollopeter *et al.*, 2014). Clathrin assembly then triggers phosphorylation of the µ2 by (adaptor- associated kinase 1 (AAK1), which stabilises its open conformation to

support further cargo recruitment (Ricotta *et al.*, 2002; Conner *et al.*, 2003). An open AP2 conformation is proposed to stabilise it at the plasma membrane and facilitate it s phosphorylation by AAK1 (Hollopeter *et al.*, 2014). The σ2 and α domain of AP2 can bind acidic dileucine motifs, marking transmembrane cargo for endocytosis (Kelly *et al.*, 2008). The α- and β2-adaptin appendages have two ligand binding sites. These are, based on their structure, referred to as platform subdomain and beta-sandwich subdomain (Owen *et al.*, 1999; Brett *et al.*, 2002). The two subdomains allow for binding of multiple proteins at the same time. These proteins often exhibit multiple copies of a binding motif, located in regions that do not have a predicted secondary structure (Kalthoff *et al.*, 2002; Mills *et al.*, 2003; Praefcke *et al.*, 2004).

The α-adaptin subunit ensures positioning of AP2 at the plasma membrane by binding to PI(4,5)P2 with its N-terminal domain (Gaidarov *et al.*, 1996; Collins *et al.*, 2002). α-adaptin binds to AP180 (in neurons) and Epsin1 (Traub *et al.*, 1999), which themselves can also interact with membrane phosphatidylinositol head groups (Itoh, 2001; Mao *et al.*, 2001; Ford *et al.*, 2001). Further binding partners comprise Eps15, Disabled 2 (Dab2), synaptojanin, arrestins, Cyclin G-associated protein kinase (GAK) and its neuronal equivalent Auxilin, and Amphiphysin (Traub *et al.*, 1999; Umeda *et al.*, 2000; Haffner *et al.*, 2000; Praefcke *et al.*, 2004). The latter is involved in dynamin recruitment for vesicle scission in late stages of CME (Shupliakov *et al.*, 1997; Wigge *et al.*, 1997b; Owen *et al.*, 1999). The β2 appendage binds to a subset of ligands that also interact with the α-adaptin ear: Eps15, Epsin, Dab2 and AP180 (Schmid *et al.*, 2006). In addition, it binds to Sorting-nexin (SNX) 9, Heat shock cognate 70 (Hsc70), Intersectin 1 and a number of other proteins (Lundmark & Carlsson, 2003; Schmid *et al.*, 2006).

Further Clathrin-associated sorting proteins serve as cargo-specific adaptors for CME: Dab2 recruits megalin and LDLR (Nagai *et al.*, 2005; Maurer & Cooper, 2006) and associates with β1-integrin (Prunier & Howe, 2005; Teckchandani *et al.*, 2012), linking cargo to AP2 (Mishra *et al.*, 2004). Numb is an endocytic adaptor for β1-integrin and links it to AP2 (Santolini *et al.*, 2000). Epsin is an adaptor for monoubiquitylated receptors (Shih *et al.*, 2002; Sorkina *et al.*, 2006) and Arrestins for β2-adrenergic receptor (Goodman *et al.*, 1996). Other proteins in the Clathrin coat assembly comprise lipid phosphatases and kinases, promoting adaptor activation and vesicle maturation (reviewed in Mettlen *et al.*, 2018).

**Clathrin coat assembly** Whereas α-adaptin binds Clathrin only weakly, the β2 subunit, together with the hinge region, has high affinity for the N-terminal domain of Clathrin (Murphy & Keen, 1992; Owen *et al.*, 2000). Dephosphorylation of the beta hinge and high concentrations of Clathrin at the plasma membrane enable binding of Clathrin triskelia (Morris *et al.*, 1990; Smith *et al.*, 1998). Clathrin has two separate binding sites for β2-adaptin (Murphy & Keen, 1992; Owen *et al.*, 2000; Miele *et al.*, 2004), allowing for proper orientation of Clathrin monomers and the formation of a Clathrin lattice. By self-polymerisation, Clathrin displaces accessory proteins bound to AP2. AP180 and EPS15 are removed to Clathrin-free locations in the Clathrin-coated pit (CCP) by directly interacting with Clathrin (Tebar *et al.*, 1996; Cupers *et al.*, 1998; Hao *et al.*, 1999) and Epsin is restricted to the edges of the CCP (Drake *et al.*, 2000; Sochacki *et al.*, 2017). Complex formation of AP2, Clathrin and accessory proteins ameliorates Clathrin assembly and contributes to the regulation of lattice formation (Hao *et al.*, 1999). Clathrin triskelia recruited from the cytosol polymerise in pentagons and hexagons at sites of the adaptor proteins (Kanaseki & Kadota, 1969; Crowther *et al.*, 1976; reviewed in Kirchhausen, 2009). Clathrin heavy chains (CHC) form the structural backbone of the coat surrounding nascent vesicles. They can be bound by Clathrin light chains (CLC), which provide further stability to the lattice and can regulate CHC polymerisation by inhibiting their spontaneous assembly (Ungewickell & Ungewickell, 1991; Liu *et al.*, 1995). However, the presence of CLC does not appear to be crucial for CHC assembly in mammalian cells, as heavy chains can polymerise independently of CLC in the presence of AP180, AP2 and auxilin (Lindner & Ungewickell, 1991) and CME ligands are still internalised when CLC is knocked down (Acton *et al.*, 1993; Huang *et al.*, 2004). CLC appear to have a more important role in endocytic cargo selection (Wu *et al.*, 2016) and Clathrin-dependent trafficking between trans-Golgi network and endosomes (Poupon *et al.*, 2008; Dannhauser *et al.*, 2015).

Many hypotheses exist for the role of the Clathrin coat in CME. It was proposed to stabilise nascent vesicle (Ehrlich *et al.*, 2004), because does not contribute to membrane bending and vesicle shaping (Avinoam *et al.*, 2015). CHCs bind to the flexible regions of most of the adaptor proteins (Murphy & Keen, 1992; Owen *et al.*, 2000) and the generated force of polymerisation would not be strong enough to bend the membrane (Dannhauser *et al.*, 2015). Instead, membrane deformation is proposed to be

induced by proteins containing membrane-bending domains like FCHo proteins (Henne *et al.*, 2010) and Epsin (Ford *et al.*, 2002). Without an already existing membrane curvature, Clathrin would most likely polymerise in a flat lattice, with its triskelia arranged in hexagons (Heuser, 1980; Saffarian *et al.*, 2009; Grove *et al.*, 2014). A recent model combines all hypotheses and describes that Clathrin intially assembles in flat lattices and starts to deform when 70 % of the final Clathrin content required for vesicle coating is required. The inition of curvature depends on a change of the AP2 to Clathrin ratio and on membrane tension (Bucher *et al.*, 2018).

**Scission of the nascent vesicle** Following Clathrin coating, membrane-sculpting BAR domain proteins (Peter *et al.*, 2004; Ferguson *et al.*, 2009) like endophilin (Sundborger *et al.*, 2011), amphiphysin (Wigge *et al.*, 1997a; Peter *et al.*, 2004) and SNX9 (Lundmark & Carlsson, 2003) assemble at the neck of the Clathrin coated pits. BAR domain proteins often form dimers and, in this formation, have a high affinity for curved membrane, like the one present at the neck of CCPs (Habermann, 2004). They furthermore exhibit membrane tubulating properties, being able to stretch the neck even further and prepare it for scission by dynamin (Wigge *et al.*, 1997a; Ferguson *et al.*, 2009; Sundborger *et al.*, 2011). Amphiphysin, SNX9 and/or intersectins then recruit dynamin, whose proline-rich domain interacts with the recruiting proteins' Src homology 3 (SH3) domains (Wigge *et al.*, 1997a; Shupliakov *et al.*, 1997; Lundmark & Carlsson, 2004; Ferguson *et al.*, 2009; Knezevic *et al.*, 2011). SH3 domain proteins furthermore generate the high membrane curvature required for binding of dynamin (Neumann & Schmid, 2013). Dynamin is present at the nascent vesicle in low levels where it is believed to be involved in the formation of a regulatory endocytic checkpoint (Taylor *et al.*, 2012; Aguet *et al.*, 2013; Reis *et al.*, 2015). During scission initiation, it is recruited in a burst to the vesicle neck to form a scission apparatus (reviewed in Ferguson & De Camilli, 2012; Mettlen *et al.*, 2018). The large GTPase dynamin is a mechanoenzyme which drives GTP-dependent fission of the CCP from the plasma membrane (Sweitzer & Hinshaw, 1998). Dynamin polymerises in rings around the neck of CCPs in a manner that seems to constrict the budding vesicle (Hinshaw & Schmid, 1995; Shnyrova *et al.*, 2013). GTP hydrolysis triggers a concerted conformational change that closes the dynamin rings and separates the vesicle from the plasma membrane (Sweitzer & Hinshaw, 1998; Stowell *et al.*, 1999; Roux *et al.*, 2006; Liu

*et al.*, 2013). Chappie *et al.* identified molecular interactions of dynamin domains which cause, what they referred to as, a hydrolysis-dependent powerstroke (Chappie *et al.*, 2011). In the absence of dynamin or with its activity blocked, vesicle formation would halt and the membrane-sculpting activity of BAR domain proteins results in the tubular elongation of the necks of vesicles connected to the plasma membrane (van der Bliek *et al.*, 1993; Macia *et al.*, 2006; Ferguson *et al.*, 2009). This marks dynamin as a crucial component in CME, which is required for vesicle fission and endocytosis progression.

**Uncoating and recycling of Clathrin components** Before pinched-off vesicles can fuse with their target endosomes, they must be relieved of the Clathrin coat. The uncoating process is mediated by the chaperone protein Hsc70 and its cofactor GAK (or auxilin in neuronal tissue). Hsc70 is an ATPase which, in concertation with its cofactor, assists in Clathrin-coated vesicle (CCV, Schlossman *et al.*, 1984; Ungewickell *et al.*, 1995) uncoating. While dynamin constricts the neck of the vesicle, GAK/auxilin is recruited in a sudden burst and binds with high affinity to the Clathrin lattice (Massol *et al.*, 2006; Taylor *et al.*, 2011). The burst of GAK/auxilin marks the onset of vesicle uncoating and GAK/auxilin presence seems to be essential for Clathrin lattice disassembly (Greener *et al.*, 2000; Taylor *et al.*, 2011). A role for auxilin was also found in non-neuronal cells, whereby it prevents nonproductive CCV-assembly (Hirst *et al.*, 2008). GTP-bound dynamin interacts with auxilin/GAK and may thereby contribute to its recruitment (Newmyer *et al.*, 2003). It is, however, more plausible that GAK/auxilin recruitment depends on its phospholipid-binding catalytically inactive PTEN domain, which is homolog to the PI(3,4,5,)P3- and PI(3,4)P2-specific 3-phosphatase domain of phosphatase and tensin homolog (PTEN, Lee *et al.*, 2006). The PTEN domain can interact with PI(3)P and PI(3,4)P2, which are late stage endocytic intermediates. 5-phosphatases such as synaptojanin and OCRL (Lowe oculocerebrorenal syndrome protein) and class II phosphatidylinositol-3-kinase C2$\alpha$ (PI(3)KC2$\alpha$) contribute to the maturation of coated vesicles by hydrolysing PI(4,5)P2. Newly formed vesicles with PI(3)P and PI(3,4)P2, are recognised by the PTEN domain of GAK/auxilin and may contribute to the burst of the co-chaperone (reviewed in Posor *et al.*, 2015). The precise mechanism of PI(4)P to PI(3)P and PI(3,4)P2 modification, however, still needs to be defined and mapped, as it was recently observed that PI(4)P and PI(3)P production might only occur after vesicle scission (He *et al.*, 2017). Polymerised dynamin at the

vesicle neck serves as a diffusion barrier for the modified phosphatidylinositols, which accumulate at the vesicle membrane until they reach the necessary concentration required for GAK/auxilin recruitment. GAK/auxilin then recruits Hsc70 and the GAK/auxilin J-domain stimulates the Hsc70 ATPase, thereby mediating the dissociation of Clathrin in an ATP-dependent manner and uncoating the vesicle (Umeda *et al.*, 2000). The nascent vesicle, matured to an early endosome by phospholipid modification executed by the lipid phosphatases synaptojanin and OCRL (Haffner *et al.*, 2000), fuses with other early endosomes and/or is processed by further phosphatases, determining the destination of its trafficking pathway (reviewed in Posor *et al.*, 2015).

Clathrin-mediated endocytosis is a hub-centrically organised process, characterised by dynamic instability. Rapid exchange of Clathrin triskelia during coat assembly is accompanied by a constantly changing network of proteins with low-affinity interactions (Aguet *et al.*, 2013; Avinoam *et al.*, 2015). It is these characteristics, however, that lead to stability of the network while providing fidelity and flexibility (reviewed in Schmid & McMahon, 2007).

While the molecular mechanism of CME is partly well resolved, a general regulation of CME activity has not yet been discovered. It was suggested that casein kinase 1 (CK1) yeast homologue, Hrr25, is involved in initiation of CME in yeast. Hrr25 phosphorylates and activates Ede1, the yeast homologue of Eps15 which binds to FCHo2, during the formation of the putative nucleation module in early phases of CME (Peng *et al.*, 2014). CME appears to be regulated at multiple stages, as was summarised by Mettlen *et al.* (2018).

#### 1.1.1.2 Role of actin in CME

Actin polymerisation is required in multiple endocytic processes, where it is involved in varying steps (Hinze & Boucrot, 2018). It is crucial for CME in yeast to overcome outward-directed turgor pressure and bend the stiff, ergosterol-rich membrane (Kübler & Riezman, 1993; Kaksonen *et al.*, 2005; Goode *et al.*, 2014). In mammalian cells, however, CME at dorsal and ventral cell surfaces does not depend on actin (Boulant *et al.*, 2011), whereas at areas of high membrane tensions, such as at apical or adherent surfaces or in mitotic cells, forces generated by actin polymerisation are required (Boulant *et al.*, 2011; Tacheva-Grigorova *et al.*, 2013; Kaur *et al.*, 2014)

**Actin involvement in CCP formation in mammals** Little is known about actin involvement in initial stages of CME in mammalian cells. When early arriving proteins Fcho1/2 are excluded from forming CCPs, levels of N-WASP, Arp2/3, actin and Syndapin 2 are increasing (Taylor *et al.*, 2011; Henne *et al.*, 2010). Intersectins 1 and 2 are guanine-nucleotide exchange factors (GEFs) for the Rho family GTPase Cdc42 (Hussain *et al.*, 2001; Novokhatska *et al.*, 2011) but can also inhibit Cdc42 GTPase-activating proteins (GAPs) (Primeau *et al.*, 2011) (Fig. 1.1.3a). Active Cdc42 intereacts with the BAR domain proteins FBP17, CIP4 and TOCA, which have an activating function towards the nucleation-promoting factor Wiskott–Aldrich syndrome protein (N-WASP) (Giuliani *et al.*, 2009; Watson *et al.*, 2016). Activated N-WASP is required for ARP2/3-dependent formation of branched actin networks (Takenawa & Suetsugu, 2007; Rotty *et al.*, 2013). Since FBP17, CIP4 and TOCA are mainly detected after vesicle scission, it is likely that they activate actin-polymerisation propulsing budded CCVs (Taylor *et al.*, 2011). While Hip1/R arrive during early steps of CCP formation and can bind actin, they do not promote actin polymerisation during that stage (Sochacki *et al.*, 2017; Engqvist-Goldstein *et al.*, 2004). Instead, they mediate assotiation of the cytoskeleton to the neck of budding CCPs (Kaksonen *et al.*, 2003; Henry, 2002; Engqvist-Goldstein *et al.*, 2004). Upon Clathrin binding, Hip1/R undergoes a conformational change which prevents its actin binding (Chen & Brodsky, 2005; Wilbur *et al.*, 2008). Additionally, Hip1R inhibits local actin assembly by association with Cortactin and blocking elongation of barbed actin filament ends (Engqvist-Goldstein *et al.*, 2004; Brady *et al.*, 2010; Le Clainche *et al.*, 2007). During CCP formation in mammalian cells, actin polymerisation is thus restricted to the Clathrin-free area at the rim and neck of nascent vesicles by Hip1/R association with the Clathrin-coat (Fig. 1.1.3b) (Wilbur *et al.*, 2008; Boettner *et al.*, 2011).

**Actin support in late stage CCP formation and vesicle scission** During late stages of CME, the vesicle neck is constricted by the BAR domains of Amphiphysin, Endophilin and SNX9 and assisted by their ENTH-domain-mediated recruitment of N-WASP, inducing local actin polymerisation (Fig. 1.1.3c) (Ferguson *et al.*, 2009; Messa *et al.*, 2014; Gallop *et al.*, 2013; Schöneberg *et al.*, 2017). Amphiphysin, Endophilin and SNX9 furthermore recruit and concentrate Dynamin at the vesicle neck (Merrifield *et al.*, 2005; Collins *et al.*, 2011). There, Dynamin assembles into ring-like structures, which catal-

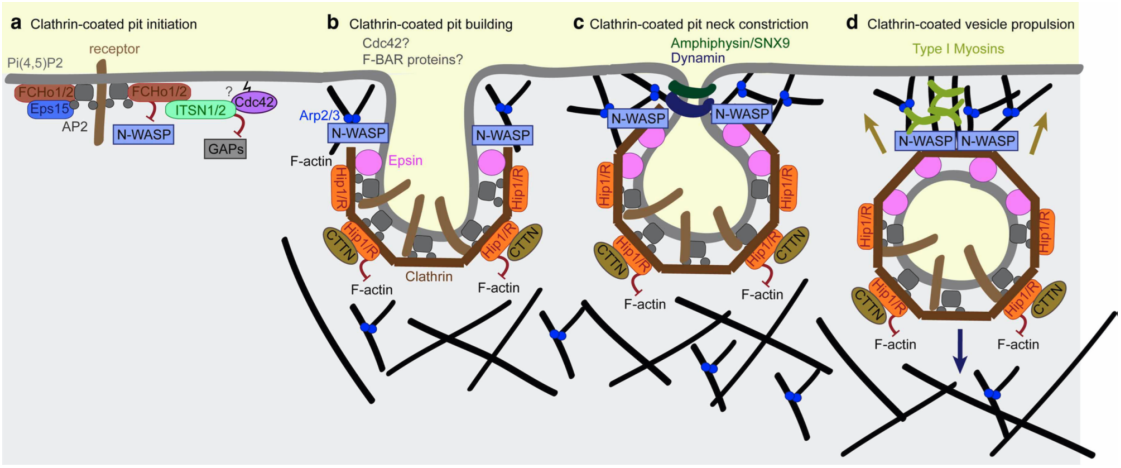


**Figure 1.1.3:** Local actin polymerisation during CME
From Hinze & Boucrot (2018).

yse GTP-hydrolysis-mediated vesicle scission (Fig. 1.1.3c) (Taylor *et al.*, 2012; Antonny *et al.*, 2016). Short, gelsolin-capped actin filaments facilitate Dynamin polymerisation which results in a feedback loop by enhancing Dynamin's GTPase activity, which in turn removes gelsolin from barbed actin ends to allow F-actin filament elongation (Gu *et al.*, 2010, 2014; Grassart *et al.*, 2014). F-actin polymerisation in turn stimulates actin-related protein 2/3 (Arp2/3)-dependent Dynamin binding to Cortactin, allowing for local remodeling of the actin cytoskeleton by Dynamin (Merrifield *et al.*, 2005; Mooren *et al.*, 2009). Unconventional type I Myosin motors, such as Myosin 1E and VI in mammals, pull the nascent vesicle away from the plasma membrane to form CCPs (Fig. 1.1.3d) (Spudich *et al.*, 2007; Taylor *et al.*, 2011).

### 1.1.1.3 FCHo proteins as nucleators of CME

**Structure** Extended Fer/Cip4 homology domain only (FCHo) 1/2 proteins belong to the family of EFC (extended FCH) or F-BAR domain proteins (Henne *et al.*, 2007). The first characterisation of FCHo2, which has homologues among mammalian species, *Drosophila* and *Caenorhabditis,* was performed *in situ* (Katoh & Katoh, 2004). SGIP1$\alpha$, a membrane binding and sculpting molecule in neuronal tissue, exhibits some degree of homology with FCHo2 (Fig. 1.1.4A; Uezu *et al.*, 2007). FCHo2 is ubiquitously expressed, whereas FCHo1 is mainly found in brain and spleen tissue, having a lower expression level than its homolog FCHo2 (Uezu *et al.*, 2011). FCHo1 can bind to SNARE

protein adaptors, a feature not exhibited by FCHo2, indicating tissue-specific differences in the function of the two proteins (Pryor *et al.*, 2008).

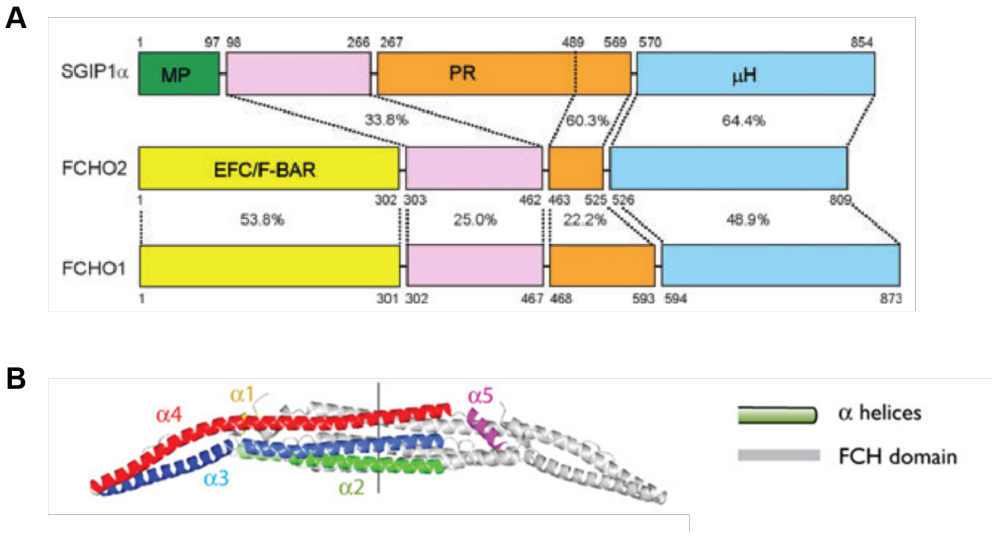


**Figure 1.1.4:** Structure of FCHo1/2 proteins
**A**: Domain organization of the FCHO family members. Percentages shown indicate identical amino acids. From Uezu *et al.* (2011). **B**: Banana-shaped FCHo2 dimer structure with highlighted α-helices and FCH domain in grey. From Henne *et al.* (2007).

FCHo2 binds to phosphatidylserines and phosphatidylinositols at the plasma membrane via its N-terminal F-BAR domain, as has been shown for other F-BAR proteins (Itoh *et al.*, 2005; Tsujita *et al.*, 2006; Henne *et al.*, 2007; Uezu *et al.*, 2011). Membrane binding occurs via antiparallel dimerisation of two FCHo2 monomers, forming an active F-BAR module (Henne *et al.*, 2007; Yu & Schulten, 2013). As a dimer, FCHo2 has a banana-shaped structure with an arc depth that is smaller than that of related BAR domain proteins (Fig. 1.1.4B) (Itoh *et al.*, 2005; Henne *et al.*, 2007). Dimerisation hides hydrophobic regions and reveals a positively charged inner surface, which mediates binding of FCHo2 to negatively charged, curved membranes (Henne *et al.*, 2007; Uezu *et al.*, 2011). Sensing membrane curvature upon dimerisation and formation of a membrane-binding region with intrinsic curvature is a common feature among F-BAR and other BAR domain proteins (Peter *et al.*, 2004; Itoh *et al.*, 2005; Henne *et al.*, 2007). BAR domain proteins, like amphiphysin, can sense high membrane curvatures (Peter *et al.*, 2004). The more shallow concave surface of F-BAR proteins, like FCHo2, allows for sensing of and binding to membranes of lower curvature (Henne *et al.*, 2007).

F-BAR domain proteins have been shown to have a membrane tubulating activity upon membrane binding (Itoh *et al.*, 2005; Tsujita *et al.*, 2006). Membrane sculpting activity induces a higher degree of membrane deformation and stabilises membrane curvature.

FCHo1/2 might therefore play a role in the formation of a nucleation module in endocytosis (Henne *et al.*, 2010). Dimerisation allows for the presentation of the flanking domains to the cytosol, and their interaction with other proteins (Henne *et al.*, 2007).

The middle region and C-terminal AP2-µ homology domain (µHD) of FCHo1/2 are not conserved, but exhibit a small degree of homology with SGIP1$\alpha$ (Uezu *et al.*, 2011). Their function remains to be discovered, but it is suggested that the central region interacts with AP2 (Umasankar *et al.*, 2012; Hollopeter *et al.*, 2014; Umasankar *et al.*, 2014) and that the µHD binds adaptor proteins of the Clathrin machinery (Henne *et al.*, 2010; Uezu *et al.*, 2011).

**Function of FCHo1/2 in CME** The initiation of CME requires nucleation sites, which are marked by induced, and maintained, membrane curvature (Motley *et al.*, 2003; Nunez *et al.*, 2011). FCHo1/2 has high affinity for PI(4,5)P2 and is recruited to the plasma membrane before the arrival of AP2 (Henne *et al.*, 2010; Uezu *et al.*, 2011; Taylor *et al.*, 2011). FCHo1/2 also serves as an allosteric activator of AP2 via its central linker region, as it has been shown that an open structure of AP2 could bypass the requirement for FCHo proteins (Umasankar *et al.*, 2012; Hollopeter *et al.*, 2014; Umasankar *et al.*, 2014). A closed conformation of AP2 prevents its binding to the membrane and adaptor proteins (Collins *et al.*, 2002). FCHo1/2 stabilises AP2 and assures the formation of CCPs with long life spans (Henne *et al.*, 2010; Cocucci *et al.*, 2012). Down regulation of FCHo1/2 drastically decreases the number of endocytic events and detectable AP2 at the plasma membrane, whereas its overexpression increases CCP nucleation events and CME activity (Henne *et al.*, 2010; Cocucci *et al.*, 2012). FCHo1/2 thus serves as an initial stabilising factor for the development of minimal AP2-Clathrin complexes into pits at the membrane (Henne *et al.*, 2010). The µHD domain of FCHo2 can furthermore interact with the LDLR adaptor Dab2 (Mulkearns & Cooper, 2012). By this interaction, Dab2 may even serve as an AP2 substitute in events of low AP2 concentrations (Mulkearns & Cooper, 2012). Similar to the C-terminal domain of the neural homolog SGIP1$\alpha$, the µHD domain can interact with Eps15 and intersectins, which are also involved in the formation of a nucleation module of CME (Uezu *et al.*, 2007; Henne *et al.*, 2010; Uezu *et al.*, 2011).

The early binding of FCHo1/2 to nucleation sites and its recruitment of accessory proteins, like Eps15, Dab2 and AP2 make it a suitable candidate for the initiation of CME. These interactions trigger clustering of FCHo1/2 into patches, which can introduce positive plasma membrane curvature (Henne *et al.*, 2010; Uezu *et al.*, 2011).

#### 1.1.1.4 Cargoes and cellular functions of CME

CME controls a variety of cellular functions, ranging from nutrient uptake to signalling, thereby regulating cell growth, proliferation, development, chemotaxis and differentiation, to the regulation of transporters and synaptic signal transduction (reviewed in Sorkin & von Zastrow, 2009; Scita & Di Fiore, 2010; Haucke *et al.*, 2011; McMahon & Boucrot, 2011).

Ligand internalisation assays of transferrin, epithelial growth factor (EGF) and low density lipoprotein (LDL) have been widely applied to study the mechanism of CME (Anderson *et al.*, 1977; Pearse, 1982; Hanover *et al.*, 1984; Jing *et al.*, 1990). It was initially believed that endocytosis would mainly serve the supply of nutrients. This holds true for the uptake of iron and cholesterol, which are carried by transferrin and LDL, respectively. TfR and LDLR are constitutively trafficking through CME (Anderson *et al.*, 1977; Goldstein *et al.*, 1985). The receptors are internalised and recycled back to the cell surface independently of binding to a substrate. Whereas transferrin interacts directly with the Clathrin machinery, LDLR recruitment requires cargo-specific adaptor proteins, such as Dab2 and ARH59 (Keyel, 2006). Binding of EGF receptor to its cognate ligand triggers its dimerisation (Yarden & Schlessinger, 1987a) and activation of its tyrosine kinase domain with subsequent autophosphorylation (Yarden & Schlessinger, 1987b; Honegger *et al.*, 1989, 1990). The multimerised and phosphorylated receptor tail is recognised by the adaptor proteins Grb2 (Lowenstein *et al.*, 1992; Kozer *et al.*, 2014) and CALM (Huang *et al.*, 2004), which mediate its recruitment to the Clathrin machinery (Huang *et al.*, 2004). The dimerised receptor furthermore recruits many signalling pathway components to the phosphorylation sites and activates conserved pathways like MAP kinase pathway as well as Ras and calcium signalling (reviewed in Disanza *et al.*, 2009; Sigismund *et al.*, 2012). Another example of CME involved in signalling are G-protein coupled receptors (GPCRs). Binding to its cognate ligand causes a conformational change of the receptor, whereupon it is recruited to CCPs by adaptors. The GPCR

β2-adrenergic receptor requires β-arrestin, upon binding its cognate ligand adrenaline, for recruitment to the Clathrin machinery (Ferguson *et al.*, 1996). Once receptor and cargo are internalised, they dissociate from their ligands and are either recycled back to the cell surface or traffic to the lysosome for degradation (reviewed in Luzio *et al.*, 2009). The main role of CME in signal transduction is the termination of the signal by removing the activated receptor from the cell surface (Sorkin & von Zastrow, 2009; Vanneste & Friml, 2009). Signalling termination is important in the canonical Wnt signalling pathway, where Frizzled is internalised via CME upon binding Wnt ligands, and degraded in the lysosomal compartment (Yu *et al.*, 2007). CME, however, also mediates signalling amplification, and under the condition of low ligand concentration, sustains the signalling by initiating recycling of receptors back to the cell surface (Sorkin & von Zastrow, 2009; Vanneste & Friml, 2009). These examples demonstrate that CME is highly involved in cellular signalling processes in non-synaptic cells, where it regulates vital functions like development, cell fate and immune response (reviewed in Sorkin & von Zastrow, 2009; McMahon & Boucrot, 2011). Therefore, impaired CME results in severe diseases, such as cancer, neurodegenerative and lysosomal storage diseases (reviewed in McMahon & Boucrot, 2011).

CME plays an important role for signal transmission in synapses (reviewed in Maritzen & Haucke, 2017; Watanabe *et al.*, 2018a). Highly active pre-synapses contain thousands of vesicles. After exocytosis, these need to be efficiently recycled for further turns of signal transmissions (Heuser & Reese, 1973; Nonet *et al.*, 1999). The regulation of size (Nonet *et al.*, 1999) and composition of synaptic vesicles is also highly dependent on CME and allows for synaptic plasma membrane homeostasis (Bazinet *et al.*, 1993; Dittman & Kaplan, 2006).

### 1.1.2 Clathrin-independent endocytic pathways

#### 1.1.2.1 Macropinocytosis

First described by Lewis (1931), macropinocytosis, also called fluid-phase uptake, is a receptor-independent endocytic pathway allowing for internalisation of large quantities of extracellular fluid and rapid plasma membrane remodelling (Buckley & King, 2017). Macropinocytosis relies on intensive actin polymerisation-dependent membrane ruffling

initiated by Ras- or receptor tyrosine kinase signalling (West *et al.*, 1989; Bryant *et al.*, 2007; Amyere *et al.*, 2000). Membrane protrusion extend from the cell and fold back upon themselves, forming large (> 0.5 µm) endocytic carriers (Kerr *et al.*, 2006; Buckley & King, 2017). The size of macropinocytic vesicles is the best characteristic to describe macropinocytosis, because to date no specific marker has been found for this pathway. Macropinocytosis initiation differs greatly from early stages of receptor-mediated endocytosis, where receptor molecules are recruited to pits at the plasma membrane. Macropinosomes form in response to receptor tyrosine kinase activation (such as EGFR and platelet-derived growth factor receptor (PDGFR)). Tyrosine kinase activation leads to an increased polymerisation and rearrangement of actin at the plasma membrane and a subsequent increase of membrane ruffling (reviewed in Kirkham & Parton, 2005; Buckley & King, 2017). Macropinosomes migrate towards the centre of the cell, whereby they acquire markers of late endosomes, such as Rab7 (Racoosin & Swanson, 1993) and eventually fuse with lysosomes (Lim *et al.*, 2008). In Ras-transformed cancer cells, macropinocytosis is constitutively active and supplies cells with nutrients, acivating mammalian target of rapamycin (mTORC) 1 by amino acid signalling from lysosomes, and stimulating growth (reviewed in Yoshida *et al.*, 2018).

Macropinosomes exhibit a unique feature which distinguishes them from trafficking vesicles formed by other endocytic pathways. The fate of the macropinosome vacuoles differs dependent on cell type, presumably serving the specific roles of macropinocytosis in each tissue. Macropinosomes in kidney cells, for example, are targeted towards late endosomes and lysosomes, whereas A-431 (human epidermoid carcinoma cells) and NIH-3T3 (mouse embryonic fibroblasts) cells keep them isolated from the endolysosomal system, so that they eventually return to and fuse with the plasma membrane (Hewlett *et al.*, 1994; Schnatwinkel *et al.*, 2004). In lymphocytes, macropinocytosis serves antigen presentation (reviewed in Liu & Roche, 2015). High levels of constitutive macropinocytosis can be furthermore observed in dendritic cells and macrophages. In these cells, macropinocytosis does not depend on Ras- or growth factor receptor signalling, but is triggered by calcium-sensing receptors (Canton *et al.*, 2016; Bretou *et al.*, 2017). This way, cells continually screen the external space for foreign, and possibly harmful, material (Norbury, 2006). However, a broad range of pathogens exploits macropinocytosis to invade cells and avoid detection by the immune system. A num-

ber of pathogens target the host cell's lipid metabolism and trigger actin reorganisation by secreting virulence factors. The ruffles formed in this way fold back on themselves and enclose the pathogen into a vacuole. Once bound to the surface of epithelial cells, pathogens employ specifically developed apparatuses, the type III/IV secretion systems, to translocate virulence proteins across the plasma membrane into the host cell's cytoplasm. Examples for this mechanism are *Salmonella* (Haraga *et al.*, 2008), *Legionella* (Shin & Roy, 2008) and *Shigella* (Schroeder & Hilbi, 2008). Other pathogens, like *Mycobacterium*, are able to induce macropinosome formation, but do not rely on a bacterial secretion system (García-Pérez *et al.*, 2008).

Even though macropinocytosis can be a potential risk for infection with pathogens, it is crucial for the survival of the cell, particularly for cancer cells which rely on vast supply of nutrients to sustain their high metabolic activity (Commisso *et al.*, 2013). Studies have shown that disruption or hyperstimulation of macropinocytosis by pharmacological or genetic manipulations leads to formation of enlarged cytoplasmic vacuoles, which can cause a form of non-apoptotic cell death ("methuosis", from Greek *methuo*: to drink to intoxication, Overmeyer *et al.* 2008). Methuosis was triggered either by overexpression of constitutively active Ras (Overmeyer *et al.*, 2008; Bhanot *et al.*, 2010) or delivery of small molecules, which induce vacuolisation, originating in the macropinosome (Overmeyer *et al.*, 2011; Robinson *et al.*, 2012). Disruption of macropinocytosis could been shown only *in vitro* and it remains unclear whether methuosis would occur *in vivo*. Nonetheless, the examples above show that macropinocytosis is a complex process that requires strict regulations in order to allow for cell survival and functionality.

#### 1.1.2.2 Caveolin-mediated endocytosis

Caveolae (which stands for "little caves") are described as flask or crater shaped plasma membrane pits and comprise, with a diameter of 60-80 nm (reviewed in Stan, 2005; Schlörmann *et al.*, 2010), a smaller volume than CCVs. They have been observed in a variety of mammalian cell types and highly enriched in endothelial cells, myocytes and adipocytes, and are involved in endocytosis, transcytosis, exocytosis, mechanosensing and signalling (reviewed in Parton & Simons, 2007; Parton & del Pozo, 2013). Caveolae were also reported to mediate pathogen infection (Branza-Nichita *et al.*, 2012). Caveolae are formed by Caveolins 1-3 (caveolin 3 in muscle cells; Scherer, 1996) (Rothberg

*et al.*, 1992). Caveolins are integral membrane proteins inserted into cholesterol-rich membrane patches by a hydrophobic hairpin domain (Murata *et al.*, 1995; Ariotti *et al.*, 2015). Therefore, the caveolin-dependent pathway appeared to be related to pathways involving lipid raft domains. These are characterized by membrane lipid reorganisation, *i. e.* clustering special kinds of lipids and cholesterol which can lead to membrane bending (Bacia *et al.*, 2005). Other lipid raft-dependent pathways show, however, no evidence for the abundance of caveolin or caveolae and a complex structural and signalling machinery as required for caveolin-mediated endocytosis (reviewed in Cheng *et al.*, 2006). Over the past years it has become evident that caveolins act together with cavins to form the caveolar pits and regulate their shape (reviewed in Parton & del Pozo, 2013). Cavin complexes additionally stabilise oligomerised caveolin in pits at the plasma membrane and stay associated with the budding caveolae (Pelkmans & Zerial, 2005; Hill *et al.*, 2008; Boucrot *et al.*, 2011). Caveolin 1 is synthesized as monomers in the rough endoplasmic reticulum and matures to oligomers when travelling through the Golgi apparatus. It subsequently forms high order oligomers in sequestering cholesterol and travels as an exocytic caveolar carrier to the plasma membrane. Internalisation of caveolae and their linear organisation at the plasma membrane are stabilised by microtubules and actin fibres of the cytoskeleton (reviewed in Parton & del Pozo, 2013). How in detail cavin is recruited and how the stabilisation occurs, as well as the function of a set of further endocytosis regulating factors, is highly discussed and remains to be elucidated. No specific cargo has been discovered for caveolin-mediated endocytosis, and there is no evidence for caveolae formation at endomembranes of intracellular vesicles (Parton & del Pozo, 2013). Emerging evidence suggests that caveolin-pits facilitate cell surface stretching and act as mechanosensors (reviewed in Nassoy & Lamaze, 2012; Echarri & Del Pozo, 2015). Earlier studies had already hinted at the involvement of caveolae in membrane stress sensing and mechanotransduction: the number of caveolae at the plasma membrane of endothelial cells increases upon applied shear stress, and caveolae formation has an impact on ERK and Akt signalling and actin remodelling (Boyd *et al.*, 2003; Radel & Rizzo, 2005; Yu *et al.*, 2006). In addition, caveolar invaginations serve as a membrane reserve, allowing for osmotically induced swelling of cells, and thereby regulate the activation of mechanosensitive ion channels (Parton & del Pozo, 2013). Mechanosensing and membrane reservoir are important functions for muscle and adipose tissue, whose cells undergo frequent shape or size changes upon

contractions, hypertrophy or lipid storage Kozera *et al.* (2009); Huang *et al.* (2013); Lo *et al.* (2015); Briand *et al.* (2014). This is reflected by the fact that the absence of caveolin-mediated endocytosis is responsible for disease phenotypes like muscular dystrophy and cardiac arrhythmia (Hayashi *et al.*, 2009; Rajab *et al.*, 2010).

#### 1.1.2.3 Clathrin- and caveolin-independent endocytic pathways

With the improvement in sample fixation strategies and the usage of electron microscopy, many more endocytic pathways have been discovered during the last years. They can be characterised by specific proteins involved, dynamin-dependence, size, morphology and kinetics and regulate specific physiological processes such as quick cell surface receptor removal, response to receptor hyper stimulation or stress hormones (’fight or flight” response), chemotaxis, and membrane retrieval upon exocytosis at synaptic hormone-containing vesicles (Ferreira & Boucrot, 2018; Watanabe & Boucrot, 2017; Johannes *et al.*, 2015).

The Clathrin-independent tubovesicular carrier (CLIC)/ glycosylphosphatidylinositol (GPI-)anchored proteins enriched carriers (GEEC) pathway, glycolipid-lectin (GL-Lect) endocytosis and internalisation of shiga and cholera toxin rely on extracellular cargo clustering for membrane deformation (Ferreira & Boucrot, 2018; Johannes *et al.*, 2015). CLIC/GEEC endocytosis of GPI-anchored proteins relies on GRAF1, Rho-GTPases and actin polymerisation, but the mechanistical details are not well understood (Lundmark *et al.*, 2008). The GL-Lect hypothesis proposes Galectin-3-mediated clustering of the extracellular domains of glycolipids and glycosylated membrane proteins, driving inward-directed membrane curvature (Lakshminarayan *et al.*, 2014). In a similar manner, Shiga and Cholera toxin bind and cluster Gb3 and GM1 glycosphingolipids, respectively, in the exoplasmic membrane leaflet (Lajoie *et al.*, 2009; Kabbani & Kelly, 2017; Johannes, 2017). In all pathways, actin polymerisation supports carrier formation (reviewed in Hinze & Boucrot, 2018).

Fast endophilin-mediated endocytosis (FEME) forms tubular carriers and occurs within seconds upon receptor activation at plasma membrane sites primed with the BAR-domain protein endophilin, which remains associated with the endocytic cariers upon budding (Boucrot *et al.*, 2015). Priming is prevalent at the leading edge and is a dynamic process mediated by FBP17 and CIP4, which recruit SHIP2 and lamellipoding to locally

generate PI(3,4)P2, resulting in recruitment of Endophilin (Chan Wah Hak *et al.*, 2018). Endophilin tubulates the cargo-containing membrane region in an actin-dependent manner (Boucrot et al., 2015). Similar to CME, dynamin is required to sever FEME carriers from the plasma membrane (Boucrot *et al.*, 2015). A subset of FEME-specific cargoes include Interleukin-2 receptor and a subset of G-protein-coupled receptors and receptor tyrosine kinases (Boucrot *et al.*, 2015).

The detailed mechanisms for these pathways remain yet to be elucidated, including the assignment of their specific cargoes and function. There might still be a large number of unexplored endocytic portals to enter cells, indicated by the variety of receptors that need to be regulated at the plasma membrane. Discovering these pathways and defining their mechanisms will be a challenging task for researchers in the future.

## 1.2 Proliferative quiescence

Continuous exponential proliferation is a state which cannot be maintained endlessly in nature. Cell proliferation is limited by the abundance of nutrients and space. Therefore, many cells in the human body as well as in other metazoan organisms and even single cellular organisms reside in a resting, non-proliferative state (Yao, 2014). However, the majority of cellular research has been performed on continuously proliferating cells. Quiescent cells, like stem cells, hepatocytes, dermal fibroblasts, endothelial cells and lymphocytes, are found in the major tissues of the human adult body, serving tissue homoeostasis and regeneration (Pol *et al.*, 1998; Brand, 1985; Iyer *et al.*, 1999; Augustin *et al.*, 2009; Arai *et al.*, 2004; Mira *et al.*, 2010; Pedersen *et al.*, 2014).

Cellular quiescence has already been observed decades ago and has been described as a proliferative inactive state that cells enter before passing the cell fate determining restriction point in the G1 phase of the cell cycle (Pardee, 1974, 1989). In contrast to senescent or terminally differentiated cells, quiescent cells resting in the G0 phase can reversibly exit the cell cycle upon natural stimuli in their environment, such as growth factors and intercellular contacts, maintaining the ability to resume proliferation (Coller *et al.*, 2006). Like the aforementioned proliferative cell states, quiescent cells exhibit a diploid (2n) genome, down regulated expression of cell cycle-promoting genes like those coding for cyclins and growth factors (Coller *et al.*, 2006) and are resistant to

senescence, differentiation and apoptosis (Sang *et al.*, 2008; Mohrin *et al.*, 2010). They are characterised by low transcriptional activity, which can be shown by low levels of RNA stained with Pyronin Y (Darzynkiewicz *et al.*, 1980; Shapiro, 1981; Rhee & Bao, 2009), decreased levels of Cyclin D1, which is excluded from the nucleus, (Baldin *et al.*, 1993; Ruiz-Miró *et al.*, 2011) and absence of Ki67 (Gerdes *et al.*, 1983, 1991). Ki67 is a proliferation marker present in all stages of the cell cycle except G0 (Gerdes *et al.*, 1991). Levels of the DNA clamp PCNA (proliferating nuclear antigen) are down regulated during cell quiescence, as DNA replication is arrested (Takasaki *et al.*, 1981; Coller *et al.*, 2006). More recent observations suggest that the activity of cyclin-dependent kinase 2 (CDK2) is a reliable monitor of cell cycle exit and re-entry, and could serve as a sensor for the commitment of cells to enter quiescence (Spencer *et al.*, 2013). Upon passing the restriction point, cells become either committed to complete the cell cycle independent of growth factors, or enter into the non-proliferative G0 phase (Zetterberg & Larsson, 1985; Spencer *et al.*, 2013). CDK2, in complex with cyclin E1, phosphorylates Retinoblastoma protein (Rb; Lundberg & Weinberg, 1998; Ren & Rollins, 2004). Rb is phosphorylated in multiple steps, first by the CDK4-cyclin D1 complex, which generates hypophosphorylated Rb, a substrate for phosphorylation by the CDK2-cyclin E1 complex (Kitagawa *et al.*, 1996; Connell-Crowley *et al.*, 1997). Inactive, fully phosphorylated Rb dissociates from its binding partners, transcription factors of the E2F family, and allows for transcription of genes involved in cell cycle progression and DNA replication (reviewed in Sears & Nevins, 2002; Stevaux & Dyson, 2002). In quiescence, cells thus exhibit low levels of cyclin D1 and hypophosphorylated Rb (Baldin *et al.*, 1993; reviewed in Zhang, 2013). While quiescent cells are often characterised and identified by their down-regulation of the expression of cell-cycle promoting genes, there is little evidence for a ubiquitous positive molecular marker. P27(Kip1), a CDK inhibitor, has been reported to block proliferation, prevent apoptosis upon growth factor withdrawal, and the onset of cellular senescence (Nourse *et al.*, 1994; Ladha *et al.*, 1998; Hiromura *et al.*, 1999; Coller *et al.*, 2006). Emerging evidence links p27 to maintenance of the stem cell pool, preventing stem cell proliferation and differentiation (Cheng *et al.*, 2000b; Oesterle *et al.*, 2011; Stein *et al.*, 2013; Chakkalakal *et al.*, 2014). Along with the cardinal feature of quiescent cells to resume proliferation after cell cycle arrest, p27 might be a potential molecular marker discriminating the G0 from terminally differentiated or senescent G1 cell populations.

First observations of the G0 cell population described this state as inactive in both proliferating activity and metabolism. Later work, however, revealed that the quiescent state is actively maintained and that quiescent fibroblasts exhibit high metabolic rates in terms of glucose turnover (Lemons *et al.*, 2010). It was observed that lysosomal and autophagic activity is increased during quiescence, which might serve maintenance of energy levels, ensure protein and organelle functionality during stress exposure and enable re-entry into the cell cycle (Onodera & Ohsumi, 2005; Valentin & Yang, 2008; Tang & Rando, 2014; Zhang *et al.*, 2017). Inhibition of autophagy has been shown to trigger apoptosis (Boya *et al.*, 2005; Dangi *et al.*, 2016). Elevated levels of autophagy are therefore cytoprotective adaptation ensuring the survival of quiescent cells in unfavourable conditions (Song *et al.*, 2013; Xu *et al.*, 2014; Dangi *et al.*, 2016).

Mammalian cells can enter the G0 phase of the cell cycle via different pathways: contact inhibition, mitogen starvation and loss of adhesion to substrate (only adherent cells, while remaining attached to each other; Coller *et al.* 2006; Ruiz-Miró *et al.* 2011; Neurauter *et al.* 2012). Each of these pathways into quiescence gives the cells a different expression signature. However, the longer cells are maintained in quiescence, the clearer a subset of common up or down regulated genes is observed (Coller *et al.*, 2006). This indicates a basic “quiescence programme”, which the cells switch on upon their reversible exit from the cell cycle. Combination of signals leads to a more effective and faster entrance into quiescence, which is then represented by a more distantly related gene expression profile compared to the profile of cycling cells (Coller *et al.*, 2006). Non-transformed proliferating cells can spontaneously exit the cell cycle and enter quiescence. The longer they reside in a quiescent state, the more pronounced the quiescence signature becomes by increased or decreased expression of quiescence-related genes (Gookin *et al.*, 2017).

Many features characterising the quiescent state have been described, but three major questions remain to be answered: Is cell quiescence a passive state or actively maintained and is it dynamic or rather static, and is there a universal positive marker identifying quiescent cells?

### 1.2.1 Quiescence in yeast

The quiescence programme in yeast can easily be switched on upon limitation of essential nutrients (reviewed in Gray *et al.*, 2004). Yeast cells sense each other and respond upon this sensing (reviewed in Hogan, 2006; Wuster & Babu, 2010). However, they do not exhibit contact inhibition because they do not form a complex organ with a regulated cellular organisation, which is the case in tissue of higher eukaryotes. Carbon, nitrogen, phosphate or sulfur starvation are unfavourable conditions for proliferation and results in entry into G0 during G1 phase. Thus, the induction of cell quiescence in yeast is distinct from cells in higher organisms which continuously obtain plenty of nutrients provided by the vascular system. However, there are a number of similarities between these populations: yeast cells enter G0 in a short time frame during G1 which is called START A and seems to be a (controversially discussed) equivalent to the restriction point in mammalian cells (reviewed in Sherlock & Rosamond, 1993). Yeast quiescence also exhibits the same reversibility because cells resume proliferative activity upon re-feeding (Lillie & Pringle, 1980). *Saccharomyces cerevisiae* and *Schizosaccharomyces pombe* were shown decades ago to be excellent eukaryotic models for genetic cell cycle studies (Hartwell *et al.*, 1973; Nurse, 1975). Usage of the two yeast strains is in particular of advantage as they are evolutionary very distant. Thus common features discovered in the two yeasts are likely to be also found in mammalian cells. Yeast cells are easy to cultivate and have a short duplication period of only 90 to 120 minutes (Bergman, 2001). Gene knock outs and knock ins can be easily performed and conditionally induced, which is represented by the many temperature-sensitive yeast strains that exist (reviewed in Littlewood, 1975; Aspuria *et al.*, 2007; Osborn & Miller, 2007). Studying quiescence in yeast gains in importance as its regulation involves many of the human homologous kinases, one of the most prominent of them being the target of rapamycin complex (TORC, reviewed in De Virgilio, 2012). By the creation of deletion and temperature sensitive mutant yeast strains, a whole set of genes required for quiescence could be elucidated, pointing out gene candidates for quiescence regulation in humans (reviewed in Yanagida, 2009). The question whether yeast is a model as good as higher differentiated cells in multicellular eukaryotes to study cellular quiescence, remains yet to be answered. It is worth noting that a key regulator for the control of quiescence and growth other than TOR protein kinase, which is the central controller of growth and

metabolism, has not yet been found (reviewed in Wullschleger *et al.*, 2006; Yanagida, 2009). Yeast studies should thus be interpreted with caution when it comes to their translation to human cells. Indeed, due to the existence of many yeast and human homologous genes, yeast cells are a great platform to study quiescence mechanisms. Yet to fully translate discoveries from yeast to humans, it remains to confirm these findings in cultures of respective human tissues, especially regarding the fact that even in distinct mammalian tissues cellular mechanisms are regulated differently. However, yeast studies along with studies in mammalian cells and *in vivo* systems can provide great contributions in identifying key players in universal regulation of quiescence in eukaryotes.

### 1.2.2 Quiescence *in vitro*

Regenerative tissues exhibit a pool of quiescent cells, which remain in a non-proliferate state until tissue damage requires cell renewal. Quiescence in endothelial cells has been studied to elaborate mechanisms triggering reversible cell cycle exit and re-entry. Mammalian cells exit the cell cycle upon different stimuli than yeast cells. Quiescence entry occurs via the exposure to different extracellular signals: i) mitogen withdrawal, ii) contact inhibition and iii) loss of adhesion to substrate (Benecke *et al.*, 1978; Coller *et al.*, 2006; Ruiz-Miró *et al.*, 2011).

The advantage of *in vitro* studies is their reproducibility at defined conditions. The establishment of non-tumorous cell lines is a great advantage in investigations of cellular quiescence, as these cells stably exhibit a diploid genome and respond to contact inhibition and stop proliferation. Inducing quiescence in primary cells is possible (Coller *et al.*, 2006), and *in vitro* experiments have been performed on quiescent cells as described below, but the variance between different donors needs to be considered (Zhu *et al.*, 2014). With the establishment of immortalised non-tumorous cell lines, like RPE1 cells (retina pigmented epithelial cells immortalised by human telomerase reverse transcriptase hTERT) or other cell lines immortalised by hTERT, like hepatocytes (Totsugawa *et al.*, 2007) or endothelial cells (Parent *et al.*, 2014) defined reproducible conditions for cell quiescence experiments are ensured (reviewed in Lipps *et al.*, 2013).

**Quiescent endothelial cells *in vitro*** Angiogenesis describes the process of formation of capillaries from pre-existing blood vessels. It has to be tightly controlled by a balance of positive and negative environmental signals, which either induce angiogenesis or inhibit proliferation of endothelial cells (ECs). Mature vascular endothelial cells rest in a quiescent state, lining the luminal surface of blood vessels (reviewed in D'Amore, 1992; Herbert & Stainier, 2011). This non-dividing state is maintained by confluent ECs in a cobblestone-like cellular monolayer, tight cell-cell junctions, predominance of angiogenic inhibitors (reviewed in Potente *et al.*, 2011). An extracellular matrix layer rich in laminin and collagen fibres, called the basement membrane, forms a barrier to surrounding tissues, contributing to quiescence maintenance and controlling the exchange of fluids, solutes and immune cell transmigration (Ingber, 1991; Mazzone *et al.*, 2009;reviewed in Adams & Alitalo, 2007; Carmeliet & Jain, 2011).

In association with wound healing or upon pro-angiogenic signals, quiescent ECs loosen their junctional contacts, the basement membrane is degraded by active proteases and angiogenesis inducers activate a subpopulation of endothelial cells (Gerhardt *et al.*, 2003). These endothelial "tip cells" then extend dynamic filopodial protrusions, thereby sensing and responding to attracting or repulsing signals in their microenvironment, which guide their motility. The acquired invasive and motile behaviour of endothelial "tip cells", together with their increased proliferative activity, marks the initiation of new blood vessel sprouting (Gerhardt *et al.*, 2003; Mazzone *et al.*, 2009). Vessel wall-stabilising factors, deposition of extracellular matrix forming the basement membrane and strengthening of cell-cell junctions slow down and suppress the sprouting of ECs and re-establish the mature quiescent phenotype (reviewed in Jain, 2003; Gaengel *et al.*, 2009).

To study the molecular mechanism of EC quiescence, *in vitro* vascular systems were shown to be a useful method. Zhang *et al.* could mimic EC quiescence by growing ECs to confluence on collagen, thereby identifying the regulation of both angiogenesis and quiescence by Angiopoietin-1 and receptor tyrosine kinase Tie2. They also observed that EC quiescence was controlled by basal Notch signalling and further downstream signalling processes (Zhang *et al.*, 2011).

In a hemodynamic flow model, Uzarski *et al.* investigated the influence of flow rates on EC quiescence properties. A physiological flow rate enhances anti-inflammatory and

anti-thrombotic characteristics of ECs, in comparison to steady flow models at a fixed pulse frequency, and represents the variability in metabolic demand of ECs, indicating that variable shear stress has a key impact on EC function (Uzarski *et al.*, 2013). These results are more consistent with the previously observed inflammation-protective quiescence phenotype (reviewed in Fiedler & Augustin, 2006) and is proof of better adaption of *in vitro* models to mimic physiological conditions in nature.

The investigations of Zhang *et al.* and Uzarski *et al.* both evaluated the regulation of signalling pathways and down-regulated cell cycle markers *in vitro*. They report, however, no cardinal feature of quiescent cells, which is the ability to resume proliferation. Pedersen *et al.* generated a quiescent phenotype of primary ECs by adding mesenchymal stem cells (MSCs) to an *in vitro* culture system (Pedersen *et al.*, 2014). Monitoring angiogenic stimulation and vascular assembly revealed decreased proliferation and maturation of ECs, and induction of EC quiescence by co-seeding MSCs (Pedersen *et al.*, 2014). They could furthermore show that the regenerative capacity of ECs was maintained, by transplanting the tissue constructs in mice where they grew into a dense network of blood vessels (Pedersen *et al.*, 2014).

**Quiescent hepatocytes *in vitro*** The liver is an organ consisting of multiple specialised cell types. It has high regenerative capacity, which is mainly generated by hepatocytes residing in proliferating quiescence. Hepatocytes, the liver parenchymal cells, form the major cell type in the liver. Upon stimulation, quiescent hepatocytes can rapidly enter the cell cycle to proliferate and maintain tissue homoeostasis (reviewed in Zimmermann, 2004). Isolated hepatocytes in primary cell culture remain in a quiescent state until proliferation is triggered by mitogenic factors, which up-regulate cyclin D1, cyclin E1 and mTOR (mammalian target of rapamycin) targets to allow for transition from G0 via the G1/S checkpoint to S phase of the cell cycle (McGowan *et al.*, 1981; Nakamura *et al.*, 1984, 1989; Oka *et al.*, 2013).

*In vitro* cultures of confluent hepatocytes have proven a suitable model to represent lipoprotein metabolism in the liver (Bouma *et al.*, 1988; Ling *et al.*, 2013). Primary hepatocytes in cell culture tend to quickly lose their hepatocyte integrity, represented by loss of mature hepatocyte markers like albumin, anti-trypsin and lipoproteins, in cell culture (Ferrini *et al.*, 1997). Improved culturing conditions have been developed to maintain

hepatocyte integrity and enable long-term culture of primary hepatocytes (Ferrini *et al.*, 1997). Immortalisation of hepatocytes allows for stable cultures of cells with differentiated hepatic functions (Cascio, 2001). Advanced studies use co-cultures of quiescent primary hepatocytes and fibroblasts to maintain pH, microfluidic chambers and 3D scaffolds or micro patterning to mimic liver geometry (Shulman & Nahmias, 2013; Hegde *et al.*, 2014; Berger *et al.*, 2015). These approaches support the maintenance of a connected cell network and allow for proper hepatocyte functions, such as albumin and bile production.

### 1.2.3 Quiescence *in vivo*

*In vivo* testing is particularly attractive, as in this system, the cells of interest are not isolated from their natural environment. Intercellular interactions and complex signalling between heterogeneous cell populations remain intact. Studying quiescence in living organisms provides insights in the natural behaviour of the cell and eliminates artefacts due to growth and physiological conditions deviating from nature. *In vivo* investigations of transgenic mice have revealed new insights into the maintenance of the quiescence of primordial follicles in mouse ovaries.

**Quiescence in adult tissue cells** Using oocyte-specific knockouts, PTEN-PI3K and the mTOR signalling cascades in the ovary were identified as key regulators of the follicle dormancy. These findings may elucidate a cause of premature ovarian failure, a condition causing infertility in women before menopause due to hyper activation of follicles and early extinction of the primordial follicle pool (Reddy *et al.*, 2008; Adhikari *et al.*, 2010).

Another striking example implies studies on lymphocytes in knockout or transgenic mice. Gene expression arrays have been shown to be a powerful tool for complex genetic analysis of B- and T-cell response upon certain stimuli or deletions in a single experiment (Glynne *et al.*, 2000; Marrack *et al.*, 2000). Tools to generate knockout and transgenic mice are well understood and with microarrays as a method to analyse a variety of genes, studies are straightforward and will contribute to our understanding of the immune system and the underlying mechanisms of its malfunctions in certain circumstances.

**Dormant adult stem cells** Adult stem cells (ASCs) are undifferentiated cells found in the major organs of the adult organism, and reside in a quiescent state in uninjured tissue (Schultz *et al.*, 1978). The pool of quiescent ASCs ensures tissue homoeostasis in adult multicellular organisms and replenishes depleted cells upon tissue injury, while maintaining a subpopulation of undifferentiated ASCs (reviewed in Rumman *et al.*, 2015). The quiescent state of ASCs protects them from oxidative stress by up-regulating ROS- and hypoxia-protective genes, and minimises mutations in their genetic material by stalling DNA replication (Pallafacchina *et al.*, 2010; Takubo *et al.*, 2010). ASCs can re-enter the cell cycle upon injury and concomitant environmental signals, and produce proliferating progenitor cells, which differentiate into functional tissue cells to restore tissue homoeostasis (Schultz *et al.*, 1978). Defects in quiescence regulation and maintenance has severe effects and can lead to exhaustion of the stem cell pool and degenerative diseases (Cheng *et al.*, 2000a; Chakkalakal *et al.*, 2012).

Hematopoietic stem cells (HSCs) are a pool of quiescent ASCs in the bone marrow, which are responsible for the production of mature blood cells (reviewed in Li, 2011). HSC quiescence is of great importance, as they need to constantly supply fresh circulating blood cells throughout the whole lifetime of a multicellular organism, thereby minimising the risk of accumulating mutations in their DNA. Only a small subpopulation of HSCs enters the cell cycle under normal conditions, ensuring the protection of the stem cell pool for long periods (reviewed in Li, 2011). The dormant state of HSCs was first observed in 1984, when their resistance towards 5-fluorouracil(5-FU)-induced apoptosis could be demonstrated in studies in mice (Van Zant, 1984). 5-FU is a pyrimidine analogue irreversibly inhibiting thymidylate synthase, an enzyme involved in thymidine monophosphate synthesis and thus an essential component of DNA synthesis. 5-FU induces apoptosis in cycling cells, while quiescent cells are not affected. It is therefore widely applied as a chemotherapeutical reagent in cancer treatment (Rich *et al.*, 2004). The quiescent nature of HSCs could furthermore be directly demonstrated by long-term *in vivo* bromodeoxyuridine (BrdU) administration, which required 12 weeks to label the DNA of HSCs in mice (Bradford *et al.*, 1997). BrdU label retention is a method often employed to detect cells in a non-proliferative state, such as dormant HSCs. In vivo BrdU labelling of the DNA was followed by a “chase” period, in which proliferating cells lose the label during cell division and chromosome segregation, and non-proliferative

cells retain the label (Potten *et al.*, 1978). While it was believed that stem cells divide asymmetrically, keeping a set of "immortal" DNA strands while segregating newly synthesised DNA to their daughter cells, this theory is now challenged (reviewed in Mull & Asakura, 2012; Tomasetti & Bozic, 2015). However, dormant cells do not synchronise new DNA which they pass on to their daughter cells and so BrdU label retention or histone label retention are still suitable methods to identify dormant stem cell populations and discriminate them from more frequently dividing progenitor cell populations (Zhang *et al.*, 2003; Arai *et al.*, 2004; Foudi *et al.*, 2009).

*In vivo* studies of HSCs gained great insights into the regulation of HSC quiescence via the niche in which they reside. Osteoblastic cells are in close contact with HSCs and were shown to regulate the hematopoietic stem cell niche, which controls HSC function by Notch signalling (Calvi *et al.*, 2003). HSC quiescence is maintained by Wnt signalling in the niche and its inhibition impedes both HSC quiescence and the HSC ability of self-renewal (Fleming *et al.*, 2008). It could also be shown that chromatin remodelling plays a major role in the regulation of HSC quiescence. Deletion of Satb1, a chromatin-remodelling protein, leads to overproliferation and enhanced commitment of HSCs, gradually depleting the stem cell pool as HSC divide in a less symmetrical manner, resulting in less self-renewal divisions and more divisions of differentiated cells (Will *et al.*, 2013).

Another *in vivo* study made use of Lrig1 (leucine-rich repeats and immunoglobulin-like domains protein 1) as an interfollicular epidermal stem cell marker of the hair follicle and regulator of stem cell quiescence in the epidermis. These stem cells keep their self-renewal potential in culture, but their natural quiescence can only be observed *in vivo*. In such a condition, investigations in living systems was the method of choice to define the cell populations regulated by Lrig1 (Jensen *et al.*, 2009).

The quiescent nature of stem cells could also be shown for other types of ASCs, among others satellite cells (muscle stem cells; Shea *et al.*, 2010), mesenchymal (reviewed in Rumman *et al.*, 2015), intestinal (reviewed in Sangiorgi & Capecchi, 2008), neuronal (Quiñones-Hinojosa *et al.*, 2006; Mira *et al.*, 2010), epidermal (reviewed in Blanpain & Fuchs, 2006) and spermatogonial stem cells (Liao *et al.*, 2014). The number of distinct adult stem cell pools for homoeostasis and regeneration of the specific tissues they reside in is vast, as is the regulation of ASC quiescence by their respective niches.

*In vivo* experiments are the method of choice to investigate dormant ASCs, as quiescence of these cells is regulated by a stem cell niche consisting of multiple factors, which comprise interacting cells and cells forming a complex extracellular matrix maintaining stem cell quiescence.

**Dormant cancer stem cells** Cancer is a heterogeneous disease and tumours are complex constructs, consisting of tissue tumour cells and various infiltrating cells, influencing tumour cells and creating different metabolic environments (reviewed in Kreso & Dick, 2014). Upon certain conditions, individual cancer cells can manage to exit the cell cycle and enter a dormant state. These quiescent cancer cells are also referred to as dormant cancer stem cells (CSCs), as they are able to metastasise and form new tumours upon resuming proliferation. CSCs have been observed in multiple cancers, ranging from hematopoietic, breast, brain, prostate, to pancreas and liver tumours (reviewed in D'Andrea *et al.*, 2014). Cancer cells can enter the dormant state upon a lack of nutrients or oxygen within the tumour mass, due to restricted blood supply, or upon detachment from their substratum. Dormant CSCs have attracted particular interest, as they evade traditional cancer treatments. These therapies, such as 5FU-chemotherapy, which was interestingly one of the first methods to discriminate dormant stem cells from cycling cells, are aimed at hyperproliferative cells and leave dormant CSCs to circulate in the blood stream and form new metastatic tumours (Van Zant, 1984; Touil *et al.*, 2014).

CSCs exhibit similar properties as ASCs, including their dependence on a stem cell niche (reviewed in Aponte & Caicedo, 2017), even though there is no proof yet whether a direct relationship between the two cell populations exists (reviewed in White & Lowry, 2015). Cell cycle exit, however does not only allow CSCs to escape anti-cancer drugs, it also enhances their survival in a similar way as quiescence protects dormant ASCs. Increased autophagy, for example, allows for survival of CSCs in environments of hypoxia and low nutrient abundance, as they can be found within tumours (Song *et al.*, 2013).

It is of great importance to identify the mechanisms by which CSC enter a dormant state and the respective quiescence markers expressed to develop new treatments that eliminate so-called "minimal residual disease", dormant CSCs resistant to primary can-

cer treatment, which can metastasise and give rise to new tumours. First progress has been made in identifying survival mechanisms or dormant CSCs of several cancers, such as ovarian, prostate and breast cancer (Abravanel *et al.*, 2015; Alvarez-Cubero *et al.*, 2016; Peart *et al.*, 2015). In response, development of new drug compounds and therapies, which target dormant cancer cells and inhibit their proliferative reactivation, is underway (Hurst *et al.*, 2015; Jain *et al.*, 2015; Ottewell *et al.*, 2015).

### 1.2.4 Endocytosis in quiescent cells

Endocytic pathways have been studied in all stages of the cell cycle, but no study has yet linked the G0 phase and endocytosis (Illinger *et al.*, 1993; Avrov *et al.*, 1999; Boucrot *et al.*, 2011). Quiescence has attracted great attention only recently. Our understanding of the regulations and mechanisms of this reversible exit from the cell cycle are still not sufficient to explain how entry, maintenance and exit from quiescence are exactly regulated. Mechanisms like the down-regulation of cell cycle-promoting genes and the up-regulation of genes keeping the cells in an undifferentiated state and resistant to apoptosis have been analysed in gene expression studies (Van Zant, 1984; Coller *et al.*, 2006). However, the regulation of protein abundance and activity does not only occur at a transcriptional level but also at the protein level by post-translational modification, ubiquitination or temporary inhibition or activation of function.

#### 1.2.4.1 Endocytosis serving cell type-specific functions

Although the mechanisms of endocytic pathways during quiescence are poorly understood, it is evident that endocytosis serves cell type-specific functions. Parenchymal hepatocytes are quiescent and the liver constitutes the major site of LDL clearance in the human body (Zimmermann, 2004; Zanoni *et al.*, 2018). Additionally, quiescent cells uptake nutrients like iron and cholesterol for storage or transport them via trans-endocytosis (also called transcytosis) across epithelia or endothelia to other tissues.

A hallmark of many quiescent cells is the development of a primary cilium to sense extracellular nutrients and growth factors (Goto *et al.*, 2017). The primary ciliium is rooted in a ciliary pocket, which is a site of high endocytic activity featuring many Clathrin-coated pits and vesicles (Molla-Herman *et al.*, 2010; Ghossoub *et al.*, 2016). Endocytosis at the

ciliary pocket regulates ciliary Sonic Hedgehog (Shh) signalling from the plasma membrane and increases TGFβsignalling in endosomes, potentially controlling cell cycle exit of quiescent cells (Pedersen *et al.*, 2016).

Quiescent tissue cells, such as epithelial or endothelial cells, form junctional cell-cell contacts on their basolateral membranes. The establishment of cell polarity with basolateral intercellular junctions regulates contact-dependent growth arrest (Matter *et al.*, 2005; Tsukita *et al.*, 2008). These are categorised as Adherens Junctions (AJs) formed by Cadherins, Tight junctions (TJs) consisting of Claudins, Occludins and ZO proteins, and Gap Junctions (GJs) composed of Connexins (Radeva & Waschke, 2018). AJs in quiescent epithelial and endothelial cells are formed and maintained by endocytosis of E- and VE-Cadherin (de Beco *et al.*, 2009; Nanes *et al.*, 2012). Junctional E-Cadherin uptake relies on CIP4 and Dynamin and local actin-polymerisation mediated by Cdc42, Arf6, N-WASP and Arp2/3 (Druso *et al.*, 2016; Georgiou *et al.*, 2008; Leibfried *et al.*, 2008; Palacios *et al.*, 2002). The precise molecular mechanism of this pathway is unclear, but the involved proteins act both in Clathrin-dependent and -independent routes. It is also unclear whether endocytosis of free Cadherins occurs via a similar mechanism as that of Cadherins clustered in AJs. Cadherins exhibit a conserved cytoplasmic AP2-binding motif, which is masked by β-catenin and p120 Catenin binding in AJs (Miyashita & Ozawa, 2007; Nanes *et al.*, 2012). When E-Cadherin is clustered by the bacterial Listeria surface protei InlA, the Clathrin adaptor Dab2, but not AP2, are recruited and followed by arrival of Clathrin as well as actin polymerisation (Bonazzi *et al.*, 2011; Veiga & Cossart, 2005; Veiga *et al.*, 2007).

TJs are present in barrier-forming epithelial and endothelial quiescent cells and restrict paracellular diffusion, which is particularly important for the impermeability of the blood-brain barrier (Stamatovic *et al.*, 2017). Stimulation by growth factors, poly-L-argingine or triggers the reomoval of Claudins, Occludin and ZO-1 from TJs by CME, resulting in decreased barrier function (Cong *et al.*, 2015; Ikari *et al.*, 2011; Yamaki *et al.*, 2014). The mechanism for a constitutive TJ remodeling without disruption of barrier function is still unclear (Dukes *et al.*, 2011; Stamatovic *et al.*, 2017). It might, however, occur by 'cross-over' endocytosis of whole TJs from one cell in a double-membrane vesicle into its neighbouring cell (Gehne *et al.*, 2017). The molecular details for this process are missing, but it appears to be constitutive.

GJs connect adjacent cells and allow for exchange of small molecules, ions and electrical impulses between them (Radeva & Waschke, 2018). Acute growth factor signalling induces PKC- and MAPK-dependent phosphorylation of Connexin 43, which licenses it for internalisation through CME and disassembly of GJs (Fong *et al.*, 2014; Nimlamool *et al.*, 2015). GJ disruption in turn disassembles quiescent cell layers and primes cells for cell cycle re-entry.

#### 1.2.4.2 Endocytosis regulating quiescence

Endocytosis serves maintenance of the quiescent state through down-regulation of mitogen-signalling or up-regulation of cell cycle arrest pathways. In quiescent cells, endocytosis is either decreased, increased or maintained to regulate growth factor and cytokine receptor cell surface availability. While Vascular Endothelial Growth Factor (VEGF) endocytosis mediates its signaling and stimulation of angiogenesis, its uptake is reduced in mature blood vessels (Nakayama *et al.*, 2013). Decreased VEGF uptake in quiescent endothelial cells is mediated by atypical PKC phosphorylation of the endocytic adaptor Dab2, which prevents Dab2 binding to VEGF Receptor (Nakayama *et al.*, 2013). Another mechanism to decrease growth factor signalling and prevent cell cycle re-entry is the removal of specific receptors from the plasma membrane by endocytosis. This is reported for the tyrosine-kinase receptor Kit, whose internalisation by CME and subsequent degradation in lysosomes of mast cells ensures their non-proliferative state (Cruse *et al.*, 2015). Intestinal Lgr5-positive stem cells escape Wnt-mediated catenin signalling by actively removing the Wnt receptor Frizzled from the cell surface (Koo *et al.*, 2012). There, Frizzled is ubiquitinated by the stem cell-specific E3 ligase RNF43, which induces its endocytosis followed by degradation in lysosomes (Koo *et al.*, 2012). CME of Lgr5 is required for stem cell fitness and Dynamin or CME inhibition induces hyper-proliferation of intestinal cells, leading to severe defects in epithelial homeostasis (Nagy *et al.*, 2016; Snyder *et al.*, 2017). Wing disc cells in developing *Drosophila* pupae stay quiescent in a similar way and sequester Notch by Crumbs at apical cell surfaces (Nemetschke & Knust, 2016). Thereby, Crumb inhibits ligand-independent endocytosis of Notch and prevents Deltex-dependent Notch signalling while its ligands Delta and Serrate are absent. Crumbs levels at the apical surface are controlled by CME and maintain epithelial polarity (Lin *et al.*, 2015). This is achieved by Stardust-mediated sta-

bilisation of Crumbs at the plasma membrane by binding to a motif in Crumbs which overlaps with its AP2 binding site.

#### 1.2.4.3 Endocytosis mediating survival of quiescent cells

Endocytosis furthermore ensures survival during quiescence. In the absence of growth factors, mTORC1 signalling is decreased in quiescent cells (Gan & DePinho, 2009). Elevated expression of β4-integrin at the cell surface of quiescent cells mediates endocytosis of Laminins, which are its extracellular matrix (ECM) ligands (Muranen *et al.*, 2017). Degradation of internalised laminins in lysosomes generates free amino acids, which are sensed by mTORC1 and restore its basal activity, thereby promoting survival (Muranen *et al.*, 2017). The endocytic pathway for β4-integrin uptake is unclear, but β4-integrin dimerises with α6-integrin, which contains a cytoplasmic YXXΦ motive that can interact with AP2 (De Franceschi *et al.*, 2016). This suggests that Laminin uptake by β4-integrin occurs by CME.

## 1.3 Endosomal trafficking of integrins

### 1.3.1 Integrins

Integrins are cell adhesion receptors and, constituting the most abundant receptor on cellular surfaces, are expressed in all cell types with the excpetion of erythrocytes (Streuli, 2016). Integrins are non-covalently linked heterodimers consisting of one β- and α-subunit from a pool of 8 β- and 18 α-subunits, allowing for the formatioin of 24 distinct integrins (reviewed in Hynes, 2002). Their β- and α-subunit composition determines their specificity to ECM ligans, such as collagen, fibronectin or laminins (Humphries, 2006; Hughes *et al.*, 1995). Upon ECM binding, integrins change their conformation from an inactive, collapsed state via an extended intermediate to an extended, open and active conformation (Askari *et al.*, 2010; Su *et al.*, 2016). They were originally characterised as links between the ECM and the actin cytoskeleton, forming a direct connection between cells and the extracellular matrix (ECM). At focal adhesions, ECM-bound integrins are connected to the cytoskeleton by a complex of focal contact proteins, such as vinculin, talin and paxillin, and a variety of scaffolding molecules (re-

viewed in Geiger *et al.*, 2001; Horton *et al.*, 2015). Kinases, including Focal adhesion kinase (FAK) and Src, are recruited to focal adhesion sites and activated to initiate downstream signalling cascades including the Ras-mediated Mitogen-activated protein kinase (MAPK) pathway for proliferation and AKT-mediated survival signalling (Wozniak *et al.*, 2004). The functions of integrins are more complex and encompass 'outside-in' signallig from the plasma membrane, 'inside-out' signalling from the cell by integrin-binding to the ECM as well as intracellular signalling, and serve adhesion, migration, mechanosensing, cell cycle regulation and are often involved in cancer (reviewed in Wang, 2012; Streuli, 2016; Seetharaman & Etienne-Manneville, 2018; Moreno-Layseca & Streuli, 2014; Multhaupt *et al.*, 2016; Alanko & Ivaska, 2016). Integrins also mediate proliferative quiescence and survival in the absence of growth factors when bound to specific ECM molecules (Naci & Aoudjit, 2014; Moreno-Layseca & Streuli, 2014).

Since integrin trafficking will be investigated in this project, the next sections will focus on integrin endocytosis and recycling.

### 1.3.2 Endocytic pathways for integrin internalisation

Endocytosis of integrins is important during cell migration and serves disassembly of focal adhesions and relocation of integrins. The endocytic pathway is thereby largely determined by the integrin subunits and ranges from CME to CLIC and Macropinocytosis (Bridgewater *et al.*, 2012). The most common endocytic pathway for integrin internalisation is CME. Many $\alpha$-integrin subunits contain a YXX$\Phi$ AP2 binding motif (De Franceschi *et al.*, 2016). In addition, the $\beta$1 subunit can interact with a range of adaptor proteins involved in CME: Dab2 associates and Numb can directly interact with the membrane-proximal NPXY motif of $\beta$1-integrin (Calderwood *et al.*, 2003; Mishra *et al.*, 2004; Prunier & Howe, 2005; Teckchandani *et al.*, 2012). Dab2 additionally mediated CME of clustered $\beta$3-integrin (Yu *et al.*, 2015) and Numb was also shown to be involved in CME of $\beta$3-integrin from focal adhesions (Nishimura & Kaibuchi, 2007). The endocytic adaptor GAIP interacting protein C terminus, member 1 (GIPC1) associates with $\alpha$5$\beta$1-integrin to mediated its endocytosis dependent on myosin VI (Myo6), which has been shown to act in CME (Spudich *et al.*, 2007), to stabilise endothelial cell adhesion on fibronectin (Valdembri *et al.*, 2009). Finally, HS1-associated protein X-1 (HAX-1) mediates CME of $\alpha$v$\beta$6-integrin (Ramsay *et al.*, 2007).

Clathrin-independent pathways, such as macropinocytosis, were also shown to rapidly remove integrins from dorsal surfaces of migrating cancer cells to allow for efficient redistribution at focal adhesions (Gu *et al.*, 2011). Additionally, Galectin-3 contributes to β1-integrin endocytosis by initiating formation of endocytic pits according to the GL-Lect hypothesis (Lakshminarayan *et al.*, 2014).

Several endocytic pathways and multiple adaptor proteins are involved in integrin endocytosis and perturbed trafficking often leads to pathophysiological conditions, with a particular focus on cancer invasion and metastasis (De Franceschi *et al.*, 2015). Integrin endocytosis also offers a complementary mechanism for focal adhesion turnover, thereby regulating integrin signalling. Additionally, integrins can be endocytosed bound to their ECM ligands, which serves ECM remodeling (Conti *et al.*, 2003; DiPersio *et al.*, 1997) or growth and survival activation by ECM degradation in lysosomes resulting in lysosmal amino acid signalling and concomitant mTORC1 activation (Rainero *et al.*, 2015; Muranen *et al.*, 2017). Furthermore, internalised active integrins can directly signal from EEA1-positive early endosomes and allow for adhesion-independent focal adhesion kinase signalling activating a MAPK/(MEK)extracellular signal-regulated kinases (ERK) signalling pathway (Alanko *et al.*, 2015; Tesfay *et al.*, 2016; Pazzagli *et al.*, 2017; Manohar *et al.*, 2004). Interestingly, β1-integrin activation was shown *in vivo* to reduce their endocytosis in non-transformed cells to stabilise integrin-matrix adhesion (López-Ceballos *et al.*, 2016).

### 1.3.3 Integrin recycling

Following internalisation, integrins associate with Rab5-positive early endosomes (Pellinen *et al.*, 2006). Rab proteins belong to the large family of small Rab GTPases, comprising of more than 60 members in humans. They confer identity to endosomes by marking them for fusion with similar, later or recycling endosomes. Rab5 is an early endosomal marker which mediates endocytic vesicle transfer to the endolysosomal trafficking pathway (Bucci *et al.*, 1992; Zerial & McBride, 2001). Fusion of endosomes is mediated by endosomal tethering factors. The early endosomal tethering factors Early endosomal antigen 1 (EEA1) and APPL1 associate with Rab5-positive endosomes and mediate their interaction and fusion with other endosomal compartments (Simonsen *et al.*, 1998; Kalaidzidis *et al.*, 2015). During their maturation, endosomes acquire or

lose Rab proteins as they approach their destination and often, distinct Rabs are found on the same endosome, marking domains targeted for different trafficking pathways (Zerial & McBride, 2001). Rab4-positive endosomes enter a fast, direct recycling pathway to the plasma membrane, Rab11 marks a slow recycling pathway via recycling endosomes, Rab7 targets endosomes for lysosomal fusion and cargo degradation and Rab9 mediates retrograde transport to the trans-Golgi network (TGN, Fig. 1.3.1) (Huotari & Helenius, 2011).

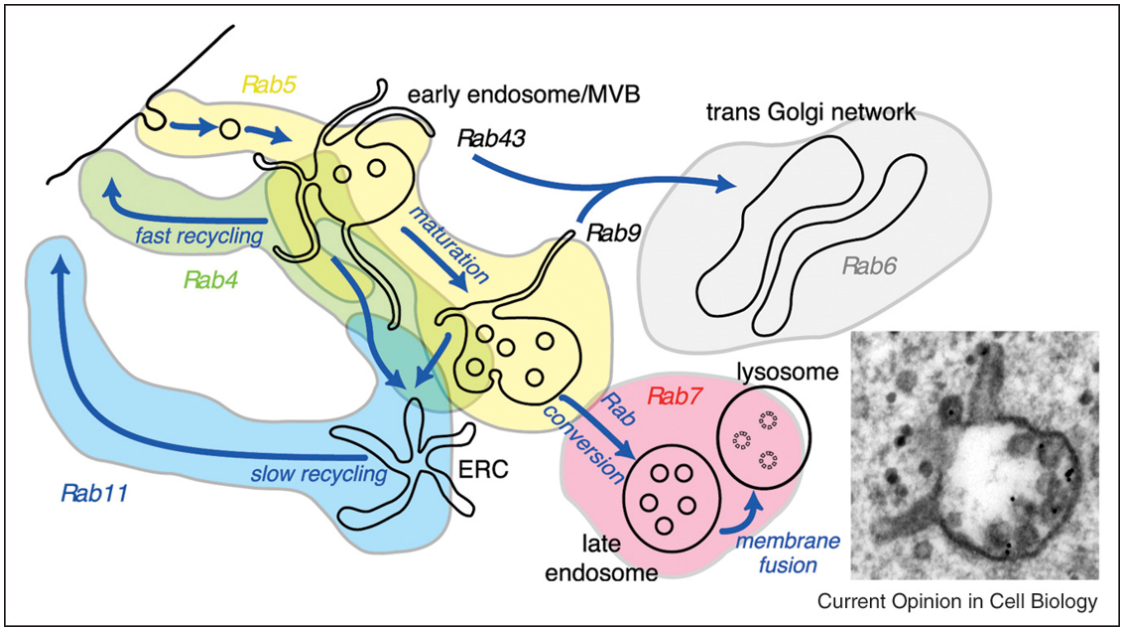


**Figure 1.3.1:** Overview of endosomal maturation
From Woodman & Futter (2008).

The majority of integrins is recycled back to the plasma mebrane to control locomotion by relocating focal adhesion sites to the leading edge Bretscher (1992). Integrins in Rab5-positive endosomes can directly interact with Rab21, which retains it in early endosomes close to the plasma membrane (Pellinen, 2006). P120RasGAP then directly interacts with integrins, replaces Rab21 and facilitate exit from Rab21-EEA1-positive endosomes for recycling (Mai *et al.*, 2011). Rab25 directly associates with β1-integrins as well and mediates their recycling to the migrating front (Caswell *et al.*, 2007). A rapid Rab25-mediated recycling pathway includes the adaptor CLIC3 and appears to be specific for tumor invasion and continued Src kinase signalling (Dozynkiewicz *et al.*, 2012). Ankyrin-B associates with PI(3)P-positive endosomes and promotes directional integri recycling to the leading edge in migrating cells by inactivating Rab22A (Qu *et al.*, 2016). Upon growth factor stimulation, internalised αvβ3-integrin is rerouted via a short-loop trafficking pathway to focal adhesions dependent on Rab11, but independent of

Arf6 (Roberts *et al.*, 2004; Woods *et al.*, 2004). The Rab11-Arf6 integrin recycling pathway is frequently reported in the literature and promotes recycling of β1-integrins as well as α4β6-integrin and (Powelka *et al.*, 2004; Hongu *et al.*, 2015; Yoon *et al.*, 2005; Lau & Chou, 2008). Interestingly, endocytosed integrins can be maintained in an active, but non-ligandbound conformation by FAK-mediated association of talin with Rab11-positive endosomes. This way, integrins remember their activated state and contribute to focal adhesion reassembly coinciding with their recycling to the plasma membrane during cell migration (Nader *et al.*, 2016). Many more integrin recycling routes have been described for different Rabs and are provided in Paul *et al.* (2015) and De Franceschi *et al.* (2015).

A VAMP3/Syntaxin 6-mediated recycling pathway was described for α3β1- and α6β1-integrin, which is exploited for chemotactic cell migration by tumor cells overexpressing Syntaxin 6 (Riggs *et al.*, 2012). Furthermore, Lipoprotein receptor-related protein 1 (LRP1) was identified as a recycling adaptor for β1-integrins in cancer cells (Theret *et al.*, 2017). A role for the Clathrin machinery protein HIP1 was discovered in recycling of inactive integrins to the plasma membrane to promote cell migration in cancer cells (Majeed *et al.*, 2014).

Multisubunit tethering complexes, such as Retromer and Retriever, contain several Rab binding sites enabling them to connect endosomes with different identities. They were also shown to play an important role in integrin recycling (Rabouille, 2017). Retromer consists of the cargo recognition subunits VPS35, VPS29 and VPS26 (Mukadam & Seaman, 2015), whereas Retriever consists of the Retromer subunit VPS29 in addition to DSCR3 and C16orf62 (McNally *et al.*, 2017). Both heterotrimers interact with cargo-specific adaptors, such as SNX17 with Retriever (Böttcher *et al.*, 2012; McNally *et al.*, 2017) or SNX27 (Temkin *et al.*, 2011; Clairfeuille *et al.*, 2016), SNX3 (Strochlic *et al.*, 2007; Lucas *et al.*, 2016) and SNX-BAR proteins, such as SNX1 and 2 (Lucas *et al.*, 2016), for Retromer. The discovery of Retriever, together with new recycling pathways for integrins including a Rab4/VPS8/VPS3-mediated fast integrin recycling pathway (Jonker *et al.*, 2018) add another level of complexity to integrin trafficking, but also open new possibilites to investigate and understand integrin trafficking-related functions.

### 1.3.4 Integrins in proliferative quiescence

To date, the role of integrins in quiescence signalling has mainly been described for outside-in signalling of ECM-bound integrins from the cell surface. Quiescence is mostly induced by Laminin-binding integrins, with Laminin111, 332, 421 or 521 being implicated in quiescence induction (Fiore *et al.*, 2017; Morgner *et al.*, 2015; Nguyen *et al.*, 2000; Govaere *et al.*, 2016; Ishii *et al.*, 2018; Susek *et al.*, 2018; Rohn *et al.*, 2018). Laminins are named with arabic numbers based on their composition, which is a heterotrimeric structure consisting of one $\alpha$, one $\beta$ and one $\gamma$ chain. According to this nomenclature, Laminin421 contains an $\alpha$4, a $\beta$2 and a $\gamma$1 chain (Aumailley *et al.*, 2005). Laminin332 and 521 are ligands for $\alpha3\beta1$-integrin, which will be investigated in this study (Nishiuchi *et al.*, 2006). Absence of $\alpha3\beta1$-integrin activates quiescent keratinocytes (Pazzagli *et al.*, 2017). Interaction of $\alpha3\beta1$-integrin with Laminin5 regulates GJ intercellular communication required for synchronisation of neighbouring cells (Lampe *et al.*, 1998). Integrins are highly involved in the establishment of epithelial cell polarity, both by inside-out signalling, polarising the assembly of the basement membrane, and outside-in signalling, controlling microtubule orientatioin (Lee & Streuli, 2014). Furthermore, $\alpha3\beta1$-integrin enhances cell survival after growth factor deprivation (Manohar *et al.*, 2004) by upregulating autophagy (Edick *et al.*, 2007; Tesfay *et al.*, 2016). Enhanced survival is additionally mediated by sequestering pro-apoptotic proteins at cytoplasmic 14-3-3 isoforms Oh *et al.* (2009).

Integrins can control cell cycle exit by several different mechanisms. Integrin interaction with their activator Kindlin-1 reduces Wnt signalling and stimulates TGF-$\beta$release. Another proposed mechanism is the down-regulation of nuclear actin by Laminin111, which upregulates Exportin-6 activity by attenuating the PI3K pathway (Fiore *et al.*, 2017; Spencer *et al.*, 2011). Which Laminin receptor attenuates PI3K signalling, is unknown. Specific $\beta1$-integrin splice variants do not localise to focal adhesions, resulting in cell cycle arrest (Meredith *et al.*, 1995). We are only at the beginning at understanding the complexity of integrin signalling and a range of ECM-integrin signalling pathways may yet be discovered.

## 1.4 Aims of this study

Endocytosis is a vital cellular process and present throughout all stages of the cell cycle. Research on endocytic mechanisms, however, has mostly been performed on proliferating cells or cancer cell lines. Endocytic pathways however, differ among cell cycle phases. During proliferative quiescence, endocytosis is modulated to down-regulate growth factor signalling, while pathways serving cell-type specific funtions are highly active. To date, no extensive characterisation of endocytosis in quiescent cells has been performed with relation to growing cells, thereby highlighting changes upon reversible cell cycle exit. In cancer cells, endocytic and recycling pathways are dysregulated to support increased nutrient demands (Commisso *et al.*, 2013), mediate migration and invasion (De Franceschi *et al.*, 2016) or permit adhesion-independent survival (Alanko & Ivaska, 2016). Quiescent cells display enhanced survival (Van Zant, 1984; Coller *et al.*, 2006; Mohrin *et al.*, 2010), which might be mediated by ECM-integrin signalling (Nguyen *et al.*, 2000; Manohar *et al.*, 2004; Sharma *et al.*, 2012; Sarper *et al.*, 2016). Differentially regulated endocytic and trafficking pathways during proliferative quiescence might play a role in ECM-mediated integrin survival signalling.

This study aims to

- Develop and validate an *in vitro* quiescence cell line model for endocytic assays
- Quantify different endocytic pathways in quiescent cells relative to proliferating cells
- Describe the mechanism and role of differentially regulated endocytic pathways
- Establish of the role of $\alpha$3-integrin trafficking for maintenance of the quiescent state

# 2 Material and Methods

## 2.1 Gene cloning

### 2.1.1 Amplification of genes of interest by polymerase chain reaction

Polymerase chain reaction (PCR) was used to amplify DNA fragments for cloning and flank them with attachment sites for introduction into the Gateway cloning system (described in sec. 2.1.3). PCR was performed using Q5 High Fidelity polymerase (M0491S, New England Biolabs) and 5X Q5 Reaction Buffer with the reaction mix listed in Tab. 2.1.1.

DNA fragments were amplified in a G-STORM GS1 thermal cycler (Gene Technologies), according to manufacturer's instructions, for 30 cycles.

**Table 2.1.1:** PCR mix

| **Reagent** | **Volume (µl)** |
|---|---|
| 5X Reaction Buffer | 4 |
| dNTP (10 mM) | 0.4 |
| Forward Primer (10 µM) | 1 |
| Reverse Primer (10 µM) | 1 |
| Polymerase | 0.2 |
| DNA | 1 (10-50 ng) |
| MilliQ water | 12.4 |

### 2.1.2 Primers

Primers were synthesised by Integrated DNA Technologies and resuspended in milliQ water to a stock concentration of 50 µM. Primers used for polymerase chain reaction

were diluted to stock concentration of 10 µM. Primers used for Gateway cloning contained attB sites required for site-specific recombination of the DNA fragment into entry vectors (sec. 2.1.3). All primers used are listed in Tab. 2.1.2.

**Table 2.1.2:** Primers used in this study

| Name | Designed for | Sequence (5'-3') |
|---|---|---|
| EB1566 | hFCHo2 pENTR1A from EcoRI for Gibson (Fwd) | CCAATTCAGTCGACTGGATCCGGTACCG AATTCGCATGGTCATGGCGTATTTCGTCG |
| EB1567 | hFCHo2 pENTR1A until EcoRI for Gibson (Rev) | ATATCTCGAGTGCGGCCGCGAATTCGTA CAATCCGCCAGGTATCGTC |
| EB1568 | hFCHo2 internal (bp1140) for Gibson (Rev1a) | CCTATAGATACTTTTAATTCATCC |
| EB1569 | hFCHo2 internal (bp1160) for Gibson (Rev1b) | GAGTGTTATATTCCCTATAGATAC |
| EB1570 | hFCHo2 internal (bp1140) for Gibson (Fwd2a) | CCTGCTGCACCATTAGCCCGG |
| EB1571 | hFCHo2 internal (bp1160) for Gibson (Fwd2b) | ACCAGCCCACCTCCTGCTGC |
| EB1668 | FCHo2 gBlocks amplification (Fwd) | GGCTTCTTTGGATGAATTAAAAG |
| EB1669 | FCHo2 gBlocks amplification (Rev) | CCGGGCTAATGGTGCAGCAGG |
| EB1761 | hFCHo2 without tag (Fwd) | GGGGACAAGTTTGTACAAAAAAGCAGGC TTCACCATGGCCGTCATGGCGTATTTCG TCG |
| EB1762 | hFCHo2 without tag (Rev) | GGGGACCACTTTGTACAAGAAAGCTGG GTCCTAACAATCCGCCAGGTATC GTCC |

### 2.1.3 Molecular cloning

DNA fragments were cloned into entry and expression vectors using the Gateway cloning system. Genes amplified by PCR (sec. 2.1.1) were cloned into entry vectors (pENTR1A or pDONR201) using 75 ng of amplified PCR product containing attB attachment sites, 75 ng of entry vector with attP attachment sites and 1 µl of BP clonase mix (11789100, Thermo-Fisher Scientific) in a total volume of 5 µl. The reaction was incubated over night at room temperature. The reaction was stopped by addition of 1 µl Proteinase K (11789100, Thermo-Fisher Scientific) and incubation at 37 °C for 10 min. Chemically competent *Escherichia coli (E.coli)* DH5α (18265-017, Thermo Fisher Scientific or C2988J, New England Biolabs) were transformed with the reaction mixture and selected for positive clones on 50 µg/ml kanamycin-containing LB agar

plates. Plasmids were extracted using GeneJET Plasmid Miniprep Kit (27106, Qiagen) and sent to Source BioScience (Cambridge) for sequencing.

DNA fragments in entry vectors, which contain attL sites, were cloned into expression vectors, containing attR sites (pDEST), by LR reaction, using 75 ng of entry vector, 75 ng of expression vector and 1 µl LR clonase (11789100, Thermo Fisher Scientific) in a total reaction volume of 5 µl. The mixture was incubated for 2 hours at 25 ℃ or over night at room temperature. Chemically competent *E. coli* DH5αwere transformed with the reaction mixture and selected for positive clones on 50 µg/ml ampicillin-containing LB agar plates. Plasmid extraction was performed as described for entry clones. Plasmids were screened for inserts by restriction digest with *Xho*I (R0146S, New England Biolabs) and subsequent agarose gel electrophoresis in a 0.9 % agarose gel.

### 2.1.4 Gibson Cloning to generate phosphomutants of FCHo2

Gibson cloning is a cloning technique that allows for quick and “seamless” in vitro assembly of a variety of gene fragments of contiguous pieces of DNA (Gibson *et al.*, 2009). In one isothermal in vitro assembly step, a 5’ exonuclease removes nucleotides of the 5’ ends of adjacent double stranded DNA fragments which have a homolog terminal sequence. The remaining complementary terminal single strands anneal, gaps are filled by a DNA polymerase and eventually ligation occurs via DNA ligase.

The phosphorylation sites of FCHo2 detected by mass spectrometry were located in clusters in the central region of the protein, so Gibson assembly was a suitable method to mutate all phosphorylation sites observed to be altered to alanines (non-phosphorylable mutant) or aspartic acids (phosphomimetic mutant). GeneArt Seamless Cloning and Assembly Enzyme Mix (A14606, Thermo Fisher Scientific) allows for simultaneous and directional assembly of up to four PCR fragments into a linearised vector of choice. Gateway entry vector pENTR-1A (Thermo Fisher Scientific) was amplified in chemically competent *E. coli* DB3.1, purified using GeneJET Plasmid Miniprep Kit and linearised by restriction digest with *Eco*RI (R0101S, New England Biolabs). The ends of the linearised vector were dephosphorylated with calf intestinal phosphatase (M0290S, New England Biolabs). The digested and dephosphorylated vector was purified on a 1 % Agarose gel using GeneJET Gel Extraction Kit (K0702, Thermo-Fischer Scientific). The central region of FCHo2, containing the mutations of

phosphorylable sites either to alanines or aspartic acid, was synthesised by IDT and will further on be referred to as gBlock. Contiguous, overlapping DNA fragments forming the flanking sites of FCHo2, were amplified by PCR. Gibson cloning was performed with the GeneArt Seamless Cloning and Assembly Enzyme Mix (Life Technologies) according to manufacturer's instructions. DNA amounts used are listed in Tab. 2.1.3.

**Table 2.1.3:** DNA fragments and amounts used for Gibson assembly of FCHo2 mutants.

| DNA fragment | DNA (ng) |
|---|---|
| pENTR1A (linear, dephosphorylated) | 50 |
| gBlock | 200 |
| Right flank of FCHo2 | 200 |
| Left flank of FCHo2 | 200 |

Chemically competent *E.coli* DH5αwere transformed with the Gibson reaction mixture and selected on 50 µg/ml kanamycin-containing agar plates for positive clones. Plasmids were extracted using GeneJET Plasmid Miniprep Kit (K0503, Thermoscientific) and sent to Source BioScience (Cambridge) for sequencing. The genes were then transferred into Myc-, EGFP-containing expression vectors via LR reaction (sec. 2.1.3). Untagged FCHo2 constructs were generated by adding a stop-codon at the end of the gene via PCR reaction with primers EB1761 and EB1762 (Tab. 2.1.2). The DNA fragment was then cloned into Gateway entry vector pDONR201 (gift from J. Pines) upon BP reaction (Gateway BP clonase II enzyme mix, Invitrogen) and subsequently into an expression vector pCi DEST-native (Safa Lucken-Ardjomande Häsler, Harvey McMahon lab) by LR reaction.

### 2.1.5 Plasmids and constructs

Generated DNA fragments were first cloned into entry (pDONR201 or pENTR1A) and subsequently in expression vectors (pDEST or pcDNA5/TO/IRES2EGFP) for expression in mammalian cells. All constructs used in this study are listed in Tab. 2.1.4 and Tab. 2.1.5.

**Table 2.1.4:** Gateway vector backbones used in this study

| Name | Vector | Tag | Promoter | Primers | Origin |
|---|---|---|---|---|---|
| GV01 | pDONR201 | N/A | N/A | pDON201 F/R | J.Pines lab |
| GV18 | pENTR1A | N/A | N/A | 0-EB133 | Invitrogen |
| GV12 | pcDNA5/TO/-IRES2EGFP | EGFP | CMV | CMV / BGH | Jackman/J. Pines lab) |
| GV34 | pCi DEST-native | N/A | CMV | CMV | H. McMahon lab |
| GV36 | pCi C-myc DEST | Myc C-term | CMV | pCi | H. McMahon lab |
| GV21 | pCi C-EGFP DEST | EGFP C-term | CMV | pCi | H. McMahon lab |

**Table 2.1.5:** Constructs used in this study
FL - full length; BP - BP reaction; LR - LR reaction

| Construct | Name | Insert | Vector | Origin | Species |
|---|---|---|---|---|---|
| EB0467 | FCHo2 FL (WT) | FCHo2 wildtype C-term taggable | pDONR201 | BP-EB4080 with GV01 | Human |
| EB0631 | FCHo2 FL (A mutant) | FCHo2 FL alanine phosphomutant (C-term taggable) | pENTR1A | Gibson cloning with EB4080 | Human |
| EB0632 | FCHo2 FL (D mutant) | FCHo2 FL aspartic acid phosphomutant (C-term taggable) | pENTR1A | Gibson cloning with EB4080 | Human |
| EB0727 | FCHo2 WT stop | FL FCHo2 wildtype with stop codon | pDONR201 | PCR 1761+1762 on 4080 | Human |
| EB0728 | FCHo2 D-mutant stop | FL FCHo2 aspartic acid phosphomutantt with stop codon | pDONR201 | PCR 1761+1762 on 4080 | Human |
| EB0729 | FCHo2 A-mutant stop | FL FCHo2 alanine phosphomutant with stop codon | pDONR201 | PCR 1761+1762 on 4080 | Human |
| EB8006 | FCHo2 wildtype untagged | FL FCHo2 WT with stop codon | GV34 | LR - EB0727 with GV34 | Human |
| EB8007 | FCHo2 D-mutant untagged | FL FCHo2 aspartic acid phosphomutant with stop codon | GV34 | LR - EB0728 with GV34 | Human |
| EB8008 | FCHo2 A-mutant untagged | FL FCHo2 alanine phosphomutant with stop codon | GV34 | LR - EB0729 with GV34 | Human |
| EB4080 | WT FCHo2-Myc FL | FCHO2 FL WT C-term Myc tag | GV36 | from Safa (clone 50) | Human |
| EB4139 | D-FCHo2-Myc FL | FL FCHo2 aspartic acid phosphomutant C-term Myc tag | GV36 | LR - EB0632 with GV36 | Human |
| EB4140 | A-FCHo2-Myc FL | FL FCHo2 alanine phosphomutant C-term tag | GV36 | LR - Eb0631 with GV36 | Human |
| EB8003 | FCHo2 wildtype | FL FCHo2 | GV12 | LR - EB0727 with GV21 | Human |
| EB8004 | FCHo2 D-mutant | FL FCHo2 aspartic acid phosphomutant | GV12 | LR - EB0728 with GV21 | Human |
| EB8005 | FCHo2 A-mutant | FL FCHo2 alanine phosphomutant | GV12 | LR - EB0729 with GV21 | Human |

## 2.2 Cell culture and transfection

### 2.2.1 Maintenance of cells

Human telomerase reverse transcriptase (hTERT)-immortalised retinal pigmented epithelial cells (RPE1; ATCC CRL-4000) were cultured in Dulbecco's Modified Eagle Medium (DMEM) supplemented 1:1 with F12 Ham's supplement, antibiotic/antimycotic and Glutamax. Medium for proliferating cells contained 10 % fetal bovine serum (FBS, PAA or MyClone). Concentrations of supplements are shown in Tab. 2.2.1. Medium was exchanged three times a week. RPE1 cells were passaged three times a week by 10 min incubation in EDTA-based cell dissociation buffer (S-014-B, Millipore) at 37 ℃, resuspension in full growth medium and re-seeding at a 1:5 to 1:10 ratio. Cells were regularly tested for mycoplasma contamination by nuclei staining with DNA-intercalating fluorescent dyes followed by high resolution confocal microscopy or by PCR with mycoplasma DNA-specific primers.

**Table 2.2.1:** Cell culture media and supplements.

| | **Manufacturer and Reference** | **Final concentration RPE1** |
|---|---|---|
| **DMEM-F12 HAM (1:1)** | Sigma-Aldrich D6421-500 ML | 1 x |
| **F-12K nut Mix** | Gibco 21127-022 | - |
| **Antibiotic/ Antimycotic 100 X** | Sigma-Aldrich A5955-100ML | 1 X |
| **Glutamax 100 X** | Gibco 35050-038 | 1 mM |
| **Hygromycin B 100 mg/ml** | Sigma-Aldrich H3274 | 5 µg/ml |
| **Sodium Bicarbonate 7.5 %** | Sigma-Aldrich S8761-100ML | 0,26 % (w/v) |
| **FBS (only for proliferating cells)** | PAA, MyClone SV30160.3 | 10 % |

### 2.2.2 Induction of cellular quiescence

To induce proliferative quiescence, RPE1 cells were counted with a CASY Cell Counter and Analyzer Model TT (Roche Applied Science) and seeded at a density

of $1.4 \times 10^4$ cells/cm$^2$ and grown in full medium for seven days to reach confluence. Medium was then exchanged for FBS-free medium, in which cells were maintained for at least 10 days to induce long-term quiescence.

For detachment of the quiescent monolayer, cells were rinsed with phosphate-buffered saline (PBS) and incubated in 0.12 % trypsin-ethylenediaminetetraacetic acid (EDTA) (Sigma-Aldrich) or in Accutase solution (AT106-500, Innovative Cell Technologies), to preserve cell surface receptors, for 5-10 min at 37 °C. FBS-free medium was added to dilute the trypsin/Accutase solution and break cell clumps by aspirating. Cells were centrifuged for 5 min at 1000 g and resuspended in FBS-free medium to obtain a single-cell solution. Detachment of cycling cells was performed in the same manner, but medium containing 10 % FBS was used.

### 2.2.3 Amino acid starvation and BSA supplementation

For amino acid starvation, 15.68 g DMEM-F12 1:1 mix without amino acids (D9811-01, United States Biological) were resuspended in 1 l miliQ water, sterile filtered through a 0.22 µm pore size filter membrane and supplemented with 1 X Antibiotic/Antimycotic (A5955, Sigma-Aldrich), 1 mM Glutamax (35050-038, Gibco) and 5 µg/ml Hygromycin and 0.26 % Sodium Bicarbonate (w/v, S8761, Sigma-Aldrich). Cells were washed three times with amino acid-free medium and cultured in it for the indicated durations. For long-term incubation in amino acid-free medium, medium exchange for fresh amino acid-free medium occured every other day.

For medium supplemented with BSA, 3 % BSA (w/v) was dissolved in the respective medium (DMEM-F12 including all supplements, with or without amino acids) and sterile filtered through a 0.22 µm pore size filter membrane.

### 2.2.4 Gene Transfection

Cells were seeded 24 hours prior to transfection and grown to 70 % confluence.

*XtremeGene HP*: XtremeGene HP (06366236001, Roche Diagnostics) was used for flow cytometry experiment because it allowed for gentle cell transfection, resulting in little cell death. High DNA concentration was needed for efficient transfection. Transfection was performed using X-tremeGENE HP DNA transfection reagent with a ratio of

500 ng DNA to 1.5 µl transfection reagent. DNA and transfection reagent were mixed in Opti-MEM (11058-021, Gibco) and incubated at room temperature for 15 min. The transfection mixture was added in a drop-wise manner to cells in full growth medium in a 1:10 volume ratio. Medium was exchanged after 3 hours and cells were used for further analysis 24 hours post transfection.

*Lipofectamine 2000:* Lipofectamine 2000 (11668019, Thermo Fisher Scientific) was used for microscopy analysis. It allowed for efficient transfection of cells while using a lower DNA concentration, resulting in lower levels of transgene expression. Transfection was performed using Lipofectamine 2000 with a ratio of 350 ng DNA to 1 µl Lipofectamine 2000 reagent. DNA and transfection reagent were diluted to 14ng/µl (DNA) or 1:25 volume ratio (Lipofectamine 2000), respectively, in Opti-MEM (Gibco). The diluted solutions were mixed, incubated at room temperature for 20 min and added to cells in full growth medium in a in a 1:10 volume ratio. Medium was exchanged after 3 hours and cells expressed the constructs for 24 hours before further analysis..

### 2.2.5 Geneknock down by RNA interference

RNA oligonucleotides (Dharmacon) were reconstituted in miliQ water to a 20 µM stock concentration. Small interfering RNAs (siRNA) used in this study are listed in Tab. 2.2.2.

#### FCHo2 knockdown in growing cells

Cells were counted with a CASY Cell Counter and Analyzer Model TT (Roche Applied Science) and seeded at $6.25 \times 10^3$ cells/cm$^2$in Greiner glass bottom 96 well microplates (655892, Greiner Bio-One) four hours prior to transfection. 1.35 pmol siRNA and 0.168 µl Lipofectamine RNAiMAX Transfection Reagent (13778150, Thermo Fisher Scientific) were each diluted in 5 µl OptiMEM (5 % of culture medium volume per well), mixed and incubated for 30 min at room temperature. 10 µl transfection mix per well was added to cells in 100 µl fresh culture medium. A second transfection was performed 24 hours later. Medium was exchanged 24 hours after the second transfection and cells were used for experiments 72 hours after the first transfection.

**Table 2.2.2:** Small interfering RNAs used in this study

| siRNA | Sequence | Reference | Manufacturer |
|---|---|---|---|
| **µ2-adaptin** | CCGCCAGAUGGAGA-GUUUGAGCUUA UAAGCUCAAACUCU-CCAUCUGGCGG | HSS101955 | Thermo Fisher |
| **Dynamin 1** | ACGACCUGCUGUG-GAUGGAUUACCA UGGUAAUCCAUCC-ACAGCAGGUCGU | HSS176208 | Thermo Fisher |
| **Dynamin 2** | GAGCGAAUCGUCA-CCACUU GAGAUCAGGUGGA-CACUCU | J-004007-08 | Dharmacon |
| **Endophilin A1** | GCUGAGUCAAGCAU-GUUCAAUCUCU AGAGAUUGAACAU-GCUUGACUCAGC | HSS109709 | Thermo Fisher |
| **Endophilin A2** | CCCAAGAUCGCAGC-UUCAUCGUCUU AAGACGAUGAAGC-UGCGAUCUUGGG | HSS109707 | Thermo Fisher |
| **Endophilin A3** | CAAUGGAGUUUCCA-CCACCUCUGUA UACAGAGGUGGUG-GAAACUCCAUUG | HSS109712 | Thermo Fisher |

**Knockdown of genes involved in endocytosis and recycling in growing and quiescent cells**

Cells were counted with a CASY Cell Counter and Analyzer Model TT (Roche Applied Science). Growing cells were seeded at 6.87 x $10^3$ cells/$cm^2$ for single knockdowns and 1.25 x $10^4$ cells/$cm^2$for double and triple knockdowns in 96 well plates (655892, Greiner Bio-One) six hours prior to transfection. Medium was exchanged for 100 µl fresh culture medium. SiRNA and Lipofectamine RNAiMAX Transfection Reagent (concentrations in Tab. 2.2.3) were each diluted in 5 µl OptiMEM (5 % of culture medium volume per well), mixed and incubated for 20 min at room temperature. 10 µl transfection mix (10 % of culture medium volume per well) to each well. The transfection step was repeated after 24 hours, culture medium exchanged after 48 hours and cells were used for experiments 72 hours after the first transfection. Quiescent cells were seeded at 1.4 x $10^4$ cells/$cm^2$ and transfected before medium exchange to serum-free medium. Mixing of siRNA and Lipofectamine RNAiMAX Transfection Reagent occured as described for growing cells, albeit at increased concentrations for both (Tab. 2.2.3). The first transfection occured 5 days after seeding, medium was replaced 24 hours later. The second transfection occured 7 days after seeding and was followed by medium exchange 24 hours later. After another two days of recovery, medium was exchanged to serum-free medium (10 days after seeding) and cells were used for experiments 17 days after seeding.

**Table 2.2.3:** Concentration of reagents for RNA interference

| **Component** | **Growing** | | | **Quiescent** |
|---|---|---|---|---|
| | **single KD** | **double KD** | **triple KD** | |
| **siRNA/cm²** | 4.22 pmol | 7.71 pmol | 12.66 pmol | 6.25 pmol |
| **siRNA/96 well** | 1.35 pmol | 2.7 pmol | 4.05 pmol | 2 pmol |
| **RNAiMAX/pmol siRNA** | 0.125 µl | 0.125 µl | 0,083 µl | 0.425 µl |

## 2.3 Quantitative proteomics and phosphoproteomics

These experiments were performed by E. Boucrot and quantified by S.Y. Peak-Chew (MRC Laboratory of Molecular Biology) and K. McGourty (E. Boucrot lab).

In brief, RPE1 cells were cultured in light or heavy Stable isotope labeling by amino acids in culture (SILAC) medium (DMEM/F12 SILAC (-K/-R), 88215, Thermo Fisher Scientific, supplemented with 50 mg/l K8, 84 mg/l R10, 200 mg/l L-Proline) with 10 % dialysed FBS for five cell divisions to allow for complete labelling. Quiescent cells were grown to confluence and medium was exchanged to serum-free light or heavy SILAC medium. Growing cells were sorted by flow cytometry according to DNA profile into G1 fractions. G1 and quiescent (G0) cells were lysed in 8 M Urea. G0 and G1 lysates from several biological repeats were amalgamated, lysates separated by SDS-PAGE, lanes cut in 20 horizontal sections and digested by tryptic in-gel digest. Phosphopeptides were enriched using TiO2 columns. Peptides were analysed by MS/MS using a Thermo Fisher Orbitrap Velos.

## 2.4 SDS-polyacrylamide gel electrophoresis and Immunoblotting

### 2.4.1 Cell lysis and protein quantification

Proliferating RPE1 cells grown in full cell culture medium were harvested with Accutase, labelled with Hoechst 33342 and sorted for the G1 (2n DNA) population by flow cytometry (MoFlo XDP cell sorter). Quiescent RPE1 cells were harvested with Accutase and, in parallel with G1 cells, lysed in 8 M urea (U1250, Sigma-Aldrich), containing phosphatase (5870S, Cell Signaling Technology) and protease inhibitors (5871S, Cell Signaling Technology), to a final protein concentration of ~ 25 mg per 1 ml lysate. For quantification of protein levels per cell, $10^6$ cells were lysed in 100 µl 8 M urea with phosphatase and proteasse inhibitor. Following lysis, samples were sonicated to fragment DNA. Sonication was performed using at maximal 7 µm amplitude for 15 seconds with 30 seconds pause intervals (5 cycles) on ice.

**Protein quantification by Bradford assay** The Coomassie Plus (Bradford) Protein Assay kit (23236, Thermo Fisher Scientific) was used to asses total protein content per cell in both proliferating and quiescent cell populations. A bovine serum albumin (BSA) standard was created according to manufacturer's instructions diluting BSA

ranging from 0 to 2000 µg/ml protein in 8 M urea containing phosphatase and protease inhibitors. Protein lysates were diluted in 8 M urea containing phosphatase and protease inhibitors to obtain protein solutions with concentrations in the linear range of the BSA standard curve. The assay was performed according to manufacturer's instructions. Triplets of each sample were analysed in a 96-well microtiter plate measuring absorbance at 594 nm using FLUOstar OPTIMA ABS absorbance microplate reader (BMG LABTECH). A linear regression function was fitted on the BSA absorbance data points in the linear range from 125-1000 µg/ml. Protein concentration of samples was determined using the mean of technical triplicates which were within the linear range of the BSA standard curve.

**Protein quantification by SDS-PAGE and Coomassie staining** Cell lysates were supplemented in a 1:4 ratio with 5 x Laemmli buffer, incubated at 95 °C for 10 min and separated by SDS-PAGE on a 10 well 12 % Bis-Tris Plus SDS gel (NW00120BOX, Thermo Fisher Scientific). Gels were stained with Coomassie staining solution for 1 hour, destained for 1 hour with Coomassie destaining solution and further destained in 1:1 (v/v) Coomassie destaining solution/d$H_2O$ over night (Tab. 2.4.1). Gels were scanned and protein levels were quantified by densitometry quantification of lanes in 8 bit images using ImageJ software and compared relative to each other.

### 2.4.2 SDS-PAGE and protein transfer

Cell lysates were supplemented in a 1:4 ratio with 5 x Laemmli buffer, incubated at 95 °C for 10 min and used for Western blots immediately or stored at -20 °C. 40 µg protein (~20 µl cell lysate with Laemmli buffer) were loaded per lane on a 10 well 12 % Bis-Tris Plus SDS gel (NW00120BOX, Thermo Fisher Scientific). SDS-PAGE was performed in MOPS running buffer (B0001, Thermo Fisher Scientific) a Bolt Mini Gel Tank (Thermo Fisher Scientific) at 300 V and 75 mA for 30-45 min. Proteins were transferred onto a nitrocellulose membrane (Lightning Blot Midi Kit, Thermo Fisher Scientific) via semi-dry transfer in a Perkin Elmer Lightning Blotter (Thermo Fisher Scientific) with fixed voltage at 24 V and variable current for 20-22 min (depending on protein size).

### 2.4.3 Protein labelling and detection

Following transfer, membranes were washed twice in homemade Tris-buffered saline supplemented with 0.05 % Tween20 (TBST) and blocked in 5 % skimmed milk (LP0031, Thermo Fisher Scientific) in TBST for one hour. Primary antibodies were diluted in TBST containing 5 % horse serum (see Tab. 2.12.1 for antibodies and dilutions) and membranes were incubated with diluted primary antibody for either 2 hours at room temperature or over night at 4 °C. After primary antibody incubation, membranes were washed three times for 5-10 min in TBST to remove unbound antibody. Membranes were incubated for 25 min in horseradish peroxidase (HRP)-conjugated secondary antibody (see Tab. 2.12.2 for antibodies and dilutions) in TBST containing 5 % horse serum. After removal of the secondary antibody, membranes were washed three times in TBST for at least 15 min, respectively, to remove excess antibody that might cause unwanted background during detection. HRP oxidises a chemiluminiscent substrate, like ECL (enhanced chemiluminescence substrate), in the presence of hydrogen peroxide. The cleavage reaction emits chemiluminescence, which is used to detect the abundance of specific proteins of interest on the membrane. Pierce ECL Plus working solution (32132, Thermo-Scientific) was freshly made by mixing the provided reagents according to manufacturer's instruction at 40:1 ratio. The membranes were covered with working solution and stimulated for 3 minutes. Following stimulation, membranes were exposed to Amersham Hyperfilm ECL (289068367, GE Healthcare) in a dark room or/and in a light-proof cassette (KODAK). The films were developed in a Compact X4 film developer (Xograph Imaging Systems). Before membranes were re-probed with another primary antibody, they were stripped twice for 15 min each in pre-warmed Western Blot stripping buffer pH 2.5, washed twice in PBS for 10 min and twice in TBST for 5 min.

**Table 2.4.1:** Buffer compositions for SDS PAGE and Immunolotting

| Solution | Compound | Concentration |
|---|---|---|
| **5X Loading Buffer** | Tris pH 6.8 | 50 mM |
| | Glycerol | 45 % (v/v) |
| | Bromphenol Blue | 0.03 % (w/v) |
| | SDS | 10 % (v/v) |
| | DTT | 500 mM |
| **TBS-Tween** | Tris pH 7.4 | 50mM |
| | NaCl | 150 mM |
| | Tween 20 | 0.05 % |
| **Coomassie staining solution** | Acetic acid (glacial) | 10 % (v/v) |
| | Methanol | 45 % (v/v) |
| | Coomassie Brilliant Blue G250 | 0.3 % (w/v) |
| **Coomassie destaining solution** | Ethanol | 40 % (v/v) |
| | Acetic acid (glacial) | 10 % (v/v) |
| **Stripping buffer pH 2.5** | Glycine | 200 mM |
| | SDS | 0.01 % |
| | Tween 20 | 1 % |

## 2.5 Fixation and immunofluorescence labelling for microscopy and flow cytometry

Growing and quiescent cells were seeded at $1.5 \times 10^4$ cells/cm$^2$ and $1.4 \times 10^4$ cells/cm$^2$ two and 17 days prior to the experiment, respectively.

### 2.5.1 Immunofluorescence labelling for confocal microscopy

Cells were grown on coverslips that were washed with acetone and 100 % ethanol and placed in in 24-well plates. Cells were washed two times with PBS and fixed with 4 % paraformaldehyde (PFA, 28908, Thermo Fisher Scientific) in PBS at room temperature for 15-20 min. 50 mM ammonium chloride ($NH_4Cl$) in PBS was added 1:1 (v/v) to the PFA solution to bind and inactivate reactive aldehyde groups of PFA and stop the fixation reaction. The solution was exchanged for fresh 50 mM $NH_4Cl$ in PBS and cells were incubated for at least 30 min at room temperature to saturate residual reactive aldehyde groups to prevent cross-reacting with antibodies and quench fluorescence originating

from free PFA aldehyde groups. Cells were stored at 4 ℃ or used immediately for immunofluorescence (IF) labelling.

Coverslips were washed for 5 seconds in PBS followed by 0.1% Saponin (47036-50G-F, Sigma-Aldrich) in PBS (Saponin buffer) and were blocked for 30 min with Saponin buffer containing 10 % horse serum or 5 % BSA. Antibodies were diluted in antibody dilution buffer (0.1 % Saponin in PBS supplemented with 10 % horse serum or 5 % BSA; see sec. 2.12.1 for primary antibodies and dilutions). Saponin permeabilises membranes reversibly and needs to be maintained throughout the whole labelling procedure. Following 90 min primary antibody labelling, cells were washed three times for 5 seconds in Saponin buffer and incubated for 25 min with antibody dilution buffer containing AlexaFluor-conjugated secondary antibody (see sec. 2.12.2 for secondary antibodies and dilutions) and 3.3 µM Draq5 (62251, Thermo Fisher Scientific) or 2 µg/ml 4',6-diamidino-2-phenylindole (DAPI) (D9542-1MG, Sigma-Aldrich). Following secondary antibody incubation, coverslips were washed for 5 seconds in Saponin buffer followed by 5 seconds in PBS and rinsed with miliQ water. Coverslips were mounted on a droplet of mounting solution containing antifading agent 1,4-diazabicyclo[2.2.2]octane (DABCO) (GTX30930, GeneTex) on a glass slide. The slides were kept at room temperature in the dark over night to solidify and then stored at 4 ℃.

### 2.5.2 Immunofluorescence labelling in microplates

Cells were grown in 96-well microplates (655892, Greiner Bio-One). Cells were washed three times with PBS and fixed with 4 % PFA in PBS for 15-20 min at room temperature. 50 mM $NH_4Cl$ in PBS was added 1:1 (v/v) to the PFA solution to stop the fixation reaction. The solution was exchanged for fresh 50 mM $NH_4Cl$ in PBS and cells were incubated for at least 30 min at room temperature. Cells were stored at 4 ℃ or used immediately for IF labelling.

Cells were washed three times in PBS and blocked for 30 min with Saponin buffer containing 10 % horse serum or 5 % BSA. Blocking buffer was exchanged for primary antibody diluted in antibody dilution buffer (see sec. 2.12.1 for primary antibodies and dilutions). Primary antibody incubation occured for 90 min at room temperature or over night at 4 ℃. Cells were washed three times for 5 min in Saponin buffer and incubated

with antibody dilution buffer containing secondary antibody (see sec. 2.12.2 for secondary antibodies and dilutions) and 2 µg/ml DAPI (D9542-1MG, Sigma-Aldrich). Following secondary antiody incubation, cells were washed three times for 5 min in Saponin buffer, two times in PBS and two times in miliQ water. Water was exchanged for Mowiol mounting solution with DABCO and plates were either imaged immediately or stored at room temperature in the dark over night before long-term storage at 4 °C.

### 2.5.3 Immunofluorescence labelling for flow cytometry

Cells were grown in T175 culture flasks or 6-well plates. Cells were pelleted at 1,000 g for 5 min and resuspended in PBS. The PBS washing step was repeated before cells were resuspended in 4 % PFA in PBS and incubated at room temperature for 15-20 min. 50 mM $NH_4Cl$ in PBS was added 1:1 (v/v) to the PFA solution and cells were pelleted at 1,000 g for 5 min and resuspended in fresh 50 mM $NH_4Cl$ in PBS and incubated for at least 30 min at room temperature. Cells were stored at 4 °C or used immediately for IF labelling.

Cells were pelleted at 1,000 g for 5 min and resuspended in PBS. The PBS washing step was repeated and cells were resuspended in antibody dilution buffer containing primary antibody (see sec. 2.12.1 for primary antibodies and dilutions) and incubated for 90 min at room temperature with occational mixing to allow for even antibody labelling. The antibody solution was diluted with Saponin buffer and cells were pelleted at 1,000 g for 5 min, resuspended in Saponin buffer and washed two more times with Saponin buffer. Cells were resuspended in antibody dilution buffer containing secondary antibody (see sec. 2.12.2 for secondary antibodies and dilutions) and 2.5 µg/ml Hoechst 33342 (H3570, Thermo Fisher Scientific) or 2 µg/ml DAPI (D9542-1MG, Sigma-Aldrich). Secondary antibody solution was diluted with Saponin buffer and cells were pelleted at 1,000 g for 5 min, resuspended in Saponin buffer and washed two more times with Saponin buffer. Pellets were resuspended in PBS, passed through a nylon mesh filter to eliminate clumps and either used immediately or stored at 4 °C in the dark until flow cytometry analysis.

**Table 2.5.1:** Composition of PBS and Mowiol with DABCO

| Solution | Compound | Concentration |
|---|---|---|
| **PBS pH 7.4** | NaCl | 137 mM |
| | KCl | 2.7 mM |
| | $Na_2HPO_4$ | 12.5 mM |
| | $KH_2PO_4$ | 2 mM |
| **Mowiol with DABCO** | Tris pH 8.5 | 100 mM |
| | Glycerol | 20 % (v/v) |
| | Mowiol 4-88 | 10 % (w/v) |
| | DABCO | 2.5 % (v/v) |

## 2.6 PyroninY - Hoechst staining and flow cytometry analysis

Cycling and quiescent RPE1 cells were grown in T-150 cell culture flasks (CC7682-4415, CytoOne). Three flasks of proliferating cells were grown for each flask of quiescent cells. Cells were rinsed with PBS and detached with Accutase. Detached cells were pelleted for 5 min at 900 g and 4 °C and washed twice in ice-cold PBS. The pellet was resuspended in 300 µl ice-cold PBS and 700 µl ice-cold 100 % ethanol were dropwise added while the cell suspension was gently mixed. Cells in the 70 % ethanol-PBS solution were kept on ice or at 4 °C for at least 3 hours before labelling.

A subset of ethanol-fixed cells were washed with PBS and labelled with anti-phospho Rb Ser 807/811 clone D20B12 (8516, Cell Signaling Technology) at a 1:400 dilution in PBS supplemented with 10 % horse serum.

4 µg/ml PyroninY and 2 µg/ml Hoechst 33342 for 25 min at room temperature in the dark. Cells were washed with PBS and analysed at the LSRII with 488 nm excitation and a 575/26 BP filter for PyroninY signal, and 350 nm excitation and a 450/50 BP filter for Hoechst signal. G0/G1 cells were discriminated in a dot plot showing Hoechst on the X-axis and PyroninY on the Y-axis.

## 2.7 Ligand uptake and recycling assays

Growing and quiescent cells were seeded at $1.5 \times 10^4$ cells/cm$^2$ and $1.4 \times 10^4$ cells/cm$^2$ two and 17 days prior to the experiment, respectively.

### 2.7.1 Ligand uptake assay for confocal microscopy imaging

Cells were grown on coverslips that were washed with acetone and 100 % ethanol and placed in in 24-well plates. Culture medium was exchanged for serum-free (transferrin, LDL and EGF uptake) or fresh culture medium (serum-free for quiescent cells) containing the respective fluorescent ligand. Ligand uptake occurred at 37 ℃ for the indicated durations (see sec. 2.12.3 for ligands and concentrations). Following ligand uptake, the 24-well plates were placed on ice, medium was removed and cells were washed twice with ice-cold PBS. Surface-bound ligand was removed by two washes in ice-cold glycine stripping buffer pH 4.5 for 2 min per stripping step. The low pH value causes the dissociation of the ligands which are bound to receptors at the outer side of the plasma membrane, so that only internalised and thus membrane-protected ligand is detected. Cells were then washed twice with ice-cold PBS to re-establish physiological pH. PBS was removed and cells were incubated in ice-cold 4 % PFA in PBS the dark for 5 min on ice and for another 15 min at room temperature. After fixation, 50 mM $NH_4Cl$ in PBS was added 1:1 (v/v) to the PFA solution. The solution was exchanged for fresh 50 mM $NH_4Cl$ in PBS and left in the dark at room temperature for at least 30 min to quench PFA autofluorescence. Coverslips were washed twice with PBS and once with Saponin buffer. They remained in the dark in Saponin buffer for at least 30 min before putting them upside down on a 40 µl droplet of Saponin buffer containing 3.3 µM Draq5 (Cell Signaling Technology) or 2 µg/ml DAPI to stain nuclei, which was placed on Parafilm laid out on milliQ water-soaked filter paper. After 25 min incubation at room temperature, coverslips were removed and washed in 0.1 % Saponin in PBS, PBS and milliQ water for ca. 5 seconds each. Excess liquid was soaked into a filter paper and coverslips were mounted on a droplet of DABCO mounting solution on a glass slide. The slides were kept at room temperature in the dark over night to solidify. Fixed and quenched cells were permeabilised and labelled with DAPI as described in sec. 2.5.

### 2.7.2 Ligand uptake assay and antibody feeding in microplates

#### Ligand uptake

Cells were grown in 96-well microplates (655892, Greiner Bio-One). Culture medium was exchanged for serum-free (transferrin, LDL and EGF uptake) or fresh culture

medium (serum-free for quiescent cells) containing the respective fluorescent ligand. Ligand-containing medium for antibody feeding assays contained 1 % BSA. Ligand uptake occurred at 37 °C for the indicated durations (see sec. 2.12.3 for ligands or antibodies and concentrations). Following ligand uptake, plates were placed on ice and cells were washed three times with ice-cold PBS containing 0.9 mM $CaCl_2$ and 0.5 mM $MgCl_2$ (PBS++; 14040117, Thermo Scientific), two times for two minutes each with ice-cold glycine stripping buffer pH 4.5 (2 min with stripping buffer pH 2.5 and two times 2 min with stripping buffer pH 2.0 for antibody feeding) and three times with ice-cold PBS++. Cells were fixed with ice-cold 4 % PFA in PBS for 5 min on ice and another 15 min at room temperature. After fixation, 50 mM $NH_4Cl$ in PBS was added in a 1:1 volume/volume ratio. The solution was exchanged for fresh 50 mM $NH_4Cl$ in PBS and incubated in the dark at room temperature for at least 30 min. Cells were then washed three times in PBS, blocked, permeabilised and labelled as described in sec. 2.5.2.

**Cell surface labelling**

Cells were grown in 96-well microplates (655892, Greiner Bio-One). Plates were placed on ice and washed three times with ice-cold PBS++. PBS++ was exchanged for ice-cold imaging medium (Tab. 2.7.2) containing 1 % BSA and primary antibody at the same concentration as used for feeding assays (see sec. 2.12.3 for ligands or antibodies and concentrations). Primary antibody incubation occured for 90 min on ice in a cold room. Following primary antibody incubation, plates were kept on ice, washed four times with ice-cold PBS++ and fixed with 4 % PFA in PBS for 5 min on ice followed by 15 min at room temperature. After fixation, 50 mM $NH_4Cl$ in PBS was added in a 1:1 volume/volume ratio. The solution was exchanged for fresh 50 mM $NH_4Cl$ in PBS and incubated at room temperature for at least 30 min. Cells were then washed three times in PBS, blocked, permeabilised and further labelling steps were performed as described in sec. 2.5.2.

**Table 2.7.1:** Ligand uptake stripping buffer composition

| Solution | Compound | Concentration |
|---|---|---|
| **Stripping buffer pH 4.5** | NaCl | 150 mM |
| | Glycine | 100 mM |
| | KCl | 5 mM |
| | $CaCl_2$ | 1 mM |
| | $MgCl_2$ | 1 mM |
| **Stripping buffer pH 2.5 or 2.0** | NaCl | 150 mM |
| | Acetic acid /glacial) | 200 mM |
| | KCl | 5 mM |
| | $CaCl_2$ | 1 mM |
| | $MgCl_2$ | 1 mM |

### 2.7.3 Macropinocytosis cargo uptake in microplates

Cells were grown in 96-well microplates (655892, Greiner Bio-One). Culture medium was exchanged for medium containing the respective fluorescent substrate. Ligand uptake occurred at 37 ℃ for the indicated durations (see sec. 2.12.3 for substrates and concentrations). 20 min before washing, Hoechst33342 was added at a final concentration of 2.5 µg to be actively taken up by the cells at 37 ℃. Following uptake, plates were placed on ice and cells were washed five times with ice-cold PBS containing 0.9 mM $CaCl_2$ and 0.5 mM $MgCl_2$. PBS was exchanged for Imaging medium (Tab. 2.7.2) containing 2.5 µM Hoechst33342 and 10 % FBS for growing cells. Cells were imaged immediately.

**Table 2.7.2:** Imaging medium for live cell imaging

| | Manufacturer and reference | Final concentration |
|---|---|---|
| **Minimal Essential Medium (MEM)** | Thermo Scientific 41061-029 | - |
| **Glutamax 100X** | Gibco 35050-038 | 1X |
| **Antibiotic/ Antimycotic 100 X** | Sigma-Aldrich A5955-100ML | 1 X |
| **Sodium Bicarbonate 7.5 %** | Sigma-Aldrich S8761 | 0,26 % (w/v) |
| **Non-essential amino acids 100 X** | Thermo Scientific 11140050 | 1X |
| **HEPES** | Thermo Scientific 15630080 | 25 mM |

### 2.7.4 Ligand uptake assay for flow cytometry analysis

**Ligand uptake:** Cycling and quiescent RPE1 cells were grown in 6-well plates (130184, Thermo Fisher Scientific). Culture medium was exchanged for FBS-free medium containing the respective fluorescent ligand and uptake occurred at 37 °C for 15 min (see sec. 2.12.3 for ligand concentrations). Following uptake, cells were washed three times with ice-cold PBS and detached with pre-warmed Accutase. Detached cells were collected using P1000 pipettes to break cell clumps by gently pipetting up and down. The cell suspension was filled in 1.5 ml reaction tubes, transferred on ice and centrifuged at 4 °C at at least 1000 g for at least 6 minutes (will be further referred to as “centrifuged”; speed and duration of centrifugation were increased for smaller cell pellet sizes). Supernatant was removed and the cell pellets resuspended in ice-cold PBS. Cells were centrifuged at 4 °C, resuspended in glycine stripping buffer pH 4.5 and incubated on ice for 2 min. Cells were centrifuged at 4 °C and the stripping step was repeated. Cells were centrifuged at 4 °C and the pellet was resuspended in ice-cold PBS. After another centrifugation step, the pellet was resuspended in ice-cold 4 % PFA in PBS and incubated in the dark for 5 min on ice and additional 15 min at room temperature. Following fixation, 50 mM $NH_4Cl$ in PBS was added in a 1:1 (v/v) ratio, cells were pelleted and resuspended in 50 mM $NH_4Cl$ in PBS in which they remained for at least 30 min in the dark at room temperature. The $NH_4Cl$ solution was exchanged for PBS and after centrifugation at room temperature the pellet was resuspended in Saponin Buffer, containing 2.5 µg/ml Hoechst 33342 (Invitrogen). After 25 min incubation at room temperature in the dark, cells were pelleted and resuspended in an appropriate volume of PBS for flow cytometry analysis.

**Cell surface labelling:** To assess the relative amount of cell surface receptors, cells were grown in 6-well plates, detached with Accutase to preserve cell surface receptors, washed with ice-cold PBS and pelleted at 4 °C. Cells were resuspended in ice-cold Alpha-MEM (41061-029, Gibco) containing fluorescence–conjugated transferrin, LDL or EGF (same concentrations as for uptake, sec. 2.12.3) or 10 % horse serum and antibodies against TfR1 (CBL47, Merckmillipore,100 ng/ml), LDLR (MAB2148, R&D Systems, 5 µg/ml) or EGFR (13A9, Genentech, 1:1000 dilution). Cells were incubated with ligands or antibodies for 90 min at 4 °C on ice in the dark. Since the antibody against

EGFR only binds to the ectopic domain of the activated, dimerised receptor, 50 ng/mL EGF (E9644, Sigma) was added to stimulate receptor dimerisation. After incubation, cells were pelleted at 4 °C and washed twice with ice-cold PBS. Fixation, DNA staining and flow cytometry analysis were performed as described for ligand uptake.

### 2.7.5 α3-integrin recycling assay

Growing and quiescent cells were seeded in 96-well microplates at $1.5 \times 10^4$ cells/cm$^2$ and $1.4 \times 10^4$ cells/cm$^2$ two and 17 days prior to the experiment, respectively. Culture medium was exchanged for medium containing 1 % BSA and 1.3 µg/ml mouse anti-α3-integrin primary antibody clone P1B5 (sc-13545, Santa Cruz) and incubated at 37 °C for 90 min to allow for saturation of uptake and recycling of α3-integrin. Next, plates were placed on ice, washed four times with ice-cold PBS++ and incubated on ice in a cold room for 90 min with ice-cold imaging medium (Tab. 2.7.2) containing 1 % BSA and 6.6 µg/ml unlabelled anti-mouse secondary antibody (A28174, Thermo Scientific) to block cell surface-bound anti-α3-integrin antibody. Plates were kept on ice and washed 4 times in ice-cold PBS++. PBS++ was exchanged for pre-warmed culture medium containing 1 % BSA and 6.6 µg/ml AlexaFluor647-conjugated anti-mouse secondary antibody (A21463, Thermo Scientific) and plates were incubated at 37 °C for the indicated durations. Due to the surface-blocking step on ice, the AlexaFluor647-conjugated secondary antibody labels only labels recycled anti-α3-integrin primary antibody and thus gives a measure of recycling efficiency. Following incubation at 37 °C, cells were placed on ice, washed four times with PBS++ and fixed with 4 % PFA in PBS for 5 min on ice followed by 15 min at room temperature. After fixation, 50 mM $NH_4Cl$ in PBS was added in a 1:1 volume/volume ratio. The solution was exchanged for fresh 50 mM $NH_4Cl$ in PBS and incubated at room temperature for at least 30 min. Cells were then washed three times in PBS, blocked, permeabilised with Saponin and labelled with AlexaFluor488-conjugated anti-mouse secondary antibody for intracellular α3-integrin and DAPI to stain nuclei as described in sec. 2.5.2.

### 2.7.6 Inhibitor treatments

A list of inhibitors and concentrations used in this study is provided in Tab. 2.7.3. All inhibitor doses were titrated and the lowest dose with maximum effect and highest cell viability was used. Endocytosis and recycling inhibitors were added to culture medium 30 min before uptake and during assay duration unless otherwise indicated. Treatment with Dyngo4A occured in serum-free medium, both for growing and quiescent cells.

**Table 2.7.3:** Inhibitor concentrations

| Reagent | Reference | Manufacturer | Concentration |
|---|---|---|---|
| **Endocytosis** | | | |
| Dyngo4A[a] | ab120689 | Abcam | 4 µM |
| Ikarugamycin | 15386 | Cayman Chemical | 50 nM |
| EIPA | 14406 | Cayman Chemical | 15 µM |
| Rottlerin | R5648 | Sigma Aldrich | 7.5 µM |
| **Recycling** | | | |
| Monensin | 16488 | Cayman Chemical | 100 µM |
| Primaquiine | 160393 | Sigma Aldrich | 50 µM |
| **mTORC1** | | | |
| Torin1 | 4247 | Tocris | 100 µM |

[a] used with serum-free medium only

## 2.8 Image acquisition

### 2.8.1 Confocal microscopy

Confocal microscopy was performed on a LSM 700 confocal microscope (Zeiss) with a 40 X Plan Apochromat oil objective (numerical aperture = 1.3) or a 63 X Plan Apochromat oil objective (numerical aperture = 1.4) equipped with a 405 nm (5 mW), 488 nm (10 mW), 555 nm (10 mW) and 639 nm (5 mW) laser laser. Using ZEN imaging software, the emission lightpath was adjusted for 488 nm and 555 nm excitation to eliminate autofluorescence in yellow wavelengths. Images were acquired at 1024x1024 pixel size with zoom factor set to 1.0-1.5. To compare signals in proliferating and quiescent cells, laser intensity and gain were kept constant when imaging the two conditions for a protein of interest.

### 2.8.2 High-throughput automated widefield microscopy

High throughput image acquisition was performed on an ImageXpress Micro XL Widefield High Content Screening System (Molecular Devices) equipped with a Nikon ELWD 20X S Plan Fluor air objective (numerical aperture = 0.45) and an environmental temperature and CO2 control module, using MetaXpress 5.3 software. Fluorophors were excited with a Lumencor Sola solid-state white-light engine with wavelengths ranging from 380 nm to 680 nm. Emission was detected with band-pass filter cubes (Tab. 2.8.1) and captured by a 4.66 megapixel complementary metal-oxide semiconductor (CMOS) camera. Images were acquired as 16 bit grayscale images at 2160x2160 pixels with one image per acquired channel.

**Table 2.8.1:** ImageXpress Micro XLS filter cubes

| Fluorophor | Excitation (nm) | Emission (nm) |
|---|---|---|
| DAPI, Hoechst33342 | 377/50 | 477/60 |
| AlexaFluor488, DiO | 482/35 | 536/40 |
| AlexaFluor555, DiI, Rhodamine | 543/22 | 593/40 |
| AlexaFluor594 | 562/40 | 624/40 |
| AlexaFluor633, AlexaFluor647 | 628/40 | 692/40 |

The workflow for setting up automated imaging of a 96 well-plate is depicted in Fig. 2.8.1. Prior to imaging, plates were calibrated to allow for plate and well bottom autofocus setup (1). After selection of the 20X objective (2), the number and location of wells and sites to be imaged were selected (3). Laser-based focussing on plate and well bottom was enabled for each image to be acquired (4). The channels of wavelengths for excitation and emission were selected and the channel serving as focus offset for each other channel determined (4). Image-based focus and exposure times, ranging from 1-2000 ms, were determined for each channel (4). To account for unevenness in plate design or differences in focus planes, a focus journal was applied after each image was acquired (5). The journal encoded a z-stack (for example 4 images with 2 µm spacing between each image, set manually) from which the image with the best focus was saved as final acquisition.

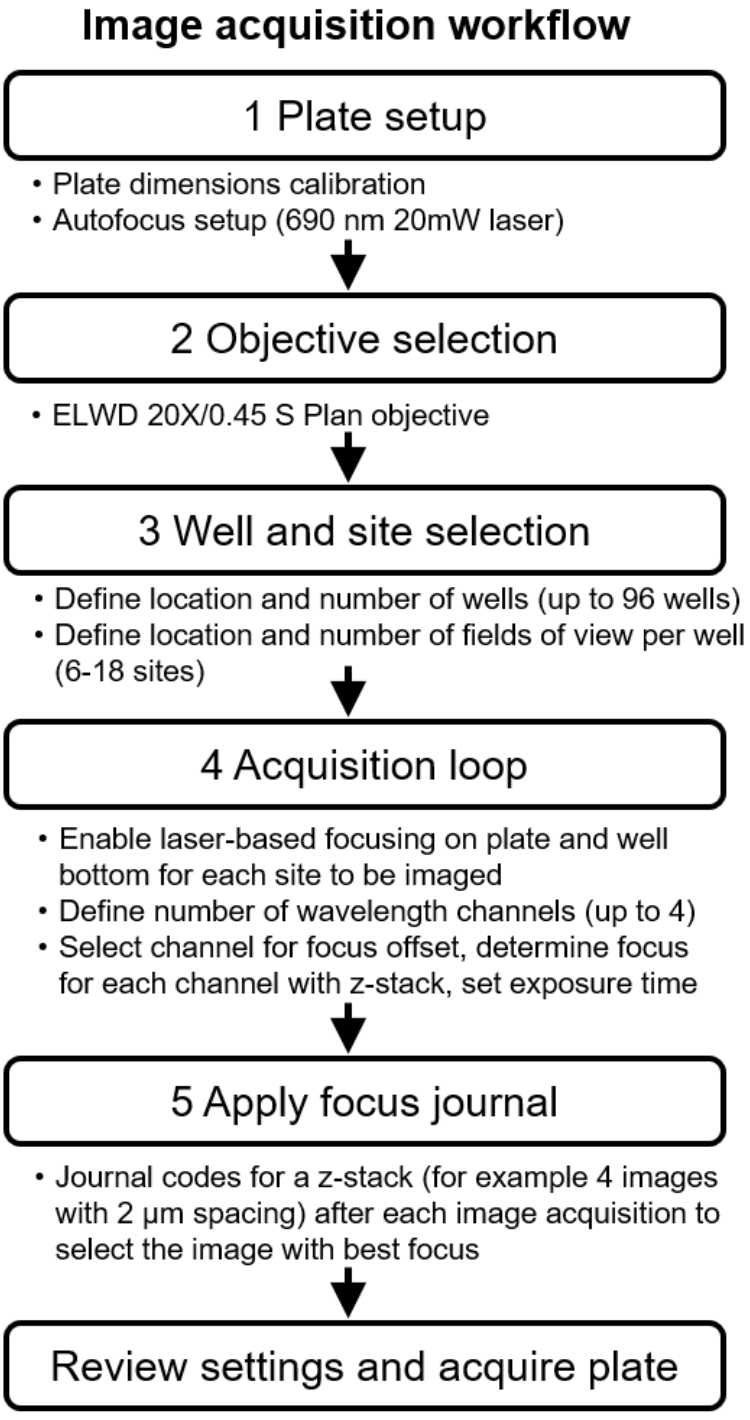


**Figure 2.8.1:** High throughput imaging workflow
Image acquisition setup with MetaXpress for ImageXpress micro XLS high content imaging system.

## 2.9 Automated image analysis

Images acquired by confocal or high throughput microscopy were analysed with CellProfiler 2.2.0 software (Carpenter *et al.*, 2006; Lamprecht *et al.*, 2007). Up to 3,000 image sets (one image sets originating from high throughput microscopy consisted of up to four separate images, one for each wavelength) were imported into CellProfiler and metadata information about experiment name, well and site number and wavelength channel extracted with regular expressions (Fig. 2.9.1).

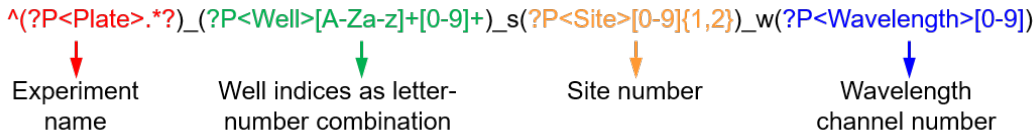


**Figure 2.9.1:** Regular expression to extract metadata information from images in CellProfiler

### 2.9.1 Cell segmentation and endosome identification

The workflow of a CellProfiler pipeline segmenting cells and endosomes is depicted in Fig. 2.9.2. The greyscale image for each wavelength channel was treated separately. An illumination function was calculated for and background-subtracted from raw images to account for uneven illumination (1). The illumination-corrected images were rescaled on a scale of 0-1 so that faint signal is visible for object identificatioin (2). In rescaled images, nuclei labelled with DAPI or Hoechst 33342 were identified as primary objects (3) and cell bodies labelled with a cytoplasmic marker (such as GAPDH or phalloidin) as secondary objects emanating from a primary object (4). A mask was created on the identified cell bodies to eliminate areas not occupied by cells from further analysis (5). Within the mask, speckles, which are small circular areas of increased intensity compared to their immediate environment, were enhanced to distinguish them from background haze or eliminate large areas of signal caused by antibody aggregation or surface-bound antibody that was not efficiently stripped (6). The speckle-enhanced image was used to identify endosomes as puncta of a defined pixel size (usually 4-15 pixels diameter) (7). Mean intensity and total area of identified puncta was measured in illumination-corrected images (8). For quantification, mean fluorescence of puncta per image was subtracted by mean fluorescence of cells per image in blank images (cells

not subjected to ligand uptake but else treated the same) and multiplied by the total area of puncta per cell.

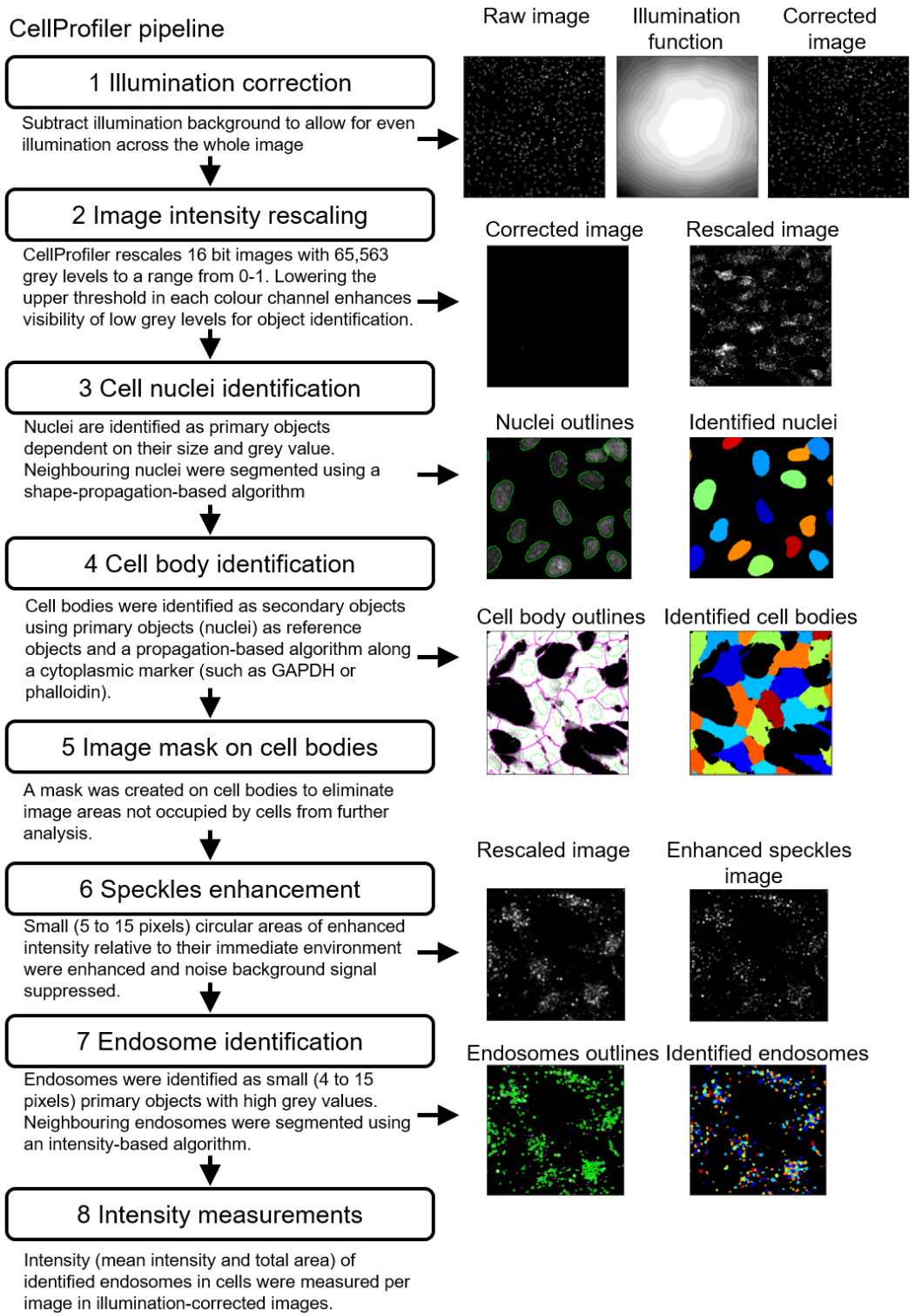


**Figure 2.9.2:** Schematic of a CellProfiler cell segmentation and endosome identification pipeline

### 2.9.2 Object-based colocalisation analysis

A schematic of a CellProfiler pipeline identifying colocalisation of endosomes is depicted in Fig. 2.9.3. Images were illumination-corrected and rescaled and speckles enhanced and endosomes identified as puncta as described in sec. 2.9.1. Identified puncta were shrunk either to a central pixel or by a specified number of pixels, determining analysis stringency (3). Colocalisation of shrunk puncta in different channels (images) was identified by relating overlapping objects in a child-parent relationship and filtering children with a parent or *vice versa* (4). To later measure intensities of the original-size endosome, shrunken puncta with a parent (or child) were related back to the initially identified puncta (5). Total intensity of colocalised and the total amount of identified puncta was measured in illumination-corrected images to evaluate the percentage of colocalisation.

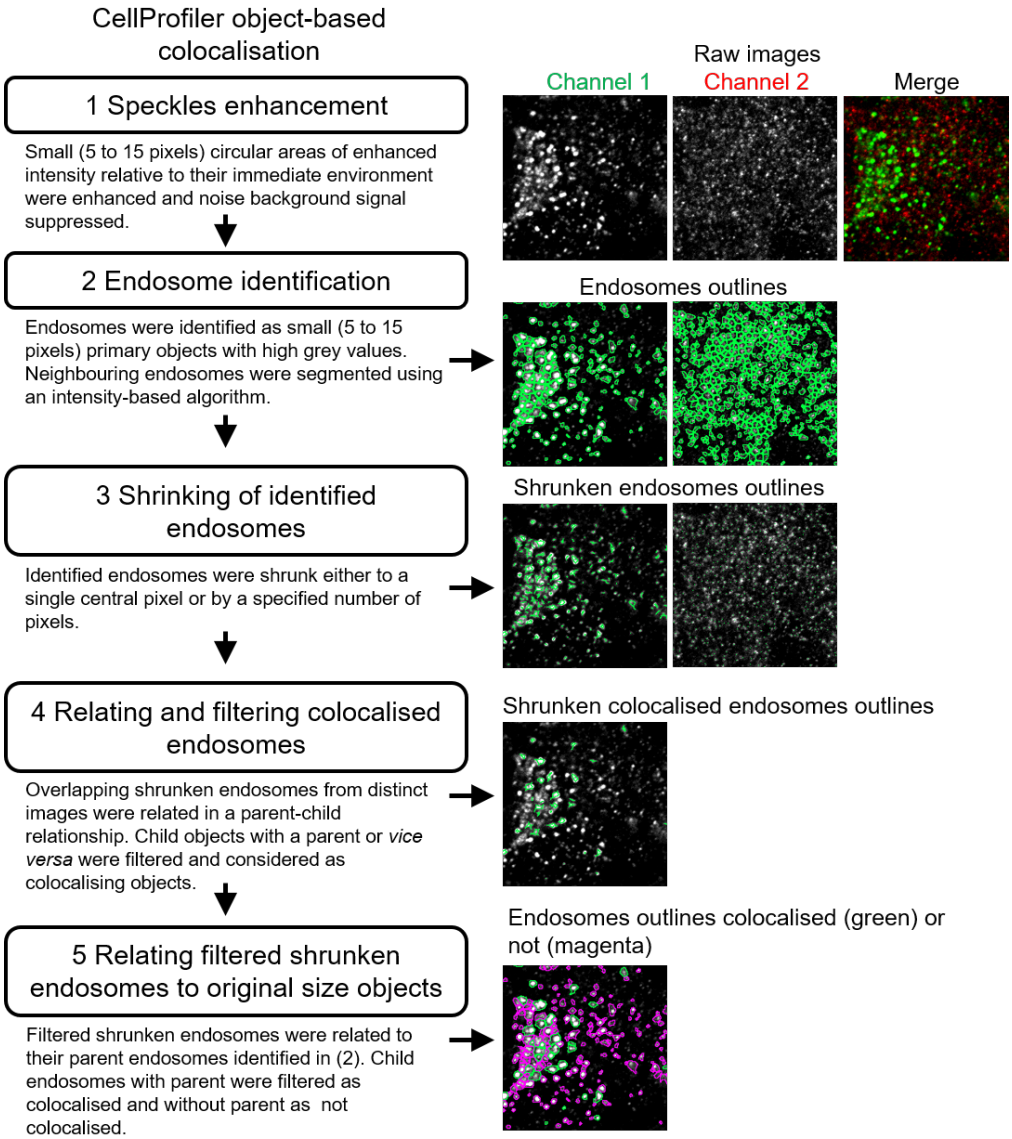


**Figure 2.9.3:** Schematic of a CellProfiler pipeline for object-based colocalisation
Object identification and filtering occured after illumination correction, image rescaling and speckle enhancement. Intensity of filtered colocalised objects was measured in illumination-corrected images.

## 2.10 Flow cytometry

Cell sorting for G1 or G0 RPE1 cells was performed on a MoFlo XDP Cell Sorter. DNA was stained with 2.5 µg/ml Hoechst33342 for 45 min at 37℃, cells were harvested with Accutase and cells with 2n DNA content sorted for further experiments (Immunoblotting or labelling for flow cytometry analysis). Flow cytometry analysis was performed on a BD Biosciences LSRII equipped with a 325 nm ultraviolet laser and 450/50 nm bandpass filter for Hoechst or DAPI, a 488 nm laser and 530/30 nm bandpass filter for AlexaFluor488 or DiO, and a 633 nm laser and 660/20 nm bandpass filter for AlexaFluor633 or -647. For red fluorescent dyes (AlexaFluor555 or DiI), a BD Biosciences FACSAriaIII with 561 nm excitation and 610/20 nm emission bandpass filter was employed. Data were analysed using FlowJo 8.8.6 (FlowJo LLC). To compare signals in proliferating and quiescent cells, laser intensity was kept constant when analysing the two cell cycle states. In a height versus area dot plot of DNA stain fluorescence intensity (Hoechst or DAPI), a gate was created on single cells to eliminate cell aggregates from further analysis. A DNA profile histogram of DNA stain fluorescence intensity was then used to gate on the cell populatioin with 2n DNA content. The 2n population of flow cytometry analysis will be referred to as “G1 cells” for proliferating samples and “G0 cells” for quiescent samples in the results chapters. The average geometrical mean of the signal area was used for quantification. Signal of labelled cells was divided by signal of control cells labelled with unspecific IgG or blank cells for activity assays and expressed as x-fold signal intensity of background signal.

## 2.11 Statistical analysis

Where not otherwise indicated, results represent mean + standard error of the mean (SEM). Gaussian distribution of samples was tested with D’Agostino & Pearson omnibus normality test. Samples following a Gaussian distribution were tested for statistical significance with Student’s unpaired two-tailed t-test (two sample groups), one-way ANOVA and Dunett’s test for multiple comparisons (more than two sample groups) or two-way ANOVA with Tukey’s test for multiple comparisons (more than two sample groups with two parameters per group). If samples did not follow a Gaussian distribution, an unpaird t-test with Welsh’s correction was used to compare two sample groups and Kruskal-

Wallis test with Dunn's multiple comparisons test for more than two sample groups. Significance of mean comparison coefficients was annotatet as follows: ****P < 0.0001, ***P < 0.001, **P < 0.01, *P < 0.05, ns, not significant.

## 2.12 Antibody and ligand concentrations

### 2.12.1 Primary antibodies

**Table 2.12.1:** Primary antibodies and concentrations
IF - immunofluorescence; FACS - Flow cytometry; IB - Immunoblot

| Antibody Name (clone) | Reference | Host | Company | Final concentration (µg/ml) or dilution | |
|---|---|---|---|---|---|
| | | | | IB | IF/FACS |
| **α3-integrin (P1B5)** | sc-13545 | Mouse | Sigma Aldrich | - | 0.66 |
| **α-adaptin (AP6)** | MA1-064 | Mouse | Thermo Scientific/Pierce Antibodies | 2 | 2 |
| **α-adaptin (clone 8/Adaptin α)** | 610501 | Mouse | BD Biosciences | 0.125 | 2.5 |
| **β1-integrin (9EG7)** | 553715 | Rat | BD Pharmingen | - | |
| **µ2-adaptin (clone 31/AP50)** | 611350 | Mouse | BD Biosciences | 0.5 | 2.5 |
| **APPL1 (D83H4)** | 3858 | Rabbit | Cell Signaling Technology | - | 1:50 |
| **APPL1 (E-17)** | sc-55063 | Goat | Santa Cruz | - | 2 |
| **CD151 (PETA-3)** | 350402 | Mouse | Biolegend | - | 1.6 |
| **Clathrin heavy chain (X22)** | MA1-065 | Mouse | Thermo Scientific | - | 6 |
| **Cyclin D1 (92G2)** | 2978 | Rabbit | Cell Signaling Technology | 1:1000 | 1:100 |
| **Dynamin 1 (41/Dynamin)** | 610245 | Mouse | BD Pharmigen | - | 1.25 |
| **Dynamin 2 (C-18)** | sc-6400 | Goat | Santa Cruz | - | 1.3 |
| **EEA1** | 2411 | Rabbit | Cell Signaling Technology | 1:1000 | 1:100 |
| **EEA1** | MAB8047 | Mouse | R&D Systems | - | 10 |
| **EGFP (clone 7.1 & 13.1)** | 11814460001 | Mouse | Roche | - | 0.8 |
| **EGFR (13A9)** | 13A9 | Mouse | Genentech | - | 1:1000 |

| Antibody Name (clone) | Reference | Host | Company | Final concentration (µg/ml) or dilution | |
|---|---|---|---|---|---|
| | | | | IB | IF/FACS |
| **EGFR (D38B1)** | 4267 | Rabbit | Cell Signaling Technology | 1:3500 | 1:100 |
| **Endophilin A2 (A-11)** | sc-365704 | Mouse | Santa Cruz | - | 0.5 |
| **FCHo2** | ab139731 | Rabbit | AbCam | 8 | 10 |
| **FCHo2** | Home made (HMM) | Rabbit | n/a | - | 1:500 |
| **GAPDH (0411)** | sc-47724 | Mouse | Santa Cruz | 0.007 | 1 |
| **GAPDH (14C10)** | 2118 | Rabbit | Cell Signaling Technology | - | 1:300 |
| **Ki67** | ab15580 | Rabbit | Abcam | 0.5 | 0.3 |
| **Lamp1 (H4A3-c)** | H4A3-c | Mouse | Developmental Studies Hybridoma Bank | - | 0.56 |
| **Lamp1 (D2D11)** | 9091 | Rabbit | Cell Signaling Technology | 1:1000 | 1:400 |
| **LDL receptor (472413)** | MAB2148 | Mouse | R&D systems | 2.5 | 2.5 |
| **p27(KIP1)** | NCL-p27 | Mouse | Novocastra (Leica) | - | 1:1000 |
| **PCNA (PC10)** | 2586 | Mouse | Cell Signaling Technology | 1:2000 | - |
| **phospho-4E-BP1 (T37/46)** | 2855 | Rabbit | Cell Signaling Technology | - | 1:400 |
| **phospho-Akt (S473) (D9E)** | 4060 | Rabbit | Cell Signaling Technology | - | 1:150 |
| **phospho-BAD (S112) (40A9)** | 5284 | Rabbit | Cell Signaling Technology | - | 1:200 |
| **phospho-Erk1/2 (T202/Y204) (D13.14.4E)** | 4370 | Rabbit | Cell Signaling Technology | - | 1:150 |
| **phospho-Erk1/2 (T202/Y204) (E10)** | 9106 | Mouse | Cell Signaling Technology | - | 1:150 |
| **phospho-FAK (Y397)** | 44-624G | Rabbit | Thermo Scientific | - | 1:150 |
| **phospho Rb (S807/811) (D20B12)** | 8516 | Rabbit | Cell Signaling Technology | | 1:300 |
| **TFR1 (CBL47)** | CBL47 | Rabbit | merckmillipore | 0,25 | 0.5 |

| Antibody Name (clone) | Reference | Host | Company | Final concentration (µg/ml) or dilution IB | IF/FACS |
|---|---|---|---|---|---|
| **VPS35** | ab97545 | Rabbit | Abcam | - | 3.1 |

### 2.12.2 Secondary antibodies

**Table 2.12.2:** Secondary antibodies and concentrations
IF - immunofluorescence; FACS - Flow cytometry; IB - Immunoblot

| Secondary Antibody | Conjugate | Reference | Manufacturer | Dilution IF/FACS |
|---|---|---|---|---|
| **Goat anti-mouse IgG** | AlexaFluor 488 | A11001 | Thermo Scientific | 1:500/1:1,000 |
| **Donkey anti-mouse IgG** | AlexaFluor 488 | A21202 | Thermo Scientific | 1:500/1:1,000 |
| **Chicken anti-mouse IgG** | AlexaFluor 488 | A21200 | Thermo Scientific | 1:500/1:1,000 |
| **Donkey anti-mouse IgG** | AlexaFluor 594 | A21203 | Thermo Scientific | 1:500/1:1,000 |
| **Goat anti-mouse IgG** | AlexaFluor 633 | A21050 | Thermo Scientific | 1:500/1:1,000 |
| **Chicken anti-mouse IgG** | AlexaFluor 647 | A21463 | Thermo Scientific | 1:500/1:1,000 |
| **Goat anti-rat IgG** | AlexaFluor 488 | A11006 | Thermo Scientific | 1:500/1:1,000 |
| **Chicken anti-rat IgG** | AlexaFluor 647 | A21472 | Thermo Scientific | 1:500/1:1,000 |
| **Goat anti-rabbit IgG** | AlexaFluor 488 | A11008 | Thermo Scientific | 1:500/1:1,000 |
| **Chicken anti-rabbit IgG** | AlexaFluor 488 | A21441 | Thermo Scientific | 1:500/1:1,000 |
| **Goat anti-rabbit IgG** | AlexaFluor 633 | A21070 | Thermo Scientific | 1:500/1:1,000 |
| **Chicken anti-rabbit IgG** | AlexaFluor 647 | A21443 | Thermo Scientific | 1:500/1:1,000 |
| **Donkey anti-goat IgG** | AlexaFluor 488 | A11055 | Thermo Scientific | 1:500/1:1,000 |
| **Donkey anti-sheep IgG** | AlexaFluor 488 | A11015 | Thermo Scientific | 1:500/1:1,000 |
| **Goat anti-Rabbit IgG** | HRP | BioRad | BioRad | IB 1:10,000 |

| Secondary Antibody | Conjugate | Reference | Manufacturer | Dilution IF/FACS |
|---|---|---|---|---|
| **Goat anti-Mouse IgG** | HRP | BioRad | BioRad | IB 1:10,000 |

### 2.12.3 Ligands for uptake assays

**Table 2.12.3:** Ligand concentrations for uptake assays and cell surface labelling

| Ligand | Conjugate | Manufacturer | Working concentration |
|---|---|---|---|
| **10 KDa dextran** | AlexaFluor 555 | Thermo Fisher D34679 | 500 µg/ml |
| **10 KDa dextran** | AlexaFluor 647 | LifeTech D22914 | 500 µg/ml |
| **10 KDa dextran**[1] | AlexaFluor 647 | LifeTech D22914 | 10 mg/ml |
| **70 KDa dextran** | TRITC | LifeTech D1818 | 1 mg/ml |
| **BSA** | AlexaFluor 647 | ThermoFisher A34785 | 100 µg/ml |
| **Cholera toxin B** | AlexaFluor 555 | LifeTech C34776 | 750 ng/ml |
| **DQ Green BSA** | BODIPY | ThermoFisher D12050 | 100 µg/ml |
| **EGF** | AlexaFluor 488 | LifeTech E13345 | 50 ng/ml |
| **EGF** | AlexaFluor 647 | LifeTech E35351 | 50 ng/ml |
| **HDL** | DiO | Kalen Biomedical 770380-9 | 50 µg/ml |
| **HDL**[2] | AlexaFluor 488 | Calbiochem 437641 | 50 µg/ml |
| **LDL** | DiI | LifeTech L3482 | 5 µg/ml |
| **LDL** | DiO | Kalen Biomedical 770280-9 | 15 µg/ml |
| **Lucifer Yellow CH** | - | LifeTech L453 | 5 mg/ml |
| **Oxidised LDL** | DiI | Intracell RP-173 | 5 µg/ml |
| **Oxidised LDL** | DiO | Kalen Biomedical 770282-9 | 30 µg/ml |
| **Shiga toxin B** | His | Sigma Aldrich SML0655 | 400 ng/ml |

[1] 10 µg/ml concentration was used when cells were fixed post uptake
[2] labelled with Alexa Fluor 488 Antibody Labeling Kit (A20181, Thermo Fisher) according to manufacturer's instructions

| Ligand | Conjugate | Manufacturer | Working concentration |
|---|---|---|---|
| **Transferrin** | AlexaFluor 488 | LifeTech T13342 | 200 µg/ml |
| **Transferrin** | AlexaFluor 555 | LifeTech T35352 | 200 µg/ml |

**Table 2.12.4:** Antibody concentrations for feeding and cell surface labelling

| Antibody Name (clone) | Reference | Host | Company | Final concentration (µg/ml) |
|---|---|---|---|---|
| **α3-integrin (P1B5)** | sc-13545 | Mouse | Sigma Aldrich | 1.3 |
| **β1-integrin (9EG7)** | 553715 | Rat | BD Pharmingen | 2.8 |
| **β1-integrin (Mab13)** | 552828 | Rat | BD Pharmigen | 2 |
| **Lamp1 (H4A3-c)** | H4A3-c | Mouse | Developmental Studies Hybridoma Bank | 1.2 |
| **CD151 (PETA-3)** | 350402 | Mouse | Biolegend | 2 |

# 3 An *in vitro* model for proliferative quiescence

## 3.1 Introduction

The majority of molecular cell biology research is carried out in continuously proliferating cell lines, which are often established by oncogenic transformations (such as HeLa cells). A notable proportion of cells in the adult human body, however, reside in a non-proliferative state, which might be characterised by modified molecular processes. Terminally differentiated and senescent cells have irreversibly left the cell cycle, but quiescent (also termed G0) cells can be triggered by specific stimuli to resume proliferation. Upon cell cycle exit, expression of cell-cycle progression markers such as Cyclin D1, CDK2, PCNA and phosphorylation of Retinoblastoma protein are down-regulated in quiescent cells (Baldin *et al.*, 1993; Ruiz-Miró *et al.*, 2011; Takasaki *et al.*, 1981; Stevaux & Dyson, 2002; Spencer *et al.*, 2013). The absence of Ki67 is another marker of cell cycle exit, as it is only present when cells are proliferating (Gerdes *et al.*, 1983, 1991). In addition to molecular markers, quiescent cells can be identified by decreased mTORC1 growth signalling (Gan & DePinho, 2009; Adhikari *et al.*, 2010) and concommitant reduced transcriptional activity, defined by low levels of mRNA (Darzynkiewicz *et al.*, 1980; Rhee & Bao, 2009). To date, research on quiescent cells has mostly been limited to naïve lymphocytes, dormant stem cells or cancer stem cells (Cheng *et al.*, 2000a; Orford & Scadden, 2008; Malumbres & Barbacid, 2001), which are difficult to maintain in culture and therefore poorly suited for complex functional assays or experiments requiring high cell numbers. Recently, human fibroblasts were identified as a qualified *in vitro* system to study molecular processes during proliferative quiescence (Mitra *et al.*, 2018). Primary cultures of human fibroblasts can enter the quiescent state via multiple routes, contact inhibition, growth factor withdrawal and loss of adhesion.

Combination of two or more of these pathways leads to a common 'deep' quiescence signature (Coller *et al.*, 2006; Mitra *et al.*, 2018). However, primary cell culture systems pose the risk of high batch-to-batch variations and variations between cell passages. In this chapter, the suitability of hTERT-immortalised RPE1 cells to serve as an *in vitro* model for proliferative quiescence will be tested. Non-transformed, hTERT-immortalised cell lines allow for the benefits of primary cells by maintaining cell type-speficic expression markers and sensitivity to contact inhibition-mediated cell cycle arrest (Vaziri & Benchimol, 1998; Bodnar, 1998).

## 3.2 Results

### 3.2.1 Inducing proliferative quiescence in RPE1 cells

Based on experiments in quiescent human fibroblasts, a protocol combining contact inhibition- and mitogen withdrawal-mediated quiescence entry was applied to hTERT-immortalised RPE1 cells (further referred to as 'RPE1 cells') (Coller *et al.*, 2006). RPE1 cells were cultured in full growth medium for seven days until they reached confluence. On day 7, medium was exchanged to growth medium without serum supplementation, in which cells were kept for 10 days to induce a deeper quiescent state (Gookin *et al.*, 2017). Subconfluent RPE1 cells did not survive medium exchange to serum-free medium (data from K. McGourty, Boucrot lab; not shown). After 10 days in serum-free medium, the DNA profile of quiescent cells was analysed by flow cytometry (Fig. 3.2.1A).

DNA quantity was measured by Hoechst 33342-staining of DNA in ethanol-fixed cells. Ethanol permeabilises cells by stripping them of lipids and allows for efficient dye incorporation into DNA. Hoechst 33342 stoichiometrically intercalates into A-T-rich minor grooves of doublestranded DNA, where it emits fluorescence when excited with UV (325 nm) or near-UV (375 nm) light. Fluorescence intensity of DNA-intercalated Hoechst 33342 is proportional to a cell's DNA content and provides information on the replicative state of its DNA (Arndt-Jovin & Jovin, 1977). Cellular DNA content can be used to distinguish between residence in G0/G1 (cells with 2n DNA content), S (between 2n and 4n DNA content) and G2 or Mitosis (G2/M, 4n DNA content with fully replicated genome) phase of the cell cycle. Proliferating (further referred to as 'growing') RPE1 cells exhibited a 2n DNA peak comprising of two thirds of the total cell population, about

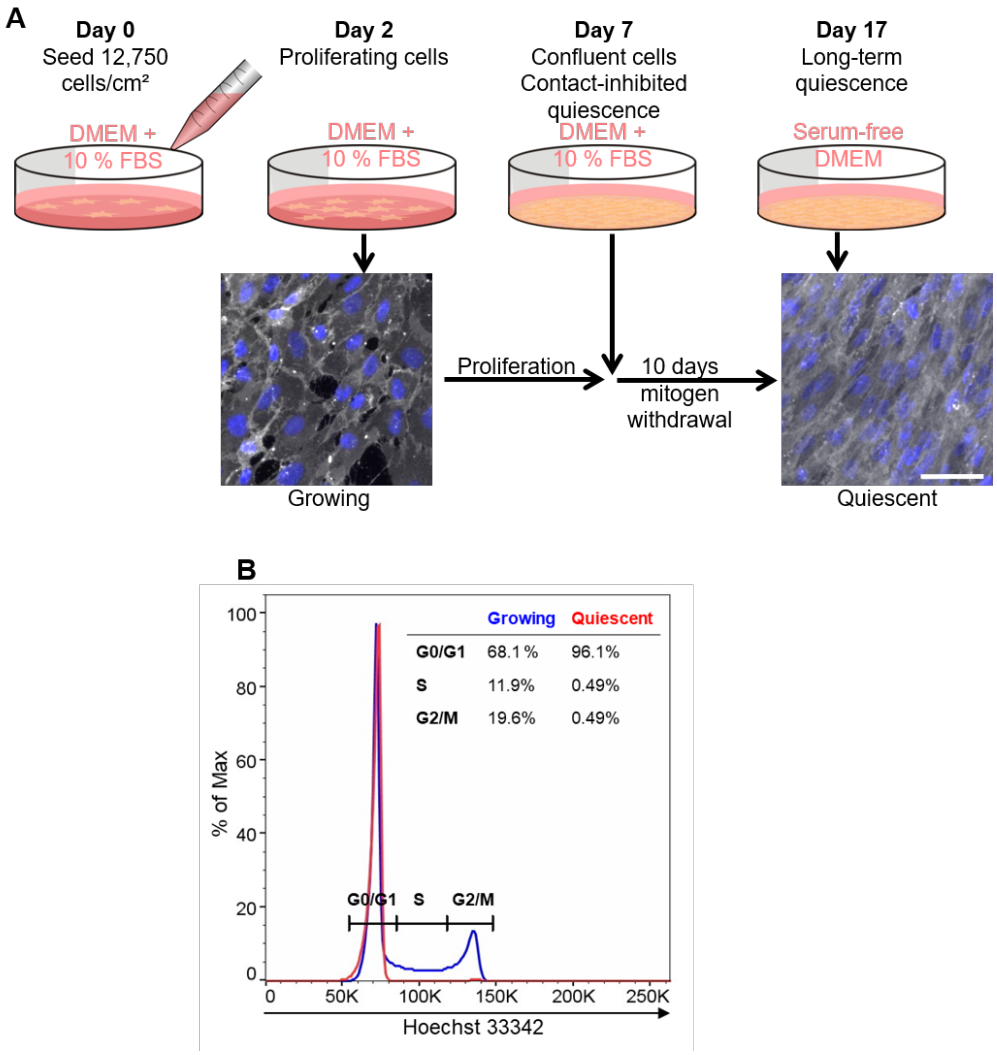


**Figure 3.2.1:** Inducing quiescence in hTERT-immortalized RPE1 cells
**A:** Upper panel: Schematic illustrating the protocol to generate proliferating ('Growing'), 7 days contact-inhibited and 10 days serum-starved RPE1 cells used throughout this study. RPE1 cells were grown in full growth medium for 7 days until they reached confluence. After 7 days, cells were cultured in medium without serum for another 10 days. Lower panel: Representative epifluorescence microscopy images of subconfluent proliferating cells at day 2 and confluent long-term quiescent cells at day 17. Nuclei are represented in blue and cell bodies (white) were labelled with a plasma membrane marker (anti-CD44). Scale bar: 50 µm. **B:** Representative histogram showing the DNA profile of ethanol-fixed growing (blue) and long-term quiescent (red) RPE1 cells stained for DNA content with Hoechst33342 analysed by flow cytometry. Gates represent the cut-off lines for cell cycle phases G0/G1, S and G2/M, which are quantified in the upper right corner. Percentage of max (% of Max) indicates the number of cells relative to the peak fraction of cells. A minimum of 50,000 cells per condition were analysed.

one tenth of cells replicated DNA in S-phase and one fifth of the population was residing in G2 or mitosis (G2/M) phase (Fig. 3.2.1B). In contrast, more than 90 % of quiescent RPE1 cells exhibited 2n DNA, suggesting cell cycle exit during G1 phase, and less than 1 % of quiescent cells were found to be replicating DNA or have duplicated genome (Fig. 3.2.1B).

The ability of quiescent RPE1 cells to re-enter the cell cycle was tested in wound-healing assays (data from Dr Kieran McGourty, not shown). This feature and reduced expression of senescence-associated β-galactosidase (K. McGourty) affirmed the temporary growth arrest and excluded the possibility of irreversible cell cycle exit (Dimri *et al.*, 1995).

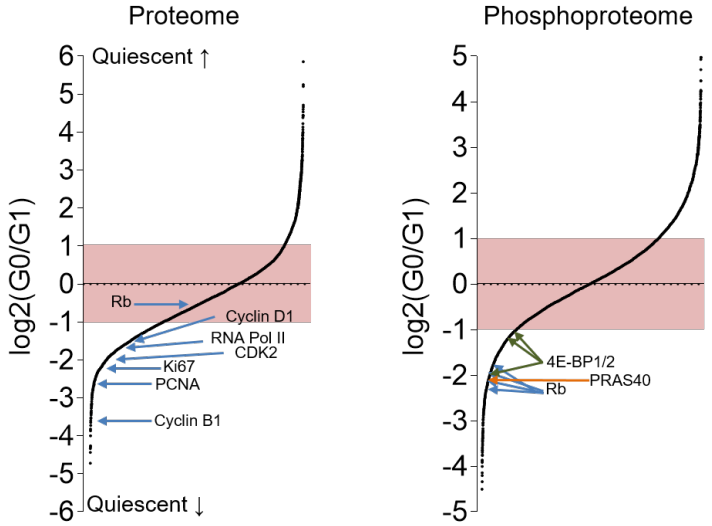


**Figure 3.2.2:** SILAC mass spectrometry data of G0 and G1 RPE1 cells
Results of a SILAC mass spectrometry screen comparing the proteome (left) and phosphoproteome (right) of G1 and G0 RPE1 cells. Displayed is the log2 ratio of protein levels in G0 relative to levels in G1. G1 cells were sorted by flow cytometry from proliferating cells. Identified key proteins involved in cell cycle progression are indicated. The ± one Log2 unit zone marked in red is considered to contain proteins whose levels did not differ (Mann & Kelleher, 2008).

To obtain an overview of the properties of quiescent RPE1 cells, the G0/G1 population of proliferating cells with 2n DNA content (further referred to as 'G1 cells') was sorted by flow cytometry and compared with quiescent, also termed G0, cells in a SILAC mass spectrometry screen. G0 cells were compared to G1 cells (and not S or G2/M phase cells) because with the protocol applied, RPE1 cells exit the cell cycle in G1 phase and we were interested in the differences occuring following cell cycle exit. This experiment was performed by E. Boucrot and MaxQuant analysis was conducted by K. McGourty (for details see sec. 2.3). Only hits with at least two peptides per protein were considered. G0 cells exhibited lower levels of cell cycle progression markers such as Cyclin D1

and B1, PCNA and CDK2 (Fig. 3.2.2). Levels of RNA polymerase II and Ki67 were also reduced. Abundance of Retinoblastoma protein (Rb) did not differ, but six identified phosphorylation sites were less phosphorylated in G0 than in G1 (Fig. 3.2.2). Furthermore, the screen hinted at a down-regulation of mTORC1 activity with hypophosphorylated substrates PRAS40 (S183, 5-fold reduced) and 4E-BP1/2 (S2, S5 both 2-fold reduced, T46 5-fold reduced) in G0. As a next step, these markers should be confirmed by biochemical and cell biological approaches.

### 3.2.2 Quiescent are smaller and contain less protein than proliferating cells

When counting growing and quiescent cells with a haemocytometer in preparation for immunoblotting and immunofluorescence experiments, quiescent cells proved to be robustly 20 % smaller than growing cells (Fig. 3.2.3A). Protein levels were determined using a Bradford-based assay. Harvested quiescent (G0) and FACS-sorted G1 cells from growing cells were lysed in equal volumes of 8 M urea per number of cells. Measuring protein concentration of equal lysate volumes, equivalent to equal cell numbers, gives conclusion on protein total protein content per cells. With this approach, it was shown that quiescent RPE1 cells contain 40 % less protein than G1 cells (Fig. 3.2.3B). As a second approach to determine differences of protein levels in G0 and G1 cells, equal volumes of total cell lysates of G0 and FACS-sorted G1 cells were analysed by SDS-PAGE. Gels were stained with Coomassie blue and band colour intensity was measured by densitometry quantification. This approach confirmed a 40 % reduction of protein content in quiescent cells (Fig. 3.2.3C). These findings are important, as results in the mass spectrometry screen were normalised to total protein levels, which has to be considered when quantitatively confirming mass spectrometry data by immunoblotting or flow cytometry. Glyceraldehyde 3-phosphate dehydrogenase (GAPDH) was tested as a potential house-keeping gene correlating with the protein level fluctuations between the two cell populations. Indeed, immunoblots of total lysates probed for GAPDH showed a 40 % reduction of GAPDH levels in quiescent cells when equal numbers of lysed cells were loaded on an SDS gel, equivalent to the reduction of total protein levels per cell (Fig. 3.2.3D). When loaded volumes were adjusted to equal total protein levels, however,

GAPDH levels were the same in G1 and G0 cells, making GAPDH a suitable loading control for future immunoblots (Fig. 3.2.3D).

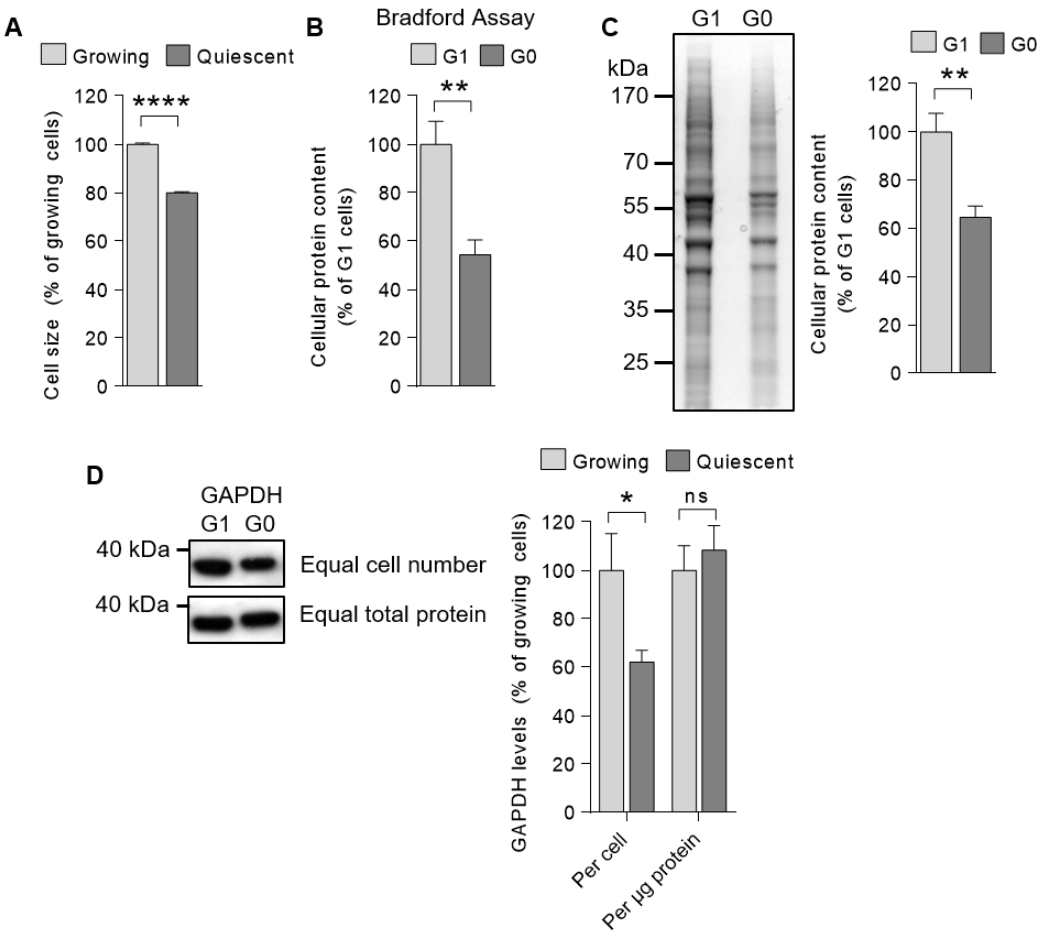


**Figure 3.2.3:** Size and protein content of quiescent RPE1 cells

**A:** Mean diameter of growing and quiescent RPE1 cells in suspension was measured with a haemocytometer. Bar graphs represent mean + SEM from n=15 (growing cells) and n=11 (quiescent cells) biological replicates. **B:** Protein concentration measurement using Bradford assay. G0 and FACS-sorted G1 cells were lysed in 8 M urea, with volumes adjusted to cell numbers. Bar graphs represent mean + SEM from n=4 biological replicates. **C:** Representative lanes of Coomassie blue-stained SDS-PAGE gel with lysates from G0 and FACS-sorted G1 cells lysed in equal volumes of 8 M urea per cell number (left). Colour intensity per lane was quantified by densitometry measurement and normalised to G1 cells (right). Bar graphs represent mean + SEM from n=5 biological replicates. **D:** Representative immunoblots of total lysates from FACS sorted G1 and G0 RPE1 cells probed against GAPDH (left). The upper blot shows loading normalised to cell number, the lower blot shows loading normalised to total protein levels. GAPDH levels per band were quantified by densitometry measurement Bar graphs represent mean + SEM from n=5 (per cell) or n=6 (per µg protein) biological replicates. Statistical significances in **A**, **B**, **C** and **D** were tested with Student's unpaired two-tailed t-test comparing G0 to G1 cells. ****P < 0.0001, **, P < 0.01, *P < 0.05, ns, not significant.

### 3.2.3 Quiescent RPE1 cells exhibit low levels of cell cycle progression markers

To confirm the observations from the mass spectrometry screen (Fig. 3.2.2), cell biological and biochemical methods (immunofluorescence (IF) microscopy, flow cytometry and immunoblotting) were employed. IF microscopy of endogenous Cyclin D1 and Ki67 levels illustrates high levels of each protein in nuclei of growing RPE1 cells, but their absence in nuclei of quiescent cells (Fig. 3.2.4A). Quantification of Cyclin D1 and PCNA levels in immunoblots of total cell extracts of G1 and G0 cells revealed presence of Cyclin D1 and PCNA in quiescent cells, but total levels were sigificantly reduced to $27.0 \pm 5.6$ % for Cyclin D1 and to $9.3 \pm 1.2$ % for PCNA compared to G1 cells (Fig. 3.2.4B and C). Ki67 was almost absent in quiescent cells with levels being $5.4 \pm 2.0$ % of Ki67 levels in G1 cells (Fig. 3.2.4B and C).

The phosphorylation state of Rb was assessed by immunolabelling of PFA-fixed growing or quiescent cells with an antibody recognising Rb phosphorylated at Serines 807 and 811 (pRb), followed by flow cytometry analysis of the cell population with 2n DNA content. G1 cells exhibited two peaks of pRb fluorescence intensity, a 'low pRb' with cells featuring hypophosphorylated Rb not recognised by the antibody and a 'high pRb' peak with cells featuring phosphorylated Rb (Fig. 3.2.4D). Percentages of cells with hypophosporylated and phosphorylated Rb were identified by drawing gates on the respective peaks. 85.8 % of G1 cells exhibited high levels of phosphorylated Rb, compared to only 2.4 % of G0 cells. 96.7 % of G0 cells contained hypophosphorylated Rb. Interestingly, a small fraction (14.2 %) of G1 cells also exhibited hypophosphorylated Rb, marking a putative quiescent subpopulation within the G1 population of proliferating cells (Fig. 3.2.4D).

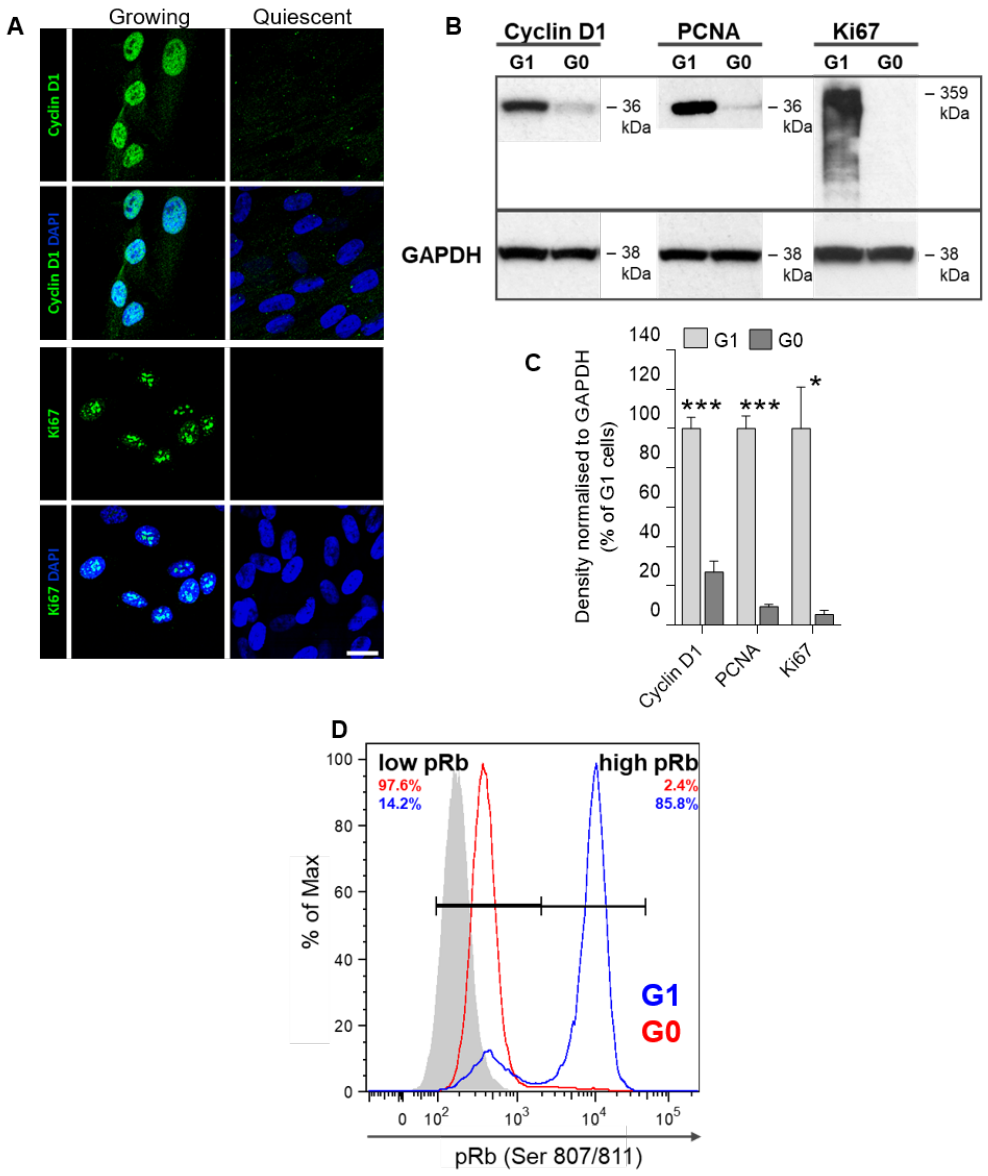


**Figure 3.2.4:** Cell cycle progression markers are down-regulated in quiescent RPE1 cells
**A:** Confocal microscopy sections of endogenous Ki67 and Cyclin D1 levels in nuclei of growing and quiescent RPE1 cells. Scale bar: 20 µm. **B:** Representative immunoblots of total lysates from G0 and FACS-sorted G1 cells probed against Cyclin D1, PCNA and Ki67. GAPDH served as loading control. **C:** Densitometry quantification of immunoblots in **B**. Band density was normalised to GAPDH and G1 cells. Bar graphs represent mean + SEM from n=3 biological replicates, Student's unpaired two-tailed t-test comparing G0 to G1 cells. ***P < 0.001, *P < 0.05. **D:** Histogram of Rb phosphorylated at Ser 807/811 (pRb) in G1 and G0 RPE1 cells. After elimination of cell doublets and dead cells, the population with 2n DNA content was used for further analysis. Gates used for pRb quantification are displayed. Percentages of G1 (blue) and G0 (red) cell populations with low and high pRb are listed in the left and right upper corner, respectively. Blank signal is shown in grey. A minimum of 50,000 cells per condition were analysed by flow cytometry.

### 3.2.4 DNA-RNA staining identifies an increased subpopulation with low RNA content in quiescent cells

As was evident from pRb labelling of proliferating cells, a cell population with 2n DNA content could be either reside G1 or G0 state of the cell cycle. The low mRNA content in quiescent cells due to their reduced transcriptional activity can be used to additionally discriminate between G1 and G0 subpopulations. According to the mass spectrometry screen, RNA Polymerase II expression was reduced in G0, supporting the hypothesis of decreased mRNA synthesis in quiescent RPE1 cells. Staining RNA with Pyronin Y (PY) and DNA with Hoechst 33342 in live cells was employed by several groups to distingruish G0 from G1 cells (Shapiro, 1981; Crissman *et al.*, 1985). PY is the xanthene homologue of Acridine Orange, a cell-permeant dye emitting green fluorescence (532 nm) when bound to double-stranded DNA and red fluorescence (637 nm) when bound to single-stranded DNA or RNA (Löber, 1981). Unlike Acridine Orange, PY is nonfluorescent both in solution and when bound to single-stranded nucleic acids (Kapuscinski & Darzynkiewicz, 1987). However, PY binds to double-stranded RNA, such as ribosomal RNA, with a four-fold higher affinity than to double-stranded DNA and emits red (565-574 nm) fluorescence when in complex with either nucleic acid (Kapuscinski & Darzynkiewicz, 1987). Thus, this method does not give a direct measurement of transcriptive activity, but considers that both mRNA and rRNA levels increase during progression through G1 phase and further when cells are dividing (Abelson *et al.*, 1974).

When staining growing and quiescent RPE1 cells for DNA and RNA content, the protocol of Shapiro (1981) was altered in that cells were fixed with 70 % ethanol before staining with Hoechst 33342 and PY to allow for better resolution of the DNA profile (Lemons *et al.*, 2010). Cells were analysed by flow cytometry and G0/G1, S and G2/M phase were identified in a DNA profile of Hoechst 33342 fluorescence as described for Fig. 3.2.1B. According to Crissman *et al.* (1985), G0 cells are the cell population with low DNA content (2n) and lower RNA content than S and G2/M cells. Following this definition, cells with 2n DNA and low or high RNA content will betermed 'low $G0^{lowRNA}$ or $G1^{hiRNA}$, respectively, in this subsection, to distinguish them from the terms G0 and G1 employed for the general quiescent and Gap1 cell cycle phases. In a linear Hoechst 33342 versus PY dotplot, gates were drawn around $G0^{lowRNA}$, $G1^{hiRNA}$, S and

G2/M phase subpopulations for growing and quiescent RPE1 cells (Fig. 3.2.5A). The upper threshold for the $G0^{lowRNA}$ subpopulation was variable according to RNA content of S phase cells (Lemons *et al.*, 2010). Quantification cell cycle distribution showed that in quiescent cells, the fraction of $G0^{lowRNA}$ cells was almost two-fold increased (53 ± 8 % versus 28 ± 1% in growing cells, Fig. 3.2.5B and C). S and G2/M phase populations in quiescent cells were negligibly small with 1.3 ± 0.3 % and 1.8 ± 0.7 % of the total population (Fig. 3.2.5B and C). Interestingly, the $G1^{hiRNA}$ subpopulation in growing cells was of equal size to the one in quiescent cells (Fig. 3.2.5B and C). These results imply, that not all quiescent cells contain low RNA levels to be classified $G0^{lowRNA}$.

To further validate the $G0^{lowRNA}$/$G1^{hiRNA}$ discrimination by DNA-RNA staining with a molecular marker, Hoechst-PY-stained cells were counterlabelled with an anti-pRb antibody recognising Rb phosphorylated at Serines 807 and 811. Cells were analysed by flow cytometry and cell cycle distribution was determined as described above. The colour code from Fig. 3.2.5A for cell cycle subpopulations was maintained when plotting the cells in a Hoechst 33342 versus pRb dotplot (Fig. 3.2.5D upper panel). In this visualisation, the majority of growing cells, including both $G0^{lowRNA}$ and $G1^{hiRNA}$ subpopulatios, exhibited high pRb levels (88.8 % and 73.1 %, respectively). Only 11.2 % of $G0^{lowRNA}$ subpoplation of growing cells had hypophosphorylated Rb. Interestingly, at least twice as many growing $G1^{hiRNA}$ cells (26.9 %) contained hypophosphorylated Rb. In contrast, the majority of quiescent $G0^{lowRNA}$ and $G1^{hiRNA}$ cells exhibited hypophosphorylated Rb (99.2 % $G0^{lowRNA}$ and 97.1 % $G1^{hiRNA}$ cells). Plotting pRb signal versus PY signal intensity confirmed the heterogenity of pRb phosphorylation in the $G0^{lowRNA}$ subpopulation of growing cells. Only 12 % of $G0^{lowRNA}$ cells exhibited hypophosphorylated Rb and twice as many $G1^{hiRNA}$ cells were also characterised by hypophosphorylated Rb (Fig. 3.2.5D lower panel). In quiescent cells, 99.2 % of the $G0^{lowRNA}$ subpopulation contained hypophosphorylated Rb, but a similar proportion of the $G1^{hiRNA}$ subpopulation (97.2 %) also contained hypophosphorylated Rb. This would suggest that the 99.2 % $G0^{lowRNA}$ cells with hypophosphorylated Rb present a *bona fide* G0 population with low DNA and RNA content and hypophosphorylated Rb. Next, pRb fluorescence intensity was plotted as a histogram of the cell cycle subpopulations identified in Fig. 3.2.5A with the pRb fluorescence signal normalised to the intensity of the peak fraction of each cell cycle subpopulation (Fig. 3.2.5E). The histogram for growing cells highlights that the majority of cells in each cell cycle phase contained pRb (precise quantifications for hypophos-

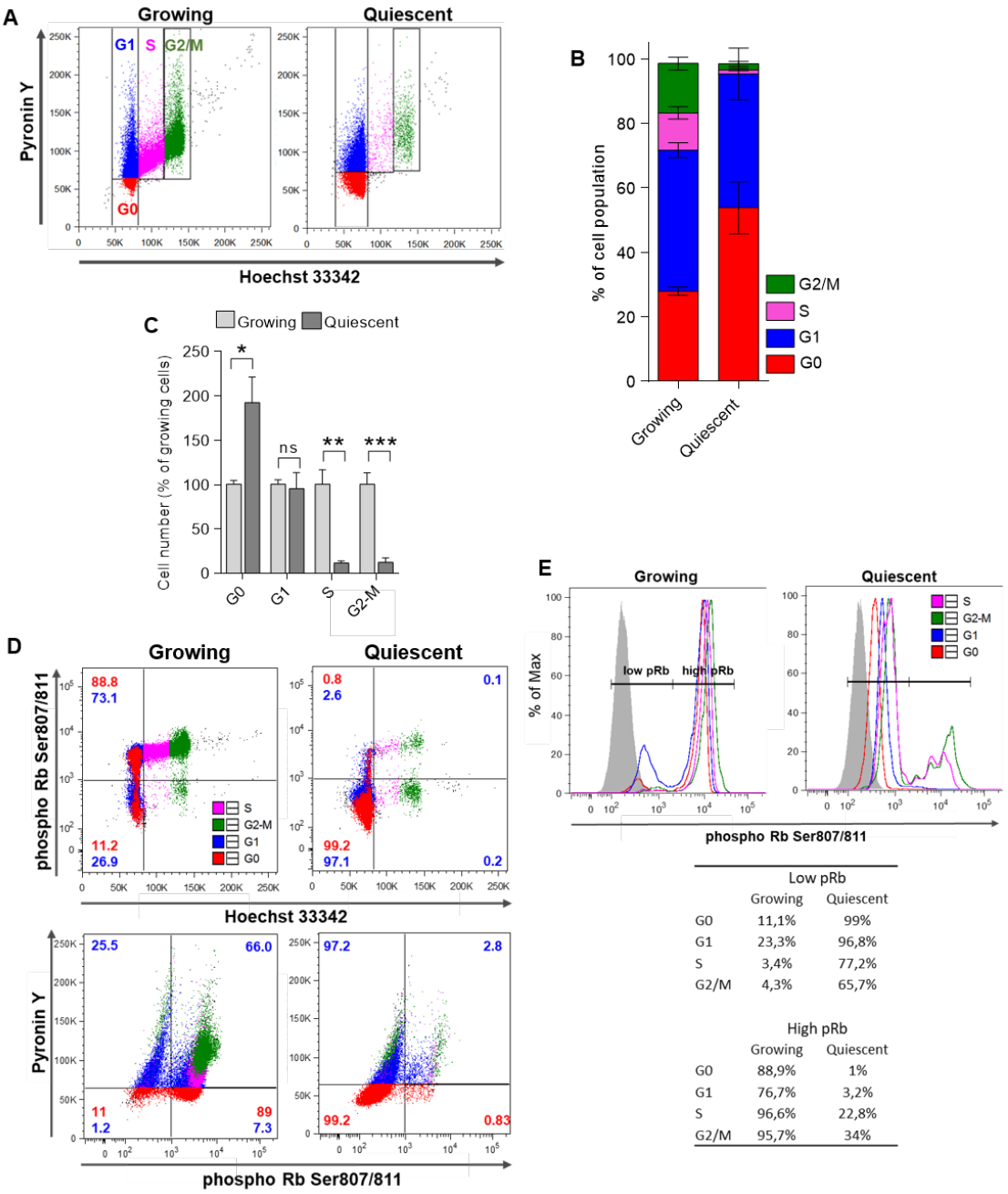


| Low pRb | Growing | Quiescent |
|---|---|---|
| G0 | 11,1% | 99% |
| G1 | 23,3% | 96,8% |
| S | 3,4% | 77,2% |
| G2/M | 4,3% | 65,7% |

| High pRb | Growing | Quiescent |
|---|---|---|
| G0 | 88,9% | 1% |
| G1 | 76,7% | 3,2% |
| S | 96,6% | 22,8% |
| G2/M | 95,7% | 34% |

**Figure 3.2.5:** Identification of a *bona fide* G0 population with DNA-RNA (Hoechst-Pyronin Y) staining and pRb colabelling

**A:** Representative dot plot of DNA (Hoechst 33342) and RNA (Pyronin Y) levels in growing and quiescent RPE1 cells with identified cell cycle phases $G0^{lowRNA}$, $G1^{hiRNA}$, S and G2/M. Cells were fixed in 70 % ethanol and stained with 2 µg/ml Hoechst 33342 and 4 µg/ml Pyronin Y. A minimum of 50,000 cells were analysed by flow cytometry. **B:** Quantification of cell cycle distribution from **A.** Column charts show mean ± SEM from n=4 biological replicates with 2 technical repeats. **C:** Cell cycle populations from **A** are represented relative to populations in growing cells as mean + SEM from n=4 biological replicates with 2 technical repeats, ***P < 0.001, **P < 0.01, *P < 0.05, ns, not significant, Student's unpaired two-tailed t-test comparing quiescent to growing cells. **D:** Flow cytometry analysis of levels of Rb phosphorylated at Serines 807 and 811 (pRb) in cell cycle phases identified by Hoechst-Pyronin Y staining. Growing and quiescent RPE1 cells were fixed with 70 % ethanol, immunolabelled for pRb and subsequently stained for DNA and RNA content as described in **A**. Dot plots represent pRb versus DNA levels (upper panel) and pRb levels versus RNA levels (lower panel). Low and high pRb levels (identified by quadrants) were quantified in cells identified as $G1_{hiRNA}$ (blue) and $G0_{lowRNA}$ (red) by Hoechst-Pyronin Y staining as percentage of the whole subpopulation. A minimum of 50,000 cells were analysed. **E:** Histograms and quantification of high and low pRb levels in cell cycle phases discriminated by Hoechst-Pyronin Y staining. Blank signal is shown in grey.

phorylated 'low pRb' and pRb 'high pRb' are below the histogram). In quiescent cells, however, the majority of each cell cycle subpopulation, including S and G2/M phase cells, exhibited hypophosphorylated Rb, with the peak of $G0^{lowRNA}$ cells at a slightly lower pRb intensity than all other subpopulations.

This experiment demonstrates that quiescence entry mediated by contact inhibition-mitogen withdrawal increased the population of low RNA-containing RPE1 cells. However, this $G0^{lowRNA}$ population did not correlate with the molecular cell cycle marker pRb. Rb was primarily hypophosphorylated both in the low and high RNA subpopulations in quiescent cells, whereas the $G0^{lowRNA}$ subpopulation in growing cells featured primarily phosphorylated Rb.

## 3.3 Discussion

### 3.3.1 RPE1 cells as an in vitro model for proliferative quiescence

Quiescent cells have been studied both *in vitro* and *in vivo*. However, the majority of cells with innate quiescence features (naïve lymphocytes, dormant stem cells, dormant cancer stem cells) are difficult to maintain *ex vivo* in cell culture systems for long term studies (Cheng *et al.*, 2000a; Orford & Scadden, 2008; Malumbres & Barbacid, 2001). Quiescence can be induced in proliferating primary cells, such as fibroblasts, by contact inhibition and mitogen withdrawal (Coller *et al.*, 2006). A quiescent state induced by these methods is more close to the physiological state of epithelial cells than perturbation by chemical compounds as shown in Crissman *et al.* (1985).To overcome the difficulties of working with primary cells, such as batch variations and variations between early and late passages, it was tested whether a non-transformed hTERT-immortalised retina pigmented epithelial cell line (RPE1 cells) can substitute primary cells to serve as a quiescence model to establish and optimise future experiments. RPE1 cells exhibit a stable diploid karyotype and are sensitive to contact inhibition (ATCC documentation). Being subjected to a combination of contact inhibition and mitogen withdrawal, RPE1 cells reversibly exited the cell cycle, halted DNA replication in G1 phase (evident by their diploid genome, Fig. 3.2.1) and were smaller and contained less protein (Fig. 3.2.3). Reduced size, and thus protein content, has been reported for multiple quiescent cell types (Yusuf & Fruman, 2003; Marguerat *et al.*, 2012) and might be a consequence of

low mTORC1 activity during quiescence and thus lacking growth stimulation (Laplante & Sabatini, 2012; Adhikari *et al.*, 2010; Gan & DePinho, 2009). Reduced mTORC1 activity in quiescent RPE1 cells was suggested in the SILAC mass spectrometry screen, which identified reduced phosphorylation of Serine 183 in the proline-rich Akt substrate of 40 kilodaltons (PRAS40) mTORC1 substrate. Hypophosphorylated PRAS40 binds to the RAPTOR subunit of mTORC1 and prevents its signalling in response to growth factors, potentially preventing fast responsiveness of quiescent cells to growth factor stimuli (Oshiro *et al.*, 2007; Hsu *et al.*, 2011). In addition to reduced growth signalling, the decreased expression of cell cycle progression markers in quiescent RPE1 cells could be shown by multiple methods (Fig. 3.2.1,Fig. 3.2.2 and Fig. 3.2.4) and is in agreement with the literature, which reports reduced Cyclin D1 (Wang *et al.*, 2011), PCNA (Cheung & Rando, 2013), absence of Ki67 (Jensen & Watt, 2006) and hypophosphorylated Rb (Leibundgut *et al.*, 2005) in naturally quiescent stem cells. Quiescent RPE1 cells also exhibited low CDK2 levels, confirming the theory of Spencer *et al.* (2013), that CDK2 is involved in the proliferation-quiescence decision. PRb labelling identified a subpopulation of growing cells with hypophosphorylated Rb (Fig. 3.2.2C). Since fully phosphorylated Rb is required for cell cycle progression, this population might reside in a spontaneous, short term quiescence (Knudsen & Wang, 1996). Proliferating cells can spontaneously enter a quiescent state under optimal growth conditions, pointing towards intrinsic, albeit unknown, features regulating this process (Gookin *et al.*, 2017). Gookin *et al.* also showed that cells spontaneously exiting the cell cycle exhibited increased levels of Cyclin D1 compared to cells residing in 'deep' longterm quiescence, which marks them as different from cells residing in a 'deep' quiescent state like dormant stem cells or cells entering quiescence by contact inhibition and mitogen withdrawal.

### 3.3.2 DNA-RNA staining as a tool to discriminate between G0/G1 populations of the cell cycle

DNA-RNA staining with Hoechst33342 and PY has been a long-standing method developed by Shapiro (1981) to discriminate between G1 and G0 cells in a heterogenic cell population and was employed successfully by Srour & Jordan (2002) to sort viable quiescent hematopoietic stem cells. It is also acknowledged in the recent volume of Methods in Molecular Biology (Eddaoudi *et al.*, 2018). DNA-RNA staining, like pRb

labelling, identified a small low-RNA population within growing RPE1 cells (Fig. 3.2.5). Surprisingly, according to this method, only about half the quiescent cells were identified as $G0^{lowRNA}$ (Fig. 3.2.5). The size of the $G0^{lowRNA}$ subpopulation was larger than the one in growing cells and agrees with the data from Lemons *et al.* (2010), but contradicted the 97 % quiescent cells with hypophosphorylated Rb (Fig. 3.2.2). In contrast, the majority of the $G0^{lowRNA}$ subpopulation in growing cells was still characterised by high pRb levels and a proportion of growing $G1^{hiRNA}$ cells featured, unexpectedly, hypophosphorylated Rb (Fig. 3.2.5). These results are in conflict with hyposphorylated Rb-mediated cell cycle exit (Ren & Rollins, 2004). Both the $G0^{lowRNA}$ and $G1^{hiRNA}$ cells in the quiescent population featured hypophosphorylated Rb, which means that all cells left the cell cycle because cell cycle progression cannot occur without Rb phosphorylation and activated cell cycle progression transcription factors (Ren & Rollins, 2004). Furthermore conflicting with the role of pRb in cell cycle progression, the majority of the $G0^{lowRNA}$ subpopulation of growing cells featured phosphorylated, and a proportion of the $G1^{hiRNA}$ subpopulation hypophosphorylated Rb (Fig. 3.2.5). The model of low RNA content for cell cycle exit might thus not be enough to conclude on a *bona fide* quiescent population, because the results presented here show that the identified $G0^{lowRNA}$ and $G1^{hiRNA}$ did not feature the corresponding levels of at least one cell cycle progression marker. This suggests that DNA-RNA staining might only be suited for cells residing in a natural quiescent state like dormant stem cells and naive lymphocytes, for which it has been successfully implemented (Fukada *et al.*, 2007; Srour & Jordan, 2002). However, it should be considered that fluorescent Pyronin Y does not represent single-stranded mRNA, but double-stranded rRNA and thus gives an indirect measurement of transcriptional activity (Kapuscinski & Darzynkiewicz, 1987). Therefore, if possible, the use of multiple molecular markers might be preferred to characterise the quiescent state, as it shed light on active or inactive cell cycle progression.

## 3.4 Conclusions

Proliferative quiescence is a naturally occuring state in which many cells in the adult mammalien body reside. Although first mentioned four decades ago, mammalian quiescent cells have attracted attention only recently when characterised to actively maintain the quiescent state (Coller *et al.*, 2006; Quinlan & Hochstadt, 1977). The work in this

chapter proposes RPE1 cells as an *in vitro* cell line model for proliferative quiescence. A robust protocol was developed to induce quiescence in RPE1 cells, upon which expression or phosphorylation of cell cycle progression markers was reduced. DNA-RNA staining to distinguish between G0 and G1 cells in a mixed population appears to be a controversial method, as it does not correlate with molecular cell cycle progression markers such as phosphorylation of Rb. Although DNA-RNA staining suggests that only part of the quiescent cells reside in a $G0^{lowRNA}$ state with reduced RNA content, the homogeneous down-regulation of cell cycle progression markers, including hypophosphorylation of Rb, whose full phosphorylation is essential for cell cycle progression, implies that all cells have exited the cell cycle. Counterlabelling of subpopulations identified by DNA-RNA staining with further cell cycle progression markers might thus be the method of choice when identifying a *bona fide* quiescence population, although this method is not applicable for intracellular markers when sorting live cells. Growth arrest in G1 phase, down-regulation of cell cycle progression markers and reduction of size and protein content were, however, encouraging evidence for us to use RPE1 cells are a suitable *in vitro* cell line model to study molecular processes in quiescent cells.

# 4 Endocytosis during proliferative quiescence

## 4.1 Introduction

### 4.1.1 Endocytic pathways

Endocytosis mediates vital cellular processes, such as nutrient uptake, receptor level regulation, plasma membrane turnover, polarisation, migration and signalling (Barbieri *et al.*, 2016). It is therefore indispensible for cellular survival and ubiquitously present in eukaryotic cells. During endocytosis, plasma membrane invaginations of varying sizes and shapes, which contain the cargo to be internalised, are generated, pushed away from the plasma membrane into the cytoplasm and finally severed to form endocytic vesicles. Various mechanisms exist for endocytic carrier formation and are distinguished according to carrier size, proteins involved and actin dependence. Clathrin-mediated endocytosis (CME) is characterised by Clathrin triskelia forming a coat around the nascent vesicle (McMahon & Boucrot, 2011; Kaksonen & Roux, 2018). Constituting the major endocytic pathway in eukaryotic cells, it occurs constitutively and is involved in many house-keeping functions (Schmid, 1997; Bitsikas *et al.*, 2014; Loerke *et al.*, 2009). Multiple Clathrin-independent pathways exist in parallel to CME, adapted to specific cargoes and cellular functions (Ferreira & Boucrot, 2018). FEME was only recently discovered and describes fast internalisation of activated receptors into Endophilin-positive carriers (Boucrot *et al.*, 2015). Cholera and Shiga toxin deform the membrane by clustering their receptors GM1 and Gb3, respectively, in the outer membrane leaflet in a process called the GL-Lect hypothesis of endocytic carrier formation (Johannes *et al.*, 2016). Macropinocytosis, also termed fluid-phase uptake, describes receptor-independent internalisation of cargo by actin-dependent membrane

ruffling, which generates membrane protrusions folding back upon themself and engulfing large amounts of cargo in micrometre-sized carriers (Buckley & King, 2017).

### 4.1.2 Endocytosis in quiescent cells

Unlike proliferating cells, quiescent cells do not depend on endocytosis for growth factor signalling to continue cell division, such as mitogen-dependent RTK signalling (Davies & Ross, 1980). Several mechanisms have been reported in quiescent cells, which down-regulate growth factor signalling-inducing endocytic events, such as inactivation of RTK adaptors (Nakayama *et al.*, 2013), stabilisation of receptors at the cell surface (Shimizu *et al.*, 2017) or decreasing cell surface receptor levels by endocytosis and subsequent receptor degradation (Koo *et al.*, 2012). However, quiescent cells still need to respond to growth factor signalling upon stimulation for cell cycle entry. Some cell types develop a primary cilium upon quiescence entry, with a ciliary pocket characterised by high endocytic activity, which serves as sensor for the cell's environment (Molla-Herman *et al.*, 2010). Cell-cell junctions of confluent, polarised cells, such as epithelial and endothelial cells, can be disrupted by acute endocytosis-mediated growth factor-signalling upon stimulation with high concentrations of mitogens (Nimlamool *et al.*, 2015). Endocytosis, however, is not only a means to exit the quiescent state but also serves cell type-specific functions or enables quiescence maintenance. Examples for the former are transport across the endothelial cell wall, involving CME and Clathrin-independent pathways (Rodriguez-Boulan *et al.*, 2005; Fung *et al.*, 2017) or nutrient acquisition and storage by Clathrin-dependent and -independent pathways (Steer & Klausner, 1983; Kanai *et al.*, 2014). Endocytosis is crucial for quiescence maintenance and survival, as was shown for CME (Snyder *et al.*, 2017; Muranen *et al.*, 2017) and requirement of dynamin in quiescent cells (Nagy *et al.*, 2016). Although the presence of endocytic pathways have been reported for quiescent cells, to date there have been no studies conducted on how their activity compares to proliferating cells. In this chapter, quiescent RPE1 cells are used to measure endocytosis in quiescent cells and establish its relation to proliferating cells.

## 4.2 Results

### 4.2.1 SILAC mass spectrometry analysis of proteins involved in CME

A SILAC mass spectrometry screen comparing the proteome of G0 and FACS-sorted G1 RPE1 cells provided an overview of the levels of proteins involved in endocytosis. Many proteins of the CME machinery, as well as CME cargo are known (Kaksonen & Roux, 2018). The screen revealed that proteins of the core CME machinery, FCHo2, AP2 subunits, Clathrin heavy chain and Dynamin 2 did not differ betewen the two cell cycle states, defined by the applied threshold of ± one Log2 unit, which is equivalent to 2-fold up- or downregulation (often applied for biological significance in mass spectrometry experiments; Mann & Kelleher, 2008) (Fig. 4.2.1). However, total levels of receptors known to be internalised by CME (TfR1, LDLR and EGFR) were decreased in G0. Interestingly, levels of the TfR1 ligand Transferrin were elevated during G0, as were those of Lamp1, which is known to have an AP2 binding site (Fig. 4.2.1; Janvier & Bonifacino, 2005). Because the mass spectrometry screen did not identify consistent up- or downregulation of proteins involved in CME, it was difficult to conclude on CME activity in G0. Moreover, as protein abundance does not necessarily prove their activity, endocytosis of CME cargo was assessed in functional assays.

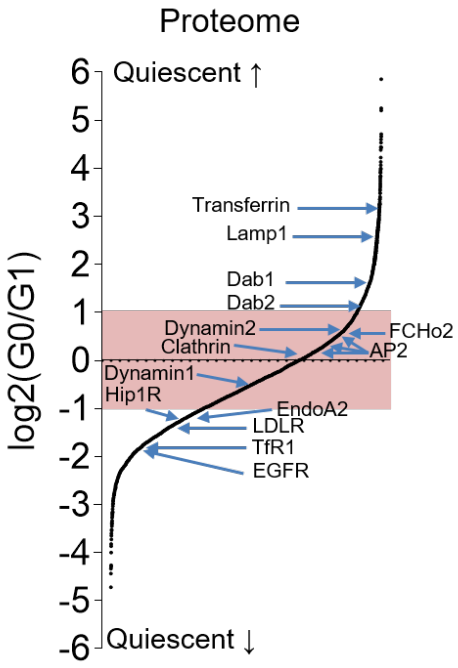


**Figure 4.2.1:** SILAC mass spectrometry analysis of proteins involved in CME
Results of a SILAC mass spectrometry screen comparing the proteome of G1 and G0 RPE1 cells. Displayed is the log2 ratio of protein levels in G0 relative to levels in G1. G1 cells were sorted by flow cytometry from proliferating cells. Identified key proteins involved in CME are indicated. The ± one Log2 unit zone marked in red is considered to contain proteins whose levels did not differ (Mann & Kelleher, 2008).

### 4.2.2 Measuring endocytosis

Endocytosis can be quantified by measuring how much cargo a cell has internalised within a specified time period. Cargo internalised by cells can be assessed by measuring cellular content of fed radioactive isotope-labelled cargoes by radioblot (Brown & Goldstein, 1975) or quantifying fluorescence intensity in cells fed with fluorescence-conjugated cargoes, an approach preferrably used nowadays (Sager *et al.*, 1984). Fluorescence intensity can be quantified by flow cytometry, which allows for quantification of large cell numbers, or by fluorescence microscopy, which gives additional spatial information, but is limited to quantification of lower cell numbers. Whereas flow cytometry analysis delivers a robust quantification of data across a large cell population, the number of samples processed at the same time is limited by time-consuming sample preparation (cell harvesting, washes are carried out by centrifugation with risk of cell loss). Furthermore, flow cytometry measures fluorescence emission from the whole cell excited by a short laser pulse, which might not be sensitive enough to measure small differences in dyes with weak fluorescence intensities due to instrument error and cell-intrinsic autofluorescence.

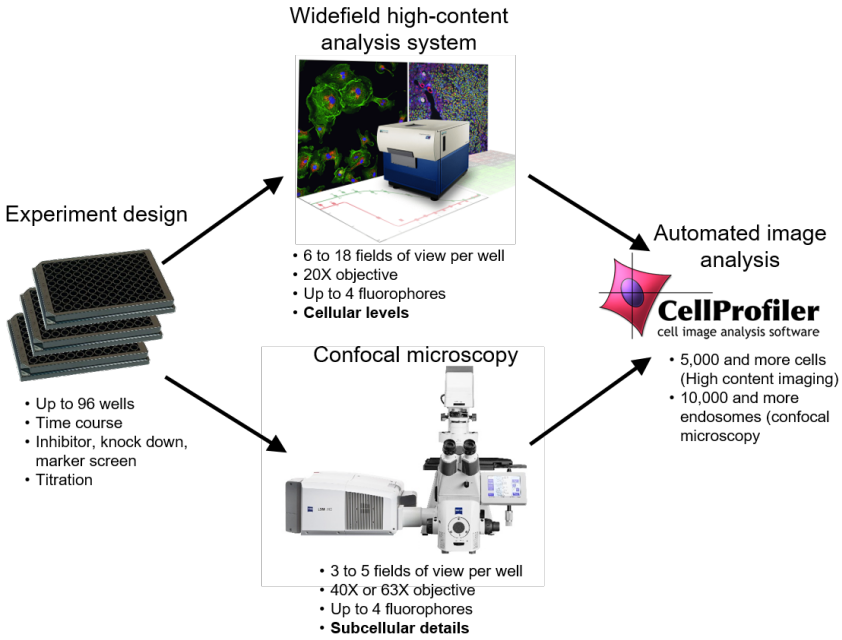


**Figure 4.2.2:** Workflow of high-thoughput experiment analysis by microscopy and automated image analysis
96 well multiwell plates were used to test for multiple conditions in parallel. Experiments can be analysed by high-content imaging with a widefield fluorescence microscope, which allows for imaging of large numbers of cells, or confocal microscopy, which allows for high intracellular resolution. Images from both imaging methods can be quantified objectively by automated image analysis using CellProfiler, resulting in quantification of thousands of cells (high-content microscopy) or thousands of organelles in up to 100 cells (confocal microscopy).

The development of automated high-content microscopy in conjunction with automated image analysis allows for quantification of fluorescence signal in specified regions within a cell, thereby omitting non-specific areas containing autofluorescence. Using multiwell plates, multiple conditions can be tested at the same time, such as cargoes, time points or inhibitors (Fig. 4.2.2). Experiments can then be imaged by automated widefield microscopy for high throughput of cell numbers or by confocal microscopy to analyse subcellular details such as colocalisation (Fig. 4.2.2). Using CellProfiler software, cells can be segmented and fluorescent dye-containing organelles identified and quantified in thousands of cells (widefild high content microscopy) or thousands of organelles (confocal microscopy), allowing for objective quantification across large populations (Fig. 4.2.2; Carpenter *et al.*, 2006).

When measuring receptor-mediated endocytosis, it is important to consider cell surface receptor levels. A cell expressing low cell surface receptor levels has a reduced ligand-binding capacity than a cell with high cell surface receptor levels. After a specific duration (for example 15 min), a cell with low ligand-binding capacity will internalise less ligands than a cell with high ligand-binding capacity (Fig. 4.2.3). Normalising inter-

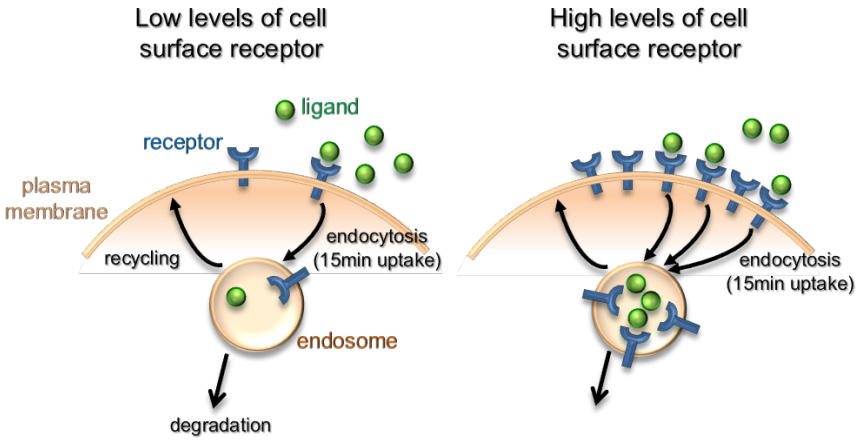


**Figure 4.2.3:** Schematic of ligand internalisation in cells with differing levels of cell surface receptors
For the same uptake duration, cells with low levels of cell surface receptors bind and internalise less ligands than cells with high levels of cell surface receptors.

nalised ligand or receptor to cell surface levels produces more accurate information on endocytic activity, as it measures both the available cargo at the cell surface and the fraction which was internalised (Marsh, 1993).

### 4.2.3 Clathrin-mediated endocytosis

#### 4.2.3.1 Endocytosis of transferrin, LDL and EGF is decreased during quiescence

To date, CME is the best characterised endocytic pathway, and a number of known CME cargoes exist. Among these are Tf, LDL and EGF (Anderson *et al.*, 1977; Pearse, 1982; Hanover *et al.*, 1984; Jing *et al.*, 1990). Growing and quiescent RPE1 cells were incubated with fluorescent dye-conjugated Tf, LDL and EGF for 15 min at 37 °C to allow for ligand internalisation. Cells were then placed on ice to prevent further uptake. Unbound ligand was removed by PBS washes, cell surface-bound ligand was stripped with acidic buffer and cells were fixed and nuclei stained with DAPI to identify separate cells in fluorescence microscopy images, or with Hoechst 33342 for flow cytometry to discriminate between G0/G1, S and G2/M phase cells. The confocal microscopy images in Fig. 4.2.4A visualise that, after 15 min, quiescent cells internalised less fluorescence-conjugated Tf, LDL and EGF than proliferating cells. Uptake of fluorescence-conjugated Tf, LDL and EGF was quantified by flow cytometry. G0 cells internalised at least 85 % less ligand than G1 cells (Fig. 4.2.4B).

Fluorescence intensity of internalised ligand was then normalised to either cell surface-bound ligand or cell surface receptor levels identified by labelling live cells at 4 °C with

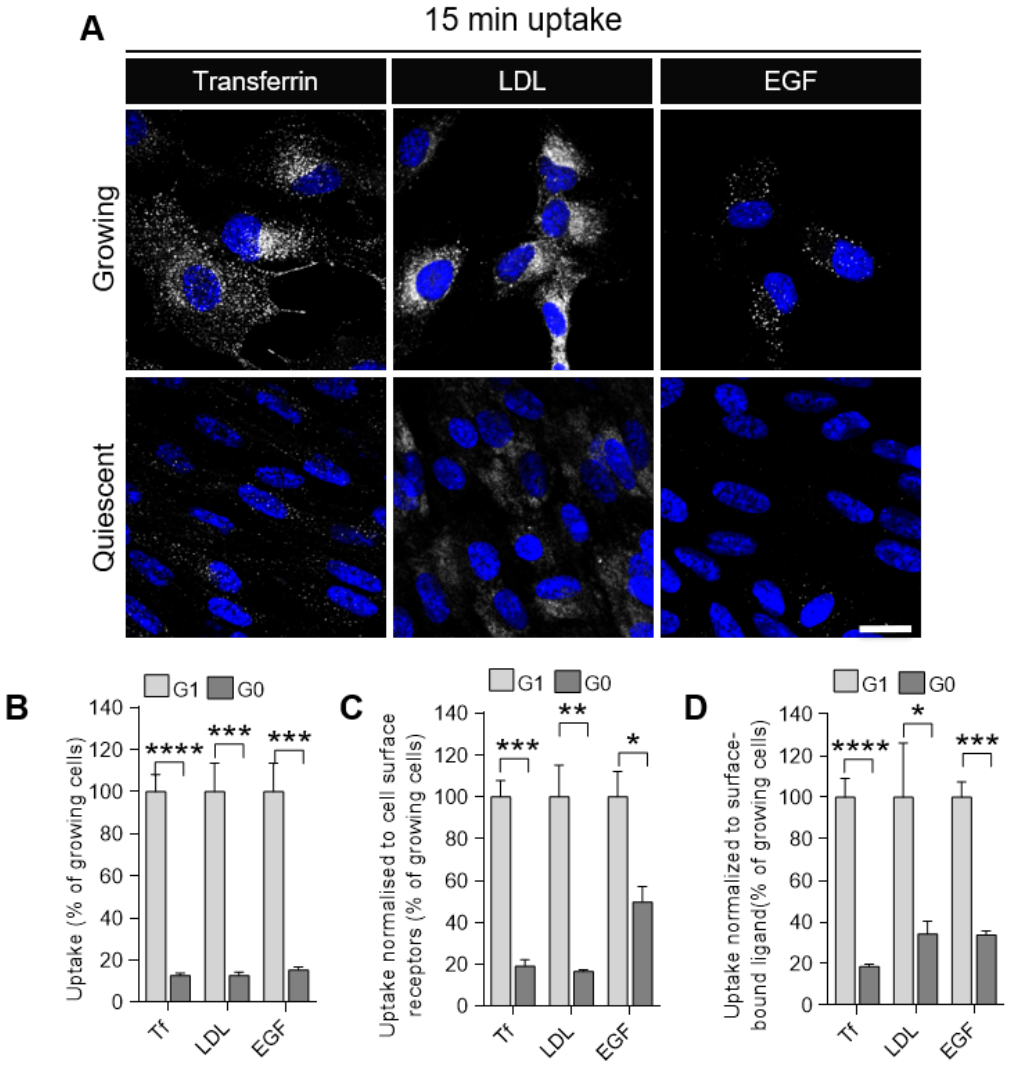


**Figure 4.2.4:** Uptake of transferrin, LDL and EGF in growing and quiescent RPE1 cells
**A:** Confocal microscopy sections of growing and quiescent RPE1 cells after 15 min uptake of fluorescence-conjugated transferrin (200 µg/ml), LDL (5 µg/ml) and EGF (50 ng/ml). Surface-bound ligand was removed by acidic washes. Cells were fixed with 4 % PFA and nuclei stained with DAPI (blue pseudocolour). Scale bar: 20 µm. **B:** Quantification of fluorescence-conjugated ligand uptake in G1 and G0 RPE1 cells by flow cytometry. Cells were treated as in **A**. Geometrical means of fluorescence intensity were normalised to blank signal and G1 cells and plotted in bar graphs as mean + SEM from n=4 biological replicates with a minimum of 5,000 RPE1 cells with 2n DNA content per sample. **C:** Cell surfaces were immunolabelled on ice with anti-TfR1, LDLR or EGFR antibodies. Ligand uptake from **B** was normalised to levels of respective cell surface receptors, transferrin to TfR1, LDL to LDLR and EGF to EGFR. Bar graphs represent mean + SEM from n=4 (LDL) or n=3 (transferrin, EGF) biological replicates with a minimum of 5,000 RPE1 cells with 2n DNA content per sample. **D:** Cells were incubated on ice with fluorescence-conjugated transferrin (200 µg/ml), LDL (5 µg/m) or EGF (50 ng/ml) and fixed with 4 % PFA. Nuclei were stained with DAPI. Ligand uptake from **B** was normalised to levels of respective cell surface-bound ligand. Bar graphs represent mean + SEM from n=4 biological replicates with a minimum of 5,000 RPE1 cells with 2n DNA content per sample. Data in **B**, **C** and **D** were tested for statistical significance with Student's unpaired two-tailed t-test; ****P < 0.0001, ***P < 0.001, **P < 0.01, *P < 0.05.

either fluorescence-conjugated ligand or anti-TfR1, anti-LDLR or anti-EGFR (EGFR dimerised upon activation by EGF-binding), respectively. Cell surface receptor levels in G1 cells were lower than in G0 cells, but endocytosis of Tf and LDL normalised to surface levels was at least 80 % lower than in growing cells and endocytosis of EGF was reduced by approximately 50 % (Fig. 4.2.4C). Uptake normalised to levels of cell surface-bound ligand confirmed reduced endocytosis during G0, with almost 90 % reduction for Tf and approximately 65 % reduction for LDL and EGF (Fig. 4.2.4D).

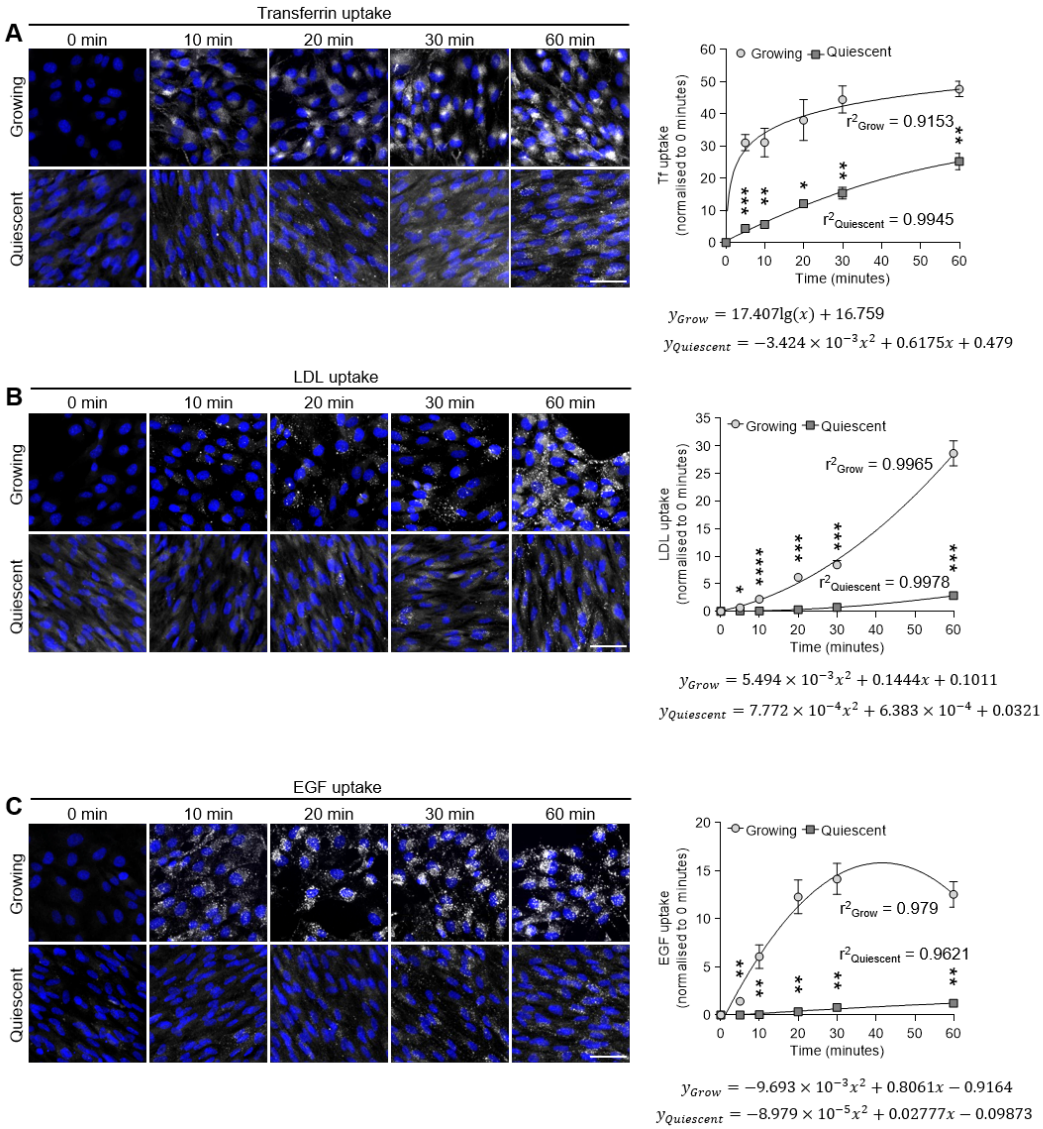


**Figure 4.2.5:** Uptake rate of transferrin, LDL and EGF in growing and quiescent RPE1 cells
Left: Representative epifluorescence microscopy images of transferrin-AlexaFluor555 (200 µg/ml; **A**), LDL-DiO (15 µg/ml; **B**) and EGF-AlexaFluor647 (50 µg/ml; **C**) uptake (represented in white) in growing and quiescent RPE1 cells at multiple time points. Surface-bound ligand was removed by acidic washes. Cells were fixed with 4 % PFA and nuclei stained with DAPI (blue pseudocolour). Scale bars: 50 µm. Right: Internalised ligand per cell was quantified in epifluorescence microscopy images and data plotted as mean ± SEM from n=3 biological replicates with a minimum of 8,000 growing and 16,000 quiescent cells per sample; ***P < 0.001, ***P < 0.001, **P < 0.01, *P < 0.05, Student's unpaired two-tailed t-test comparing quiescent with growing cells. Uptake rate curves were fitted according to the highest coefficient of determination ($r^2$). Respective functions and $r^2$ are shown for growing and quiescent cells.

To test whether uptake of Tf, LDL and EGF was only reduced for the observed timepoint of 15 min, time-course experiments were performed measuring ligand internalisation from 5 to 60 min. During this time, other cell-biological processes such as recycling and degradation will affect the observed amount of internalised ligand. Since we were interested whether quiescent cells would accumulate the same amount of ligand as proliferating cells over a longer period of time, additional trafficking of degradative processes would not interfere with the interpretation of results. Ligand uptake assays were performed as described above but analysed by high-throughput epifluorescence image acquisiton and automated image analysis across the whole population of proliferating (growing) or quiescent RPE1 cells. Only 'puncta' of fluorescent ligand were considered for quantification to omit cell-intrinsic autofluorescence from the analysis. Autofluorescence in yellow wavelengths is higher in quiescent cells (visible as white haze in quiescent cell images in Fig. 4.2.5A and B, reported in Cho & Hwang, 2012) and would lead to an overestimation of internalised ligand fluorescence. Uptake of Tf in growing cells occured fast within the first 10 min, reaching 50 % of the maximum uptake at 60 min after almost 5 min, whereupon the rate increased more slowly, which can be described by a logarithmic function (Fig. 4.2.5A). The logarithmic nature of Tf uptake is due to a steady-state of Tf gain by endocytosis and Tf loss by recycling or degradation. Tf uptake in quiescent cells followed an downward-opening quadratic parabola with a steeper slope than Tf uptake in growing cells after 10 min, but due to a slowly decreasing rate, even after 60 min uptake, Tf intensity per cell remained half that of growing cells (Fig. 4.2.5A). LDL uptake in growing cells continually increased following a quadratic function with a significantly steeper slope in growing than in quiescent cells (Fig. 4.2.5B), indicating a continuous acquisition of ligand without loss due to degradation or recycling. After 60 min, however, at least some degradation of LDL would be expected. LDL was labelled by the lipophilic carbocyanine derivative DiI, which might have diffused into cellular membranes and remained there, continuing to emit fluorescence, after LDL was degraded in lysosomes (Reynolds & St. Clair, 1985). Thus, DiI-LDL uptake represents accumulation of LDL over time, without effects of LDL degradation or recycling. In quiescent cells, LDL uptake was strongly decreased for all assessed timepoints (Fig. 4.2.5B). EGF uptake was also strongly decreased in quiescent cells during the 60 min time course (Fig. 4.2.5C). EGF uptake rate in growing cells was described by a downward-opening parabola, with maximum EGF content per cell at

around 40 min. After 40 min, degradation might have outweighed acquisiton of EGF, likely due to a loss of cell surface receptor levels due to increased stimulated EGFR endocytosis and degradation (surface-levels of EGFR were not assessed), as reported in Vieira *et al.* (1996). Only little EGF accumulated in quiescent cells over the time course of 60 min, with an uptake rate described by a downward-opening parabola with a very small slope (Fig. 4.2.5C). Summarised, over a time course from 5 to 60 min, quiescent cells accumulated less Tf, LDL and EGF than proliferating cells at all time points.

#### 4.2.3.2 Level of core proteins of the Clathrin-machinery are elevated during quiescence

Down-regulated expression of core proteins of the CME machinery as cause for the reduced endocytosis of CME cargo could be excluded by the SILAC mass spectrometry screen results, which suggested little difference of CME machinery levels between G1 and G0 RPE1 cells (Fig. 4.2.1). The screen results were verified by cell biological and biochemical methods (immunofluorescence and immunoblotting) to exclude the possibility of the levels of CME machinery proteins presenting a bottleneck for CME activity in quiescent cells. Confocal microscopy sections of growing and quiescent RPE1 cells immunolabelled for FCHo2 or α-adaptin suggests that both proteins were actually present in significantly higher levels in quiescent cells (Fig. 4.2.6A). Flow cytometry analysis of G1 and G0 RPE1 cells confirmed that FCHo2 and α-adaptin levels were increased in G0 (Fig. 4.2.6B). Additionally, flow cytometry analysis showed that μ2-adaptin and Clathrin heavy chain levels were also increased in G0 (Fig. 4.2.6B). Immunoblots of total lysates of G0 and FACS-sorted G1 RPE1 confirmed elevated levels of FCHo2, α- and μ2-adaptin in G0 cells (Fig. 4.2.6C and D). In both flow cytometry analysis and immunoblots, FCHo2 levels were significantly increased by about 50 % and levels of AP2 subunits α and μ2 by at least 100 % in G0. Additionally, flow cytometry analysis revealed a 72 ± 3 % increase in Clathrin heavy chain levels in G0 cells.

These results suggest that the decreased endocytosis of multiple CME cargoes might not be caused by a shortage of CME machinery core proteins forming CCPs. Of course, many more proteins such as intersectins, Hip1/R and Epsin1/2 are involved in CME and were not tested. However, the fact that the levels of proteins most central to CME were

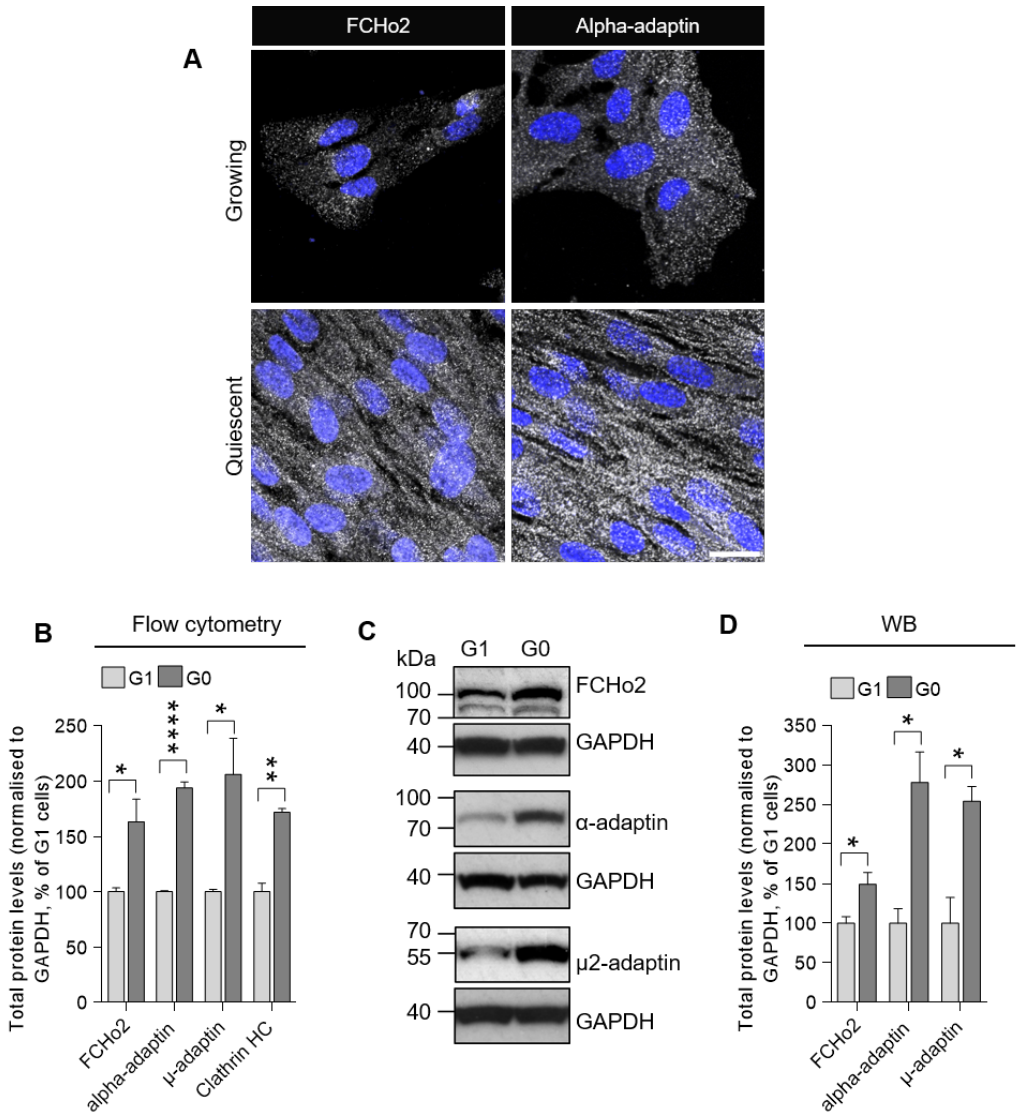


**Figure 4.2.6:** Levels of core proteins of the CME machinery in growing and quiescent RPE1 cells
**A:** Confocal microscopy sections of immunolabelled FCHo2 and alpha adaptin in growing and quiescent RPE1 cells. Nuclei are represented in blue pseudocolour. Scale bar: 20 µm. **B:** Flow cytometry analysis of total levels of endogenous FCHo2, alpha adaptin, µ2 adaptin and Clathrin heavy chain (Clathrin HC) in G1 and G0 RPE1 cells. Geometrical means were normalised to blank signal, GAPDH levels and G1 cells and plotted in bar graphs as mean + SEM from n=3 biological replicates with a minium of 10,000 cells with 2n DNA content per sample; ****P < 0.0001,**P < 0.01, *P < 0.05, Student's unpaired two-tailed t-test. Clathrin HC - Clathrin heavy chain **C:** Representative immunoblots (out of three biological replicates) of total lysates from G0 and FACS-sorted G1 RPE1 cells probed against FCHo2, alpha adaptin and µ2 adaptin. GAPDH served as loading control. **D:** Densitometry quantification of immunoblots in **C**. Background-subtracted band densities were normalised to GAPDH and G1 cells. Bar graphs represent mean + SEM from n=3 biological replicates; *P < 0.05. Student's unpaired two-tailed t-test comparing G0 to G1 cells.

present in higher levels in quiescent cells, made the assumption that CME might be regulated by a mechanism other than protein abundence an attractive hypothesis.

#### 4.2.3.3 The role of FCHo2 phosphorylation in CME

The presence of proteins alone is often not enough to conclude on their activity. Protein activity can be triggered or inhibited by posttranslational modifications, causing changes in the conformation of a protein to reveal or block binding sites or by blocking binding sites directly. Regulation of the activity of endocytic proteins has been reported for AP2 subunits (Olusanya *et al.*, 2001; Hollopeter *et al.*, 2014; Umasankar *et al.*, 2014) or BAR domain proteins (Zhao *et al.*, 2013; Salzer *et al.*, 2017). We considered proteins arriving during early stages of CME, such as Epsin1/2 and FCHo2, to be most likely responsible as regulators for Clathrin-coated pit formation. In a first MaxQuant analysis of the SILAC mass spectrometry screen, using version 1.4.1.2, phosphorylation sites in Epsin1/2, Eps15 and FCHo2 were identified to be differentially phosphorylated in G0 RPE1 cells (Fig. 4.2.7A). Interestingly, the six phosphorylation sites in FCHo2, which were hypophosphorylated in G0, were located in two clusters in the central regions of the protein (Fig. 4.2.7B). To date, these regions are not well characterised but they are located proximal to the AP2-activating region identified by Umasankar *et al.* (2014) and Hollopeter *et al.* (2014) and pose a putative module regulating the role of FCHo2 in CME. It should be noted that a second MaxQuant analysis was performed on the G0/G1 dataset using MaxQuant version 1.5.3.8, which did not identify a significant difference between phosphorylation at the identified FCHo2 phosphorylation sites in G0 and G1 cells. This, however, was not yet known at the time the experiments described below were carried out.

Based on the six identified phosphorylation sites, nonphosphorylable mutants with all sites mutated to Alanines or phosphomimetic mutants with all sites mutated to Aspartic acid were generated by Gibson cloning (see sec. 2.1.4). Since addition of a large fluorescent protein tag to FCHo2 impairs its function (Henne *et al.* (2010), conversation with Prof Tom Kirchhausen), either a C-terminal Myc tag was attached to the constructs or untagged wildtype FCHo2 (wildtype and phospho mutants) was used for transient overexpression in subconfluent, growing RPE1 cells. Based on the rationale that quiescent cells exhibit hypophosphorylated FCHo2 and decreased CME, overexpression of the hypophsphorylated FCHo2 mutant (A-FCHo2) in growing cells should decrease and overexpression of the phosphomimetic FCHo2 mutant (D-FCHo2) should increase Tf uptake. Endogenous FCHo2 was initially not knocked down based on the assump-

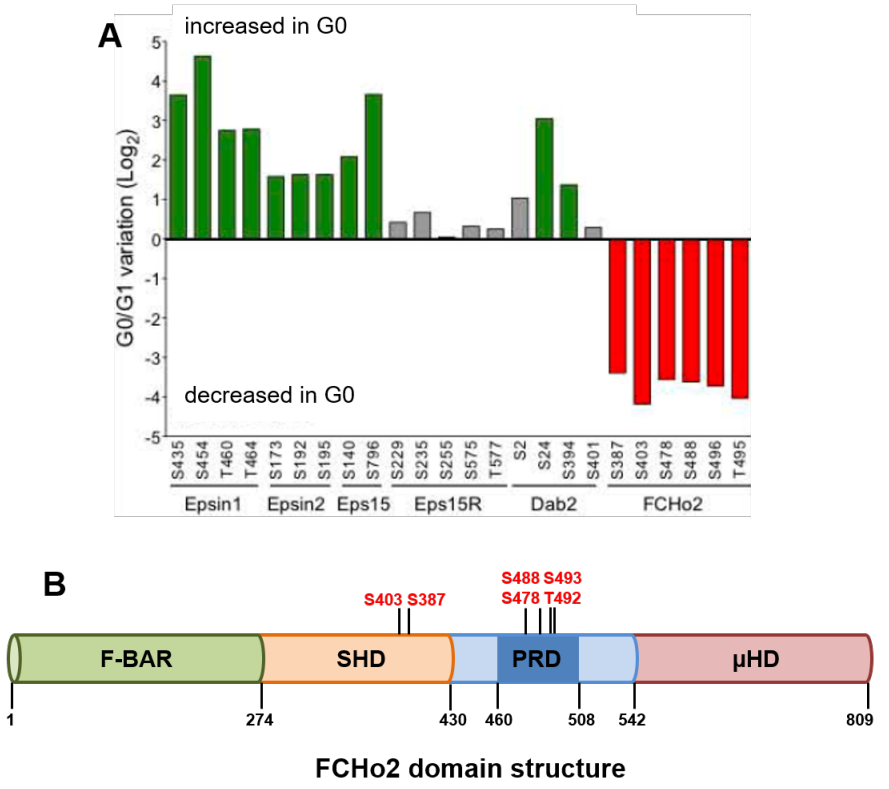


**Figure 4.2.7:** Changes of phosphorylation of endocytic proteins in G0 and G1 RPE1 cells
**A:** Fold changes of Epsin1 and 2, Esp15, Eps1R, Dab2 and FCHo2 phosphorylation in G0 and G1 RPE1 cells as identified by a SILAC mass spectrometry screen. Six phosphorylation sites of FCHo2 were hypophosphorylated during G0. **B:** The identified FCHo2 phosphorylation sites are located in clusters in the central regions of FCHo2. F-BAR - Fes/CIP4 homology Bin/amphiphysin/Rvs domain, SHD - putative Src homology 2 domain, PRD - putative proline-rich domain, µHD - AP2 µ2-homology domain.

tion that overexpression of FCHo2 phosphomutants might have a dominant effect. This would reduce further stress placed on cells by knock down followed by overexpression and might prevent aberrant phenotypes due to unfitness of cells. Overexpression of wildtype FCHo2 (WT-FCHo2) and FCHo2 phospho mutants 24 hours post transfection was assessed by flow cytometry. Anti-FCHo2 immunolabelling in fixed and permeabilised cells was employed to identify overexpressed untagged FCHo2 constructs. Mock-transfected cells immunolabelled with anti-FCHo2 antibody were used as control for non-transfected cells and the excitation laser intensity adjusted so that they were located at the same position as blank cells (Fig. 4.2.8A left). Analysis of anti Myc-labelled cells transiently overexpressing Myc-tagged FCHo2 suggested that the anti-Myc antibody labelled non-transfected as well as transfected cells, since the majority of cells exhibited similar signal to FCHo2-labelled mock-transfected cells (Fig. 4.2.8A middle, further experiments were conducted with non-transfected anti Myc-labelled cells showing similar results). Gates drawn on the two identified populations with low and high Myc signal identified 9.4 % transfection efficiency, but did not correlate with gates drawn on non-transfected cells because of the low resolution between transfected and non-transfected populations (Fig. 4.2.8A middle). Anti-FCHo2 labelling of cells transiently overexpressing untagged WT-FCHo2 and FCHo2 phosphomutants proved a more robust way to identify transfected cells, as it allowed for increased resolution between FCHo2 signals of non-transfected and transfected cells and discrimination between cells with low and high levels of transgene overexpression (Fig. 4.2.8A right). Fig. 4.2.8B highlights transfected cells in anti FCHo2-labelled cells as a tail of high FCHo2 fluorescence, whereas Myc-tagged cells only exhibited a small shoulder of cells with increased Myc levels. Transfection efficiencies are listed in Fig. 4.2.8C and range from 7.6 to 13 % when labelled for FCHo2. Using the same conservative gate to identify transfected cells labelled for Myc did not identify a recoverable transfected cell population (Fig. 4.2.8C).

Because anti-FCHo2 staining seemed more appropriate to discriminate transfected from non-transfected cells, untagged constructs of WT-FCHo2 and FCHo2 phosphomutants were used for further experiments analysing transferrin uptake. Within the transfected cell population, subpopulations with low and high overexpression levels were identified to assess whether higher levels of FCHo2 phospho mutant overexpression have a different effect on Tf uptake than lower overexpression levels (Fig. 4.2.8A right). Internalisation of AlexaFluor488-conjugated transferrin for 15 min was measured

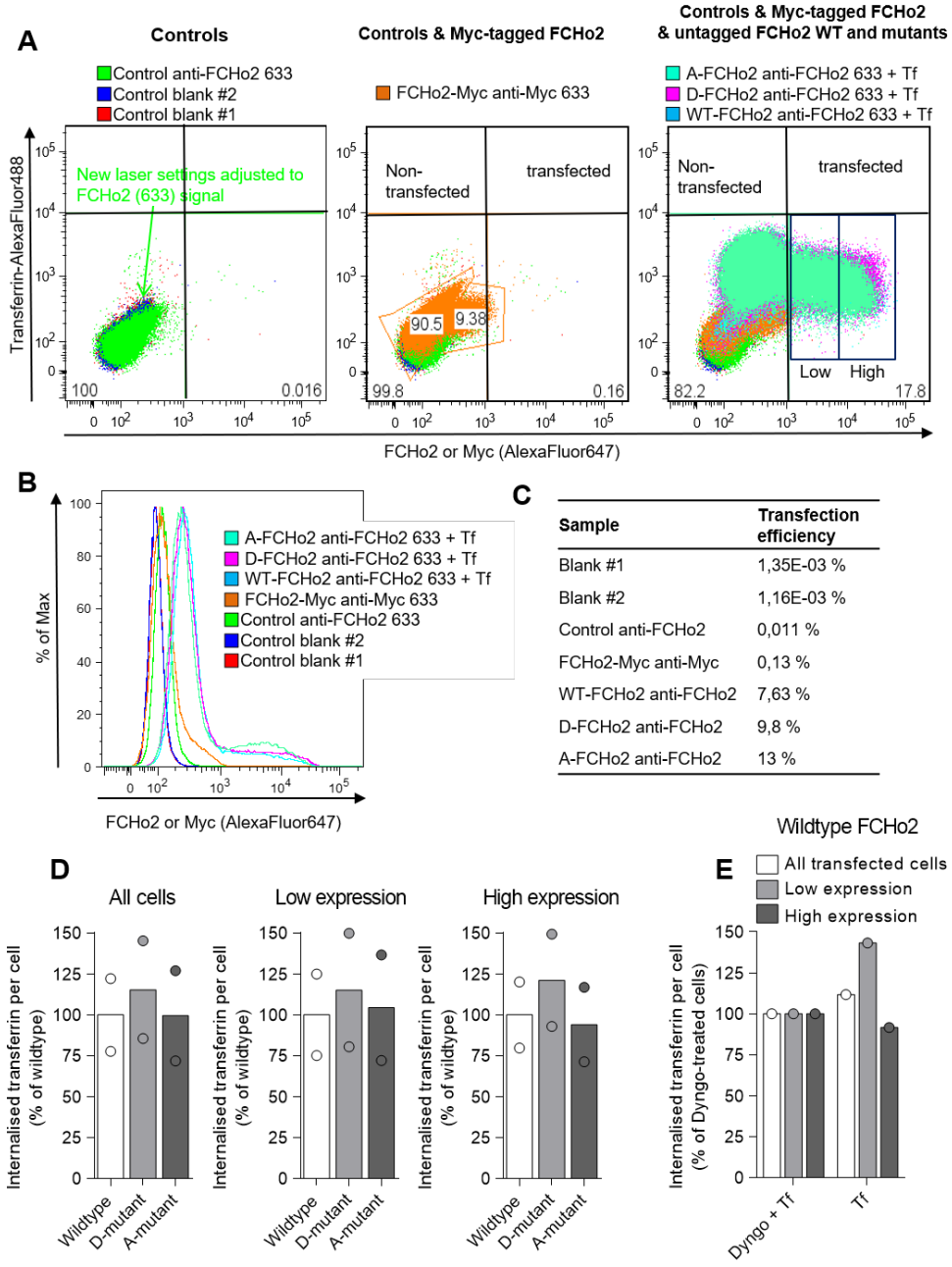


**Figure 4.2.8:** Flow cytometry analysis of transferrin uptake in RPE1 cells overexpressing FCHo2 phosphomutants

Subconfluent RPE1 cells were transiently transfected with FCHo2 wildtype or FCHo2 phosphomutants for 24 hours and subjected to 15 min uptake of AlexaFluor488-conjugated transferrin (Tf), fixed with 4 % PFA and immunolabelled against FCHo2 or Myc. A minimum of 100,000 cells were analysed by flow cytometry. **A:** Representative FCHo2 expression versus transferrin uptake dot plots of blanks (unlabelled, no transferrin uptake) and anti-FCHo2-labelled untransfected control cells (left), cells overexpressing myc-tagged wildtype FCHo2 labelled with anti-myc antiody (middle) and cells overexpressing untagged wildtype (WT-FCHo2), phosphomimetic (D-FCHo2) or nonphosphorylable (A-FCHo2) labelled with anti-FCHo2 antibody. Gates discriminating between transfected and non-transfected cells were oriented on untagged, anti-FCHo2 labelled samples. Low and High gate discriminate between low and high overexpression levels. **B:** Representative histogram of FCHo2 expression levels of samples in **A**. **C:** Representative transfection efficiency of samples in **A** as percentage of population of viable single cells. **D:** Transferrin uptake per cell was quantified as geometrical mean in all transfected cells (left) and cells with low (middle) or high (right) transgene expression level (as identified in **A**). Bar graphs represent mean and single data points of n=2 biological replicates; ns, not significant, two-way ANOVA with Tukey's multiple comparisons test. **E:** Cells overexpressing untagged wildtype-FCHo2 were subjected to uptake of 15 min AlexaFluor488-conjugated transferrin. A subset of samples was pre-treated with 4 µM Dyngo4A for 30 min and had Dyngo present throughout uptake. Bar graphs represent geometrical mean of transferrin fluorescence intensity per cell for one experiment in all transfected cells and low or high overexpressing populations (as identified in **A**).

by flow cytometry in the whole population of transfected cells (Fig. 4.2.8D left) as well as for cells overexpressing lower (Fig. 4.2.8D middle) or higher levels (Fig. 4.2.8D right) of WT-FCHo2 and FCHo2 phospho mutants. Internalised Tf in D- or A-FCHo2 was compared to Tf uptake in WT-FCHo2. Tf uptake was increased by 15 % in the total and low-expressing populations of D-FCHo2-transfected cells, and by 21 % in the high-expressing population. The total population of A-FCHo2 mutants internalised equal amounts of Tf as wildtype, with the low-expressing population internalising 4 % more and the high-expressing population 6 % less Tf than wildtype. These minor differences did not represent the severe down-regulation of Tf uptake in quiescent cells and might have partially been caused by instrument error and not the effect of FCHo2 phosphorylation. Furthermore, quiescent cells still exhibited low levels of Tf uptake despite hypophosphorylated FCHo2. The dynamin-inhibitor Dyngo4A was used as a control representing a baseline level of inhibited Tf endocytosis (McCluskey *et al.*, 2013). A first test run of 15 min AlexaFluor488-conjugated Tf uptake in cells overexpressing WT-FCHo2 resulted in slightly increased Tf uptake in the total transfected cell population (11 %) and 40 % higher uptake in the low-expressing population compared to samples treated with 30 µM Dyngo4A (Fig. 4.2.8E). However, Tf quantification in the high-expressing population suggested that Tf uptake was 9 % less than in Dyngo4A-treated cells with high WT-FCHo2 expression levels (Fig. 4.2.8E). This result appears conflicting with research showing that FCHo2 overexpression increases Tf uptake (Henne *et al.*, 2010), but might have been caused by the high levels of FCHo2 overexpression, which can result in a dominant-negative effect, or by the increased autofluorescence in green and yellow wavelengths in cells treated with Dyngo (data not shown). Dyngo-induced autofluorescence was not accounted for by including an additional blank treated with Dyngo but not subjected to Tf uptake.

Taken together, flow cytometry analysis of Tf uptake in cells overexpressing phosphomimetic or non-phosphorylable FCHo2 revealed only small variations in Tf uptake compared to WT-FCHo2-expressing cells. Importantly, fluorescence signal of internalised Tf is quite faint, demonstrated by a large proportion of cells with internalised Tf overlapping with blank cells (Fig. 4.2.8A right). Detecting a faint signal, and even more challenging, measuring differences in faint signal by flow cytometry, is difficult as signal precision is limited by background noise such as autofluorescence (Snow, 2004). An LSRII flow cytometer, as used in this study, only measures the total fluorescence intensity per cell,

which causes a high background signal in green to yellow wavelength that interferes with fluorescence from AlexaFluor488-conjugated Tf, thus decreasing the signal-to-noise ratio and negatively impacting the robustness of the quantification.

Fluorescence microscopy and automated image analysis based on Tf-containing vesicles in cells were considered as a solution to increase the signal-to-noise ratio. Cells were transiently transfected with untagged WT-FCHo2 and FCHo2 phospho mutants in a vector co-expressing EGFP from a separate promoter (pcDNA/TO/IRES2EGFP) and allowed to overexpress transgenes for 24 hours. Instead of AlexaFluor488-conjugated Tf, AlexaFluor555-conjucated Tf was used for 15 min uptake, because its fluorescence was brighter in microscopy images (data not shown). PFA-fixed and permeabilised cells were labelled with anti-FCHo2 antibody and AlexaFluor647-conjugated secondary antibody. Transfected cells were identified with CellProfiler software based on brighter AlexaFluor647 fluorescence (Fig. 4.2.9A). Total fluorescence intensity per cell in identified Tf-positive puncta (see sec. 2.9.1 for puncta identification) was quantified in cells overexpressing WT-, D- and A-FCHo2 and normalised to Tf uptake in cells transfected with empty pcDNA/TO/IRES2EGFP (further referred to as 'control vector'), which were identified based on EGFP fluorescence. Transfection of cells with empty pcDNA/TO/IRES2EGFP as control vector accounted for the (unspecific) effect of transgene expression on other cellular processes, such as endocytosis. Tf uptake in cells transfected with WT-FCHo2 or FCHo2 phospho mutants was at least 12 % higher than in cells transfected with control vector, but did not differ between WT- and D-FCHo2 (Fig. 4.2.9B left). Interestingly, cells overexpressing nonphosphorylable FCHo2 internalised 25 ± 3 % more Tf than cells overexpressing empty vector, and significantly more Tf than WT- or D-FCHo2. To introduce the baseline of blocked CME, cells were treated with Dyngo4A prior to and throughout Tf uptake. A control for increased autofluorescence was carried through this experiment, to which Tf uptake in Dyngo4A-treated cells was normalised. Tf uptake in vehicle (DMSO)-treated cells overexpressing control vector or WT-, D- and A-FCHo2 was then normalised to Dyngo4A-treated cells. Relative to cells overexpressing control vector, Tf uptake was increased by 11 ± 3 % in cells overexpressing WT-FCHo2, by 65 ± 5 % in cells overexpressing D-FCHo2 and by 117 ± 6 % in cells overexpressing A-FCHo2 (Fig. 4.2.9B right). This suggests that both phosphomimetic and nonphosphorylable FCHo2 increase CME of Tf, whereas nonphosphorylable FCHo2 increased Tf uptake twice as much as phosphomimetic

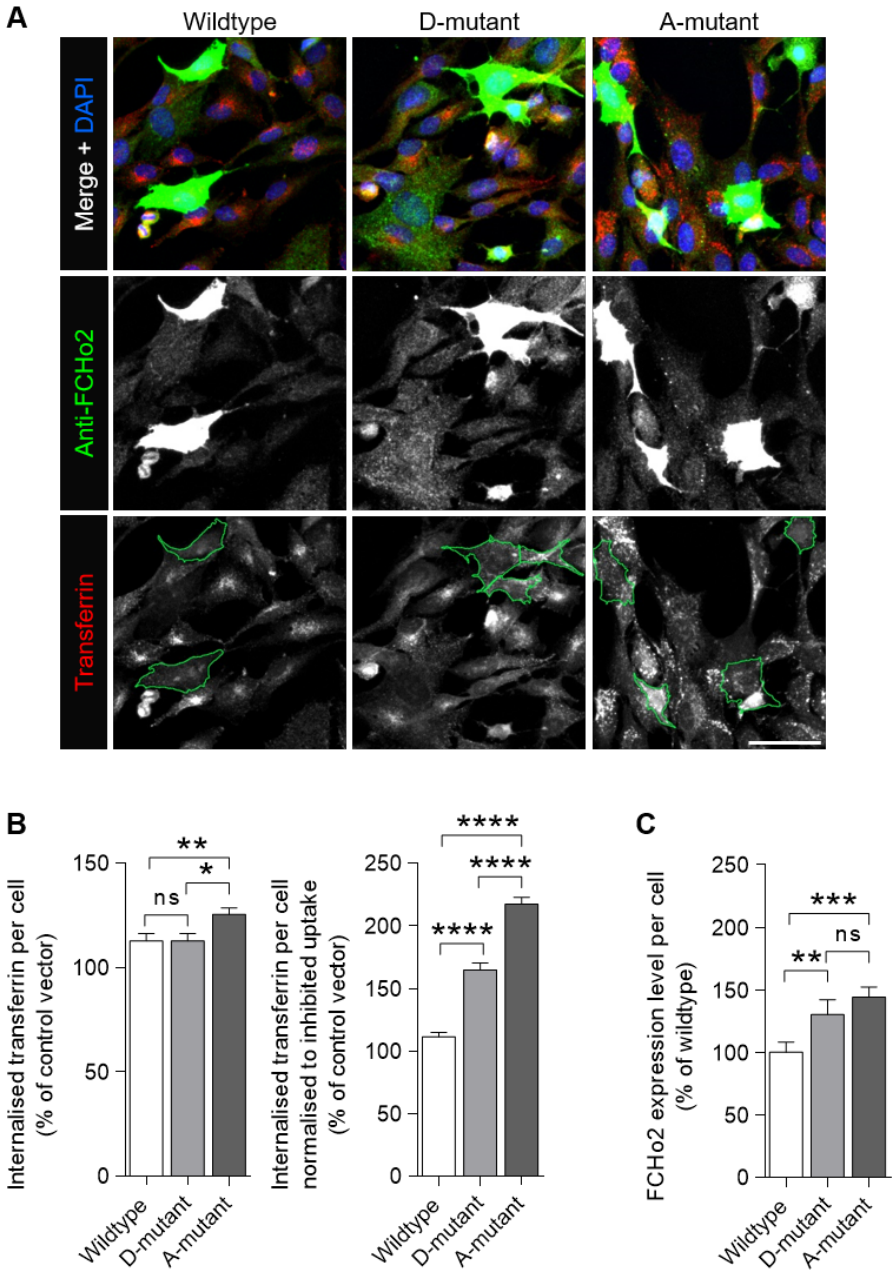


**Figure 4.2.9:** Effect of FCHo2 phosphorylation on transferrin uptake
**A:** Representative epifluorescence microscopy images of 15 min uptake of AlexaFluor555-conjugated transferrin in subconfluent RPE1 cells transfected with wiltdype, phosphomimetic (D-mutant) and non-phosphorylable (A-mutant) full length FCHo2 in pcDNA5/TO/IRES2EGFP. Transfected cells are outlined in green in the lower panel. Following uptake, surface-bound transferrin was removed with acidic buffer, cells were fixed with 4 % PFA, permeabilised and labelled with anti-FCHo2 antibody and AlexaFluor647-conjugated secondary antibody. DNA was stained with DAPI. Scale bar: 50 µm. **B:** Transferrin internalisation per transfected cell was quantified in images from **A** and normalised to cells transfected with control vector (left) or cells treated with 4 µM Dyngo4A and subsequently to cells containing control vector (right). Bar graphs represent mean + SEM from n=148 (wildtype), 115 (D-mutant), 210 (A-mutant) or 207 (control vector) fields of view, equivalent to a minimum of 10,000 transfected cells, pooled from three biological replicates; ****P < 0.0001,**P < 0.01, *P < 0.05, ns, not significant, Kruskal-Wallis test with Dunn's multiple comparisons test. **C:** FCHo2 expression levels in transfected cells used for transferrin uptake quantification in **B** normalised to WT-FCHo2; *P < 0.05, ns, not significant, Kruskal-Wallis test with Dunn's multiple comparisons test.

FCHo2 (Fig. 4.2.9B right). Although D- and A-FCHo2 expression levels were 30 ± 12 % (D-FCHo2) and 44 ± 8 % (A-FCHo2) elevated compared to WT-FCHo2, they did not correlate with the even higher increase of Tf uptake (Fig. 4.2.9C). Moreover, levels of overexpressed protein did not significantly differ between cells overexpressing D- and A-FCHo2, contrary to levels of internalised Tf, which were significantly higher in cells overexpressing A-FCHo2 (Fig. 4.2.9C). This suggests that elevated Tf uptake in D- and A-FCHo2-expressing cells compared to cells overexpressing WT-FCHo2 did not correlate with levels of overexpressed D- or A-FCHo2, indicating that they were caused by FCHo2 phosphomimesis or hypophosphorylation. Unexpectedly, nonphosphorylable FCHo2 increased Tf uptake more than both wildtype and phosphomimetic FCHo2, suggesting a more complex underlying mechanism regulating FCHo2 activity to decrease CME of Tf in quiescent cells.

### 4.2.4 Clathrin-independent endocytosis

#### 4.2.4.1 Uptake of HDL and posttranslationally modified LDL do not differ in growing and quiescent cells

When the ApoB-100 subunit of LDL is chemically modified at a minimum number of lysine residues, it is no longer recognised by the LDL receptor, but instead by scavenger receptors (Parthasarathy *et al.*, 1987; Holvoet, 2006). The mechanisms of scavenger receptor endocytosis pathways are not fully understood, which might be due to their ability to bind a variety of ligands (PrabhuDas *et al.*, 2017; Kzhyshkowska *et al.*, 2012). Oxidised LDL (oxLDL) is recognised and endocytosed by a set of scavenger receptors, such as LOX1 and CD36, which undergo Clathrin-independent endocytosis (Collins *et al.*, 2009; Zeng *et al.*, 2003; Murphy *et al.*, 2008). Similar to chemically modified LDL, high density lipoprotein (HDL) is bound by scavenger receptors (CD36, SRBI and ecto-$F_1$-ATPase/ P2Ys) and internalised by Clathrin-dependent and -independent pathways (Röhrl & Stangl, 2013).

Growing and quiescent RPE1 cells were incubated with fluorescent-conjugated HDL and oxLDL for 15 min at 37 °C to allow for ligand uptake. Removal of surface-bound ligand and nuclei staining was carried out as described in Fig. 4.2.4. Confocal microscopy sections visualise that growing and quiescent RPE1 cells internalised only little HDL and oxLDL within 15 min (Fig. 4.2.10A), which might be a physiological property of RPE cells,

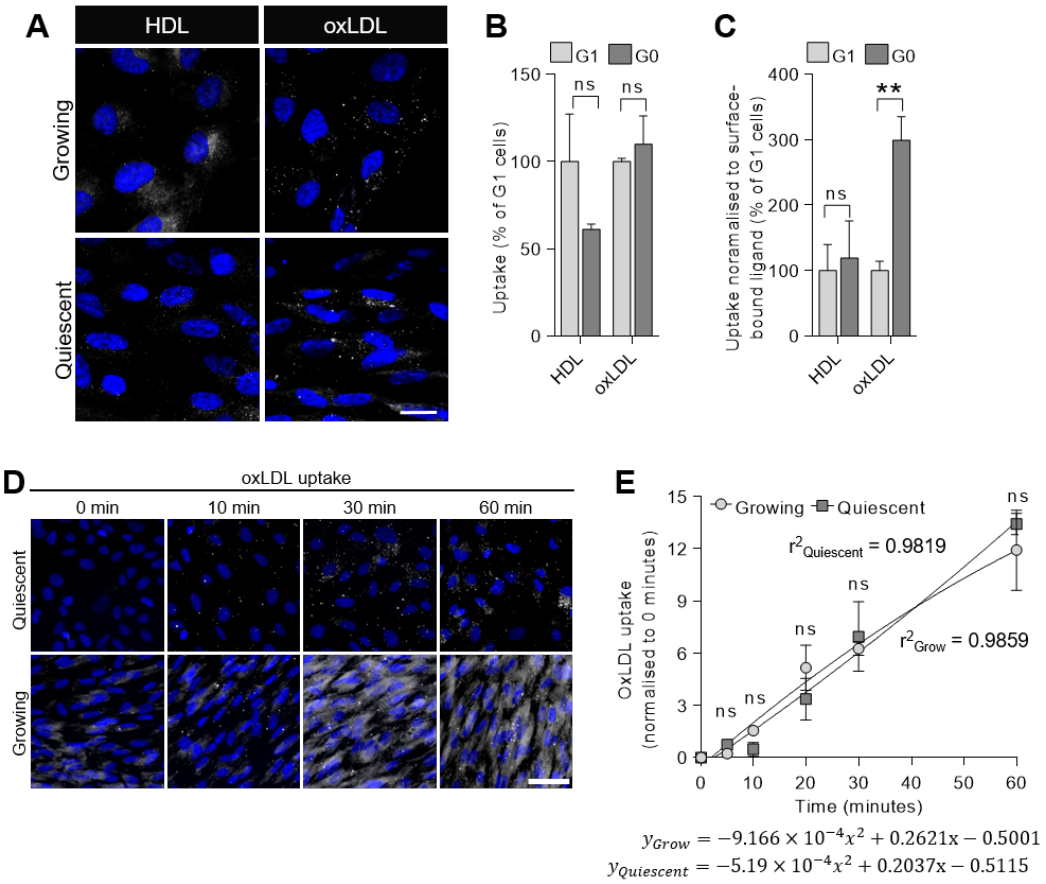


**Figure 4.2.10:** HDL and oxidised LDL uptake in growing and quiescent RPE1 cells

**A:** Confocal microscopy sections of 15 min DiO-HDL (50 µg/ml) and DiO-oxidised LDL (oxLDL; 30 µg/ml) uptake in growing and quiescent RPE1 cells. Surface-bound ligand was removed by acidic washes. Cells were fixed with 4 % PFA and nuclei stained with Hoechst33342 (blue pseudocolour). Scale bar: 20 µm. **B:** Flow cytometry analysis of 15 min HDL-AlexaFluor488 (50 µg/ml) and DiI-oxLDL (5 µg/ml) uptake in G1 and G0 RPE1 cells. Geometrical means were normalised to blank signal and G1 cells. Bar graphs represent mean + SEM from n=3 biological replicates with a minimum of 5,000 cells with 2n DNA content per sample; ns, not significant, Student's unpaired two-tailed t-test. **C:** To assess levels of cell surface-bound ligand, cells were incubated on ice with fluorescence-conjugated HDL (50 µg/ml) and oxLDL (5 µg/ml), fixed with 4 % PFA and nuclei stained with Hoechst33342. Cells were analysed by flow cytometry and HDL and oxLDL uptake from **B** were normalised to levels of cell surface-bound ligand. Bar graphs represent mean + SEM from n=3 biological replicates with a minimum of 5,000 cells with 2n DNA content per sample; **P < 0.01, ns, not significant, Student's unpaired two-tailed t-test. **D:** Representative epifluorescence microscopy images of DiO-oxLDL (30 µg/ml) uptake (represented in white) in growing and quiescent RPE1 cells at multiple time points. Scale bar: 50 µm. Surface-bound ligand was stripped by acidic washes. Cells were fixed with 4 % PFA and nuclei stained with DAPI (blue pseudocolour). **E:** OxLDL internalisation per cell for multiple time points was quantified in epifluorescence microscopy images from **D**. Data are plotted as mean ± SEM from n=3 biological replicates with a minimum of 8,000 growing and 16,000 quiescent RPE1 cells per sample; ns, not significant, Student's unpaired two-tailed t-test comparing quiescent with growing cells. Uptake rate curves were fitted according to the highest coefficient of determination ($r^2$). Respective functions and $r^2$ are shown for growing and quiescent cells.

since they are neither involved in clearance of modified cholesterol like macrophages nor in reverse cholesterol transport like hepatocytes (Wüstner *et al.*, 2004; Swirski *et al.*, 2014). Internalised HDL and oxLDL quantified by flow cytometry showed no difference between G0 and G1 RPE1 cells for the uptake of either complex after 15 min uptake (Fig. 4.2.10B). Internalised HDL and oxLDL were then normalised to cell surface-bound HDL and oxLDL, respectively. This approach was chosen instead of normalising uptake to cell surface receptor levels, because multiple receptors contribute to endocytosis of both HDL and oxLDL. HDL uptake normalised to cell surface levels did not differ between G0 and G1 cells, but oxLDL uptake was three-fold increased in G0 (Fig. 4.2.10C). OxLDL uptake was then analysed over the time course of 60 min by high-throughput epifluorescence microscopy and automated image quantification (Fig. 4.2.10D). For all time points assessed, uptake of oxLDL did not differ between growing and quiescent RPE1 cells (Fig. 4.2.10E). These results highlight that endocytic pathways are differentially regulated during proliferative quiescence and support the hypothesis that quiescent cells are not simply in a dormant state, but actively up- and downregulate cellular processes (Coller *et al.*, 2006).

#### 4.2.4.2 Uptake of Shiga toxin is decreased and Cholera toxin uptake occurs homogeneously across the quiescent cell population

A recently described form of endocytic carrier generation is the clustering of glycosylated receptors or glycolipids located in the exoplasmic plasma membrane leaflet by extracellular proteins (lectins), leading to membrane deformation and endocytic pit formation (Johannes *et al.*, 2016). Both Shiga and Cholera toxin subunit B (StxB and CtxB) bind to the gangliosides Gb3 and GM1, respectively, as their cognate receptors, in a similar way lectins bind to glycoproteins (Van Heyningen, 1974; Lindberg *et al.*, 1987; Johannes, 2017). Interestingly, Gb3 is primarily found in the plasma membrane of cells residing in G2 phase of the cell cycle, whereas GM1 is primarily expressed in G1 phase cells, limiting StxB uptake to G2 phase cells and CtxB uptake to cells in G1 phase (Majoul *et al.*, 2002). Considering that quiescent RPE1 cells exit the cell cycle in G1 phase, it is likely that they internalise CtxB, but not StxB. To test this hypothesis, growing and quiescent cells were incubated with His-tagged StxB and AlexaFluor555-conjugated CtxB for 60 min at 37 °C to allow for toxin accumulation in cells, facilitating

toxin-positive cell recognition in fluorescece microscopy images by automated image analysis. Cell surface-bound toxin was removed by washes with strongly acidic buffers (1x pH 2.5, 2x pH 2.0 for 2 min each). Cells were fixed with PFA, permeabilised and nuclei stained with DAPI. StxB was visualised by immunolabelling with an anti-His antibody. Experiments were analysed by high-throughput epifluorescence microscopy and automated image analysis of toxin-positive cells. Images were rendered on cells positive for toxin uptake and a smoothing algorithm applied, so that signal from toxin-containing vesicles spread across a larger area and merged, facilitating cell body identification, which is (among others) based on a wathershed algorithm. Toxin-positive cell outlines were then identified in the toxin fluorescence channel and related to the DAPI-stained nuclei they colocalised with. Fluorescence microscopy images demonstrate that StxB uptake occured in a small proportion of growing cells, but was almost absent in quiescent cells (Fig. 4.2.11A). Growing cells positive for StxB represented almost 2 % of the cell population, whereas only 1 % of the quiescent cell population were identified as StxB positive (Fig. 4.2.11B). The 1 % StxB-positive quiescent cells might have left the cell cycle in G2 phase (Otsuki & Brand, 2018; Laporte *et al.*, 2011, small G2/M phase population observed in Fig. 3.2.1), because it is unlikely that cell cycle progression continues during prolonged lack of growth factor stimulation. The level of StxB internalised by StxB-positive quiescent cells, however, was three times lower than in StxB-positive growing cells (Fig. 4.2.11D). Due to the low amount of StxB-positive growing cells, levels of internalised StxB per cell did not differ when averaged across the whole cell population (Fig. 4.2.11D). CtxB was, similar to StxB, internalised by a small population of growing cells, but contrary to StxB, CtxB uptake occured across the whole population of quiescent cells (Fig. 4.2.11A and B). Whereas only $8.2 \pm 0.4$ % of growing cells internalised CtxB, $86 \pm 2$ % of quiescent cells were CtxB-positive (Fig. 4.2.11C). Some CtxB-positive cells might have evaded identification due to low CtxB fluorescence intensity or only a few CtxB-positive vesicles present in a cell, which did not allow for a mask big enough to be colocalised with a nucleus. This event is likely, because microscopy images demonstrate that every quiescent cell nucleus is associated with at least some CtxB-positive puncta, indicating that CtxB uptake occured in more than 86 %, if not all quiescent cells (Fig. 4.2.11B). This portrays a limit of automated image analysis, however, despite the conservative approach of CtxB-positive cell identification, nearly all quiescent cells internalised CtxB, compared to a small percentage of growig cells. CtxB

levels did not differ between CtxB-positive growing and quiescent cells, but when averaged across the whole cell population, quiescent cells internalised at least 6.5 times more CtxB than growing cells (Fig. 4.2.11D). The fact that almost all quiescent cells internalise CtxB agrees with the hypothesis that they exited the cell cycle in G1 phase and suggests that they did not change membrane composition with respect to GM1 gangliosides. However, only less than 10 % of growing cells were positive for CtxB uptake. Considering that usually 60-70 % of growing RPE1 cells reside in G1 phase (Fig. 3.2.1), only a subpopulation of G1 cells appears to express GM1 at sufficient levels to mediate CtxB uptake at this concentration.

Summarised, StxB appears not to be internalised into quiescent cells and ChtxB uptake occurs homogeneously across the quiescent cell population. These results are consistent with quiescence entry from G1 phase cells which express GM1 as receptor for CtxB and show that endocytosis via the glycolipid-lectin pathway occurs in quiescent cells (Majoul *et al.*, 2002).

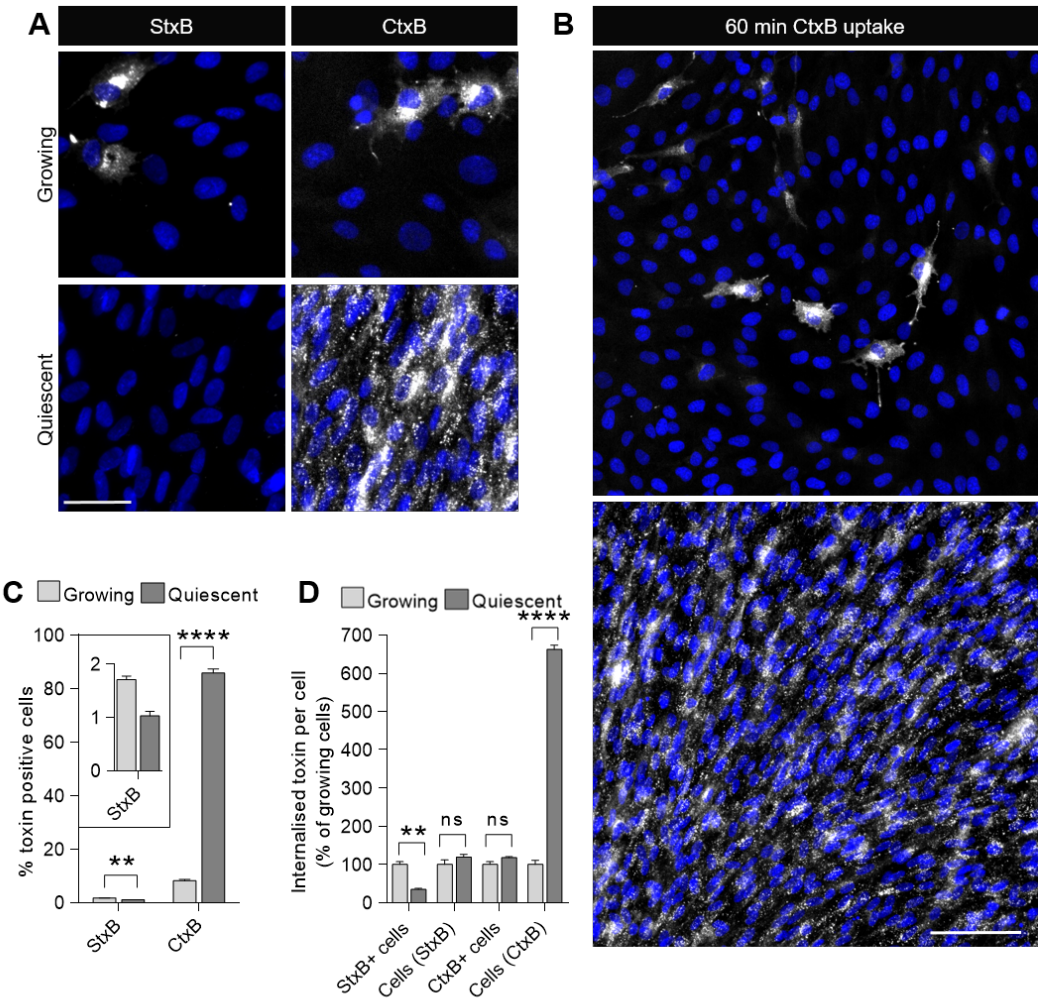


**Figure 4.2.11:** Uptake of Shiga and Cholera toxin B in growing and quiescent RPE1 cells
**A:** Epifluorescence microscopy images of 60 min Shiga (StxB; 400 ng/ml) and Cholera toxin subunit B (CtxB; 750 ng/ml) uptake in growing and quiescent RPE1 cells. Surface-bound ligand was removed by acidic washes. Cells were fixed with 4 % PFA and nuclei stained with DAPI (blue pseudocolour). Scale bar: 50 µm. **B:** Larger field of view of 60 min CtxB uptake illustrating uniform uptake of CtxB across the quiescent cell population, whereas only few growing cells internalise CtxB. Scale bar: 100 µm. **C:** Cells containing internalised toxin ('toxin positive cells') were quantified from images and plotted as percent of the total cell population. Inlet shows StxB uptake for growing cells with shrunken y axis. Bar graphs represent mean + SEM from n=3 biological replicates with a minimum of 6,000 growing and 12,000 quiescent RPE1 cells per sample; ****P < 0.0001, **P < 0.01, Student's unpaired two-tailed t-test comparing quiescent to growing cells. **D:** Total fluorescence intensitiy of internalised StxB and CtxB per cell was quantified in cells positive for toxin uptake (StxB+, CtxB+) or the whole cell population (Cells) and normalised to growing cells. Bar graphs represent mean + SEM from n=3 biological replicates with a minimum of 6,000 growing and 12,000 quiescent cells per sample; ****P < 0.0001, **P < 0.01, ns, not significant. Student's unpaired two-tailed t-test comparing growing to quiescent cells.

#### 4.2.4.3 Macropinocytosis is elevated during proliferative quiescence

Macropinocytosis is a receptor-independent endocytic pathway relying indirectly on growth factor receptor signalling to activate a Ras signalling-dependet cascade which initiates actin cytoskeleton remodelling and membrane ruffling (West *et al.*, 1989; Bryant *et al.*, 2007). In transformed cells with constitutively activated Ras, growth factor signalling can be bypassed and as a result, macropinocytosis is constitutively active (Amyere *et al.*, 2000). Macropinocytosis occurs on a baseline level in RPE1 cells cultured in full growth medium, making them a suitable model to investigate differences between growing and quiescent cells (preprint from Schink *et al.* (2017)). The water-soluble dye Lucifer Yellow as well as fluorescent-conjugated Dextrans or albumin (BSA) were reported as macropinocytosis cargoes and were therefore used for endocytic assays to measure macropinocytosis (Commisso *et al.*, 2013; Swanson, 1989).

Growing and quiescent RPE1 cells were incubated for 120 min with Lucifer Yellow (LY) and for 60 min with fluorescent-conjugated 70 kDa dextran, 10 kDa dextran and BSA at 37 ℃ to allow enough time for cargo uptake and accumulation in endosomes. Self-quenched BSA (DQBSA), which becomes fluorescent only in lysosomes upon enzymatic digestion, served as control that BSA was internalised and not simply bound to the plasma membrane. 20 min before uptake termination, Hoechst33342 was added to the cells to label nuclei for image-based quantification. Because most of the reagents used were not fixable, cells were washed and immediately imaged live on a high-content widefield fluorescence microscope after uptake (Fig. 4.2.14A). Fluorescence microscopy images illustrate that while growing cells internalised moderate amounts of LY, dextran and BSA, uptake in quiescence cells was highly increased (Fig. 4.2.14A). For image quantification, cells were identified based on nuclear Hoechst33342 signal and the area surrounding the nucleus within a 26.5 µm radius. For all cargoes tested, quiescent cells exhibited more macropinocytosis than growing cells (Fig. 4.2.14B). However, the differences in cargo uptake appeared to be related to its size and constitution. Uptake of Lucifer Yellow, a lithium salt dissociating in aqueous buffers, was 2.5-fold increased in quiescent cells (Fig. 4.2.14B). 70 kDa dextran uptake was almost 10-fold increased in quiescent cells and 10 kDa dextran almost 13-fold (Fig. 4.2.14B). BSA uptake in quiescent cells was more than 70 times higher than BSA uptake in growing

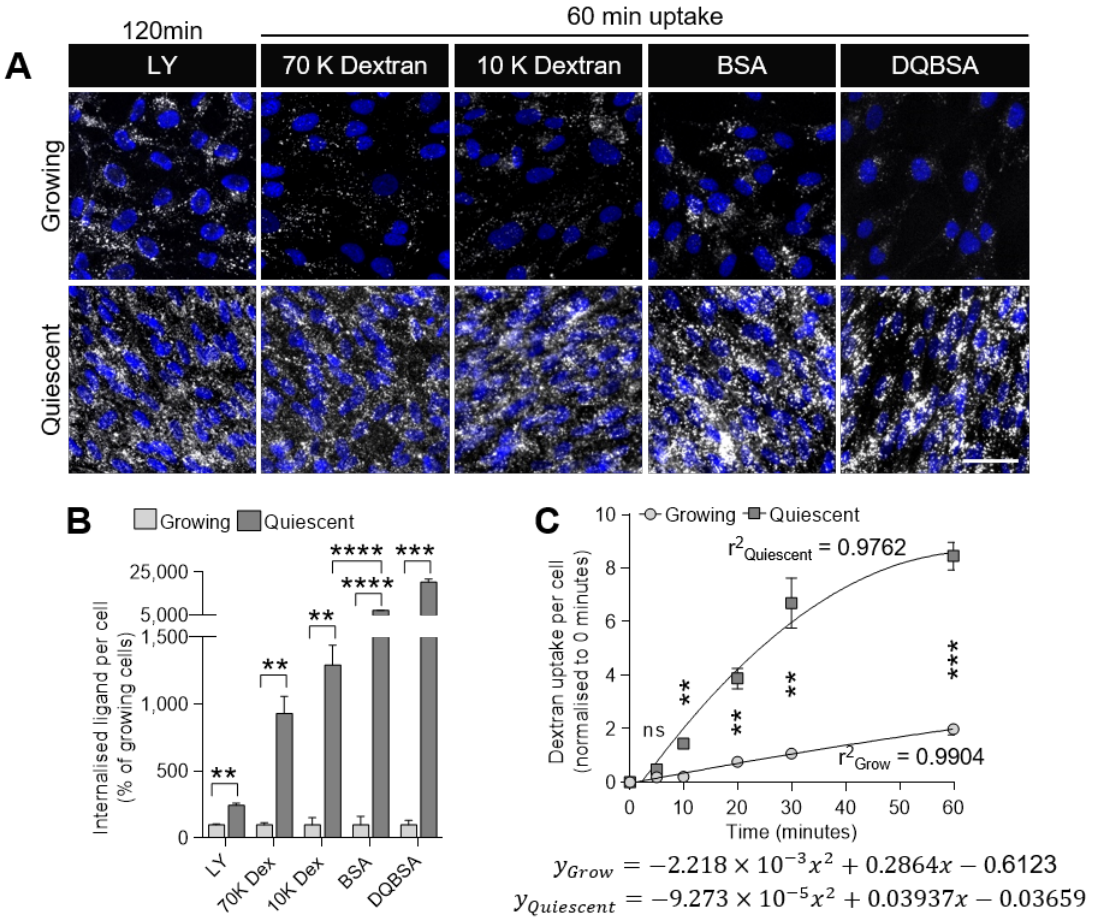


**Figure 4.2.12:** Macropinocytosis in growing and quiescent RPE1 cells
**A:** Representative epifluorescence microscopy images of Lucifer Yellow (5 mg/ml), 70 KDa TMR-dextran (1 mg/ml), 10 KDa dextran-AlexaFluor647 (500 µg/ml), BSA-AlexaFluor647 (100 µg/ml) and DQBSA (100 µg/ml) uptake in growing and quiescent RPE1 cells for the indicated durations. Nuclei were stained with Hoechst 33342 in live cells at 37 ℃ (blue pseudocolour). Following uptake, live cells were washed in PBS and imaged immediately in imaging medium (see Tab. 2.7.2 in sec. 2.7.3). Scale bar: 50 µm. **B:** Quantification of epifluorescence microscopy images from **A**. Total fluorescence intensity of internalised cargo per cell was normalised to growing cells. Bar graphs represent mean + SEM from n=3 biological replicates with a minimum of 3,000 growing and 6,000 quiescent RPE1 cells per sample; ****P < 0.0001, ***P < 0.001, **P < 0.01, Student's unpaired two-tailed t-test comparing quiescent to growing cells or two-way ANOVA with Tukey's multiple comparisons test comparing conditions between quiescent cells. **C:** 10 KDa dextran-AlexaFluor647 (10 mg/ml) internalisation per cell for multiple time points was quantified in epifluorescence microscopy images. Cells were washed in PBS, fixed with 4 % PFA, labelled for cytoplasmic marker GAPDH and nuclei were stained with DAPI. Data are plotted as mean ± SEM from n=3 biological replicates with a minimum of 8,000 growing and 16,000 quiescent cells per sample; **P < 0.01, ***P < 0.001, ns, not significant, Student's unpaired two-tailed t-test comparing quiescent to growing cells. Uptake rate curves were fitted according to the highest coefficient of determination ($r^2$). Respective functions and $r^2$ are shown for growing and quiescent cells.

cells, which was a significantly higher difference than the uptake of 10 kDa dextran (Fig. 4.2.14B). Fluorescence of DQBSA in quiescent cells was 200 times higher than in growing cells (Fig. 4.2.14B). This observation confirms that BSA was internalised and suggests that lysosomal degradation is elevated during quiescence, a phenomenon which has been reported in the literature (Legesse-Miller *et al.*, 2012; Zhang *et al.*, 2017). Uptake of 10 kDa dextran was also evaluated for durations shorter than 60 min to ascertain the endocytic nature of the previous observations by eliminating recycling and degradation events following endocytosis. Growing and quiescent RPE1 cells were incubated with lysine-fixable 10 kDa dextran for varying time points, washed and fixed with 4 % PFA to ensure uptake did not occur for longer time periods, which was particularly important for uptake durations of 5 or 10 min. No difference in dextran uptake could be detected for 5 min uptake, which might be due to resolution limits, since macropinosome formation is a process typically requiring 5-10 min (Fig. 4.2.14C, Kerr *et al.* (2006)). From 10 min onward, quiescent cells internalised significantly more dextran than growing cells (Fig. 4.2.14C). The rate of dextran uptake could be fitted with a function exhibiting a steeper average rate change than the function for dextran uptake rate in growing cells, moving towards an equilibrium of uptake and degradation after 50-60 min (Fig. 4.2.14C).

To exclude the hypopthesis that quiescent cells exhibit increased macropinocytosis to internalise nutrients, since the contact-inhibition/serum withdrawal protocol might starve them of serum proteins such as albumin, uptake of 10 kDa dextran and BSA was studied in cells that entered quiescence only by long-term contact inhibition (10 days contact-inhibited in growth medium containing 10 % FBS, see also Lemons *et al.*, 2010; further referred to as 'CI quiescent'). 60 min uptake of 10 kDa dextran, BSA and DQBSA in growing, quiescent and CI-quiescent cells occured as described above and was analysed by widefield epifluorescence microscopy and image-based analysis. Both quiescent and CI-quiescent cells exhibited elevated uptake of dextran and BSA and increased DQBSA degradation when compared to growing cells (Fig. 4.2.13). Relative dextran uptake and DQBSA degradation did not differ between quiescent and CI-quiescent cells, but BSA uptake was almost 2-fold reduced when quiescence was induced by contact-inhibition only (Fig. 4.2.13B). This might suggest that serum-withdrawal induces increased protein uptake, however, BSA uptake was still increased in CI-quiescent cells

compared to growing cells (Fig. 4.2.13), so there might be further underlying mechanisms increasing BSA uptake upon quiescence entry.

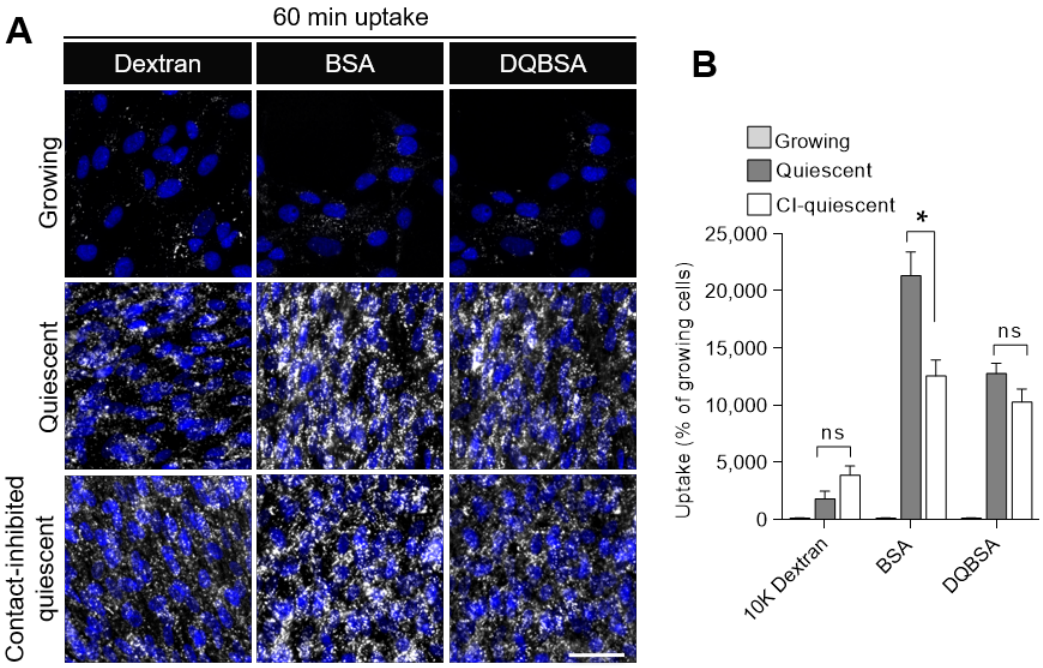


**Figure 4.2.13:** Macropinocytosis in contact-inhibited quiescent RPE1 cells
**A:** Representative epifluorescence microscopy images of 60 min uptake of 10 KDa dextran-AlexaFluor647 (500 µg/ml), BSA-AlexaFluor647 (100 µg/ml) and DQBSA (100 µg/ml) in growing, quiescent and contact-inhibited (CI) quiescent RPE1 cells. CI-quiescent cells were maintained in full growth medium for 10 days following confluence and were not subjected to mitogen withdrawal. Nuclei were stained with Hoechst 33342 in live cells at 37 ℃ (blue pseudocolour). Following uptake, live cells were washed in PBS and imaged immediately in imaging medium (see Tab. 2.7.2 in sec. 2.7.3). Scale bar: 50 µm. **B:** Quantification of epifluorescence microscopy images from **A**. Fluorescence intensity of internalised cargo per cell was normalised to growing cells. Bar graphs represent mean + SEM from n=3 biological replicates with a minimum of 3,000 growing and 6,000 quiescent cells per sample; *P < 0.05, ns, not significant, one-way ANOVA with Tukey's multiple comparisons test comparing uptake in quiescent and CI-quiescent cells.

## 4.2.5 Dedicated CME during proliferative quiescence

### 4.2.5.1 Uptake of a subset of macropinocytosis cargoes is reduced but not completely blocked by amiloride

The next step was to determine whether the increased uptake of the cargoes studied in sec. 4.2.4.3 really occured because of elevated macropinocytosis. Macropinocytosis can be blocked by amiloride or, more efficiently, its 5-(N-ethyl-N-isopropyl)-derivative EIPA (West *et al.*, 1989; Ivanov, 2008). EIPA blocks the NHE1 isoform of $Na^+/H^+$ exchangers. Its inhibitory effect on macropinocytosis, however, appears to be indirect and is thought to occur due to uncompensated $Na^+/H^+$ antiporter activity resulting in acidification of the submembranous environment, impairing actin polymerisation required

for plasma membrane ruffling and macropinocytosis (Koivusalo *et al.*, 2010). Although cytosolic acidification also blocks other endocytic pathways, macropinocytosis seems to be more sensitive to low submembraneous pH changes than pathways such as CME, so that lower concentrations of EIPA inhibit macropinocytosis of dextran, but not CME of transferrin (Koivusalo *et al.*, 2010; Sandvig, 1987). Since no specific macropinocytosis inhibitor is known to date, EIPA treatment is widely accepted to test for macropinocytosis.

Growing and quiescent RPE1 cells were treated with 15 µM EIPA (which is below the threshold of 100 µM for off-target effects and thus specific for macropinocytosis; Koivusalo *et al.*, 2010; Sandvig, 1987) 30 min prior to and throughout 120 min uptake of LY and 60 min uptake of fluorescence-conjugated 70 kDa dextran or fluorescence-conjugated BSA. EIPA concentrations were titrated for macropinocytosis inhibition versus cytotoxicity of growing cells, which were more vulnerable to high drug concentrations than quiescent cells (data not shown). The same EIPA concentration was used for treatment of growing and quiescent cells to avoid off-target effects which might occur when using different concentrations. 20 min before uptake termination, Hoechst33342 was added to the cells to label nuclei for image-based quantification. Because the used reagents were not fixable, cells were washed immediately after uptake and imaged on a high-content widefield fluorescence microscope (Fig. 4.2.14A). Internalised cargo per cell was quantified as described in sec. 4.2.4.3. In growing cells, EIPA treatment reduced LY and 70 kDa dextran uptake by about 90 % and BSA uptake by approximately 75 % (Fig. 4.2.14B). In quiescent cells, LY uptake was reduced by 77 ± 3 %, 70 KDa dextran uptake by 90 ± 3 % and BSA uptake by only 58 ± 1 % when cells were treated with EIPA (Fig. 4.2.14C). Levels of internalised cargo with and without EIPA treatment were then compared between quiescent and growing cells. As shown in sec. 4.2.4.3, uptake in vehicle-(DMSO) treated quiescent cells was higher than in vehicle-treated growing cells for all three cargoes (Fig. 4.2.14D). When treated with EIPA, quiescent cells still internalised more LY (6-fold) and BSA (7-fold) than growing cells, but inhibition of 70 kDa dextran uptake did not significantly differ in both cell populations (Fig. 4.2.14D). EIPA treatment reduced LY and 70 kDa uptake to a level similar to that of vehicle-treated growing cells. However, even with EIPA treatment, uptake of BSA in quiescent cells was still almost 2-fold higher than BSA uptake in vehicle-treated growing cells (Fig. 4.2.14D).

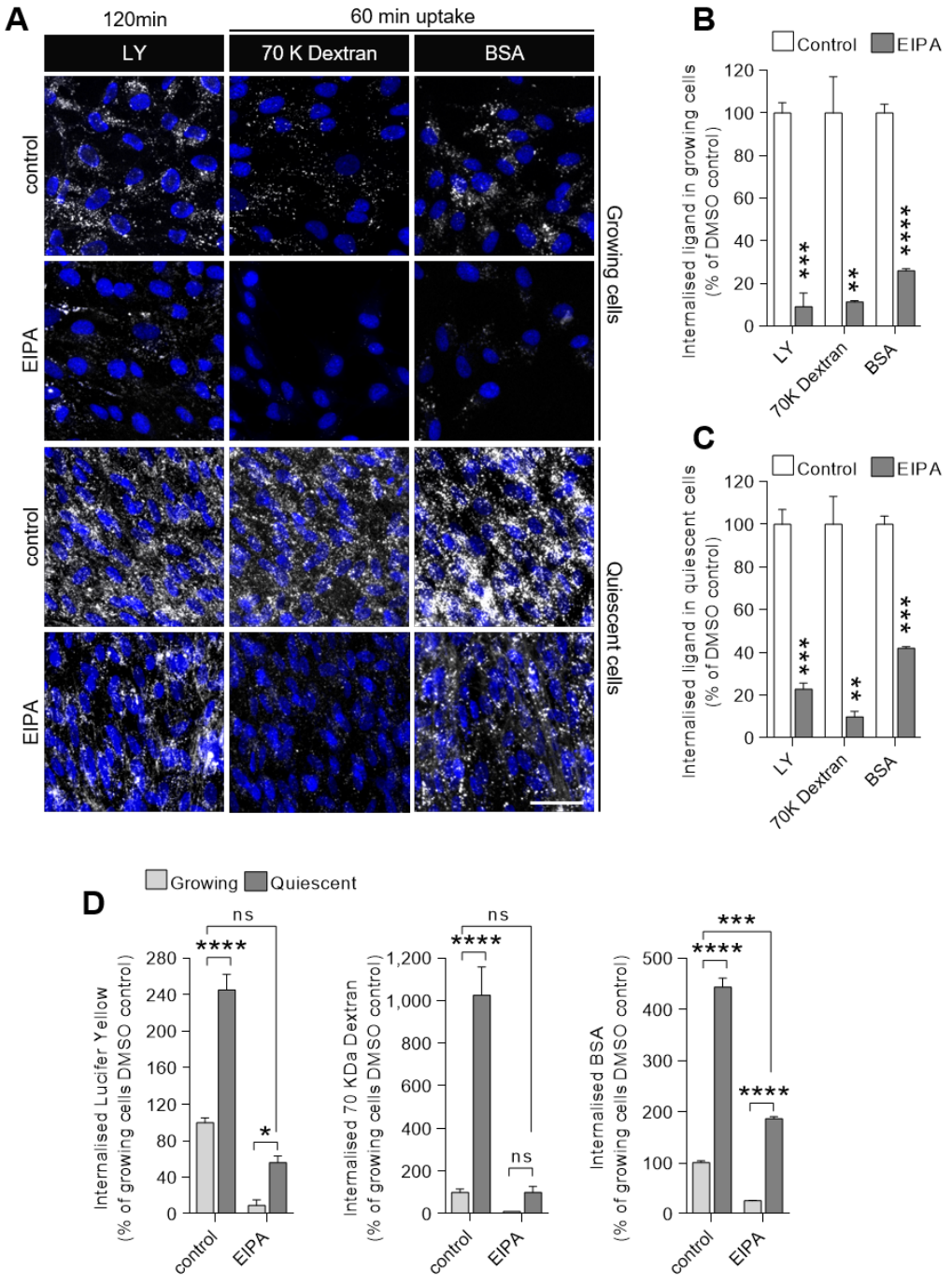


**Figure 4.2.14:** Inhibition of macropinocytosis by amiloride in growing and quiescent RPE1 cells
**A:** Representative epifluorescence microscopy images of Lucifer Yellow (5 mg/ml), 70 KDa TMR-dextran (1 mg/ml), 10 KDa dextran-AlexaFluor647 (500 µg/ml), BSA-AlexaFluor647 (100 µg/ml) uptake in growing and quiescent RPE1 cells for the indicated durations. Prior to uptake, cells were treated with vehicle (DMSO) or 15 µM EIPA for 30 min. DMSO and EIPA were present during uptake. Nuclei were stained with Hoechst 33342 in live cells at 37 ℃ (blue pseudocolour). Following uptake, live cells were washed in PBS and imaged immediately in imaging medium (see Tab. 2.7.2 in sec. 2.7.3). Scale bar: 50 µm. **B** and **C:** Quantification of epifluorescence microscopy images from **A.** Total fluorescence intensity of internalised ligand per cell was normaised to DMSO control. Bar graphs represent mean + SEM from n=3 biological replicates with a minimum of 3,000 growing (**B**) and 6,000 quiescent (**C**) cells per sample; ****P < 0.0001, ***P < 0.001, **P < 0.01, Student's two-tailed unpaired t-test comparing EIPA-treated samples to respective control. **D:** Quantification of epifluorescence microscopy images from **A.** Total fluorescence intensity of internalised Lucifer Yellow (left), 70 KDa dextran (middle) and BSA (left) per cell was normalised to DMSO control of growing cells. Bar graphs represent mean + SEM from n=3 biological replicates with a minimum of 3,000 growing and 6,000 quiescent cells per sample; ****P < 0.0001, ***P < 0.001, **P < 0.01, two-way ANOVA with Tukey's multiple comparisons test.

The fact that BSA uptake, particularly in quiescent cells, cannot be efficiently inhibited by EIPA treatment, suggests that it might be internalised by additional pathways. BSA can bind to cell surface receptors, including megalin (LRP2), neonatel Fc receptor (FcRN) and Secreted protein acidic and rich in cysteine (SPARC) (Bern *et al.*, 2015). Of these, only SPARC was identified by our SILAC mass spectrometry screen to be expressed by RPE1 cells. Not much is known about SPARC-dependent endocytosis of albumin, except that it might occur in a α5-integrin- and Clathrin-dependent manner (Nakamura *et al.*, 2014; Sage *et al.*, 1984). Interestingly, LRP2 also internalises albumin in a Clathrin-dependent manner, by recruitment of the adaptor Dab2, whose levels were up-regulated in quiescent RPE1 cells (Fig. 4.2.1; Buchäckert *et al.* 2012; Yumoto *et al.* 2012; Koral & Erkan 2012).

#### 4.2.5.2 AP2 knock down decreases endocytosis of the CME cargo Lamp1 in quiescent RPE1 cells

Endocytosis of the typical CME cargoes Tf, LDL and EGF is highly reduced in quiescent RPE1 cells (sec. 4.2.3.1). A decrease in endocytosis of either of these cargoes by AP2 knockdown might hence be difficult to observe. Lysosomal-associated membrane protein 1 (Lamp1) is an endocytic protein with a conserved YXXΦ motif in its cytoplasmic tail, which interacts with AP2 to deliver newly synthesised Lamp1 to lysosomes via endocytosis from the plasma membrane (Obermüller *et al.*, 2002; Janvier & Bonifacino, 2005). Its levels are highly increased in quiescent cells, making it a potential candidate to observe CME during G0 and confirm CME activity upon inhibition of the CME machinery (Fig. 4.2.1; Zhang *et al.* 2017).

Since Clathrin is involved in many cellular trafficking events ranging from endocytosis to recycling, it is not an optimal knockdown candidate to investigate endocytic processes (Dacks & Robinson, 2017). AP2 action is limited to the plasma membrane, so that it only acts at endocytic pits and is therefore more specific for endocytic events (Rohde *et al.*, 2002). Knockdown of the μ2-adaptin subunit results in the degradation of the remaining AP2 subunits, such as α-adaptin, because disruption of the subunit level stoichiometry destabilises the tetrameric complex AP2, resulting in the degradation of the unbound subunits (Boucrot *et al.*, 2010; Motley *et al.*, 2003). Therefore, knockdown of the AP2 μ2 subunit was employed to inhibit CME in growing and quiescent RPE1 cells.

Growing cells were treated with scrambled or µ2-adaptin siRNA on the day of seeding, 24 hours later and were used for experiments 72 hours after seeding. Because quiescent cells were resistant to knockdowns once medium was exchanged to serum-free (communication with K. McGourty, Boucrot lab), the knockdown protocol was modified. SiRNA treatment for quiescent cells occured 5 and 7 days after seeding, while cells were still dividing and in serum-containing medium. Medium exchange to serum-free occured 10 days after seeding and cells were used for experiments 17 days after seeding. AP2 knockdown efficiency was tested by IF labelling with anti-α-adaptin antibody, high-content widefield fluorescence microscopy and image-based quantification (Fig. 4.2.15A). Total levels of α-adaptin were significantly reduced by approximately 90 % in both growing and quiescent RPE1 cells treated with µ2-adaptin siRNA (Fig. 4.2.15B).

Endocytosis of Lamp1 was assessed by anti-Lamp1 antibody feeding. Cells were incubated with anti-Lamp1 antibody for 30 min at 37 °C. Surface-bound antibody was removed by washes in acidic buffer. After fixation, permeabilisation and labelling with secondary antibody and DAPI, cells were imaged at a high-content widefield fluorescence microscope. Lamp1 uptake was quantified by image-based analysis identifying Lamp1-positive endosomes as 'puncta' (Fig. 4.2.15C and D). Lamp1 uptake in scrambled siRNA-treated (further referred to as 'control') quiescent cells was 77 ± 9 % higher than in control growing cells. This difference was significant using Student's unpaired two-tailed t-test ($P < 0.002$), but the employed two-way ANOVA with Tukey's post hoc test did not determine significance due to 3-fold increase of Lamp1 uptake after AP2 knockdown (AP2 KD) in quiescent cells, which was 1.5-fold higher than Lamp1 uptake in AP2 KD growing cells (Fig. 4.2.15D left). The increased Lamp1 uptake after AP2 KD is in conflict with the findings of Janvier & Bonifacino (2005), who observed a decrease in Lamp1 uptake when AP2 was knocked down. In quiescent AP2 KD cells, however, it was evident that a large proportion of Lamp1 uptake was blocked because it accumulated at the plasma membrane and was still present despite washes with acidic buffer which should compete with the antibody for receptor binding (Fig. 4.2.15C). The measured increase of Lamp1 uptake upon AP2 KD thus might have been caused by increased cell surface levels of Lamp1. Indeed, although they did not differ between growing and quiescent control cells, Lamp1 cell surface levels increased 2.5-fold in growing and 20-fold in quiescent AP2 KD cells (Fig. 4.2.15D middle). Because elvated Lamp1 cell surface levels increase the pool of Lamp1 which can be endocytosed, Lamp1 uptake

was normalised to cell surface levels to conclude on endocytic activity (see Fig. 4.2.3). Quiescent control cells exhibited 2-fold higher Lamp1 endocytosis than growing control cells but endocytosis in AP2 KD quiescent cells was significantly lower (six-fold) than in control quiescent cells and AP2 KD growing cells (four-fold) (Fig. 4.2.15D right). However, Lamp1 endocytosis in growing AP2 KD cells was not reduced compared to growing control cells, potentially because the increase of cell surface levels rescued Lamp1 uptake to levels in control cells with the residual levels of AP2 left in the cells (Fig. 4.2.15D right).

The results show that CME can be decreased by knockdown of AP2 in quiescent cells and identify Lamp1 as a CME cargo whose endocytosis is augmented in quiescent RPE1 cells. The fact that Lamp1 cell surface levels were drastically increased upon AP2 knockdown emphasises the pivotal function of lysosomal activity during quiescence and highlights that CME plays an important role in quiescent cells. This suggests that CME ist not generally decreased, but specifically regulated for different cargoes during quiescence. These results are important, because they support a potential role of CME in BSA uptake and show that CME can be reduced by AP2 KD.

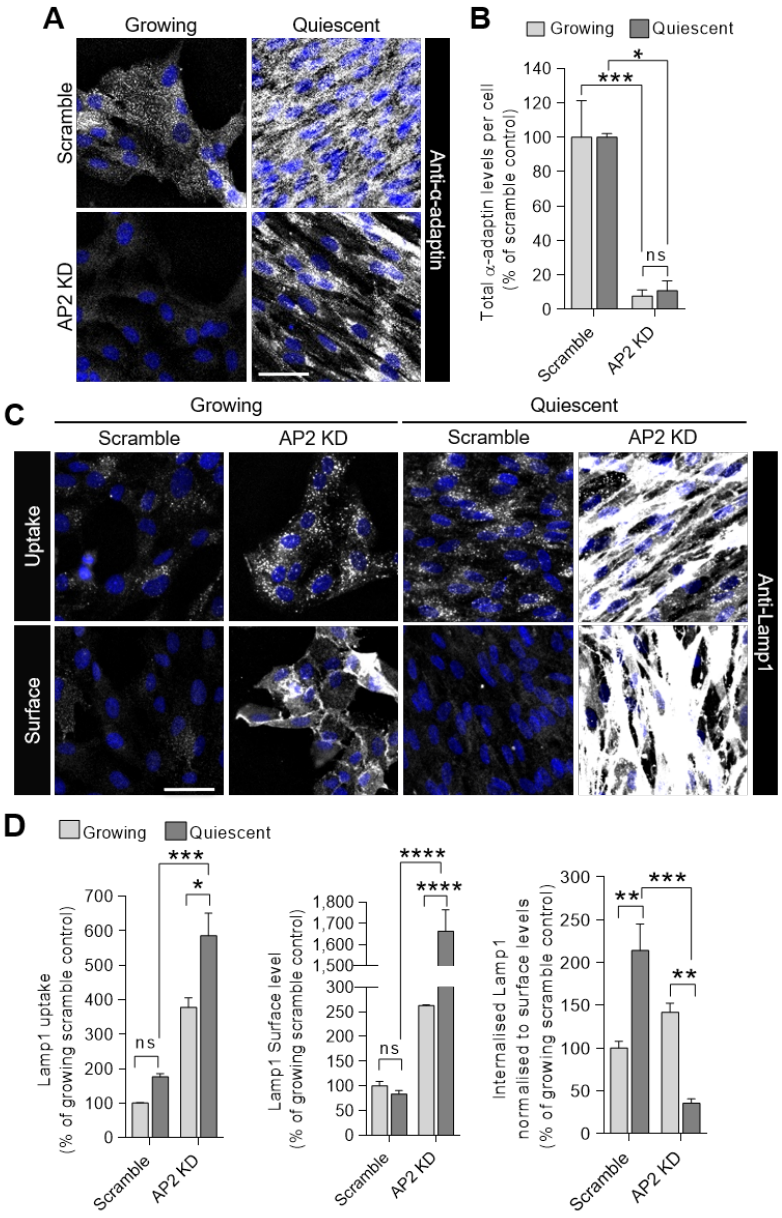


**Figure 4.2.15:** Anti-Lamp1 antibody feeding in growing and quiescent RPE1 cells in the context of AP2 knock down

**A:** Representative epifluorescence microscopy images of growing and quiescent RPE1 cells treated with scrambled or µ2-adaptin siRNA (AP2 KD) and immunolabelled for anti-α-adaptin and nuclei (DAPI, represented in blue). Growing cells were treated with siRNA on the day of seeding, 24 hours later and were used for experiments 72 hours after seeding. Quiescent cells were treated with siRNA 5 and 7 days after seeding. Medium exchange to serum-free occured 10 days after seeding. Quiescent cells were used for experiments 17 days after seeding. Scale bar: 50 µm. **B:** Quantification of epifluorescence microscopy images from **A.** Total α-adaptin fluorescence intensity per cell was normalised to respective scrambled control**.** Bar graphs represent mean + SEM from n=3 biological replicates with a minimum of 500 growing and 2,000 quiescent cells per sample; ***P < 0.001, *P < 0.05, ns, not significant; two-way ANOVA with Tukey's multiple comparisons test. **C:** Representative epifluorescence microscopy images of 30 min anti-Lamp1 monoclonal antibody feeding and anti-Lamp1 cell surface labelling in growing and quiescent RPE1 cells treated with scrambled or µ2-adaptin siRNA. Following uptake, surface-bound antibody was removed by acidic washes. Cells were fixed with 4 % PFA, permeabilised, incubated with fluorescence-conjugated secondary antibody (represented in white) and nuclei were stained with DAPI (blue pseudocolour). Scale bar: 50 µm. **D:** Quantification of epifluorescence microscopy images from **C.** Total fluorescence intensity of internalised Lamp1 puncta or cell surface-Lamp1 per cell was normalised to growing cells scrambled control. Lamp1 internalisation (left), internalised Lamp1 normalised to cell surface Lamp1 levels (middle) and Lamp1 cell surface levels (right) are showm. Bar graphs represent mean + SEM from n=3 biological replicates with a minimum of 500 growing and 2,000 quiescent cells per sample; ****P < 0.0001, ***P < 0.001, **P < 0.01, *P < 0.05, ns, not significant, two-way ANOVA with Tukey's multiple comparisons test.

#### 4.2.5.3 AP2 knock down decreases uptake of low molecular weight dextran and BSA

Next, the role of CME in uptake of dextran and BSA was investigated. AP2 knockdown was performed by μ2-adaptin siRNA treatment of growing and quiescent cells as described in the previous section. To analyse whether macropinocytosis inhibitors would have an additive effect on endocytosis reduction, scrambled siRNA control and AP2 KD cells were treated with vehicle (DMSO), EIPA or Rottlerin. Rottlerin was first described as a Protein kinase C delta (PKCδ) inhibitor, but was found to inhibit a broad spectrum of protein kinases (Bain *et al.*, 2007). Despite its unspecific inhibitory activity on protein kinases, it could be employed as a specific macropinocytosis inhibitor when used at small micromolar doses, but the mechanism of macropinocytosis inhibition is unclear (Sarkar *et al.*, 2005; Fenyvesi *et al.*, 2014). Rottlerin was employed as a second macropinocytosis inhibitor to test the impact of CME versus macropinocytosis on uptake of BSA.

Knockdown and quantification of μ2-adaptin occured as described in sec. 4.2.5.2. Cellular levels of α-adaptin were reduced by at least 90 % in growing cells, but AP2 KD was not as efficient in quiescent cells as illustrated in Fig. 4.2.15A, reducing α-adaptin levels only by 55-70 % (Fig. 4.2.16). EIPA and Rottlerin treatment for 60 min had no effect on α-adaptin levels in AP2 KD cells (Fig. 4.2.16).

Uptake of fluorescence-conjugated 10 kDa dextran, BSA and DQBSA was performed and analysed as described in sec. 4.2.4.3. Dextran uptake was performed to identify effects of AP2 KD spefic to macropinocytosis cargoes. DQBSA was carried as a control for internalised BSA, because it only fluoresces once enzymatically cleaved in lysosomes. AP2 knockdown did not decrease uptake of 10 kDa dextran and BSA in growing cells, but significantly reduced uptake of both cargoes in quiescent cells by at least 85 % when compared to siRNA-treated cells (Fig. 4.2.17A and B). BSA degradation, analysed as DQBSA fluorescence, decreased upon AP2 knockdown in both growing (42 ± 4 %) and quiescent cells (71 ± 1 %), which might be because Clathrin-dependent endocytosis of multiple proteins, such as Lamp1, Lamp2 and CD68, is dysregulated and thus lysosomal function impaired (see sec. 4.2.5.2, Janvier & Bonifacino 2005). Treatment with EIPA and Rottlerin reduced uptake of 10 kDa dextran and BSA in growing cells, both when compared to control and to AP2 KD (Fig. 4.2.17A and B). However, whereas

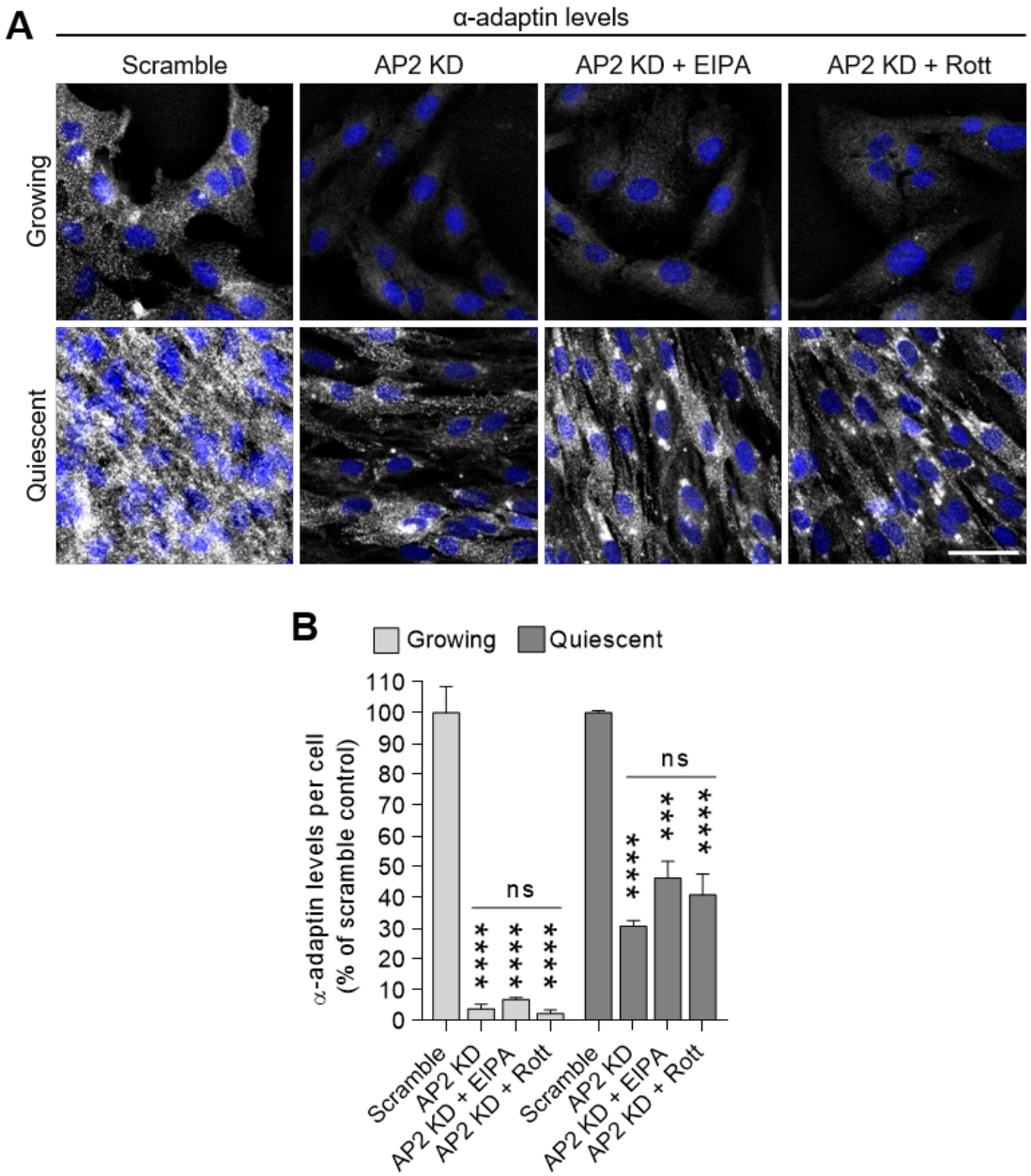


**Figure 4.2.16:** AP2 knock down efficiency in growing and quiescent RPE1 cells

**A:** Representative epifluorescence microscopy images of α-adaptin (represented in white) in growing and quiescent RPE1 cells treated with scrambled or µ2-adaptin siRNA (AP2 KD). Growing cells were treated with siRNA on the day of seeding, 24 hours later and were used for experiments 72 hours after seeding. Quiescent cells were treated with siRNA 5 and 7 days after seeding. Medium exchange to serum-free occured 10 days after seeding. Quiescent cells were used for experiments 17 days after seeding. AP2 KD cells were treated with vehicle (DSMO), 15 µM EIPA or 7.5 µM Rottlerin (Rott) for 60 min. Cells were fixed with 4 % PFA, permeabilised and immunolabelled for α-adaptin. DNA was stained with DAPI (blue pseudocolour). Scale bar: 50 µm. **B:** Quantification of epifluorescence microscopy images from **A**. Total fluorescence intensity of α-adaptin per cell was normalised to scrambled control of growing or quiescent cells, respectively. Bar graphs represent mean +SEM from n=3 biological replicates with a minimum of 500 growing and 3,000 quiescent cells per sample; ****P < 0.0001, ***P < 0.001, ns, not significant; one-way ANOVA with Tukey's multiple comparisons test comparing siRNA-treated cells to scrambled control and AP2 KD with vehicle to EIPA and Rottlerin treatment.

EIPA and Rottlerin reduced dextran uptake by approximately 60 % and 80 %, respectively (compared to scrambled control), BSA uptake was only decreased by about 45 % and 55 %, respectively (Fig. 4.2.17B). In quiescent cells, EIPA and Rottlerin had no additive effect on AP2 KD-mediated endocytosis reduction for either cargo. Interestingly, although AP2 KD decreased uptake of 10 kDa dextran and BSA by at least 85 % in quiescent cells, they still internalised more cargo than growing cells (Fig. 4.2.17C). Dextran and BSA uptake in quiescent cells was signifcantly increased compared to growing cells for control, AP2 KD and AP2 KD with EIPA or Rottlerin treatment, except for dextran uptake in AP2 KD cells and AP2 KD cells treated with EIPA. With the apparent AP2-dependence of dextran and BSA uptake, it might be possible that a more efficient AP2 knockdown would have achieved a dextran and BSA uptake decrease to the levels of EIPA and Rottlerin treatment in growing cells.

These results confirm, together with Fig. 4.2.14, that in growing cells, dextran and BSA uptake might occur primarily via macropinocytosis. In quiescent cells, however, AP2 and thus CME might be key players mediating uptake of cargo that is usually considered to be internalised by macropinocytosis. This is supported by electron microscopy images of quiescent RPE1 cells incubated with HRP, which imply that few HRP-positive macropinosomes exist and instead many Clathrin-coated pits and vesicles are present (R. G. Parton, data not shown). It is, however, controversial that EIPA reduced uptake of BSA and dextran in quiescent cells (Fig. 4.2.14), but that neither EIPA nor Rottlerin treatment had an effect on uptake after AP2 knockdown (Fig. 4.2.17). Both inhibitors, however, are not specific macropinocytosis inhibitors. EIPA has been shown to inhibit other endocytic pathways such as Clathrin-dependent endocytosis and FEME (Sandvig, 1987; Boucrot *et al.*, 2015). Rottlerin unspecifically inhibits a set of protein kinases and the mechanism of its inhibitory effect on macropinocytosis is still unclear (Bain *et al.*, 2007; Fenyvesi *et al.*, 2014). Additionally, there might be an interplay between macropinocytosis and other endocytic pathways or organisation of the actin cytoskeleton which change upon AP2 KD. Quiescent cells exhibit an elongated, spindle-like shape after AP2 KD and do not pack as tightly as quiescent cells treated with scrambled siRNA (Fig. 4.2.16A). The effect of AP2 KD on macropinocytosis during quiescence might thus not only be directly, but also indirectly mediated by an interplay of factors that remain to be elucidated.

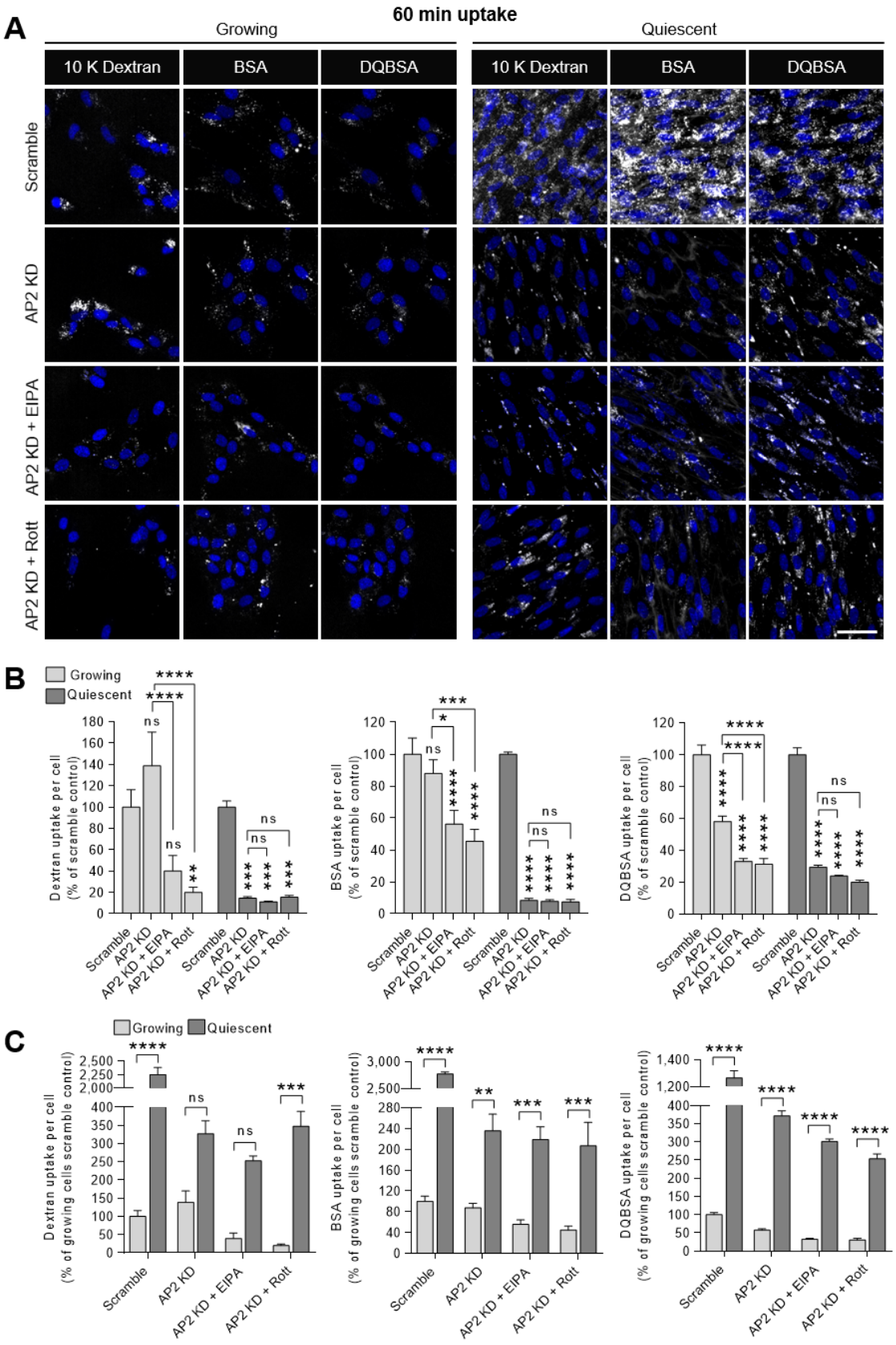


**Figure 4.2.17:** Uptake of low molecular weight dextran and BSA in growing and quiescent RPE1 cells in the context of AP2 knock down
Figure legend on next page

**Figure 4.2.17:** Uptake of low molecular weight dextran and BSA in growing and quiescent RPE1 cells in the context of AP2 knock down
AP2 knock down (KD) protocols differ between cell populations: Growing cells were treated with µ2-adaptin siRNA on the day of seeding, 24 hours later and were used for experiments 72 hours after seeding. Quiescent cells were treated with siRNA 5 and 7 days after seeding. Medium exchange to serum-free occured 10 days after seeding. Quiescent cells were used for experiments 17 days after seeding. **A:** Representative epifluorescence microscopy images of 60 min uptake of 10 KDa dextran-AlexaFluor555 (500 µg/ml), BSA-AlexaFluor647 (100 µg/ml) and DQBSA (100 µg/ml) in growing and quiescent RPE1 cells treated with scrambled or µ2-adaptin siRNA and with vehicle (DMSO; in scrambled and AP2 KD samples), 15 µM EIPA or 7.5 µM Rottlerin (Rott). Cells were treated with drug or vehicle 30 min prior to and throughout uptake. Nuclei were stained in live cells at 37 ℃ with Hoechst 33342 (blue pseudocolour). Following uptake, live cells were washed in PBS and imaged immediately in imaging medium (see Tab. 2.7.2 in sec. 2.7.3). Scale bar: 50 µm. **B:** Quantification of epifluorescence microscopy images from **A**. Total fluorescence intensity of internalised ligand per cell was normalised to scrambled control of growing and quiescent cells, respectively. Bar graphs represent mean +SEM from n=16 sites pooled from two biological replicates (dextran, BSA; equivalent to a minimum of 1,200 growing and 4,200 quiescent cells) or n=24 sites pooled from three biological replicates (DQBSA; minimum 1,700 growing and 6,500 quiescent cells); ****P < 0.0001, ***P < 0.001, **P < 0.01, *P < 0.05, ns, not significant; two-way ANOVA with Tukey's multiple comparisons test. **C:** Quantification of epifluorescence microscopy images from **A.** Total fluorescence intensity of internalised ligand per cell was normalised to scrambled control of growing cells. Bar graphs represent mean +SEM from n=16 sites pooled from two biological replicates (dextran, BSA; equivalent to a minimum of 1,200 growing and 4,200 quiescent cells) or n=24 sites pooled from three biological replicates (DQBSA; minimum 1,700 growing and 6,500 quiescent cells); ****P < 0.0001, ***P < 0.001; **P < 0.05, ns, not significant, two-way ANOVA with Tukey's multiple comparisons test.

### 4.2.6 Uptake of extracellular protein by quiescent cells is not sufficient for amino acid supply and survival

The highly increased dextran and BSA uptake in quiescent cells poses the question: Why do quiescent cells exhibit upregulated endocytic pathways for these cargoes? Ras-mutated cancer cells can rely on uptake of extracellular proteins to activate mTORC1 signalling pathways via lysosomal degradation, which are down-regulated under amino acid starvation conditions (Palm *et al.*, 2015). Serum-starved cells internalise protein (laminin) from the extracellular matrix for the same purpose (Muranen *et al.*, 2017). Quiescent cells are, however, characteristed by low mTORC1 activity, which distinguishes them from senescent cells, who continue to grow in size after cell cycle exit (Cho & Hwang, 2012).

In quiescent RPE1 cells, down-regulated mTORC1 activity could be shown by low phosphorylation levels of the mTORC1 substrates 4E-BP1 and p70S6 kinase (data from K. McGourty, Boucrot lab, not shown), but mTORC1 activity could be further decreased by mTORC1 inhibition with Torin1, an mTORC1-specific inhibitor (Thoreen *et al.*, 2009) (Fig. 4.2.18).

To test, whether quiescent RPE1 cell survival is mediated by extracellular protein uptake, medium was exchanged for amino acid-free medium or amino acid-free

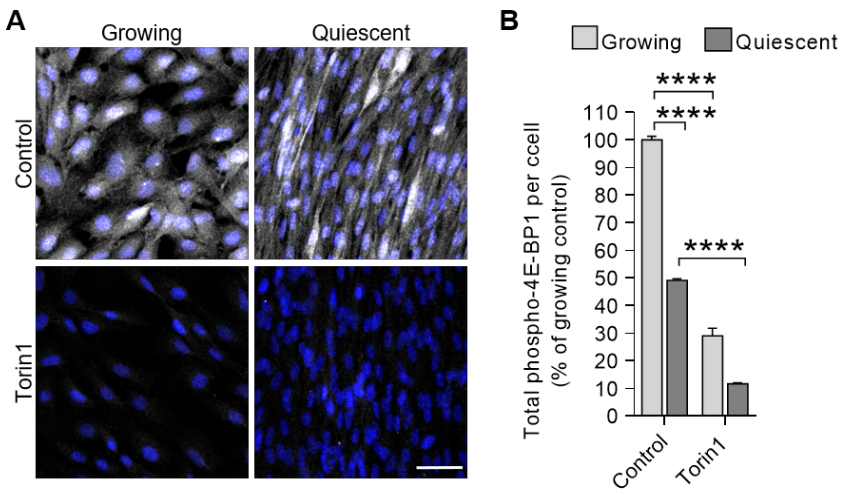


**Figure 4.2.18:** Activity of mTORC1 in growing and quiescent RPE1 cells assessed by phosphorylation of 4E-BP1
**A:** Representative epifluorescence microscopy images of growing and quiescent quiescent cells treated for 4 hours with vehicle (DMSO) or 100 µM Torin 1. Cells were fixed, permeabilised and immunolabelled for the mTORC1 substrate phospho 4E-BP1 (T37/46, white). Nuclei were labelled with DAPI. Scale bar: 50 µm. **B:** Quantification of epifluorescence microscopy images from **A**. Total fluorescence intensity of p4E-BP1 per cell was normalised to growing control cells. Bar graphs represent mean +SEM from n=3 biological replicates with a minimum of 8,000 growing and 24,000 quiescent cells per sample; ****P < 0.0001; two-way ANOVA with Tukey's multiple comparisons test.

medium supplemented with 3 % BSA. 3 % BSA was chosen because it sustains viability of non-transformed cells and allowed for proliferation of Ras-transformed cells (Palm *et al.*, 2015). Quiescent RPE1 cells cultured in amino acid-free medium showed no decrease in viability for 24 hours of amino acid starvation, but after 48 hours nuclear chromatin began to condense and nuclei to shrink, a sign of apoptosis (Fig. 4.2.19A; Toné *et al.*, 2007). Furthermore, mTORC1 activity, measured by phosphorylation of 4E-BP1 (T37/46) immunolabeling in PFA-fixed and permeabilised cells was slightly reduced after 5 and 24 hours of amino acid starvation, and almost absent after 48 hours of amino acid starvation (Fig. 4.2.19B). However, mTORC1 activity did not decrease as much as reported by Palm *et al.*, who observed almost complete abrogation of mTORC1 signalling after 1 hour of amino acid starvation. BSA supplementation in amino acid-deprived medium rescued the apoptotic phenotype observed after 48 hours of amino acid starvation (Fig. 4.2.19A). With BSA present, mTORC1 activity was not decreased during the first 24 hours of amino acid starvation, indicating that internalised BSA might be degraded in lysosomes so that released amino acids activate mTORC1 (Zoncu *et al.*, 2011). Interestingly, after 48 hours of amino acid starvation and BSA supplementation, 4E-BP1 phosphorylation was higher than in control cells

(Fig. 4.2.19B). To assess cell death induced by amino acid starvation, quiescent cells were cultured in amino acid-free medium with or without 3 % BSA supplementation for 24, 48 or 72 hours. Based on the rationale that apoptotic cells eventually detach, medium was removed from culture wells by gently pipetting up and down three times to detach losely adherent cells and the concentration of detached cells was measured with a haemocytometer. After 48 hours, no difference in the number of detached cells was observed between control, amino acid starvation or BSA supplementation (Fig. 4.2.19C), indicating that amino acid starvation-induced apoptosis begins after around 48 hours when cells are still adherent (Fig. 4.2.19A). However, after 72 hours of amino acid starvation, the number of floating cells was 10 times increased compared to control (Fig. 4.2.19C). BSA supplementation in amino acid-free medium did not prevent cell death. Although the number of dead cells was only half that of dead cells upon 72 hours amino acid starvation, it was still 5 times higher than under control conditions (Fig. 4.2.19C). This suggests that the elevated mTORC1 activity observed for 48 hours amino acid starvation and BSA supplementation might have been an attempt for increased survival, but was not enough to prevent cell death. It should be noted that this is a preliminary experiment and further research needs to be undertaken to establish the time frame of apoptosis induction and mTORC signalling after 48 hours, when cells begin to detach. The number of dying cells was only measured once, so more replicates are required for significant results. It would furthermore be interesting to assess whether lysosomal degradation is required for mTORC1 activity rescue by BSA supplementation, for example by treatment with Bafilomycin 1A for the shorter starvation periods.

The preliminary conclusions from this experimental setup, however, are:

1. Although quiescent RPE1 cells produce large amounts of extracellular matrix (data from K. McGourty, Boucrot lab), they do not internalise extracellular matrix as nutrient supply for maintainance mTORC1 activity and survival. This could be shown by apoptosis induction and starvation and highly reduced mTORC1 activity after prolonged amino acid starvation.

2. BSA supplementation in amino acid-free medium might delay the onset of amino acid starvation effects, but upon prolonged feeding on BSA as sole amino acid

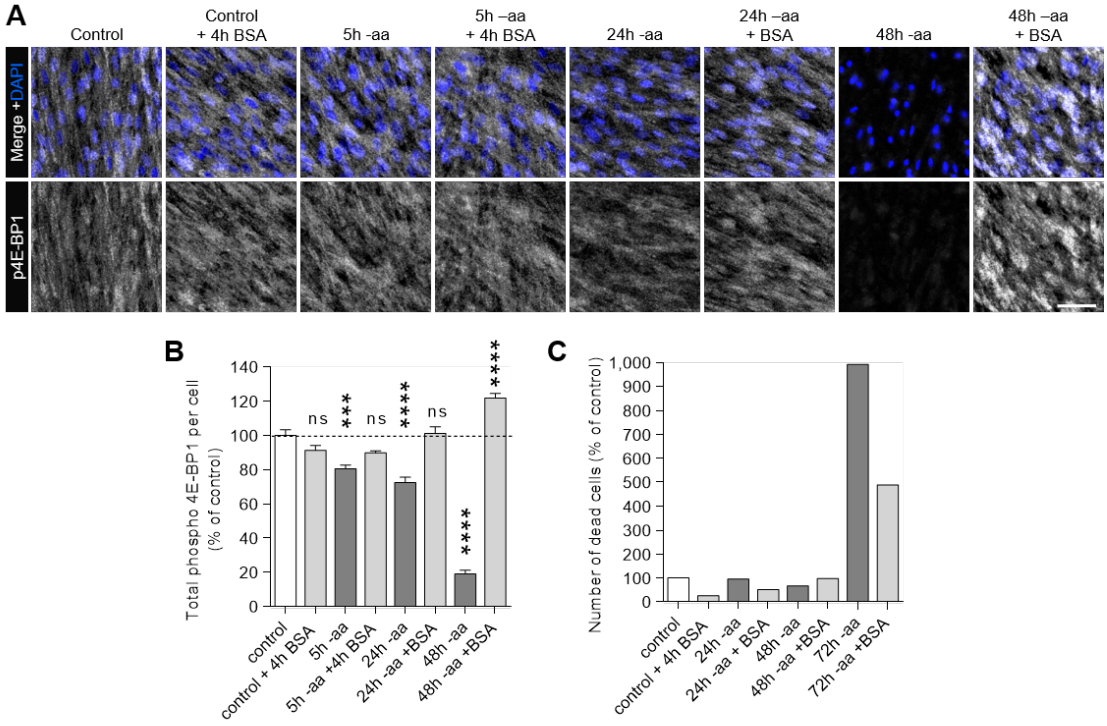


**Figure 4.2.19:** Long-term amino acid starvation with or without BSA supplementation in quiescent RPE1 cells

**A:** Representative epifluorescence microscopy images of quiescent cells cultured in amino acid-containing (control) or amino acid-free (-aa) growth medium supplemented with or without 3 % BSA. After the indicated timepoints, cells were fixed, permeabilised and immunolabelled for the mTORC1 substrate phospho 4E-BP1 (T37/46). Nuclei were labelled with DAPI. Scale bar: 50 µm. **B:** Quantification of epifluorescence microscopy images from **A**. Total fluorescence intensity of p4E-BP1 per cell was normalised to control cells. Bar graphs represent mean +SEM from n=3 biological replicates with a minimum of 500 growing and 3,000 quiescent cells per sample; ****P < 0.0001, ***P < 0.001, ns, not significant; one-way ANOVA with Dunnett's multiple comparisons test comparing amino acid-starved cells to control. **C:** Assessment of dead cell numbers after culturing in amino acid-free medium supplemented with or without 3 % BSA for the indicated timepoints. Medium was removed from wells after gently pipetting up and down three times and detached cells were counted with a heamocytometer. Bar graphs represent numbers of dead cells from one experiment normalised to growing control cells in amino acid-containing medium.

source (72 hours), mTORC1 signalling is disrupted and quiescent cells begin to die.

## 4.3 Discussion

Endocytosis is a process inherent to all eukaryotic cells and mediating vital processes such as nutrient uptake from the environment, signalling, plasma membrane turnover and migration (Barbieri *et al.*, 2016). As such, it occurs throughout all phases of the cell cycle, including mitosis and quiescence (Tacheva-Grigorova *et al.*, 2013; Majoul *et al.*, 2002; Illinger *et al.*, 1993). Since the observation and first descriptions of macropinocytosis in the beginning of the 20th century (described in Chapman-Andresen, 1984) and Clathrin-mediated endocytosis in the 1960s (Roth & Porter, 1964), a range of Clathrin-independent pathways have been identified. Although our understanding of the molecular details characterising each pathway varies greatly from being able to define the spatio-temporal process for CME to identifying key regulators and cargoes of FEME, CLIC/GEEC or endocytosis via the GL-Lect hypothesis, the role these pathways play in different stages of the cell cycle - and to what extend - remains to be uncovereed.

In this chapter, endocytosis in quiescent cells was compared to growing cells or, more specifically, cells in the G1 phase of the cell cycle. Although it is evident that endocytosis persists during quiescence, its relative activity in comparison to other phases of the cell cycle has not been assessed (Hinze and Boucrot, review to be published). Here, internalisation of cargo of a variety of endocytic pathways was measured by fluorescence-based techniques in an *in vitro* model of quiescent RPE1 cells to highlight differences or commonalities of endocytosis in cycling cells and cells that reversibly left the cell cycle.

### 4.3.1 Regulation of Clathrin-mediated endocytosis during quiescence

#### 4.3.1.1 CME activity in quiescent cells is adapted to cargo proteins

CME is by far the best characterised endocytic pathway with a number of classical cargoes and proteins operating in the Clathrin machinery being identified (Kaksonen & Roux, 2018; McMahon & Boucrot, 2011). Uptake of the CME cargoes Tf, LDL and EGF by their cognate receptors was down-regulated in quiescent cells, but levels of core

proteins of the Clathrin machinery such as AP2 subunits and Clathrin, were elevated (Fig. 4.2.4 and Fig. 4.2.6). This suggested a general down-regulation of the activity of proteins involved in CME. Results from a SILAC mass spectrometry screen identified the F-BAR domain protein FCHo2, a protein arriving at early sites of forming CCPs, as a putative regulator of CME (Henne *et al.*, 2010). Its levels were increased in G0 cells in comparison to G1 and six phosphorylation sites were identified to be hypophosphorylated during G0 (Fig. 4.2.7). Furthermore, the identified phosphorylation sites were located in the central region of FCHo2, which has been shown to play a role in AP2 activation (Hollopeter *et al.*, 2014; Umasankar *et al.*, 2014). Phosphorylation has been demonstrated to regulate the activity of BAR domain proteins (Zhao *et al.*, 2013; Salzer *et al.*, 2017). With CME being decreased in quiescent cells, which exhibit hypophosphorylated FCHo2, we hypotehesised that FCHo2 phosphorylation at one or more of the six identified phosphorylation sites might be required for FCHo2 function in CME. Hence, a nonphosphorylable FCHo2 mutant might decrease CME in growing cells. Interestingly, not only did overexpression of a phosphomimetic FCHo2 phosphomutant (with all six identified phosphorylation sites mutated to Aspartic acid) increase Tf uptake compared to overexpression of wildtype FCHo2. Overexpression of a nonphosphorylable FCHo2 phosphomutant with all identified phosphorylation sites mutated to Alanines increased Tf uptake even further (Fig. 4.2.9). An explanation for this effect could be a more complex mechanism of FCHo2 phosphorylation, requiring sequential phosphorylation of one or more of the identified binding sites. Furthermore, FCHo2 is not the only early-arriving protein at sites of CCP formation. Eps15 and intersectins form a nucleation module together with FCHo2 (McMahon & Boucrot, 2011; Ma *et al.*, 2016). Activity of these proteins might also be dependent on phosphorylation, as the mass spectrometry screen identified two phosphorylation in Eps15 to be hyperphosphorylated in G0 relative to G1, in addition to four hyperphosphorylated sites in Epsin1 (Fig. 4.2.7). Although the identified Epsin1 phosphorylation sites were identified in mass spectrometry screens in the literature and mapped on PhosphoSitePlus.org, they are not yet functionally linked to endocytosis. Phosphorylation of Eps15 at Serine 796 was reported to occur by p38 (MAPK14) upon EGF or TNF-$\alpha$ stimulation (Zhou *et al.*, 2014) and the same kinase is responsible for ligand-independent EGFR endocytosis following stimulation with EGF (Tanaka *et al.*, 2018). EGF receptors following non-canonical, p38-mediated endocytosis are recycled back to the plasma membrane, contrary to ligand-bound EGFR which

trafficks to lysosomes (Tanaka *et al.*, 2018). P38 activity in quiescent cells remains to be investigated, but it might pose a candidate for EGFR endocytosis regulation in these cells. It should, however, be mentioned that after FCHo2 mutant experiments were performed, the SILAC mass spectrometry screen was re-analysed by K. McGourty (E. Boucrot lab) using a newer version of MaxQant (1.5.3.8). A selection of results from this run are displayed in (Fig. 4.2.1), as they did not conflict with results from the previous MaxQuant analysis. One notable difference between the two analysis was that the identified FCHo2 phosphorylation sites were slightly hyperphosphorylated in G0 in the new MaxQuant analysis, but this difference was within the cut-off of ± one log2 unit. Although parameters were kept similar between the two MaxQuant analyses, identification of peaks might have followed different algorithms in each version. As described in sec. 2.3, several biological replicates were pooled together for mass spectrometry analysis and results of heavy G0/light G1 ratio and light G0/heavy G1 ratio were combined in the MaxQuant quantification. With this approach, the statistical evaluation is less powerful than when multiple samples are analysed separately and identified biological differences become less robust, explaining the variations in data generated by analysis with two different MaxQuant versions. Therefore, the mass spectrometry screen only served as a guide and results were biochemically, cell biologically and functionally confirmed. Another consideration explaining the unexpected effect of hypophosphorylated FCHo2 is that cell surface levels of TfR1 were not accounted for in this experiment and that only endocytosis of a single CME cargo was studied. CME appears to be active in quiescent cells, as could be shown for endocytosis of Lamp1, which is increased in quiescent compared to growing cells (Fig. 4.2.15). Lamp1 has a YXXΦ motif in its cytoplasmic tail which marks it for AP2-binding and CME (Obermüller *et al.*, 2002; Janvier & Bonifacino, 2005). In contrast to TfR, LDLR and EGFR, total and surface levels of Lamp1 are higher in quiescent than in growing RPE1 cells ((Fig. 4.2.1),(Fig. 4.2.4) and (Fig. 4.2.15)). In accordance with the literature, which reports increased Lamp1 levels during quiescence, it might be a suitable candidate for further CME studies in quiescent cells (Zhang *et al.*, 2017).

#### 4.3.1.2 The role of CME-mediated BSA and low molecular weight dextran uptake in quiescent cells

Surprisingly, AP2, the central adaptor complex of CME, seems to be required for the up-regulated uptake of BSA and low molecular weight (10 kDa) dextran in quiescent cells, but is not required for endocytosis of these cargoes in growing cells (Fig. 4.2.17). That uptake of low molecular weight dextran (further referred to as LMW-dextran) might be mediated via endocytic routes other than macropinocytosis has been shown by Cao *et al.* (2007) and Li *et al.* (2015). Both groups concluded on a dynamin-dependent, Clathrin-independent pathway, but none tested for AP2 dependence. Surprisingly, Cao *et al.* (2007) found out that low serum levels seem to shift the LMW-dextran uptake pathway from macropinocytosis to dynamin-dependence, which would fit with the fact that quiescent RPE1 cells are cultured in serum-free medium. However, uptake of LMW-dextran was also highly increased in contact-inhibited quiescent RPE1 cells, which were kept in medium with 10 % serum. It will be interesting to find out whether LMW-dextran and BSA uptake in contact-inhibited quiescent cells is also AP2-dependent. Furthermore, it should be considered that knockdown in quiescent cells occurs over a period of 12 days, with serum withdrawal from the medium occuring 5 days after first siRNA treatment. During this time, compensatory endocytic and trafficking mechanisms can take over, which might be one of the explanations why LMW-dextran and BSA uptake were still higher in AP2 KD cells than in growing cells (Fig. 4.2.17). Moreover, if quiescent cells are so dependent on AP2 to mediate endocytosis of vital proteins such as Lamp1 for the maintenance of lysosomal function, AP2 KD might not allow for entry into a 'deep' quiescent state, such as described in chapter 3. The transient overexpression of a dominant-negative AP2 mutant might be more appropriate in abrogating AP2 function to prevent CCP formation, as transfections can be performed within 48 hours on quiescent cells (data not shown) (Kadlecova *et al.*, 2016). If AP2 can be confirmed as a key mediator of LMW-dextran and BSA uptake, a thorough analysis of LMW-dextran and BSA uptake will give a more detailed picture of the endocytic mechanism involved and whether it occurs by classical CME. Dynamin-dependence should be confirmed in quiescent RPE1 cells by small compound inhibitors such as Dyngo4A, dominant-negative Dynamin (K44 mutant) overexpression or Dynamin knockdown. To further assess the receptor-mediated, and thus non-macropinocytic, nature of LMW-dextran and BSA up-

take in quiescent cells, surface labelling will show whether dextran or BSA are able to bind to cell surface receptors (Buckley & King, 2017). Receptors for dextran and BSA binding have been reported, such as Mannose receptor for dextran (Kato *et al.*, 2000) and, among others, LRP2 in conjunction with the adaptor Dab2 for BSA (Koral & Erkan, 2012; Buchäckert *et al.*, 2012; Yumoto *et al.*, 2012; Larsen *et al.*, 2016). These receptors, however, were not identified in RPE1 cells by the SILAC mass spectrometry screen nor by a cell surface mass spectrometry screen performed by K. McGourty. It is likely they might bind to other cell surface molecules. Furthermore, the effect of AP2 KD on fluid uptake (labelled by LY) or high molecular weight dextran uptake, which were not studied in this chapter, needs to be established and might confirm receptor dependance.

Summarised, CME is active in quiescent RPE1 cells and mediates uptake of specific cargoes such as Lamp1 and, potentially, LMW dextran and BSA. However, endocytosis of classical CME cargoes such as Tf, LDL and EGF is highly decreased. The selective endocytosis of CME cargoes might be due to phosphorylation regulating CME machinery or adaptor protein activity and might thus be adapted to the needs during the quiescent state and to maintain it. Further experiments should be carried out in different cell types to confirm that the observations shown here are of general significance.

### 4.3.2 Clathrin-independent endocytic pathways in quiescent cells

#### 4.3.2.1 Scavenger receptor-mediated endocytosis of oxLDL and HDL

Chemically modified LDL, such as oxidised LDL (oxLDL), is not recognised by LDLR and internalised by CME, but instead binds to a set of scavenger receptors and is internalised by poorly characterised pathways, generally termed 'scavenger receptor-mediated endocytosis' (Parthasarathy *et al.*, 1987; Holvoet, 2006; PrabhuDas *et al.*, 2017; Kzhyshkowska *et al.*, 2012). Scavenger receptor-mediated endocytosis is thought to be mostly Clathrin-independent, as has been shown for the oxLDL receptors LOX1 and CD36 (Collins *et al.*, 2009; Zeng *et al.*, 2003; Murphy *et al.*, 2008). Uptake of chemically modified LDL is of particular importance for quiescent endothelial cells lining blood vessel walls, as LDL residing in the blood for a long time has a high probability of being modified and poses a risk for atherosclerosis development when accumulating in blood vessels (Young & McEneny, 2001). Endocytosis of oxLDL by quiescent endothelial cells would facilitate macrophage-mediated clearance of modified LDL and

prevent foam cell formation of oxLDL-overloaden of macrophages (Yu *et al.*, 2013). Although net oxLDL uptake did not differ between growing and quiescent RPE1 cells, surface-normalised oxLDL endocytosis was increased in quiescent cells, indicating an upregulation of one or more scavenger receptor-mediated pathways during quiescence Fig. 4.2.10. Since oxLDL is bound and internalised by multiple scavenger receptors, including LOX1 and CD36, the precise pathway remains to be identified and its mechanism elucidated (Collins *et al.*, 2009; Zeng *et al.*, 2003; Murphy *et al.*, 2008).

HDL plays a major role in hepatic cholesterol clearance, which predominantly occurs by selective cholesteryl ester transfer, a process which does not involve endocytosis of the full HDL particle, but allows for cholesteyl ester uptake via SRBI (Nieland *et al.*, 2005; Rigotti *et al.*, 2003). However, HDL can also be endocytosed by scavenger receptors (CD36, SRBI and ecto-$F_1$-ATPase/ P2Ys) in a variety of cells via Clathrin-dependent and -independent pathways (Röhrl & Stangl, 2013). Since hepatocytes primarily reside in a quiescent state, investigating HDL endocytosis in quiescent cells was an attractive idea (Zimmermann, 2004). However, no difference in HDL endocytosis was observed between quiescent and growing RPE1 cells (Fig. 4.2.10). The low levels of internalide HDL might also confirm that HDL uptake is not the primary route of cholesterol delivery. It might be interesting to compare HDL uptake in quiescent and proliferating hepatocytes, as their cell surface receptor levels might be better adjusted for HDL interactions. An attempt to do so was made in an hTERT-immortalised human hepatocytes cell line (IHH cells) produced in the group of K. Srai, but the immortalisation occured by viral transduction and might have transformed the cells so that they did not stop proliferation upon contact inhibition, prevening them from entering a quiescent state. Non-transformed hTERT-immortalised hepatocytes were not available and other cell lines like HEPG2 or similar are transformed and do not enter the quiescent state.

Studies of oxLDL and HDL endocytosis confirm the differentially regulated endocytic activity during proliferative quiescence. While endocytosis of HDL did not differ between growing and quiescent RPE1 cells, oxLDL endocytosis was increased during quiescence. While it is difficult to conclude a molecular mechanism determining the increased endocytosis of oxLDL because of the multitude of receptors affecting its uptake, the results show that quiescent cells are by no means in a dormant state down-regulating all cellular processes.

#### 4.3.2.2 Endocytosis of bacterial toxins via the GL-Lect mechanism

Endocytic pits do not only form upon deformation of the plasma membrane by cytosolic proteins, but can also be initiated by extracellular clustering according to the GL-Lect hypothesis (Johannes *et al.*, 2016). Shiga and Cholera toxin B subunits were identified to act as lectins, clustering their cognant glycosphingolipid receptors, Gb3 and GM1, respectively, in the exoplasmic plasma membrane leaflet, thereby inducing inward-bound curvature of the plasma membrane (Van Heyningen, 1974; Lindberg *et al.*, 1987; Johannes, 2017). Interestingly, Gb3 is mainly expressed in cells in G2 phase of the cell cycle, whereas GM1 is expressed in G1 phase cells, limiting Shiga and Cholera toxin uptake to distinct cell cycle phases and excluding uptake of both toxins in the same cell (Majoul *et al.*, 2002). A small population of growing cells was identified as StxB positive (Fig. 4.2.11). It was smaller than the G2/M population identified by cell cycle analysis in Fig. 3.2.1, which might be due to a conservative approach to automatically identify StxB-positive cells with CellProfiler software due to high background because of StxB-His tag labelling. It was established in chapter 3 that quiescent RPE1 cells exhibit a 2n genome and are therefore likely to have left the cell cycle in G1 phase. Accordingly, only a small fraction of quiescent RPE1 cells was found to internalise StxB (Fig. 4.2.11). StxB positive cells within the quiescent cell population might have either left the cell cycle in G2 phase or undergone cell cycle arrest in G2 due to DNA damage, as a small G2/M phase fraction within the quiescent cell population was observed by cell cycle analysis in Fig. 3.2.1. Cell cycle exit to quiescence during G2 has been reported, however to date it has only been observed in yeast, *D. melanogaster* and zebrafish (Otsuki & Brand, 2018; Laporte *et al.*, 2011; Nguyen *et al.*, 2017). Since continuous proliferation can be excluded under conditions of contact inhibition and absence of growth factor stimulation, cell cycle arrest in G2 could also have been caused by DNA damage, with subsequent cell cycle arrest at the G2/M restriction point (Pedraza-Alva *et al.*, 2006). A fraction of G2/M cells was also present in quiescent fibroblasts generated by varying protocols in Lemons *et al.* (2010), but their nature remains to be elucidated. However, to assure that StxB-positive cells in the quiescent population really are in G2/M phase, their cell cycle profile should be analysed by flow cytometry.

Unlike StxB, CtxB was internalised across the entire quiescent cell population (Fig. 4.2.11), supporting the assumption in chapter 3 that quiescent RPE1 cells have

left the cell cycle during G1 phase and proposing that quiescent RPE1 cells might maintain some plasma membrane constituents, such as GM1, from G1 phase (Majoul *et al.*, 2002). GM1 is also present in the plasma membrane of quiescent monocytes, where it facilitated integrin-mediated cell adhesion and might serve a similar purpuse in quiescent RPE1 cells (Cambi *et al.*, 2006). Among growing cells, only a small fraction internalised CtxB. Conflicting the hypothesis of CtxB-binding to G1 phase cells, the CtxB positive fraction was smaller than the G1 fraction identified by cell cycle analysis (Fig. 3.2.1). This suggests that either GM1 expression is only high enough for CtxB internalisation for a short time during G1 phase, most likely before the G1/G0 restriction point. Another possibility might be that CtxB-positive cells in the growing poppulation reside in a short-term quiescence (or pseudo-quiescence, in case of cancer cells like HeLa, which also internalise CtxB as shown by Torgersen *et al.*, 2001), like the RPE1 cell subpopulation with both hypophosphorylated Rb or low RNA levels identified in growing cells in sec. 3.2.4 and Fig. 3.2.5. Cyclin D1, Ki67 or pRb counterstaining would identify whether CtxB-positive cells in the growing cell population are actively dividing. If CtxB is only internalised by a quiescent subpopulation lacking any of the aforementioned proliferation markers, CtxB uptake might be another marker identifying quiescent cells. A likely alternative is that the CtxB concentration used in this study was too low to induce membrane bending and be internalised in all G1 cells expressing GM1. The CtxB doses were kept low because it was shown that CtxB enters cells via multiple pathways when it is present at high concentrations of (20 nM; Massol *et al.*, 2004), which might be because of increased GM1 clustering at this concentration (Wolf *et al.*, 2008). The concentration of 750 ng/ml used in Fig. 4.2.11 was slightly less than the 1 µg/ml used by Ewers *et al.* (2010) and 10 times lower than in Howes *et al.* (2010), where it might have contributed to observing highly active CIE, and at least 100 times lower than in Day *et al.* (2015). Renard *et al.* (2015) used AlexaFluor555-conjugated CtxB at 285 ng/ml, which is almost three times less than the concentration used here, to study the intracellular machinary involved in CtxB uptake. Because internalised CtxB was difficult to identify by widefield fluorescence microscopy, the dose was set to 750 ng/ml, which translates to 13 nM, when a molecular weight of 57 kDa per pentameric CtxB complex is considered, and maximum 11 nM, when the molecular weight of up to 7 AlexaFluor555 molecules/mol CtxB pentamer is added. This is almost half the dose used for uptake assays in the study of Massol *et al.* (2004). It is also

worth noting that endocytic uptakes performed throughout this project occured without prior ligand incubation on ice or at room temperature, which would lead to changes in membrane fluidity and induce receptor clustering, potentially activating additional endocytic pathways or preventing their occurence Boucrot *et al.* (2015).

#### 4.3.2.3 Macropinocytosis and uptake of extracellular protein

The purposes of macropinocytosis range from environmental sampling (macrophages, dendritic cells) to elevated nutrient uptake (cancer cells) and rapid plasma membrane turnover (Buckley & King, 2017). It occurs constitutively only in specific cell types such as dendritic cells, macrophages and Ras-transformed cells and else is stimulated indirectly by growth factor receptor signalling (West *et al.*, 1989; Bryant *et al.*, 2007; Amyere *et al.*, 2000). In cells cultured in growth factor-containing medium, such as growing RPE1 cells cultured in medium containg 10 % FBS, permanent base-line EGF signalling allows for a baseline level of macropinocytosis activity (preprint from Schink *et al.* (2017)). Acute stimulation with high levels of EGF increases plasma membrane ruffling and elevated macropinocytosis (West *et al.*, 1989; Bryant *et al.*, 2007; Nakase *et al.*, 2015). A baseline level of macropinocytosis activity could be observed in growing RPE1 cells, but surprisingly, quiescent RPE1 cells, which are not exposed to growth factor signalling, exhibited highly elevated levels of macropinocytosis for multiple cargoes, such as fluorescent salt-labelled fluid (LY), high molecular weight dextran (70 kDa, HMW-dextran), low molecular weight dextran (10 kDa, LMW-dextran) and BSA (Fig. 4.2.12). Amiloride (EIPA) treatment strongly reduced uptake of LY and HMW-dextran, indicating that it is macropinocytosis (Koivusalo *et al.*, 2010; Ivanov, 2008), but BSA uptake, although decreased after EIPA treatment, was still higher than the uptake in growing control cells (Fig. 4.2.14). Increased extracellular matrix protein uptake was shown to supply serum-starved cells with amino acids, activate mTORC1 and promote survival (Muranen *et al.*, 2017). This is not the case for quiescent RPE1 cells, as they undergo apoptosis when cultured in amino acid-free medium for longer than 24 hours and protein from the ECM would be the only source of amino acids (Fig. 4.2.19). Furthermore, quiescent RPE1 cells exhibited increased uptake of dextran and BSA even when maintained in serum-containing medium (Fig. 4.2.19), implying that serum starvation is not the key mediator of elevated BSA uptake. Moreover, mTORC1 activity in quiescent

RPE1 cells was shown not to be as succeptible to short-term amino acid starvation as it is in proliferating or cancer cells (Palm *et al.*, 2015). Although the small decrease in mTORC1 activity caused by amino acid starvation was rescued by BSA for a time period of 24 hours, BSA uptake did not prevent cell death of quiescent RPE1 cells under long-term amino acid starvation, in spite of increased mTORC1 activity (Fig. 4.2.19). This is in accordance with results of the work from K. McGourty, who identified an AKT/mTORC1-independent quiescence survival signalling pathway.

Summarised, the absence or presence of growth factors did not significantly contribute to the elevated uptake of macropinocytosis cargo in quiescent cells. This would imply constitutively active macropinocytosis, similar to macrophages and dendritic cells. However, electron microscopy images of HRP uptake indicate that only few HRP-positive macropinosomes exist in quiescent RPE1 cells, whereas a multitude of Clathrin-coated pits and vesicles are present (R. G. Parton, not shown). Since each micropinocytic vesicle not only internalises specific cargo, but also a certain volume of extracellular fluids, it might be possible that the sum of upregulated receptor-mediated/micropinocytic pathways contributes to increased uptake of extracellular fluid, including dextran and BSA. The important role of CME in quiescent cells was established in sec. 4.3.1 and would support this argument. Additionally, it should be tested how much BSA uptake can be inhibited by a newly described macropinocytosis inhibitor, imipramine (Buyya & Pandey, 2018). Imipramine did not inhibit CME, which will be important to identify the proportion of BSA that is internalised by CME.

## 4.4 Conclusions

The work in this chapter presents the first extensive study quantifying endocytic pathways in quiescent cells and comparing them to proliferating cells. It was shown that a variety of pathways, such as CME, scavenger receptor-mediated endocytosis, endocytic carrier formation according to the GL-Lect hypothesis and macropinocytosis occur during proliferative quiescence. Interestingly, the activity of endocytic pathways during quiescence was differentially regulated for specific cargoes. Endocytosis of the classical CME cargoes Tf, LDL and EGF was reduced, in agreement with reduced requirement for nutrients and signalling factors needed for cell growth and division. On the other hand, endocytosis of proteins vital for quiescence, such as the lysosomal protein

Lamp1, was increased. These observations support the theory that quiescence is not a passive state in which cells wait for stimuli to divide, but is actively maintained. An interesting adaptation observed for quiescent RPE1 cells is the highly elevated uptake of extracellular protein (BSA) and cargo usually internalised by macropinocytosis, which appears to occur by CME. Future work will have to establish whether this is a common feature in quiescent cells by studying different cell types, such as quiescent endothelial cells (HUVECS) or quiescent fibroblasts. It also remains to be established whether this pathway is classical CME or dependent on specific adaptors by a combination approach of knockdown, dominant-negative mutant overexpression and chemical inhibitors. The next step will be to identify how uptake of the same cargo within the same cell type can be regulated differently depending on its cell cycle phase and might lead to a better understanding of the regulation of endocytic pathways.

The purpose of increased fluid and protein uptake in quiescence maintenance remains to be elucidated. The work presented here suggests that increased protein uptake does not serve mTORC1-mediated survival signalling upon starvation conditions. However, it may prime cells for efficient plasma membrane receptor turnover upon environmental changes or samplig of the environment itself. It might also be linked to quiescence-specific signalling events, which can be identified by specific kinase inhibitors.

Concluding, using an *in vitro* cell line model of two cell cycle phases allows not only to identify cell cycle-specific differences in endocytic activity, but might also reveal underlying or induced signallig processes which will enhance our understanding of molecular mechanisms linking endocytosis and signalling.

# 5 Integrin endocytosis and recycling during quiescence

## 5.1 Introduction

### 5.1.1 Integrin signalling in proliferative quiescence

Integrins are heterodimeric cell adhesion receptors providing a direct connection between the cell and its environment, mediating a variety of cellular functions such as cell adhesion, differentiation, proliferation and survival (Streuli, 2016). 24 distinct integrins can be formed by a noncovalent bond between a β- and α-subunit pooled from 8 β- and 18 α-subunits (Hynes, 2002). Integrins in the plasma membrane can interact with their ligands, ECM molecules such as collagen, fibronectin and laminins, with a specificity determined by their β- and α-subunits (Humphries, 2006; Hughes *et al.*, 1995). This interaction can trigger an 'outside-in' signalling mechanism, activating signalling cascades regulating proliferation, growth arrest or survival (Moreno-Layseca & Streuli, 2014). In this chapter, the effect of α3-integrin endocytosis and recycling on quiescence maintenance will be investigated. α3-integrin dimerises with β1, binds to laminins (Pattaramalai *et al.*, 1996) and was shown to be required for keratinocyte adhesion to their secreted ECM (Pazzagli *et al.*, 2017), for quiescence signalling and epithelium formation upon Laminin332-binding (Nguyen *et al.*, 2000) and for survival signalling (Manohar *et al.*, 2004; Oh *et al.*, 2009).

### 5.1.2 Integrin endocytosis and recycling

Integrins are highly endocytic molecules which, upon internalisation, are either degraded in lysosomes or recycled back to the plasma membrane (De Franceschi *et al.*,

2015). Both the α- and β-subunit are involved in integrin endocytosis. The cytoplasmic tail of α3-integrin contains two YXXΦ motifs, which are binding motifs for AP2, and a membrane-proximal GFFKR region (De Franceschi *et al.*, 2016). Endocytosis of β1-integrin can be mediated by both the adaptor proteins Numb and Dab2, which bind to its membrane-proximal NPXY motif and recruit endocytic adaptor proteins, such as AP2 (Calderwood *et al.*, 2003; Teckchandani *et al.*, 2012; Mishra *et al.*, 2004). Integrin recycling can occur via different pathways and might again be determined by their subunits. Retromer and Retriever complexes are highly involved in integrin recycling, and both participate in α3β1 subunit recycling, with α3-integrin depending on SNX17 and SNX35 and β1-integrin dependent solely on SNX17 (McNally *et al.*, 2017). However, a recently discovered recycling pathway, consisting of Vps3, Vps8 and the CHEVI complex, is also involved in β1-integrin recycling via Rab11-positive endosomes (Jonker *et al.*, 2018).

The endocytic nature of integrins reflects their sensitivity to changes in the ECM, as might happen during migration. It also serves ECM remodelling, as was shown for α3β1-dependent regulation of Laminin511 in the interfollicular basal lamina (Conti *et al.*, 2003; DiPersio *et al.*, 1997). Furthermore, integrins can mediate survival by endocytosis of their ECM ligands, which, when degraded in lysosomes, activate mTORC1 (Rainero *et al.*, 2015; Muranen *et al.*, 2017), or by directly signalling from endosomes, rendering cell survival independent from the extracellular environment (Alanko *et al.*, 2015; Tesfay *et al.*, 2016; Pazzagli *et al.*, 2017; Manohar *et al.*, 2004).

## 5.2 Results

### 5.2.1 Integrin endocytosis

When comparing the proteome of G1 and G0 RPE1 cells by SILAC mass spectrometry, levels of α3-integrin were four-fold higher in G0 than in G1 cells (data not shown). Furthermore, a matrisome analysis of the ECM of growing and quiescent RPE1 cells (3 biological replicates, 3 technical repeats per biological sample, performed and analysed by K. McGourty, E. Boucrot lab and A. Cryar, K. Thalassinos lab) identified a subset of Laminins as key components of the quiescent ECM (personal communication with E. Boucrot and K. McGourty). Laminins are ECM ligands for α3-integrin and might regulate proliferative quiescence by outside-in signalling via α3β1-integrin, which is known

to regulate cell adhesion, proliferation and survival (Nakada *et al.*, 2013; Manohar *et al.*, 2004; Pazzagli *et al.*, 2017; Tesfay *et al.*, 2016; Nguyen *et al.*, 2000).

#### 5.2.1.1 Colocalisation of internalised α3- with active or inactive β1-integrin

Integrins can endocytose bound to their ECM ligands (Muranen *et al.*, 2017). It was studied whether α3β1-integrin is internalised in a ligand-bound or unbound state. Monoclonal antibodies (mAb) specific for α3-integrin (mAbP1B5) and ligand-bound, extended β1 (mAb9EG7) or non-ligand bound collapsed β1-integrin (mAb13) were used (Byron *et al.*, 2009). The monoclonal anti-α3-integrin antibody P1B5 specifically binds to its extracellular beta propeller when it is dimerised with the β1 subunit and competes with α3 binding of laminins (Nicolaou *et al.*, 2012). It was also used in studies examining trafficking of α3-integrin (Das *et al.*, 2017).

MAb13 binds the βα-domain of β1 when it is not bound to ECM ligands and in a non-extended, or collapsed, conformation (Paul Mould *et al.*, 1996). MAb9EG7 binds the EGF-like repeats in the β1 subunit and stabilises its extended conformation, thereby enhancing ligand binding (Bazzoni *et al.*, 1995; Su *et al.*, 2016). It was confirmed that binding of mAb13 or 9EG7 does not alter integrin signalling, which makes these antibodies adequate tools to study integrin trafficking without inducing aberrant signalling events (Arjonen *et al.*, 2012).

To test whether α3-integrin internalisation occurs when it is bound to ligand-bound active or non-ligand-bound inactive β1-integrin, its colocalisation with anti-β1 mAb13 or mAb9EG7 was assessed in antibody feeding assays. Growing and quiescent RPE1 cells were incubated with primary antibody for 10 or 30 min at 37 °C to allow for antibody internalisation. Following uptake, endocytosis was halted by placing plates on ice, unbound antibody was removed by washes with ice-cold PBS and surface-bound antibody was removed by 2 min washes with ice-cold acidic buffer (1x pH 2.5, 2x pH 2.0). After fixation and permeabilisation, internalised antibody was labelled with fluorescence-conjugated secondary antibody and nuclei were stained with DAPI. Plates were imaged on a confocal microscope and colocalisation of α3- and β1-positive puncta was quantified by automated image analysis. The diameter of identified puncta was shrunk so that only overlaps of puncta centres were considered for colocalisation to avoid false-positives (see sec. 2.9.2 for details).

Microscopy images suggest that active β1-integrin labelled by mAb9EG7 was internalised to a lesser extend both after 10 and 30 min uptake than inactive β1-integrin labelled by mAb13 (Fig. 5.2.1A and C). This differs with the observation of Arjonen *et al.* (2012), who report increased uptake of active β1-integrin in cancer cells, but might be due to the non-tumourigenic nature of the cells used here. Arjonen *et al.* showed that ligand-bound β1-integrin traffics to lysosomes, which might serve as an additional amino acid supply to satisfy the increased demand of nutrients in cancer cells or to remodel the ECM. *In vivo* studies reported that activation of β1-integrin reduces their mobility and endocytosis (López-Ceballos *et al.*, 2016), which would explain reduced endocytosis of active β1-integrin particularly in quiescent RPE1 cells, which exhibit high cell surface levels of active β1-integrin (data not shown). The fraction of α3-integrin colocalising with ligand-bound β1-integrin did not differ between growing and quiescent cells after both 10 (about 20 %) and 30 min uptake (about 50 %) and colocalisation of α3- with non-ligand-bound β1-integrin in quiescent cells was marginally lower than in growing cells for both timepoints (Fig. 5.2.1B and D left). Interestingly, the percentage of colocalised α3- and ligand-bound β1-integrin increased by about 30 % after 30 min uptake compared to 10 min. Colocalisation of α3 with non-ligand-bound β1-integrin was generally higher than with ligand-bound β1 and did not differ with respect to the duration of antibody feeding (81.7 ± 0.4 % and 86.8 ± 0.1 % after 10 min, and 80.9 ± 1.2 % and 88.8 ± 0.4 % after 30 min in quiescent and growing cells, respectively) (Fig. 5.2.1B and D left). Thus, the majority of α3-integrin internalised when bound to non-ligand-bound β1. The sum of the α3-integrin fraction colocalising with active and inactive β1 is about 100 % after 10 min uptake in both growing and quiescent cells, which implies that the two complexes might enter cells via different endocytic pathways. After 30 min uptake, the sum of colocalisation with active and inactive β1 is higher than 100 %, suggesting that endosomes have fused during trafficking and contain both β1 conformers.

Analysis of internalised β1-integrin fractions showed a significantly smaller fraction colocalising with α3-integrin in quiescent cells than in growing cells for both ligand-bound and non-ligand-bound β1 after 10 and 30 min uptake (Fig. 5.2.1B and D right). Furthermore, colocalisation of non-ligand-bound β1 with α3 was significantly higher than that of ligand-bound in both growing and quiescent cells. This suggests that a larger proportion of both ligand-bound and non-ligand-bound conformer interacts with other α-subunits in

quiescent cells and that a larger proportion of ligand-bound β1 is dimerised with other α-subunits than α3 both in growing and quiescent cells.

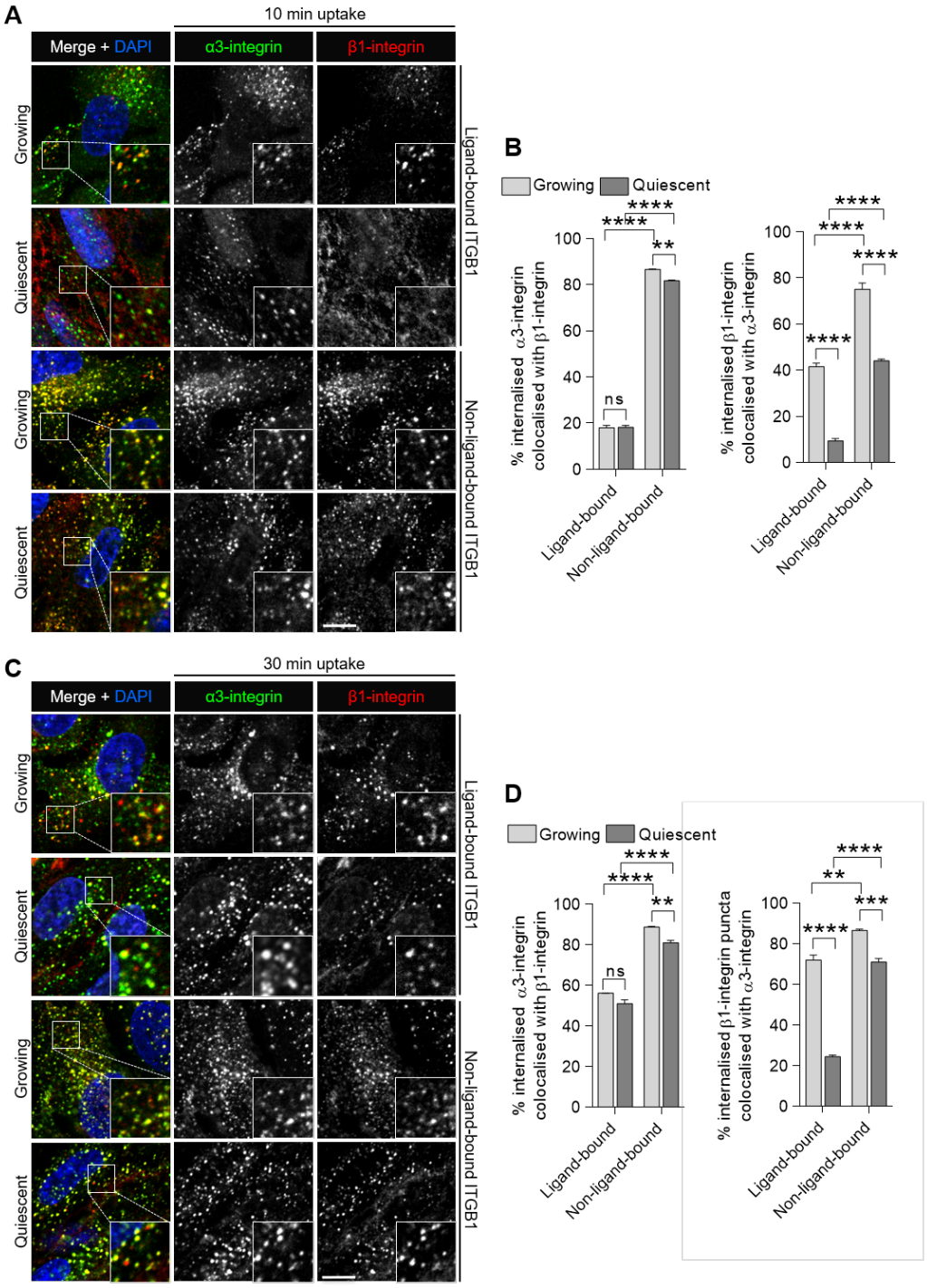


**Figure 5.2.1:** Colocalisation of internalised α3-integrin with ligand-bound and non-bound β1-integrin
**A** and **C:** Representative confocal microscopy sections of 10 min (**A**) amd 30 min (**D**) anti-β1- and α3-integrin antibody feeding in growing and quiescent RPE1 cells. Inlets show 2.2 x magnified view of boxed areas. Two distinct anti-β1-integrin antibodies were used, binding either to non-ligand-bound β1-integrin competing with ligand-binding, and binding to β1-integrin when it is bound to its ligand. Surface-bound antibody was stripped by acidic washes. Cells were fixed with 4 % PFA, permeabilised, incubated with fluorescence-conjugated secondary antibody and nuclei were stained with DAPI. Scale bars: 10 µm. **B** and **D:** Object-based quantification of α3- and β1-integrin colocalisation in images from **A** and **C**. α3- and β1-integrin-positive vesicles were identified as puncta, their perimeter shrunk by 2 pixels to account for true colocalisation and overlapping (colocalising) puncta were filtered and related back to the original-size puncta. Total fluorescence intensity of colocalised puncta per cell was normalised to total fluorescence intensity of all identified puncta. Bar graphs represent mean + SEM from n=3 biological replicates with a minimum of 80 growing and 120 quiescent cells per sample. Statistical significances of **B** and **D** were determined with , two-way ANOVA and Tukey's multiple comparisons test, comparisons as indicated by the brackets; ****P < 0.0001, ***P < 0.001, **P < 0.01, ns, not significant.

#### 5.2.1.2 Endocytosis of α3β1-integrin and CD151

To assess whether uptake of α3-integrin differs between growing and quiescent cells, antibody feeding assays were performed using mAbP1B5 for α3- and mAb13 for β1-integrin, because α3 was primarily internalised together with non-ligand-bound β1-subunit (sec. 5.2.1.1).

Growing and quiescent RPE1 cells were incubated with primary antibody for 10 or 30 min at 37 °C to allow for antibody internalisation. Following uptake, endocytosis was halted by placing plates on ice, unbound antibody was removed by washes with ice-cold PBS and surface-bound antibody was removed by 2 min washes with ice-cold acidic buffer (1x pH 2.5, 2x pH 2.0). In parallel, cell surface integrin levels were labelled by incubating cells on ice at 4 °C with respective primary antibody. After fixation and permeabilisation, internalised or surface primary antibody was labelled with fluorescence-conjugated secondary antibody and nuclei were stained with DAPI. Plates were imaged on a high-content widefield fluorescence microscope and images quantified by automated image analysis. Internalised antibody was identified as puncta to eliminate non-specific background signal. Mean fluorescence intensity of puncta was normalised to that of surface-labelled cells from which antibody was stripped by acidic washes to account for incomplete removal of surface-bound antibody. Normalised puncta mean fluorescence was then multiplied by puncta area per cell, which results in total fluorescence intensity in puncta per cell. Cell surface integrin levels of cells were normalised to blank samples labelled with secondary antibody to account for autofluorescence and total fluorescence intensity per cell calculated as described for puncta.

After 10 min, quiescent RPE1 cells internalised 91 ± 1 % less β1-integrin and 79 ± 2 % less α3-integrin than growing cells (Fig. 5.2.2A and B). Normalised to cell surface levels, which were lower in quiescent cells for both β1 and α3 (Fig. 5.2.2G and H), endocytosis of the two subunits was reduced by 76.8 ± 0.5 % for β1 and by 59 ± 2 % for α3 (Fig. 5.2.2C). The differences in endocytosis between the two subunits make sense, because β1 associates with many other alpha subunits, which might be internalised with different efficiency or are expressed at different levels at the cell surface (Hynes, 2002). The tetraspanin CD151 has been shown to interact strongly with α3β1-integrin (Berditchevski *et al.*, 2001; Sterk *et al.*, 2002) and to promote endocytosis of its associated integrins, among which is the α3-integrin subunit (Liu *et al.*, 2007). Because

mAbP1B5 against α3 does not interfere with CD151 complex formation, the potential effect CD151 might have on α3 β1-integrin endocytosis should not be disrupted (Nicolaou *et al.*, 2012). Endocytosis of CD151 was studied by monoclonal antibody feeding as described above to discover whether it might be responsible for the decreased endocytosis of α3-integrin in quiescent cells. Surprisingly, uptake and surface level-normalised endocytosis of CD151 did not differ after 10 min antibody feeding (Fig. 5.2.2A-C), indicating that it might not be the limiting factor. After 30 minutes uptake, quiescent cells still contained about 75 % β1 and 60 % less α3 than growing cells (Fig. 5.2.2D and E). However, α3 endocytosis did not differ when normalised to cell surface receptors, although that of β1 was still reduced by about 35 % (Fig. 5.2.2F). Interestingly, endocytosis of CD151 was about two-fold elevated in quiescent cells compared to growing cells when normalised to cell surface levels. After 30 minutes of internalisation, recycling and degradative pathways might affect the amount of internalised integrin observed. This implies that α3-integrin might either be retained longer in quiescent cells or degraded faster in growing cells.

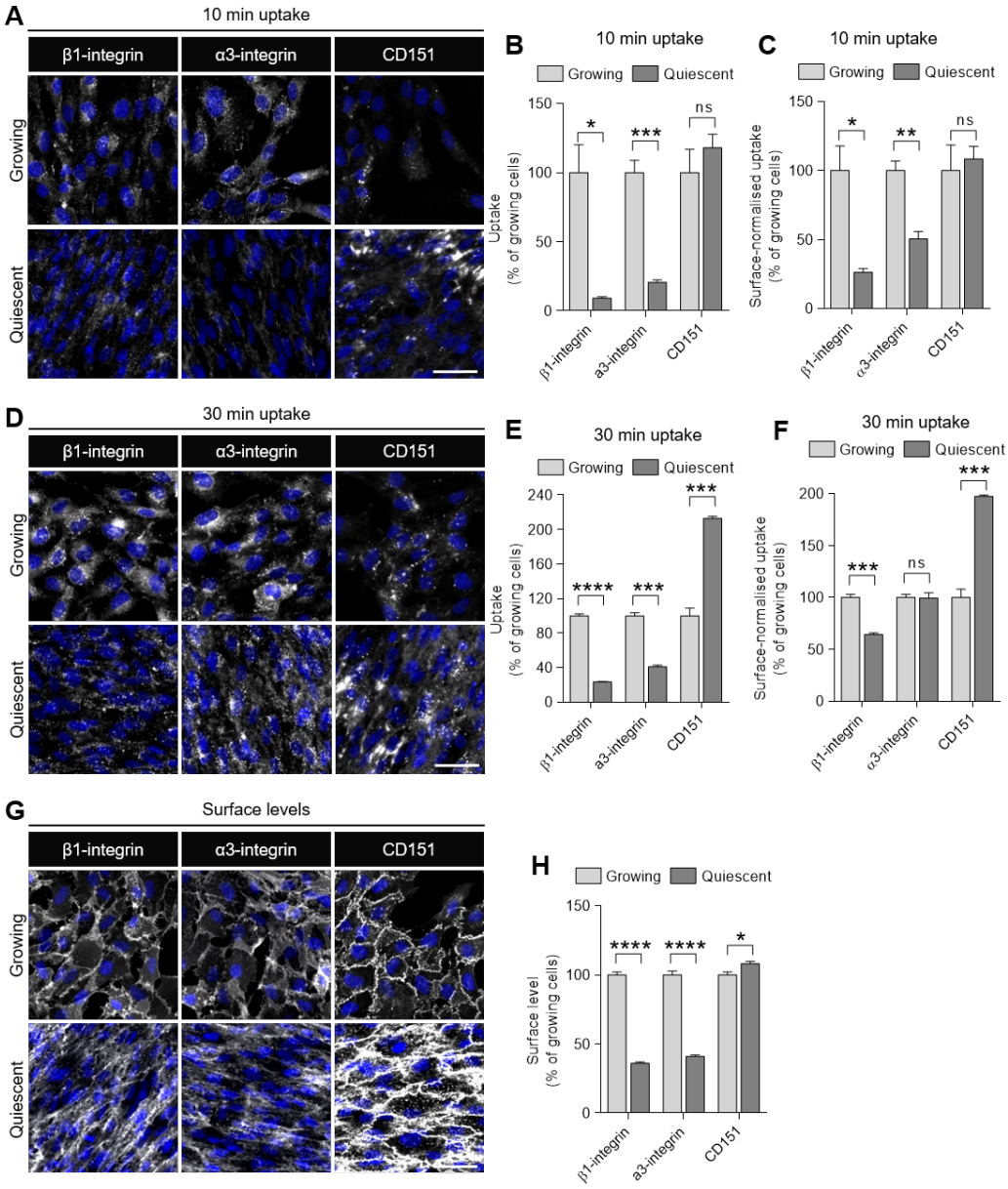


**Figure 5.2.2:** Uptake of β1- and α3-integrin and CD151 in growing and quiescent RPE1 cells
**A** and **D:** Representative epifluorescence microscopy images of 10 min (**A**) amd 30 min (**D**) anti-β1- and α3-integrin and anti-CD151 antibody feeding in growing and quiescent RPE1 cells. Surface-bound antibody was stripped by acidic washes. Cells were fixed with 4 % PFA, permeabilised, incubated with fluorescence-conjugated secondary antibody and nuclei were stained with DAPI (blue pseudocolour). Scale bars: 50 µm. **B** and **E:** Quantification of epifluorescence microscopy images from **A** and **D:** Total fluorescence intensity of internalised antibody per cell was normalised to growing cells. Bar graphs represent mean + SEM from n=3 biological replicates with a minimum of 5,000 growing and 10,000 quiescent cells per sample. **C** and **F:** Total fluorescence intensity of internalised antibody per cell was normalised to cell surface levels and growing cells. Bar graphs represent mean + SEM from n=3 biological replicates with a minimum of 5,000 growing and 10,000 quiescent cells per sample. **G:** Representative epifluorescence microscopy images of β-1 and α3-integrin and anti-CD151 cell surface immunolabelling. Cells were incubated on ice with primary antibody, washed, fixed with 4 % PFA, permeabilised and incuated with secondary fluorescence-conjugated antibody and DAPI to stain nuclei (blue pseudocolour). Scale bar: 50 µm. **H:** Total fluorescence intensity of cell surface-bound antibody per cell was normalised to growing cells. Bar graphs represent mean + SEM from n=3 biological replicates with a minimum of 5,000 growing and 10,000 quiescent cells per sample. Statistical significances of **B, C, E, F** and **H** were determined with Student's unpaired two-tailed t-test comparing quiescent to growing cells; ****P < 0.0001, ***P < 0.001, **P < 0.01, *P < 0.05, ns, not significant.

### 5.2.2 Quiescence signalling is not mediated by endosomal focal adhesion kinase

An explanation for prolonged residence of α3-integrin in quiescent cells could be that it might mediate endosomal FAK survival signalling, as discovered by (Alanko *et al.*, 2015; Alanko & Ivaska, 2016). Quiescent cells were shown to exhibit enhanced survival properties (Cheung & Rando, 2013; Coller *et al.*, 2006) and a quiescence survival signalling pathway was discovered by K. McGourty (Boucrot lab, data not shown). In brief, while proliferating cells rely on AKT/mTORC1 and nuclear ERK signalling for growth, proliferation and survival, quiescent cells downregulate AKT/mTORC1 signalling and upregulate a survival signalling pathway mediated by cytosolic ERK (Fig. 5.2.3).

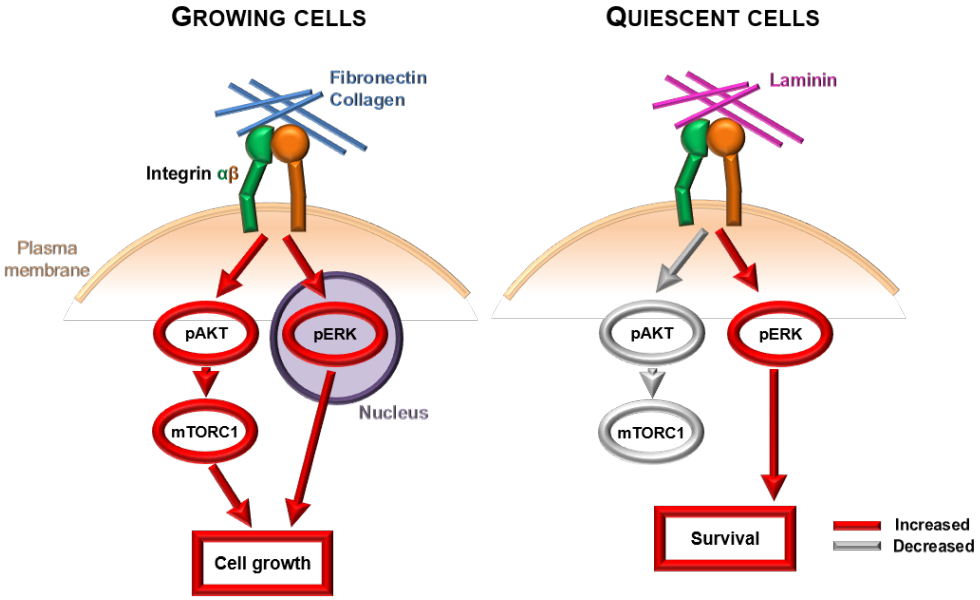


**Figure 5.2.3:** Quiescence survival signalling
Simplified schematic of AKT/mTORC1/nuclear ERK-mediated growth, proliferation and survival signalling in growing cells and cytosolic ERK-mediated survival signalling in quiescent cells with downregulated AKT/mTORC1 signalling. Active signalling pathways are displayed in red and pathways with decreased activity in grey. (K. McGourty, unpublished work)

To test whether FAK signalling from EEA-positive endosomes is elevated in quiescent RPE1 cells, colocalisation of FAK phosphorylated at Tyr397 (pFAK) with EEA1 was studied (Alanko *et al.*, 2015). Growing and quiescent RPE1 cells were fixed with PFA, permeabilised and immunolabelled for EEA1 and pFAK. Imaging occured by confocal microscopy and object-based colocalisation was performed with automated image analysis as described for sec. 5.2.1.1 and in sec. 2.9.2. The focal plane section was chosen based on EEA1 signal and was above the cell bottom where focal adhesion sites were. Although pFAK in quiescent cells exhibited a distinct punctate pattern in the plane of

EEA1-positive endosomes, the total intensity of pFAK colocalised with EEA1-positive endosomes was about half of that in growing cells (Fig. 5.2.4A and B left). To consider differences in levels of all pFAK and EEA1 puncta between growing and quiescent cells, colocalised puncta were normalised to all identified puncta. Consistently, a higher fraction of EEA1-positive endosomes (44 ± 4 %) colocalised with pFAK in growing cells than in quiescent cells (29 ± 2 %) and the fraction of pFAK colocalised with EEA1 puncta did not differ (Fig. 5.2.4B right). Hence, pFAK recruitment to EEA1-positive endosomes is not increased in quiescent cells and might therefore not result in elevated endosomal pFAK signalling. An interesting observation was furthermore that quiescent cells exhibit smaller focal adhesions (Fig. 5.2.4C). Perhaps focal adhesion signalling might not be prevalent during quiescence.

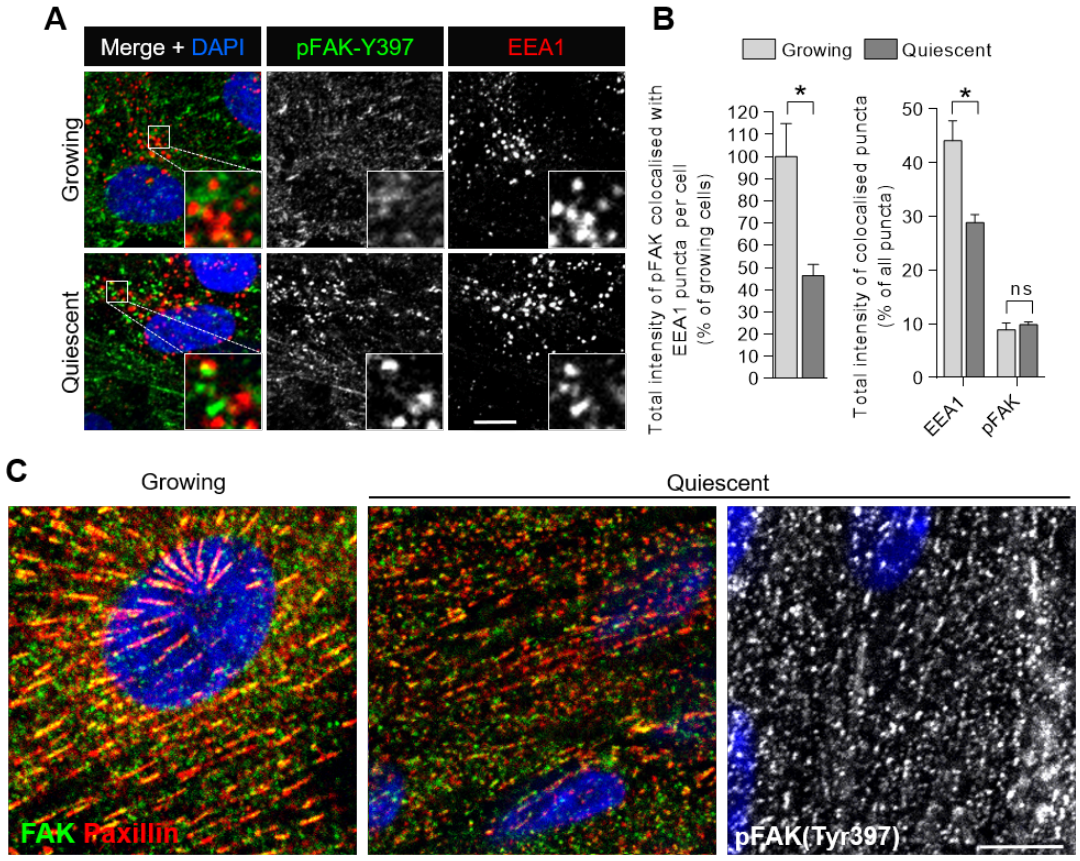


**Figure 5.2.4:** Colocalisation of phosphorylated FAK (Tyr397) with EEA1-positive endosomes
**A:** Representative confocal microscopy sections of PFA-fixed permeabilised growing and quiescent RPE1 cells immunolabelled for phosphorylated FAK (Tyr397; pFAK) and EEA1. Inlets show 3.5 x magnified view of boxed areas. Scale bar: 10 µm. **B:** Left: Total intensity of pFAK puncta colocalised with EEA1 puncta per cell. Left: Total intensity of EEA1 puncta containing pFAK or of pFAK puncta colocalised with EEA1 as percentage of total EEA1 or pFAK puncta intensity, respectively. Bar graphs represent mean + SEM from n=3 biological replicates with a minimum of 75 growing and 180 quiescent cells per sample, *P < 0.05, ns, not significant, Student's unpaired two-tailed t-test comparing quiescent to growing cells.

### 5.2.3 α3-integrin trafficking through endosomal compartments

The next step was to identify the subcellular localisation of internalised α3-integrin to find out where it was retained within quiescent cells after 30 min trafficking, or whether it was simply degraded faster in growing cells. Trafficking of α3-integrin was studied by quantifying its colocalisation with markers of endosomal compartments. As early endosomal markers, EEA1 and APPL1 were chosen. Both reside on Rab5-positive early endosomes. They can be found there either together or separately, the latter defining independent endosomal sorting compartments (Kalaidzidis *et al.*, 2015). VPS35 was chosen as marker for recycling endosomes, because it is a subunit of the Retromer cargo recognition complex (Mukadam & Seaman, 2015), which is involved in α3-integrin recycling (McNally *et al.*, 2017). Finally, Lamp1 was selected as lysosomal marker to evaluate lysososmal degradation (Williams & Fukuda, 1990).

Anti-α3-integrin antibody feeding was performed as described in sec. 5.2.1.1. Fixed and permeabilised cells were counterlabelled for endosomal markers and plates were analysed by confocal microscopy. Based on the rationale that a higher occupancy of a specific endosomal compartment is equivalent to an extended residence of internalised α3-integrin within that compartment at a steady state (*i.e.* fixed cells), colocalisation of α3-integrin-positive endosomes with marker-labelled endosomes was quantified as described in sec. 5.2.1.1. Total fluorescence intensity of α3-positive puncta colocalising with a specific endosomal compartment was normalised to the total amount of internalised α3 to obtain fractions of α3 for each endosomal compartment analysed.

After 10 min uptake, α3-integrin was present in significantly more EEA1- and Lamp1-positive endosomes in growing (68 ± 1 % EEA1, 28 ± 1 % Lamp1) than in quiescent cells (32 ± 1 % EEA1, 7 ± 1 % Lamp1 Fig. 5.2.5A and B). In quiescent cells, 10 % more α3-integrin co-localised with the Retromer subunit VPS35 (70 ± 3 %) than in growing cells (60 ± 1 %). Because VPS35 localises to EEA1-positive endosomes (Temkin *et al.*, 2011) and the resolution of the acquired microscopy images was not enough to differentiate endosomal subdomains, α3-integrin colocalisation might have been quantified redundantly for endosomes associated with both EEA1 and Retromer, resulting in a sum larger than 100 % when adding up all endosomal α3 fractions. Therefore, the sum of endosomal α3 fractions was normalised to 100 % and represented as stacked bar graph for better comparison of subcellular α3 distribution in growing and quiescent cells

(Fig. 5.2.5C). This approach does not represent the absolute levels of α3-integrin per endosomal compartment, but highlights that in quiescent cells, internalised α3 resided primarily in endosomes associated with Retromer, whereas in growing cells α3 was almost equally distributed between EEA1-positive and VPS35-positive endosomes.

It was now interesting to find out whether the majority of α3-integrin would remain in VPS35-positive endosomes in quiescent cells after 30 min uptake, or whether its trafficking would change upon prolonged internalisation of 30 min. For this time point, α3 colocalisation with the early endosomal marker APPL1 (Adaptor protein, phosphotyrosine interacting with PH domain and leucine zipper 1) was quantified in addition to EEA1, in case APPL1 would mark an early endosomal sorting compartment favoured to EEA1 in quiescent cells. Interestingly, APPL1 was shown to regulate cell migration by modulating Rab5-controlled endocytosis and recycling of β1-integrin, resulting in decreased adhesion dynamics (Diggins *et al.*, 2018). However, only little α3-integrin colocalised with APPL1 in both growing and quiescent cells (Fig. 5.2.6A and B). The distribution of α3-integrin in early endosomes was similar to that after 10 minutes, with significantly more α3 in APPL1-positive as well as EEA1-positive endosomes in growing cells (25 ± 1 % APPL1, 66 ± 1 % EEA1) compared to quiescent cells (11 ± 1 % APPL1, 36 ± 2 % EEA1). This might rule out a specific role for early endosomal markers in α3-integrin trafficking and signalling in quiescent RPE1 cells. Lysosomal levels of α3-integrin were also higher in growing (27 ± 1 %) than in quiescent cells (8 ± 1 %). However, 25 % more α3-integrin resided in VPS35-positive vesicles in quiescent cells (55 ± 2 %) than in growing cells (30 ± 3 %), which is 15 % more than after 10 min uptake. When the sum of all endosomal α3-integrin fractions was normalised to 100 %, the differrence became even more striking, highlighting that Retromer appears to play a major role in α3-integrin trafficking in quiescent cells, whereas in growing cells, α3 seems to traffick mainly through EEA1-positve endosomes (Fig. 5.2.6C). This suggests a trafficking route of fast early endosomal recycling in addition to a significant proportion of one fifth being degraded in lysosomes in growing cells (Fig. 5.2.6B and C). The data here propose a pivotal role of Retromer-dependent recycling for α3-integrin function in quiescence. Of course, many more endosomal recycling markers exist, such as Retriever, recycling pathways identified slow Rab11 and fast Rab4 recycling or Rab9-mediated retrograde transport to the TGN, and are tempting markers to look at to determine the recycling mechanism of α3-integrin in quiescent cells.

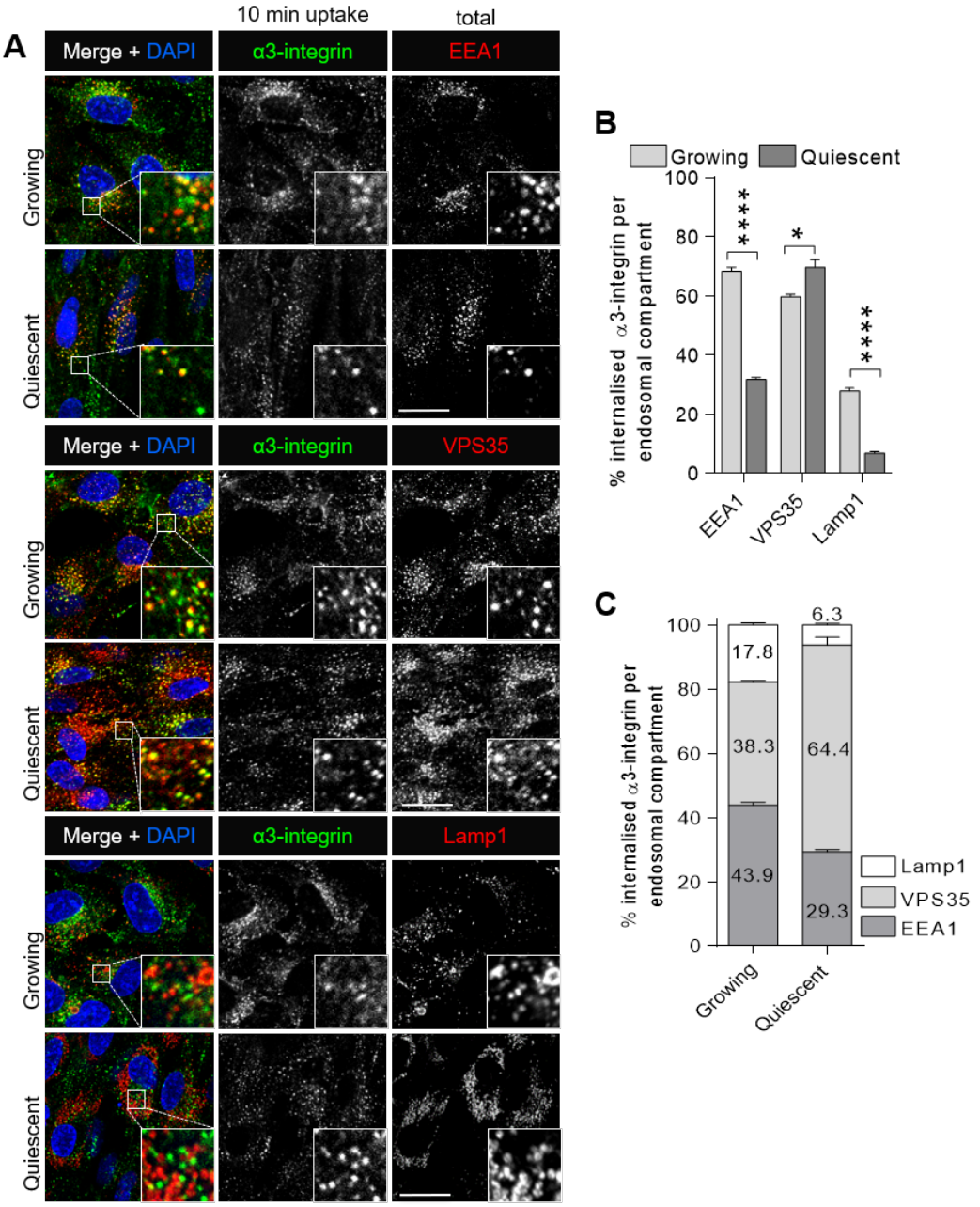


**Figure 5.2.5:** Colocalisation of α3-integrin with endosomal compartments after 10 minutes uptake
**A:** Representative confocal microscopy sections of 10 min anti-α3-integrin antibody feeding in growing and quiescent RPE1 cells colabelled for endosomal markers EEA1, VPS35 and Lamp1. Inlets show 4.3 x magnified view of boxed areas. Surface-bound α3-integrin antibody was stripped by acidic washes after uptake. Cells were fixed with 4 % PFA, permeabilised, colabelled for endosomal markers, incubated with fluorescence-conjugated secondary antibody and nuclei were stained with DAPI. Scale bars: 25 µm. **B:** Object-based quantification of α3-integrin colocalisation with endosomal markers in images from **A**. α3-positive endosomes and EEA1-, VPS35- or Lamp1-positive vesicles were identified as puncta, their perimeter shrunk by 2 pixels to account for true colocalisation and overlapping (colocalising) shrunken puncta were filtered and related back to the original-size puncta. Total fluorescence intensity of colocalised puncta per cell was normalised to total fluorescence intensity of all identified puncta. Bar graphs represent mean + SEM from n=3 biological replicates with a minimum of 100 growing and quiescent cells per sample, ****P < 0.0001, *P < 0.05; Student's unpaired two-tailed t-test. **C:** Quantifications from **B** represented as stacked bar graphs (mean + SEM from n=3 biological replicates) with α3-integrin fractions in all endosomal compartemnts normalised to 100 % to visualise differences in its subcellular distribution between growing and quiescent cells.

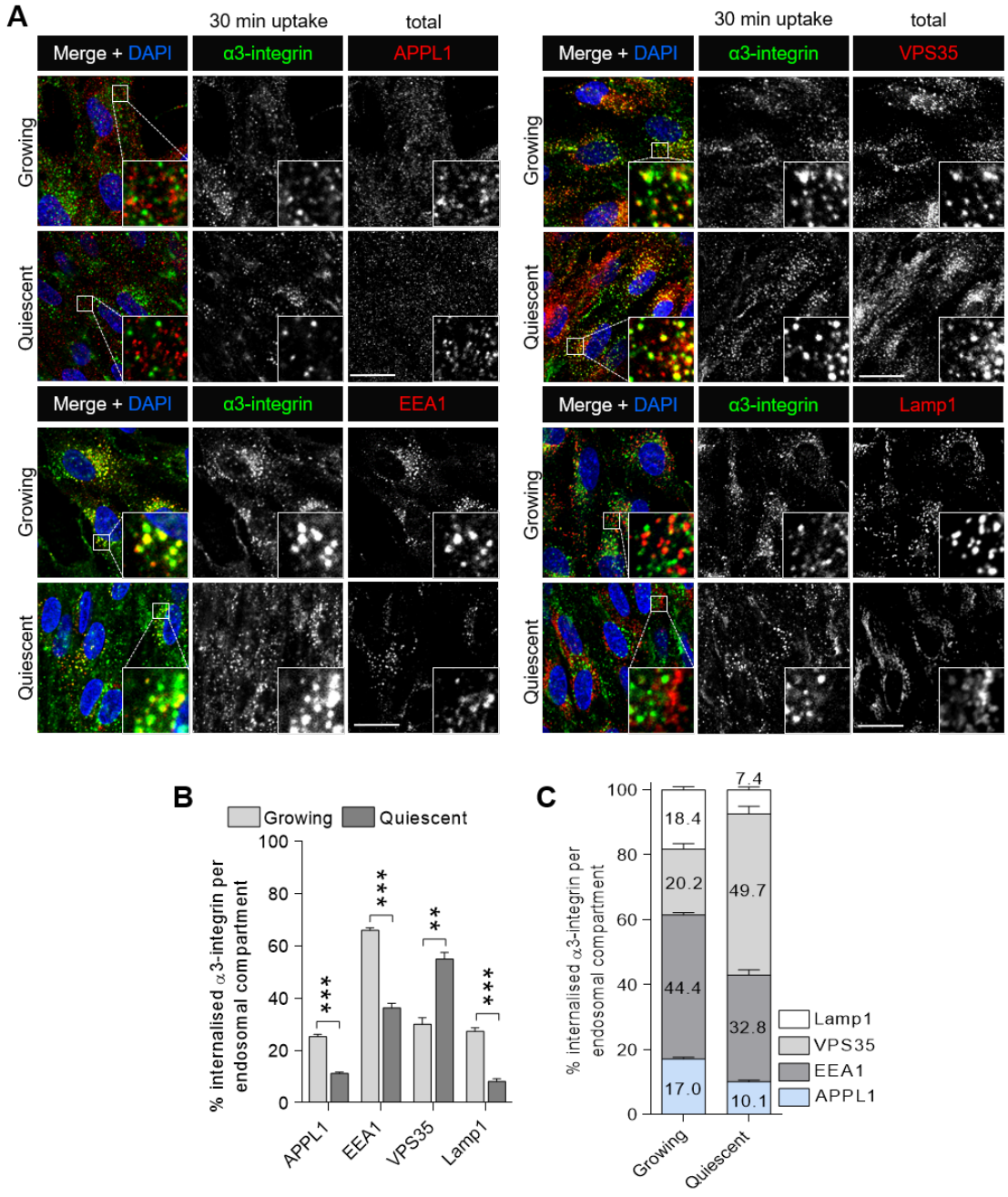


**Figure 5.2.6:** Colocalisation of α3-integrin with endosomal compartments after 30 minutes uptake
**A:** Representative confocal microscopy sections of 30 min anti-α3-integrin antibody feeding in growing and quiescent RPE1 cells colabelled for endosomal markers APPL1, EEA1, VPS35 and Lamp1. Inlets show 4.3 x magnified view of boxed areas. Surface-bound α3-integrin antibody was stripped by acidic washes after uptake. Cells were fixed with 4 % PFA, permeabilised, colabelled for endosomal markers, incubated with fluorescence-conjugated secondary antibody and nuclei were stained with DAPI. Scale bars: 25 µm. **B:** Object-based quantification of α3-integrin colocalisation with endosomal markers in images from **A**. α3-positive endosomes and APPL1-, EEA1-, VPS35- or Lamp1-positive vesicles were identified as puncta, their perimeter shrunk by 2 pixels to account for true colocalisation and overlapping (colocalising) shrunken puncta were filtered and related back to the original-size puncta. Total fluorescence intensity of colocalised puncta per cell was normalised to total fluorescence intensity of all identified puncta. Bar graphs represent mean + SEM from n=3 biological replicates with a minimum of 100 growing and quiescent cells per sample, ***P < 0.001, **P < 0.01; Student's unpaired two-tailed t-test. **C:** Quantifications from **B** represented as stacked bar graphs (mean + SEM from n=3 biological replicates) with α3-integrin fractions in all endosomal compartemnts normalised to 100 % to visualise differences in its subcellular distribution between growing and quiescent cells.

### 5.2.4 α3-integrin recycling appears to be slower in quiescent cells

Since Retromer is involved in recycling of integrins (McNally *et al.*, 2017), recycling of α3-integrin was measured in a functional assay which allows quantification of both recycled and non-recycled receptors for multiple time points (Manna *et al.*, 2010). Growing and quiescent RPE1 cells were incubated with anti-α3-integrin mAbP1B5 for 90 minutes at 37 ℃ to saturate endocytic and recycling compartments. Since cell surface antibody removal with highly acidic buffer (pH 2.5 and lower) diminishes cell fitness, particularly when cells are transferred back to 37 ℃, cell surface-bound mAbP1B5 was instead blocked with an unlabelled secondary antibody on ice for 60 min (Fig. 5.2.7A). Cells were then transferred back to 37 ℃ and incubated with an AlexaFluor647-conjugated secondary antibody for the indicated time points. Only recycled mAbP1B5 will be labelled by this secondary antibody. Following recycling, cells were placed on ice, unbound AlexaFluor647-conjugated secondary antibody was removed by washes with ice-cold PBS and cells were fixed with PFA, permeabilised and labelled with an AlexaFluor488-conjugated secondary antibody to detect non-recycled mAbP1B5. Plates were imaged at a high-content widefield fluorescence micoscope and images analysed by automated image analysis quantifying total fluorescence intensity per cell for recycled and non-recycled mAbP1B5. Microscopy images confirm that, using this assay, distinct populations of recycled and non-recycled α3-integrin, which do not colocalise, can be identified (Fig. 5.2.7B). The kinetics of recycled α3-integrin appeared faster in growing than in quiescent cells over the period of 60 min, the amount of recycled α3 being significantly higher than in quiescent cells at each time point measured (Fig. 5.2.7C). When, however, the efficiency of the surface-blocking step by incubation with unlabelled secondary antibody was assessed, the surface blocking proved not to be complete, because residual α3-integrin was labelled by a fluorophor-conjugated secondary following the 60 min incubation with unlabelled secondary antibody, while unlabelled secondary antibody was still present (data not shown). To account for differing surface blocking efficiency, recycled α3-integrin was normalised to 5 min recycling in both growing and quiescent cells. If α3-integrin recycled indeed faster in growing cells, it would also do so after 15, 30 and 60 min. However, levels of recycled α3-integrin did not differ between growing and qiescent cells for 15 and 30 min of recycling. Only after 60 min of recycling, approximately 16 % more recycled α3-integrin was measured in growing cells when

compared to quiescent cells. While this experiment might need a better control to account for incomplete surface blocking by the unlabelled secondary antibody, it suggests that no severe difference exists for $\alpha$3-integrin, particularly when recycling is assessed for 30 min.

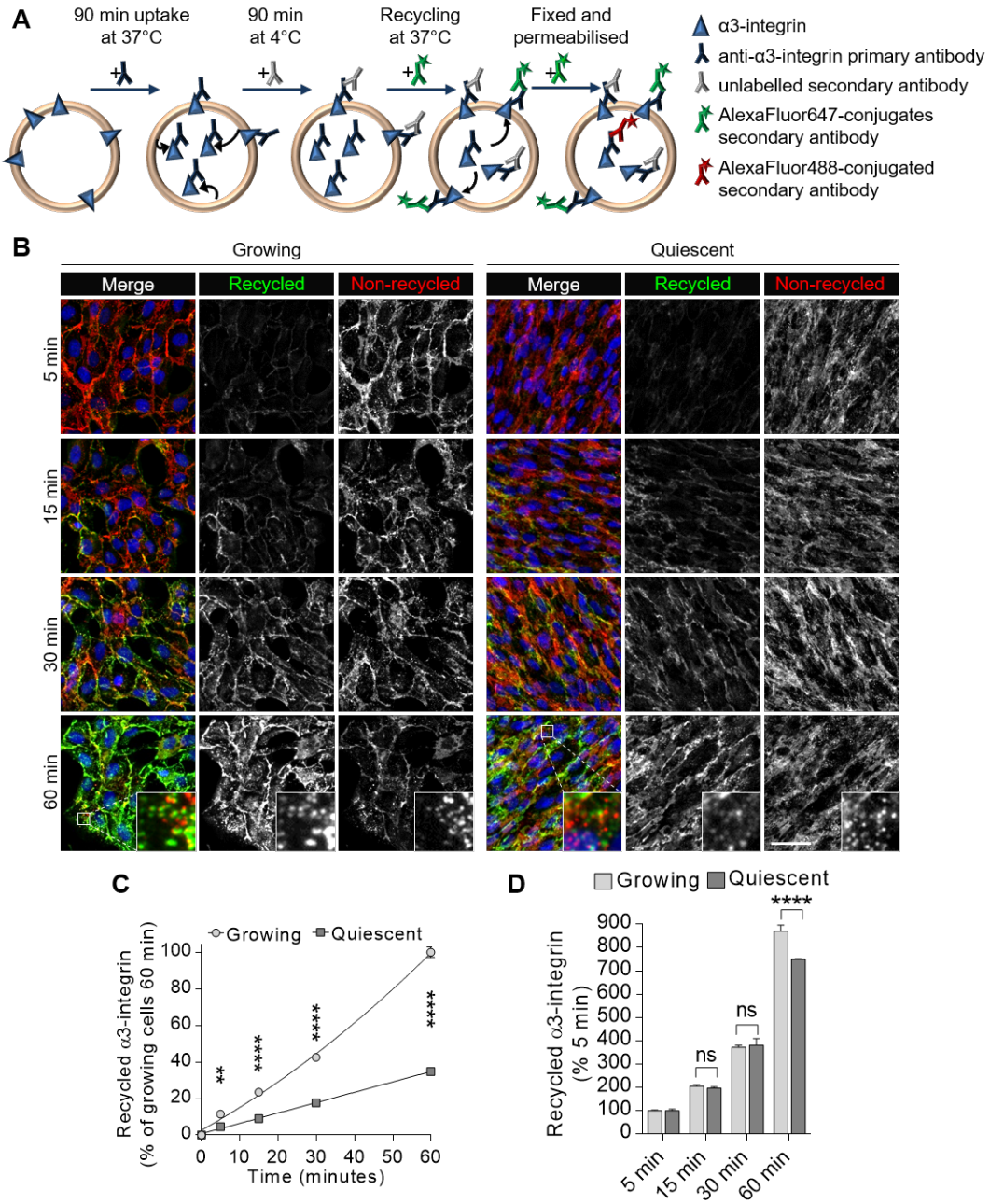


**Figure 5.2.7:** Recycling of α3-integrin in growing and quiescent RPE1 cells

**A:** Schematic overview of α3-integrin recycling assay. Cells were subjected to anti-α3-integrin antibody feeding for 90 min at 37 ℃, followed by blocking of surface-bound antibody with an unlabelled secondary antibody on ice for 90 min. Cells were then transferred back to 37 ℃ and incubated with AlexaFluor647-conjugated secondary antibody for multiple time points to label recycled α3-integrin primary antibody. Following recycling, cells were fixed with 4 % PFA and α3-integrin which was not recycled was labelled with AlexaFluor488-conjugated secondary antibody. Inlets show 5 x magnified view of boxed areas. scale bar: 50 µm. **B:** Representative epifluorescence microscopy images 5, 15, 30 and 60 min α3-integrin recycling in growing and quiescent RPE1 cells. Cells were treated as described in **A**; nuclei are represented in blue pseudocolour. Inlets show 5.3X magnified boxed areas. Scale bar: 50 µm. **C:** Quantification of epifluorescence microscopy images from **B**. Total fluorescence intensity of per cell was normalised to growing cells after 60 min recycling. Data represent mean ± SEM of recycled α3-integrin from n=3 biological replicates with a minimum of 6,000 growing and 12,000 quiescent cells per sample. **D:** Quantification from **C** normalised to 5 min recycling α3-integrin in growing and quiescent cells, respectively. Bar graphs represent mean + SEM from n=3 biological replicates with a minimum of 6,000 growing and 12,000 quiescent cells per sample. Statistical significances in C and D were derived from two-way ANOVA with Sidak's multiple comparisons test comparing growing and quiescent cells, ****P < 0.0001, **P < 0.01, ns, not significant.

### 5.2.5 Monensin and Primaquine trap more recycling α3-integrin vesicles in quiescent than in growing cells

Next, it was assessed whether recycling inhibition by chemical compounds would trap more α3β1-integrin in quiescent cells. Primaquine (PQ) and Monensin were both shown to inhibit integrin recycling (Woods *et al.*, 2004; Marre *et al.*, 2010). PQ is an amphiphilic weak base which can cross membranes in a non-protonated form. Once in acidic endosomal compartments, including lysosomes (Schwartz *et al.*, 1985), it becomes protonated due to the acidic endosomal pH, which traps it in endosomes, thereby neutralising endosomal pH (Van Weert *et al.*, 2000). Monensin is a sodium ionophore acting as a sodium-potassium antiporter preventing endosomal acidification, but also has an effect on lysosomal pH (Wileman *et al.*, 1984).

Growing and quiescent cells were treated with vehicle (DMSO), 50 µM PQ or 100 µM Monensin for 2 hours, fixed with PFA, permeabilised and immunolabelled for α3β1-integrin and TfR1 as a positive control of recycling inhibition. Plates were analysed by high-content widefield fluorescence microscopy and automated image analysis. Microscopy images show that upon PQ and Monensin treatment, α3- and β1-integrin are located primarily at the plasma membrane, but distinct puncta become visible upon PQ and Monensin treatment and are interpreted as trapped vesicles (Fig. 5.2.8A and B). These speckles, defined as distinct foci with increased intensity relative to its immediate neighbourhood, were enhanced in CellProfiler software. This results in the suppression of intensities which are not distinct foci of a specified diameter, leaving only vesicle-like punctate structures of bright intensity for object identification. The total intensity of identified puncta per cell was then measured, normalised to total levels per cell and compared to vehicle-treated growing or quiescent cells, respectivey. PQ and Monensin treatment lead to a significantly higher trapping of both α3- and β1-vesicles in quiescent than in growing cells (Fig. 5.2.8A and B). The fraction of trapped β1-vesicles in quiescent cells was almost 8 times higher than control upon PQ treatment and almost 13 times higher than control and upon Monensin treatment (Fig. 5.2.8A). The relative β1-vesicle accumulation in quiescent cells was also 5 times higher than in growing cells upon both PQ and Monensin treatment. The fraction of trapped α3-integrin vesicles in quiescent cells was 9 times higher than control upon PQ treatment and 7 times higher than control upon Monensin treatment (Fig. 5.2.8B). This was 6.5 times higher than in growing

cells upon PQ treatment and almost 5 times higher than in growing cells upon Monensin treatment. These results suggest that α3β1-integrin recycles more actively in quiescent than in growing cells and recycling inhibition by two chemical compounds with different inhibitory mechanisms results in increased accumulation of both integrins in quiescent cells.

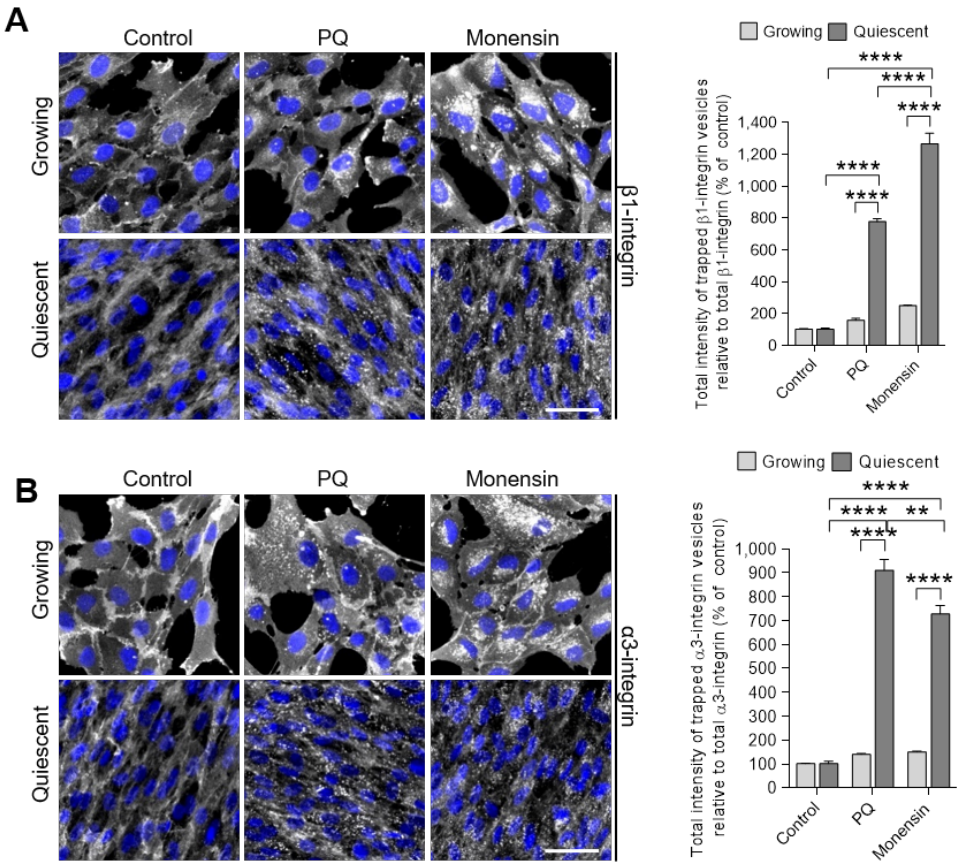


**Figure 5.2.8:** Treatment with Monensin and Primaquine traps recycling α3β1-integrin
**A** and **B** Left: Representative epifluorescence microscopy images of growing and quiescent RPE1 cells treated with vehicle (DMSO), 50 µM Primaquine (PQ) or 100 µM Monensin for 2 hours, fixed with 4 % PFA and immunolabelled with anti-β1-integrin mAb13 or anti-α3-integrin mAbP1B5 (represented in white). DNA was stained with DAPI (blue pseudocolour). Scale bars: 50 µM. **A** and **B** right: β1-integrin or α3-integrin vesicles were identified as enhanced puncta in images, while background intensity without distinct puncta of high intensity was suppressed (left). Total fluorescence intensity of puncta was normalised to total fluorescence intensity per cell and respective DMSO control in growing and quiescent cells. Bar graphs represent mean + SEM from n=3 (uptake) biological replicates with a minimum of 5,000 growing and 15,000 quiescent cells per sample; ****P < 0.0001, ***P < 0.001, **P < 0.01, *P < 0.05, ns, not significant, two-way ANOVA with Tukey's multiple comparisons test.

### 5.2.6 Pharmacological recycling inhibition leads to accumulation of internalised α3-integrin in quiescent cells

To confirm that the trapped vesicles observed in sec. 5.2.5 originated from endocytosis, accumulation of α3-positive vesicles upon PQ and Monensin treatment was measured

for an anti-α3-integrin antibody feeding assay. 30 min uptake of anti-mAbP1B5 was performed as described in sec. 5.2.1.1 in cells treated with vehicle (DMSO), 50 µM PQ or 100 µM Monensin for 30 min prior to and throughout uptake and was imaged on a high-content widefield epifluorescence microscope. Internalised α3-integrin was quantified by automated image analysis as described in sec. 2.9.1. In DMSO-treated control cells, α3-integrin utpake in quiescent cells was lower than in growing cells, but after Monensin treatment, the amount of internalised α3-integrin did not differ between growing and quiescent cells, which was partially due to a 35 ± 0.5 % decrease of internalised α3-integrin in growing cells and partially because of a more than two-fold increase in quiescent cells (Fig. 5.2.9A and B). PQ treatment elevated levels of internalised α3 in both growing (about 1.7 fold) and quiescent (about 1.85 fold) cells, resulting in lower α3-integrin in quiescent than in growing cells. Interestingly, the cellular localisation of α3-positive vesicles both in control and Monensin-treated cells appears rather perinuclear, whereas in PQ-treated cells it is more disperse (Fig. 5.2.9A). This suggests that the drugs inhibit α3 trafficking in different endosomal compartments, which might explain their differing effect on the levels of internalised α3-integrin in growing cells. In quiescent cells, however, both Monensin and PQ treatment resulted in accumulation of α3-integrin, with Monensin having a significantly higher effect (233 ± 4 %) than PQ (183 ± 10 %) compared to levels in DMSO-treated cells (Fig. 5.2.9C).

Because Monensin reduced α3-integrin uptake in growing and increased it in quiescent cells, it was assessed whether 90 min Monensin treatment, which is even longer than the 30 min preincubation used for mAbP1B5 feeding assays, changed α3-integrin cell surface levels. Elevated cell surface α3-integrin would affect the pool availabe for internalisation. Following vehicle (DMSO) or Monensin treatment, live cells were incubated on ice with mAbP1B5 for 90 min, fixed with PFA and labelled with secondary antibody and DAPI, imaged on a high-content widefield epifluorescence microscope and total levels of cellular surface α3-integrin quantified by automated image analysis. Cell surface α3-integrin levels in quiescent cells were lower than in growing cells as established in sec. 5.2.1.2, but were not changed by Monensin treatment, potentially because 90 min of treatment are too short to significantly decrease cell surface levels by integrin endocytosis or because newly synthesised α3-integrin replenished the surface pool (Fig. 5.2.9D and E). When normalised to cell surface level, the amount of internalised α3-integrin was two-fold increased in quiescent cells compared to growing cells

(Fig. 5.2.9F). α3-integrin uptake in DMSO-treated cells was slightly lower in quiescent than growing cells (16 ± 3 %), which conflicts with unchanged endocytosis observed in sec. 5.2.1.2 but could have been caused by an effect of DMSO. Importantly, Monensin treatment decreased α3-integrin endocytosis in growing cells but lead to a more than two-fold accumulation of endocytic α3-integrin levels in quiescent RPE1 cells, supporting a potential role of its recycling during quiescence (Fig. 5.2.9G).

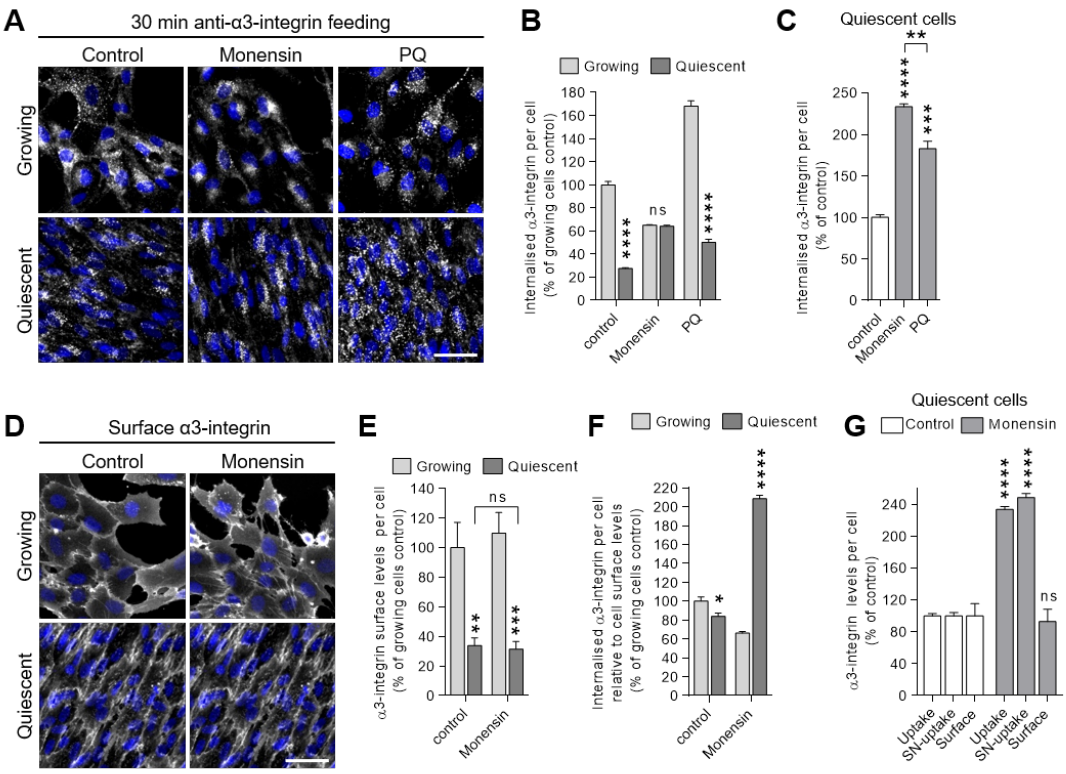


**Figure 5.2.9:** Effect of recycling inhibitors on α3-integrin uptake in growing and quiescent RPE1 cells
**A** and **D:** Representative epifluorescence microscopy images of 30 min anti-α3-integrin (**A**) antibody feeding and α3-integrin cell surface levels (**D**) in growing and quiescent RPE1 cells in the presence of vehicle (DMSO control), 100 µM Monensin or 50 µM Primaquine (PQ). Scale bars: 50 µm. **A**: Cells were pre-treated with drugs 30 min prior to uptake. Following uptake, surface-bound antibody was stripped by acidic washes. Cells were fixed with 4 % PFA, permeabilised, incubated with fluorescence-conjugated secondary antibody and nuclei were stained with DAPI (blue pseudocolour). **D:** After 90 minutes drug treatment, live cells were incubated on ice with primary anti-α3-integrin antibody, fixed with 4 % PFA, permeabilised, incubated with fluorescence-conjugated secondary antibody and nuclei were stained with DAPI (blue pseudocolour). **B** and **E:** Quantification of epifluorescence microscopy images from **A** and **D:** Total fluorescence intensity of internalised or surface-bound antibody per cell was normalised to growing cells DMSO control. Bar graphs represent mean + SEM from n=3 (uptake) or n=6 (surface) biological replicates with a minimum of 5,000 growing and 15,000 quiescent cells per sample. **C:** Data from quiescent cells in **B** were normalised to quiescent cells DMSO control; ****P < 0.0001, ***P < 0.001, **P < 0.01, one-way ANOVA with Tukey's multiple comparisons test comparing inhibitor-treated samples to respective DMSO control and Monensin- and PQ-treated cells as indicated. FF**:** Total fluorescence intensity of internalised antibody per cell was normalised to cell surface levels and growing cells. Bar graphs represent mean + SEM from n=3 biological replicates with a minimum of 5,000 growing and 15,000 quiescent cells per sample. **G:** Total fluorescence intensity of internalised, surface bound-normalised (SN-uptake) internalised or surface-bound α3-integrin in Monensin-treated quiescent cells was normalised to respective quiescent cells DMSO control. Bar graphs represent mean + SEM from n=3 (uptake, surface bound-normalised uptake) or n=6 (surface) biological replicates with a minimum of 5,000 growing and 15,000 quiescent cells per sample; ****P < 0.0001, ns, not significant, one-way ANOVA with Dunett's multiple comparisons test comparing inhibitor-treated samples to respective DMSO control. Statistical significances of **B, E** and **F** were determined with two-way ANOVA with Tukey's multiple comparisons test comparing quiescent and growing cells; ****P < 0.0001, ***P < 0.001, **P < 0.01, *P < 0.05, ns, not significant.

### 5.2.7 Recycling inhibition with monensin reduces quiescence survival signalling

K. McGourty (Boucrot lab) established that quiescent RPE1 cells secrete an ECM with laminins as key components, differing from the ECM secreted by growing cells (unpublished work). Laminins are integrin ligands and mediate outside-in signalling which can regulate the cell cycle to, for example, mediate quiescence entry. Associated with cell cycle exit, he identified a quiescence survival signalling pathway, which effectuates resistance to apoptosis and depends on reduced AKT/mTORC1 signalling concomitant with elevated ERK activity (Fig. 5.2.3). Laminins are ECM ligands for $\alpha$3-integrin and a role for $\alpha$3-integrin in ERK signalling was described in glioma stem-like cells, which reside in a laminin-rich niche (Nakada *et al.*, 2013). However, how precisely quiescence survival signalling is mediated by integrins is unknown. The results in the previous chapter suggest that recycling of $\alpha$3-integrin might be required for its signalling. It was therefore tested whether recycling inhibition by chemical compounds, such as Monensin or PQ, would perturb quiescence signalling. The advantage of small chemical compounds is the short exposure for their immediate effect, whereas knockdown or overexpression might change homeostatic balances over a long period of time and the observed effect might not be directly linked to the manipulation.

Growing and quiescent cells were incubated with vehicle (DMSO), 100 µM Monensin or 50 µM PQ for 90 min, fixed with PFA, permeabilised and immunolabelled with monoclonal antibodies for activity of key players in quiescence survival signalling. AKT activity was assessed by its phosphorylation at Serine 473 (pAKT) with a monoclonal antibody (Persad *et al.*, 2001) For mTORC1 activity, phosphorylation of its substrate 4E-BP1 at Threonines 37 and 46 (p4E-BP1) was identified with a monoclonal antibody (Gingras *et al.*, 2001). ERK activity was assessed by its phosphorylation at Threonine 202 and Tyrosine 204 (pERK) recognised by a monoclonal antibody (Roskoski, 2012). Finally, activated Bcl2-associated agonist of cell death (BAD), a downstream target of pERK, was identified by a monoclonal antibody binding to its phosphorylated Serine 112, whose phosphorylation is required for survival signalling (Scheid *et al.*, 1999). Plates were analysed by high-content widefield fluorescence microscopy and images quantified by automated image analysis.

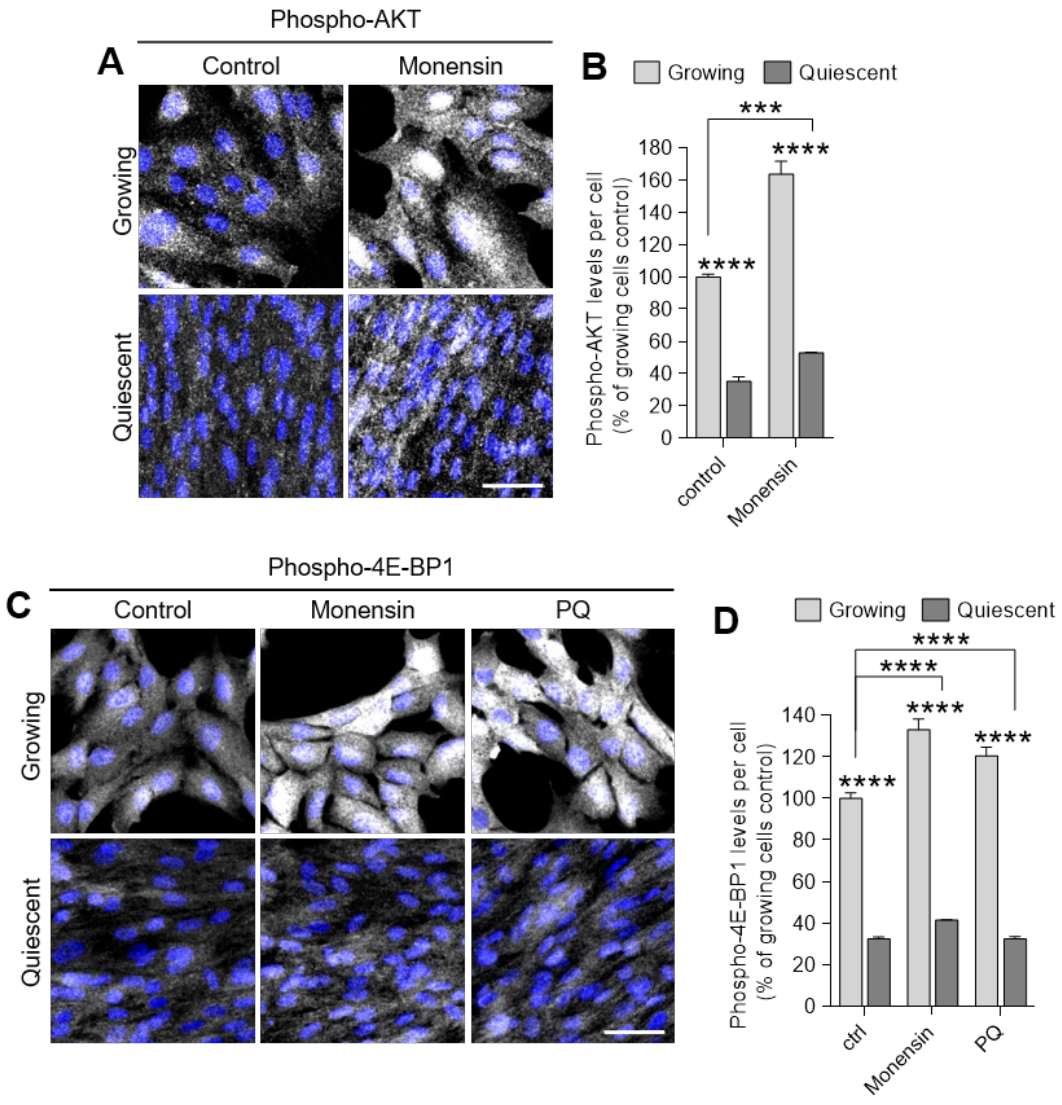


**Figure 5.2.10:** Effect of recycling inhibitors on growth signalling in growing and quiescent RPE1 cells
**A** and **C:** Representative epifluorescence microscopy images of growing and quiescent RPE1 cells treated with vehicle (DMSO control), 100 µM Monensin or 50 µM Primaquine (PQ, **C** only) for 90 minutes, fixed with 4 % PFA and immunolabelled with anti-phospho-AKT (S473) (**A**) or anti-phospho-4E-BP1 (T37/46) (**C**) antibody. DNA was stained with DAPI (blue pseudocolour). Scale bars: 50 µm. **B** and **D:** Quantification of epifluorescence microscopy images from **A** and **C**.Total fluorescence intensity per cell was normalised to growing cells DMSO control. Bar graphs represent mean + SEM from n=3 (uptake) biological replicates with a minimum of 5,000 growing and 15,000 quiescent cells per sample; two-way ANOVA with Tukey's multiple comparisons test comparing quiescent and growing cells and as indicated; ****P < 0.0001, ***P < 0.001.

AKT phosphorylation in quiescent RPE1 cells was 65 ± 3 % reduced when compared to growing cells (Fig. 5.2.10A and B). Treatment with Monensin increased AKT phosphorylation in growing cells by 64 ± 8 % and in quiescent cells by 47 ± 0.3 %, but pAKT levels in quiescent cells were still significantly lower than in growing control and Monensin-treated cells. Similarly, 4E-BP1 phosphorylation was not changed much by Monenensin or PQ treatment (Fig. 5.2.10C and D). Levels of p4E-BP1 in quiescent cells were about 60 % lower than in growing cells for DMSO, Monensin or PQ treatment. Upon treatment with either drug, p4E-BP1 levels remained significantly lower in quiescent than growing control cells. Phosphorylation of ERK at T202/Y204 did not differ between growing and quiescent control cells and upon PQ treatment, but was significantly reduced in quiescent cells treated with Monensin, both when compared to growing control cells (by 34 ± 5 %) or to growing Monensin-treated cells (by about 40 %; Fig. 5.2.11A and B). Concomitant with reduced pERK, BAD phosphorylation at Serine 112 was also reduced in quiescent Monensin-treated cells: Under control conditions (DMSO), pBAD levels were 30 ± 2 % higher in quiescent than in growing cells (Fig. 5.2.11C and D). Treatment with Monensin decreased pBAD by approximately 35 % in quiescent and by 25 % in growing cells compared to respective control, so that Monensin-treated quiescent cells still exhibited significantly more pBAD than Monensin-treated growing cells. However, pBAD levels in Monensin-treated quiescent cells did not differ from those in growing control cells. Finally, quiescence integrity was assessed by immunolabelling Monensin-treated cells for p27, whose expression is elevated in quiescent cells to keep CyclinD1-CDK4 cell cycle progression complexes inactive (Ladha *et al.*, 1998; Toyoshima & Hunter, 1994). P27 contains a nuclear localisation signal and translocates to the nucleus to inhibit cell cycle progression (Zeng *et al.*, 2000). Nuclear p27 levels were at least 3.5 times higher in quiescent than in growing control cells (Fig. 5.2.11E and F), but interestingly, they were 5.7 times higher upon Monensin treatment than in nuclei of Monensin-treated growing cells and 4.6 times higher than in those of control growing cells. Summarised, Monensin treatment perturbed quiescence survival signalling by elevating pAKT (50 ± 1 %) and p4E-BP1 (27 ± 1 %) levels, which mediate growth signalling, and by decreasing pERK (39 ± 4 %) and pBAD (27 ± 2 %) levels, which mediate survival, in quiescent cells compared to quiescent control cells (Fig. 5.2.11G). Increased levels of p27 (27 ± 7 %) are not in agreement with elevated growth signalling defined by increased AKT and mTORC1 activity. It might, however, be possible that the perturbed

quiescence signalling pathways lead to the onset of senescence. Although p27 is not a marker of ageing senescent cells, its expression was shown to be increased when senescence was artificially induced (Malavolta *et al.*, 2018).

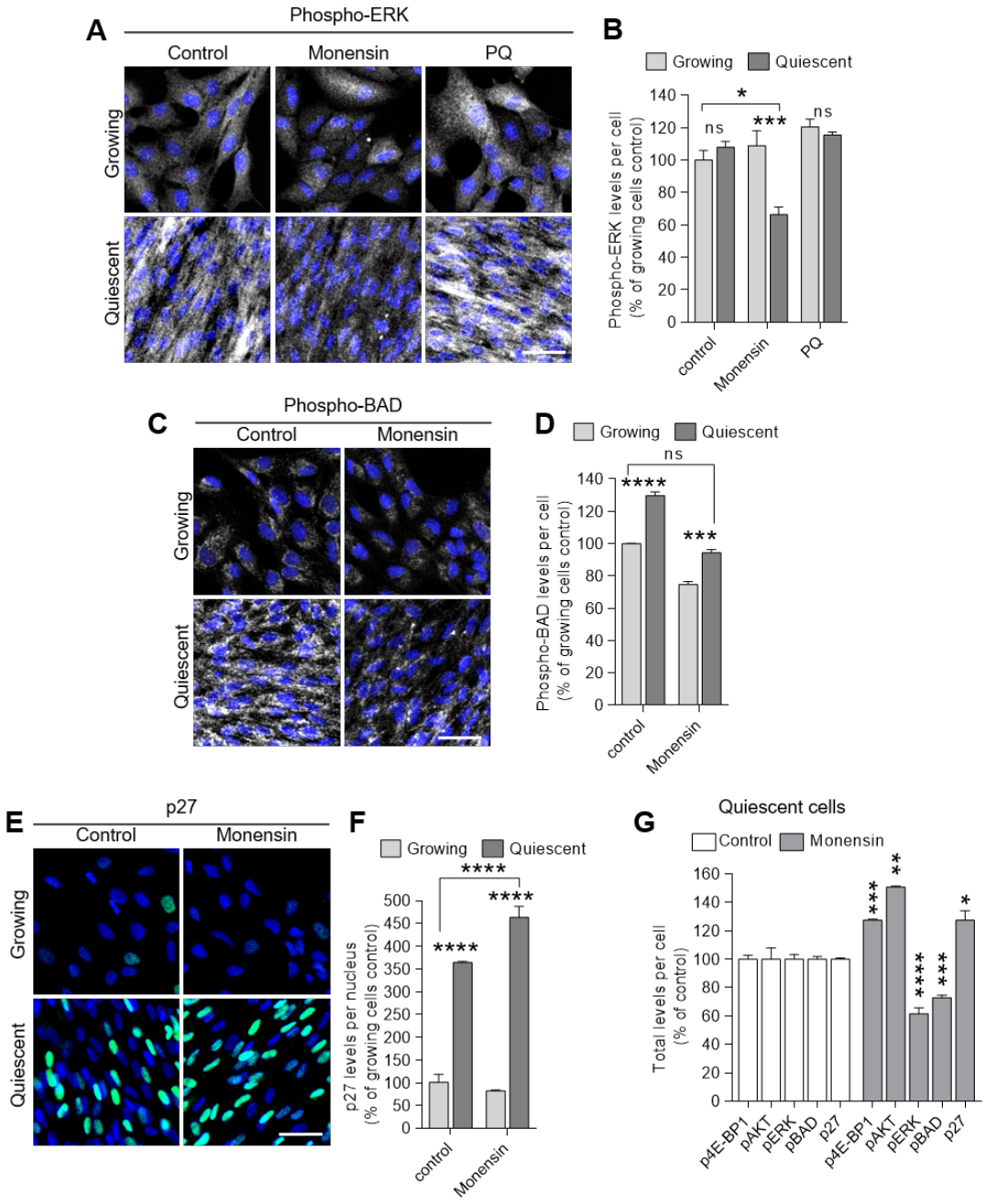


**Figure 5.2.11:** Effect of recycling inhibitors on quiescence survival signalling in growing and quiescent RPE1 cells

**A**, **C** and **E:** Representative epifluorescence microscopy images of growing and quiescent RPE1 cells treated with vehicle (DMSO control), 100 µM Monensin or 50 µM Primaquine (PQ, **A** only) for 90 minutes, fixed with 4 % PFA and immunolabelled with anti-phospho-ERK (T202/Y204) (**A**), anti-phospho-BAD (S112) (**C**) or anti-p27 (**E**) antibody. DNA was stained with DAPI (blue pseudocolour). Scale bars: 50 µm. **B**, **D** and **F:** Quantification of epifluorescence microscopy images from **A**, **C** and **E**. Total fluorescence intensity per cell was normalised to growing cells DMSO control. Bar graphs represent mean + SEM from n=3 or n=6 (phospho-ERK control and Monensin) biological replicates with a minimum of 5,000 growing and 15,000 quiescent cells per sample; two-way ANOVA with Tukey's multiple comparisons test comparing quiescent with growing cells and as indicated; ****P < 0.0001, ***P < 0.001, ns, not significant. **G:** Quantification of epifluorescence microscopy images from **A**, **C** and **E** and **A** and **C** in Fig. 5.2.10 in vehicle (DMSO)- and Monensin-treated quiescent cells. Total fluorescence intensity per cell was normalised to respective quiescent cells DMSO control. ****P < 0.0001, ***P < 0.001, **P < 0.01, *P < 0.05, Student's unpaired two-tailed t-test comparing treated samples to respective control.

### 5.2.8 Inhibition of Dynamin with Dyngo slightly reduces α3-integrin uptake in quiescent cells

While recycling is an important cellular function to maintain cell surface receptor levels, it is preceded by endocytosis. To find out by which endocytic route α3-integrin is internalised and whether it differs between growing and quiescent cells, a range of endocytosis inhibitors was screened for their ability to block endocytosis α3-integrin in growing and quiescent RPE1 cells. Dyngo4A (Dyngo) is a dynamin inhibitor and often used to block CME, but it also blocks other endocytic pathways relying on dynamin, such as FEME (McCluskey *et al.*, 2013; Boucrot *et al.*, 2015). Ikarugamycin (Ika) was shown to inhibit endocytosis of CME cargo by an unknown mechanism, but also reduced uptake of oxLDL, which is internalised by multiple, often Clathrin-independent, pathways, in macrophages (Elkin *et al.*, 2016; Hasumi *et al.*, 1992). EIPA and Rottlerin were used as macropinocytosis inhibitors, as described in sec. 5.2.1.1.

Growing and quiescent RPE1 cells were treated with 4 µM Dyngo, 50 nM Ika, 15 µM EIPA or 15 µM Rottlerin 30 min prior to and throughout 30 min uptake of anti-α3-integrin mAbP1B5, which was performed as described in sec. 5.2.1.2. To assess whether drug treatment would result in an increase of surface levels of α3-integrin because of blocked endocytosis, growing and quiescent RPE1 cells were treated with the respective inhibitors at the same concentrations for 90 min. Following inhibitor treatment, live cells were incubated on ice with anti-α3-integrin mAbP1B5 for 90 min, unbound antibody was removed by washes with PBS, cells were fixed and permeabilised and labelled with secondary antibody and DAPI. Plates were imaged on a high-content widefield fluorescence microscope and images quantified by automated image analysis as described in sec. 5.2.1.2.

30 min α3-integrin uptake in quiescent cells was not much affected by any of the endocytosis inhibitors used and for any condition significantly lower than in growing cells, exept when treated with Dyngo (Fig. 5.2.12A and B). Under control conditions, α3-integrin uptake in quiescent cells was 72 ± 1 % lower than in growing cells, and consistently 78-79 % lower than the growing control when treated with endocytosis inhibitors. α3-integrin uptake did not significantly differ between growing and quiescent cells upon Dyngo treatment, but that was caused by a significant decrease of α3-integrin uptake in growing cells (by 67 ± 3 %), indicating that dynamin plays a crucial role in α3-integrin

uptake in growing cells. Similarly, only Dyngo and Ika increased cell surface levels of α3-integrin in growing cells, whereas they remained unaffected in quiescent cells (Fig. 5.2.12C and D) and were significantly decreased compared to those in growing cells. Although drug treatment for cell surface-α3 labelling was 30 min longer than the 60 min treatment used for the endocytic uptake, their negligible effect on cell surface-α3 levels in quiescent cells allowed for normalisation of α3-integrin uptake to cell surface levels, which did not identify an inhibitor that would have reduced α3-integrin endocytosis in quiescent cells relative to growing cells (Fig. 5.2.12E). α3-integrin endocytosis for 30 min did not differ in vehicle(DMSO)-, Ika-, EIPA- or Rottlerin-treated cells, but Dyngo significantly decreased α3-integrin endocytosis in growing cells both compared to DMSO-treated growing and Dyngo-treated quiescent cells. To compare the effect of endocytosis inhibitors within quiescent cells, α3-integrin uptake, uptake was normalised to cell surface levels and cell surface levels were normalised to DMSO-treated quiescent cells (Fig. 5.2.12F). Although all drugs reduced α3 uptake by about 18-21 % relative to control, only Dyngo had a significant effect, decreasing α3-integrin uptake and surface-normalised uptake by 23 % ± 4 % and 25 % ± 3 %, respectively. Cell surface α3-integrin levels were increased by Ikarugamycin treatment, but the effect was not significant. This suggests that neither CME, dynamin-dependent endocytic pathways or macropinocytosis mediate α3-integrin endocytosis in quiescent cells. It should, however, be considered that quiescent cells were less succeptible to the inhibitory drugs used in this experiment. Titration of each inhibitor was optimised according to the viability of subconfluent, growing cells, because they died at concentrations which quiescent cells survived (data not shown). This might have resulted in a working concentration lower than necessary to inhibit an endocytic pathway in quiescent cells. Quiescent RPE1 cells are a confluent, tightly packed monolayer, exposing less surface area which drugs can enter. This might affect the drug concentration which actually reaches the cells and thus the inhibitory effect and might be reflected by the small effect of Dyngo on α3 uptake in quiescent cells. Inhibition of α3-integrin uptake would be in agreement with the fact that it contains an AP2-binding motif in its cytoplasmic tail, which would destine it for CME (De Franceschi *et al.*, 2015).

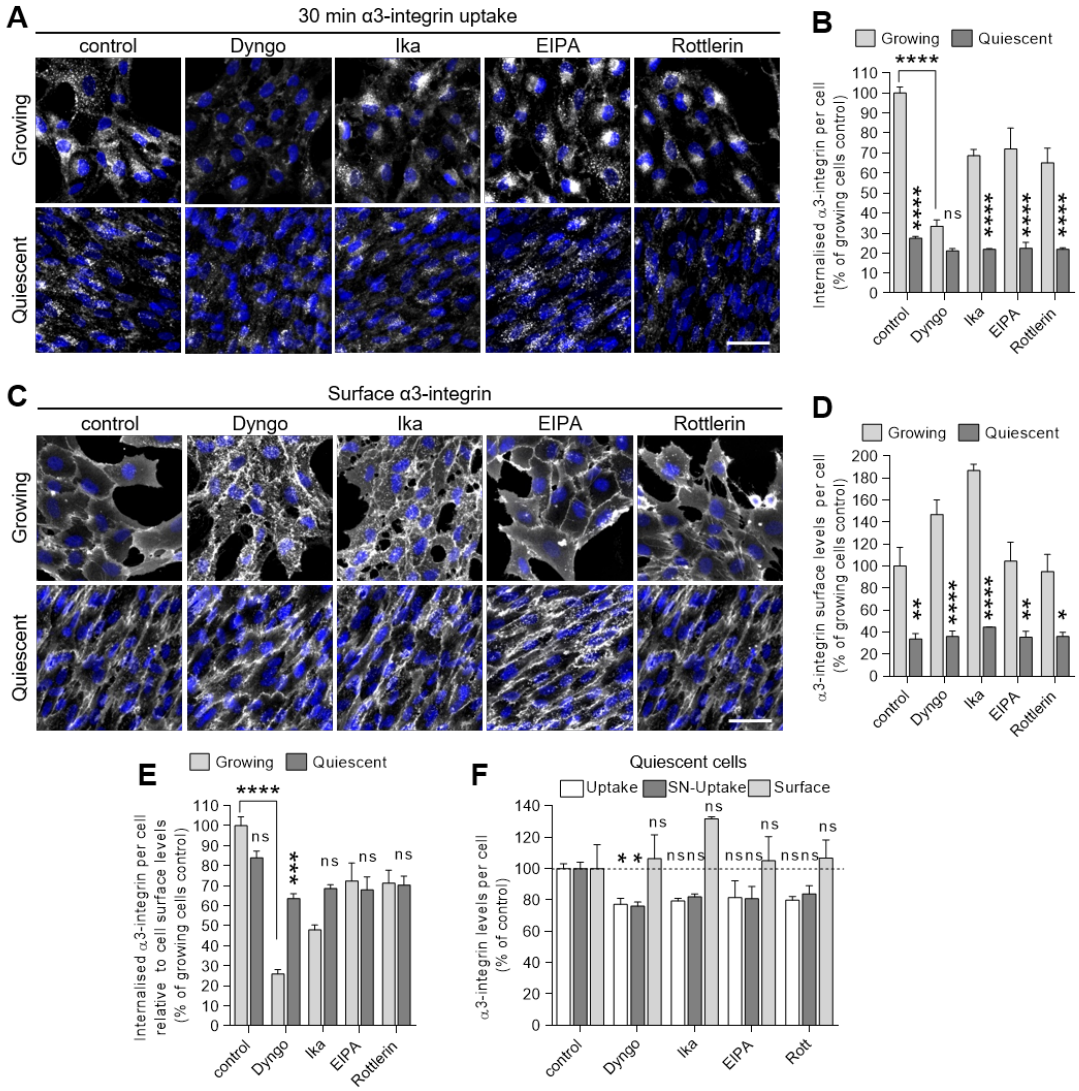


**Figure 5.2.12:** Effect of endocytosis inhibitors on α3-integrin uptake in growing and quiescent RPE1 cells **A** and **C:** Representative epifluorescence microscopy images of 30 min anti-α3-integrin antibody feeding (**A**) and α3-integrin cell surface levels (**C**) in growing and quiescent RPE1 cells in the presence of vehicle (DMSO control), 4 µM Dyngo4A, 50 nM Ikarugamycin (Ika), 15 µM EIPA or 7.5 µM Rottlerin (Rott). cells Scale bars: 50 µm. **A**: Prior to uptake, cells were pre-treated with drugs for 30 minutes. Following uptake, surface-bound antibody was removed by acidic washes. Cells were fixed with 4 % PFA, permeabilised, incubated with fluorescence-conjugated secondary antibody and nuclei were stained with DAPI (blue pseudocolour). **C:** After 90 minutes drug treatment, live cells were incubated on ice with primary anti-α3-integrin antibody, fixed with 4 % PFA, permeabilised, incubated with fluorescence-conjugated secondary antibody and nuclei were stained with DAPI (blue pseudocolour). **B** and **D:** Quantification of epifluorescence microscopy images from **A** and **C:** Total fluorescence intensity of internalised or surface-bound antibody per cell was normalised to growing cells DMSO control. Bar graphs represent mean + SEM from n=3 (uptake and Ikarugamycin-treated surface) or n=6 (surface) biological replicates with a minimum of 5,000 growing and 15,000 quiescent cells per sample. **E:** Total fluorescence intensity of internalised antibody per cell was normalised to cell surface levels and growing cells. Bar graphs represent mean + SEM from n=3 biological replicates with a minimum of 5,000 growing and 15,000 quiescent cells per sample. **F:** Quantification of epifluorescence images from **A** and **C:** Total fluorescence intensity of internalised, surface bound-normalised (SN-uptake) internalised or surface-bound α3-integrin in inhibitor-treated quiescent cells was normalised to respective DMSO control. Bar graphs represent mean + SEM from n=3 (uptake, surface bound-normalised uptake and Ikarugamycin-treated surface) or n=6 (surface) biological replicates with a minimum of 5,000 growing and 15,000 quiescent cells per sample; *P < 0.05, ns, not significant, one-way ANOVA with Dunett's multiple comparisons test comparing inhibitor-treated samples to respective DMSO control. Statistical significances of **B, D** and **E** were determined with two-way ANOVA with Tukey's multiple comparisons test comparing quiescent with growing cells and as indicated; ****P < 0.0001, ***P < 0.001, **P < 0.01, *P < 0.05, ns, not significant.

### 5.2.9 Pharmacological inhibition of macropinocytosis, but not CME, affects quiescence survival signalling

Despite the discouraging effect of endocytic inhibitors on α3-integrin endocytosis, their effect on quiescence survival signalling was studied. It is likely that α3-integrin is not the only integrin required for quiescence survival signalling from a set of G0 ECM-specific laminins. Consistently, α3 was shown to act in conjunction with other integrins, such as α6β1 (Fujiwara *et al.*, 2001).

Growing and quiescent RPE1 cells were treated with 4 µM Dyngo, 50 nM Ika, 15 µM EIPA or 15 µM Rottlerin for 90 min, fixed with PFA, permeabilised and labelled with monoclonal primary antibodies specific for activity-indicating phosphorylation sites of AKT, the mTORC1 substrate 4E-BP1, ERK and BAD as described in sec. 5.2.7. Plates were analysed by high-content widefield fluorescence microscopy and images quantified by automated image analysis.

Levels of pAKT and p4E-BP1 in quiescent cells remained significantly lower than those in growing cells for all endocytosis inhibitors tested (Fig. 5.2.13A-D). Levels of pERK, which did not differ between growing and quiescent control cells, were 1.4 fold higher in quiescent Dyngo-treated cells than in growing Dyngo-treated cells and 1.5 fold higher in quiescent Rottlerin-treated cells than in growing Rottlerin-treated cells, while neither treatment significantly changed pERK levels in growing cells, although pERK was slightly reduced upon Dyngo treatment (Fig. 5.2.13E and F). Levels of pBAD were significantly higher in quiescent cells than in growing cells both for control cells (30 %) and for cells treated with endocytosis inhibitors (ranging from 20-40 %) (Fig. 5.2.14A and B).

Finally, nuclear levels of p27 were quantified to test for cell cycle exit (see sec. 5.2.7). P27 was highly expressed in nuclei of quiescent cells and was significantly 3.6-4.4-fold higher than in growing control cells when treated with endocytosis inhibitors (Fig. 5.2.14C and D). Dyngo, Ika and EIPA had a larger effect on increased p27 expression in nuclei of growing cells, indicating the importance of CME and macropinocytosis in proliferation. Nonetheless, nuclear levels of p27 in quiescent cells were significantly higher than in growing cells for all inhibitors tested. In summary, 90 min treatment with endocytosis inhibitors did not revert quiescence signalling to signalling reminiscent of growing cells, but EIPA treatment resulted in elevated phosphorylation of ERK.

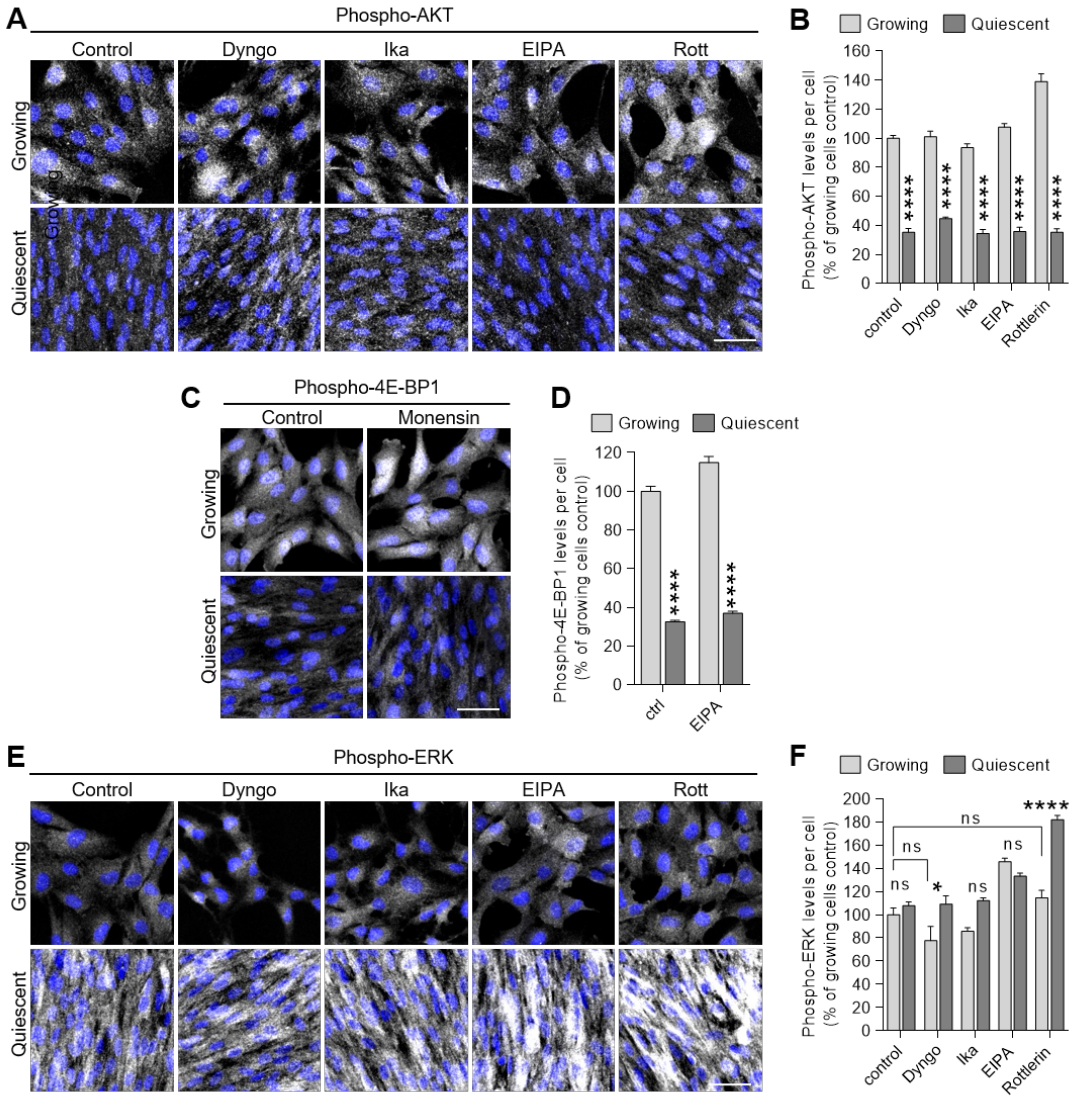


**Figure 5.2.13:** Effect of endocytosis inhibitors on growth signalling in growing and quiescent RPE1 cells **A**, **C** and **E:** Representative epifluorescence microscopy images of growing and quiescent RPE1 cells treated with vehicle (DMSO control), 4 µM Dyngo4A (Dyngo), 40 nM Ikarugamycin (Ika), 15 µM EIPA or 7.5 µM Rottlerin (Rott) for 90 minutes, fixed with 4 % PFA and immunolabelled with anti-phospho-AKT (S473) (**A**), anti-phospho-4E-BP1 (T37/46) (**C**) or anti-phospho-ERK (T202/Y204) (**E**) antibody. DNA was stained with DAPI (blue pseudocolour). Scale bars: 50 µm. **B**, **D** and **F:** Quantification of epifluorescence microscopy images from **A**, **C** and **E**. Total fluorescence intensity per cell was normalised to growing cells DMSO control. Bar graphs represent mean + SEM from n=3 or n=6 (phospho-ERK except Ika treatment) biological replicates with a minimum of 5,000 growing and 15,000 quiescent cells per sample; two-way ANOVA with Tukey's multiple comparisons test comparing quiescent with growing cells and as indicated; ****P < 0.0001, *P < 0.05, ns, not significant.

The effect of endocytosis inhibitors on signalling in quiescent cells was then compared to quiescent cells treated with vehicle (DMSO) (Fig. 5.2.14E). The CME inhibitors Dyngo and Ika did not change quiescence signalling significantly except for a 6 ± 1 % decrease in nuclear p27 levels caused by Dyngo treatment. The macropinocytosis inhibitors EIPA and Rottlerin both increased ERK phosphorylation (24 ± 3 % and 69 ± 4 % respectively) and did not affect AKT phosphorylation. Additionally, EIPA treatment resulted in increased p27 levels (21 ± 2 %), but conflictingly, BAD phosphorylation was reduced (13 ± 1 %) and 4E-BP1 phosphorylation was increased (14 ± 4 %) upon EIPA treatment. This suggests that macropinocytosis might play a role in quiescence survival signalling. It should be considered that EIPA inhibits macropinocytosis indirectly via increasing submembraneous pH, which affects Rac1 and Cdc42 signalling as well as actin polymerisation (Koivusalo *et al.*, 2010). Furthermore, EIPA inhibits FEME, likely because of impaired Cdc42 signalling (Boucrot *et al.*, 2015). Finally, changes of cytoplasmic pH alter membrane lipid mobility (Libera *et al.*, 1997), which can change membrane curvature or interaction of proteins with membranes constituting of different lipids.

### 5.2.10 AP2 knockdown decreases α3-integrin endocytosis in growing and quiescent cells

The rapid effect of chemical inhibitors is advantageous, however, off-target effects cannot be ruled out. In addition, quiescent cells were more resistant to inhibitor lethality than growing cells and potentially to inhibitory effects as well, because they expose less cell surface area for the drug to penetrate, resulting in lower effective intracellular inhibitor concentrations. To account for these issues, a knockdown approach was employed to specifically downregulate proteins mediating endocytosis. Knockdown efficiency can be assessed by quantifying remaining protein levels and thus gives a measure of how much an endocytic pathway is inhibited. α3-integrin contains two YXXΦ AP2 binding motifs in its cytoplasmic tail and might thus be internalised by CME (De Franceschi *et al.*, 2016). This is supported by Dyngo having a strong and weak inhibitory effect on α3-integrin endocytosis in growing and quiescent RPE1 cells, respectively (sec. 5.2.8), because Dyngo was shown to reduce endocytosis of CME cargoes, as CME vesicle scission is Dynamin-dependent (McCluskey *et al.*, 2013). However, Dyngo also reduces uptake of 10 kDa dextran (Park *et al.*, 2013).

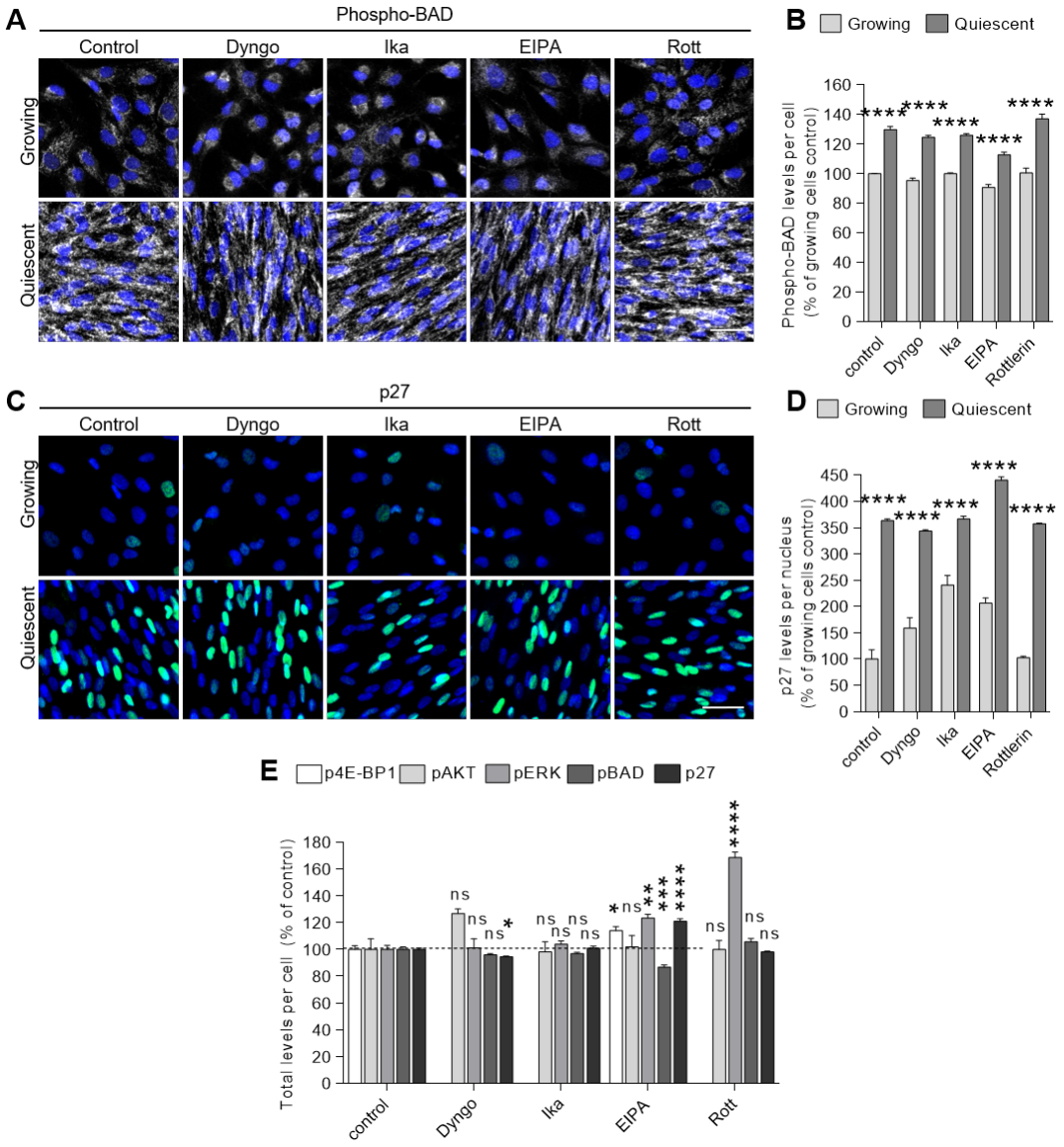


**Figure 5.2.14:** Effect of endocytosis inhibitors on quiescence survival signalling in growing and quiescent RPE1 cells

**A** and **C:** Representative epifluorescence microscopy images of growing and quiescent RPE1 cells treated with vehicle (DMSO control), 4 µM Dyngo4A (Dyngo), 40 nM Ikarugamycin (Ika), 15 µM EIPA or 7.5 µM Rottlerin (Rott) for 90 minutes, fixed with 4 % PFA and immunolabelled with anti-phospho-BAD (S112) (**A**) or anti-p27 (**C**) antibody. DNA was stained with DAPI (blue pseudocolour). Scale bars: 50 µm. **B** and **D:** Quantification of epifluorescence microscopy images from **A** and **C**. Total fluorescence intensity per cell was normalised to growing cells DMSO control. Bar graphs represent mean + SEM from n=3 biological replicates with a minimum of 5,000 growing and 15,000 quiescent cells per sample; two-way ANOVA with Tukey's multiple comparisons test comparing quiescent and growing cells; ****P < 0.0001, **E:** Quantification of epifluorescence microscopy images from **A** and **C,** and **A** and **C** in Fig. 5.2.13 in quiescent cells. Total fluorescence intensity per cell was normalised to respective quiescent cells DMSO control. ****P < 0.0001, ***P < 0.001, **P < 0.01, *P < 0.05, Student's unpaired two-tailed t-test (phospho-4E-BP1) or one-way ANOVA with Dunett's multiple comparisons test comparing treated samples to respective control.

To test whether α3- and β1-integrin are internalised by CME, the central hub linking Clathrin, adaptor proteins and cargo, AP2, was knocked down in growing and quiescent RPE1 cells by transiently transfecting cells with μ2-adaptin siRNA (Motley *et al.*, 2003; Boucrot *et al.*, 2010). Growing cells were treated with scrambled or μ2-adaptin siRNA on the day of seeding, 24 hours later and were used for experiments 72 hours after seeding. Because quiescent cells were resistant to knockdowns once medium was exchanged to serum-free (communication with K. McGourty, Boucrot lab), the knockdown protocol was modified and siRNA treatments started before cells entered quiescence. SiRNA treatment for quiescent cells occured 5 and 7 days after seeding, while cells were still dividing and in serum-containing medium. Medium exchange to serum-free occured 10 days after seeding and cells were used for experiments 17 days after seeding. To account for α3β1-integrin internalised by macropinocytosis, μ2-siRNA-treated samples were additionally treated with EIPA or Rottlerin for 60 min. AP2 knockdown efficiency was tested by IF labelling with anti-α-adaptin antibody, high-content widefield fluorescence microscopy and image-based quantification (see sec. 4.2.5.3). Levels of α-adaptin were reduced by at least 90 % in growing cells and by 55-70 % in quiescent cells (Fig. 5.2.6). EIPA or Rottlerin treatment did not significantly affect the down-regulation of α-adaptin expression.

First, cell surface levels of α3- and β1-integrin were quantified. Growing and quiescent RPE1 cells treated as described above were incubated on ice with anti-α3 mAbP1B5 or anti-β1 mAb13 for 90 min, unbound antibody was removed by washes with ice-cold PBS and cells were fixed with PFA, permeabilised and labelled with secondary antibody and DAPI. Plates were imaged on a high-content widefield fluorescence microscope and cell surface levels of α3- and β1-integrin were quantified in images by automated image analysis. Cell surface levels of α3-integrin in quiescent cells treated with vehicle (DMSO) and scrambled siRNA were 72 ± 0.5 % lower than in growing cells, but were elevated and did not differ from growing cells when cells were treated with μ2-adaptin siRNA (Fig. 5.2.15A and B). Levels of β1-integrin looked similar in microscopy images (Fig. 5.2.15A). When comparing α3-integrin cell surface levels within growing cells, neither AP2 KD nor treatment of EIPA or Rottlerin in addition to AP2 KD had a significant effect and cell surface levels of β1-integrin did not significantly differ from scrambled control either (Fig. 5.2.15C left). Upon AP2 KD, quiescent cells were less densely packed than under control conditions and thus were larger, exhibiting an increased cell surface

area (Fig. 5.2.15A). This is reflected by a significant increase of both α3- and β1-integrin surface levels by 235 ± 25 % and 248 ± 35 %, respectively (Fig. 5.2.15C right). Surface levels of both integrin subunits were increased by a similar extent upon EIPA and Rottlerin treatment in quiescent AP2 KD cells and did not significantly differ from AP2 KD. Next, it was studied whether increased cell surface levels of α3- and β1-integrin were related to decreased endocytosis of the integrins. AP2 KD, EIPA and Rottlerin treatment in growing and quiescent RPE1 cells occured as described above. α3- and β1-integrin uptake was assessed by 30 min mAbP1B5 and mAb13 feeding as described in sec. 5.2.1.1. Experiments were analysed by high-content widefield fluorescence microscopy and automated image analysis as described in sec. 5.2.1.2.

In growing cells, a significant reduction of α3- (by 79 ± 1 %) and β1-integrin (by 55 ± 6 %) uptake was observed when AP2 was knocked down (Fig. 5.2.16A and B top). EIPA and Rottlerin treatment did not decrease uptake further. In quiescent cells, α3 uptake was significantly reduced by 48 ± 8 % upon AP2 knockdown and did not significantly differ from EIPA- or Rottlerin-treated AP2 KD cells, although the 27 ± 4 % reduction of α3 uptake in EIPA-treated cells was not identified as significant (Fig. 5.2.16A and B bottom). Uptake of β1-integrin did not differ from control for any of the conditions tested. This is not surprising, because β1-integrin can dimerise with many more α-integrin subunits than just α3 (Hynes, 2002). Normalisation to cell surface levels of α3- or β1-integrin did not change the observations made for uptake alone in growing cells, because the surface levels were not significantly altered by AP2 KD or inhibitor treatments (Fig. 5.2.16C left). Briefly, AP2 KD decreased α3-integrin endocytosis by 79 ± 2 % and β1-integrin endocytosis by 63 ± 4 %. EIPA or Rottlerin treatment did not significantly affect endocytosis of either integrin. In quiescent cells, where cell surface levels of both α3- and β1-integrin were significantly elevated after AP2 KD, normalisation of uptake to cell surface integrin levels resulted in a significant decrease of α3- (by 83 ± 4 %) and β1-integrin (by 71 ± 6 %) (Fig. 5.2.16C right). Again, EIPA or Rottlerin treatment had no significant effect on endocytosis of either integrin. Finally, surface level-normalised uptake of α3-integrin was compared between growing and quiescent cells and highlighted that for all conditions, no significant difference existed between the two cell populations (Fig. 5.2.16D).

These results show that uptake of α3-integrin in both growing and quiescent RPE1 cells was strongly dependent on AP2 and is therefore likely to be mediated by CME. In both cell populations, the majority of β1-integrin relied on AP2 for internalisation as well,

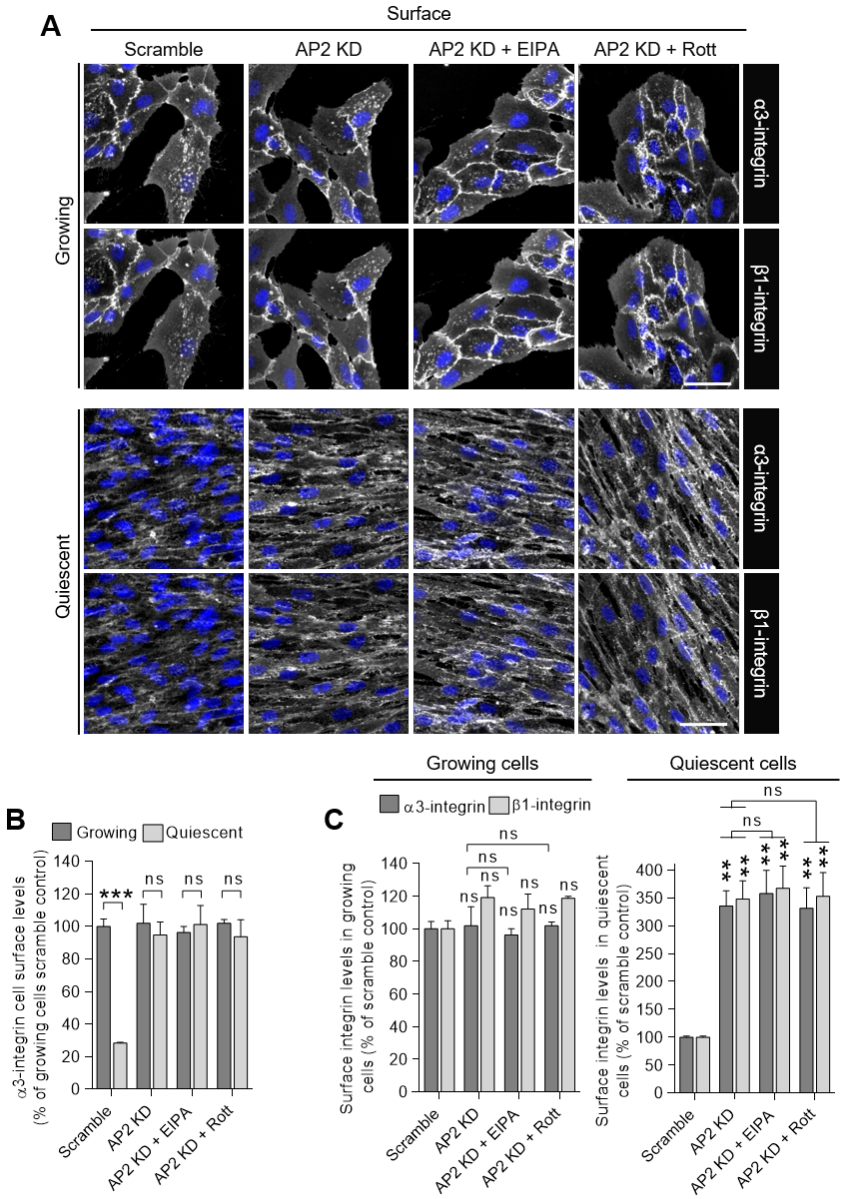


**Figure 5.2.15:** α3β1-integrin cell surface levels increase in quiescent RPE1 cells when AP2 expression is reduced

AP2 knock down (KD) procedure protocols differ between cell populations: Growing cells were treated with µ2-adaptin siRNA on the day of seeding, 24 hours later and were used for experiments 72 hours after seeding. Quiescent cells were treated with siRNA 5 and 7 days after seeding. Medium exchange to serum-free occured 10 days after seeding. Quiescent cells were used for experiments 17 days after seeding. **A:** Representative epifluorescence microscopy images of α3- and non-ligandbound β1-integrin cell surface immunolabelling in growing and quiescent RPE1 cells treated with scrambled or µ2-adaptin siRNA and with vehicle (DMSO; in scrambled and AP2 KD samples), 15 µM EIPA or 7.5 µM Rottlerin (Rott). Cells were treated with drug or vehicle for 60 minutes, incubated with primary antibody on ice, fixed with 4 % PFA, permeabilised and stained with secondary antibody and DAPI (blue pseudocolour). Scale bars: 50 µm. **B:** Quantification of epifluorescence microscopy images from **A:** Total fluorescence intensity of surface-bound α3-integrin per cell was normalised to growing cells scrambled control. Bar graphs represent mean + SEM from n=3 biological replicates with a minimum of 500 growing and 2,500 quiescent cells per sample; ***P < 0.001, ns, not significant, two-way ANOVA with Tukey's multiple comparisons test. **C:** Quantification of epifluorescence microscopy images from **A:** Total fluorescence intensity of surface-bound α3- and β1-integrin per growing or quiescent cell was normalised to respective growing or quiescent cells scrambled control. Bar graphs represent mean + SEM from n=3 biological replicates with a minimum of 500 growing and 2,500 quiescent cells per sample; **P < 0.01, ns, not significant, one-way ANOVA with Dunnet's multiple comparisons test comparing treated samples to respective scrambled control; two-way ANOVA with Tukey's multiple comparisons test comparing AP2 KD to AP2 KD treated with EIPA or Rottlerin as indicated.

which can be explained by its partial dimerisation with α3-integrin and by the fact that it can interact with endocytic adaptors such as Numb and Dab2, which themselves are able to recruit AP2 (Calderwood *et al.*, 2003; Teckchandani *et al.*, 2012; Mishra *et al.*, 2004). The two macropinocytosis inhibitors EIPA and Rottlerin had no additive effect on reduction of integrin endocytosis, implying that α3 and β1-integrins are not internalised by macropinocytosis.

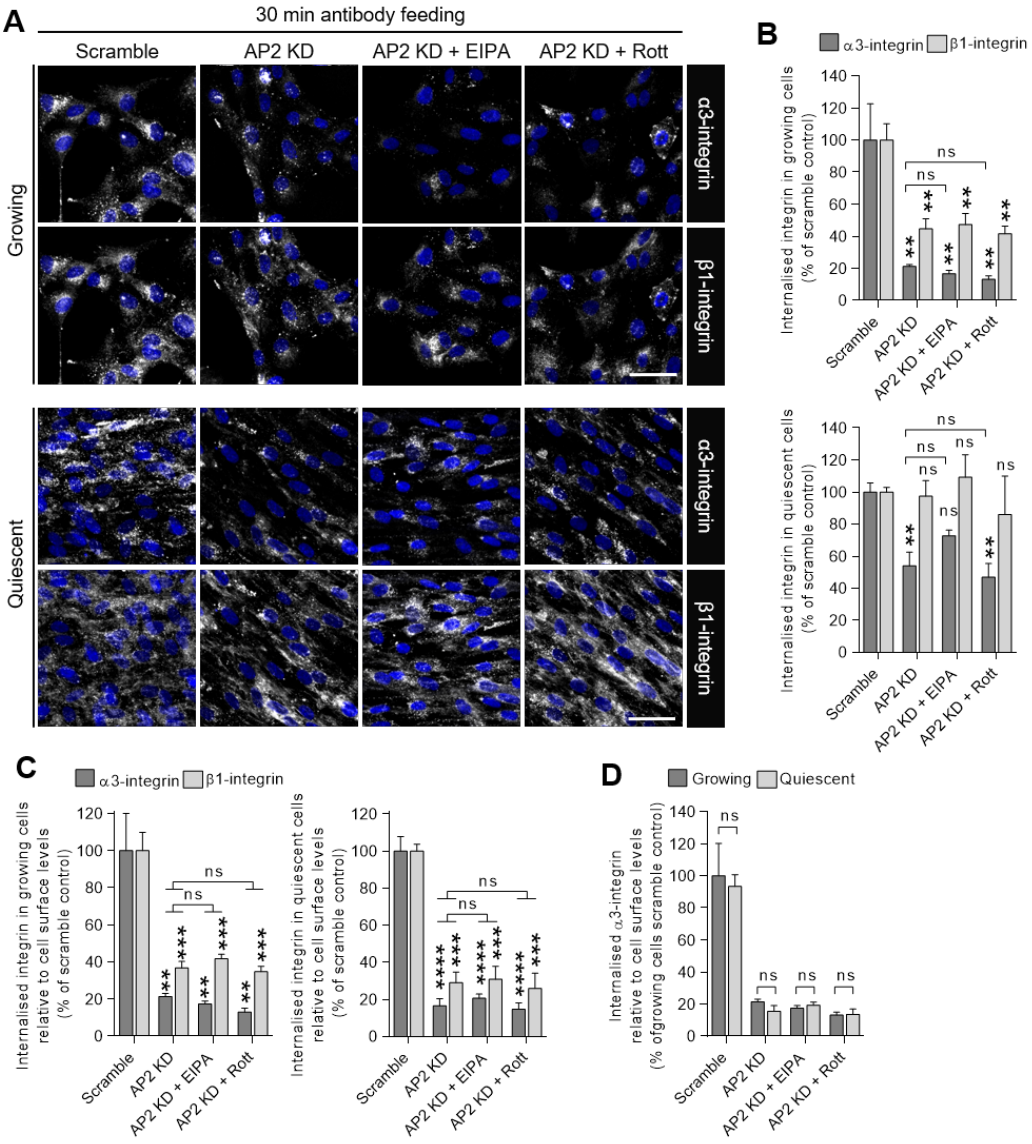


**Figure 5.2.16:** Uptake of α3β1-integrin decreases when AP2 expression is reduced
AP2 knock down (KD) procedure protocols differ between cell populations: Growing cells were treated with µ2-adaptin siRNA on the day of seeding, 24 hours later and were used for experiments 72 hours after seeding. Quiescent cells were treated with siRNA 5 and 7 days after seeding. Medium exchange to serum-free occured 10 days after seeding. Quiescent cells were used for experiments 17 days after seeding. **A:** Representative epifluorescence microscopy images of 30 min anti-α3- and anti-non-ligandbound β1-integrin antibody feeding in growing and quiescent RPE1 cells treated with scrambled or µ2-adaptin siRNA and with vehicle (DMSO; in scrambled and AP2 KD samples), 15 µM EIPA or 7.5 µM Rottlerin (Rott). Cells were treated with drug or vehicle for 30 minutes prior to and throughout uptake, washed with acidic buffer to remove surface-bound antibody, fixed with 4 % PFA, permeabilised and stained with secondary antibody and DAPI (blue pseudocolour). Scale bars: 50 µm. **B:** Quantification of epifluorescence microscopy images of growing (upper graph) or quiescent cells (lower graph) from **A:** Total fluorescence intensity of internalised α3- and β1-integrin per cell was normalised to scrambled control. Bar graphs represent mean + SEM from n=3 biological replicates with a minimum of 500 growing and 2,500 quiescent cells per sample. **C:** Data from **B** were normalised to α3- or β1-integrin cell surface levels from Fig. 5.2.15 and to scrambled control. Bar graphs represent mean + SEM from n=3 biological replicates of growing (left) or quiescent (right) cells with a minimum of 500 growing and 2,500 quiescent cells per sample. Statistical significances for **B** and **C** were derived from one-way ANOVA with Dunnet's multiple comparisons test comparing treated samples to scrambled control and two-way ANOVA with Tukey's multiple comparisons test comparing AP2 KD to AP2 KD treated with EIPA or Rottlerin as indicated, ****P < 0.0001, ***P < 0.001, **P < 0.01, ns, not significant. **C:** Quantification of α3-integrin uptake relative to cell surface levels from **C** normalised to growing cells scrambled control to compare uptake between growing and quiescent cells. Bar graphs represent mean + SEM from n=3 biological replicates with a minimum of 500 growing and 2,500 quiescent cells per sample; ns, not significant, two-way ANOVA with Tukey's multiple comparisons test.

### 5.2.11 Dynamin and Endophilin knockdown decrease endocytosis of α3-integrin

In addition to AP2, CME relies on Dynamin for vesicle scission and the BAR-domain protein Endophilin was shown to be involved in CCV-uncoating in neurons (Kaksonen & Roux, 2018; Watanabe *et al.*, 2018b; Milosevic *et al.*, 2011). Dynamin and Endophilin are also required in other endocytic pathways, such as FEME or for scission events in Shiga and Cholera toxin endocytosis, and are therefore not as specific for CME as AP2 (Boucrot *et al.*, 2015; Renard *et al.*, 2015; Simunovic *et al.*, 2017). On that account, the effect of Dynamin and Endophilin knockdown on α3-integrin uptake was tested for a more complete characterisation of its endocytosis in quiescent - and also growing - RPE1 cells.

Dynamin knockdown was performed as double knockdown (Dyn DKD) using siRNAs for Dynamin 1 and Dynamin 2. EndophilinA knockdown was a triple knockdown (EndoA TKD) of EndophilinA 1, A 2 and A 3. In parallel, AP2 was knocked down using μ-adaptin siRNA (for experiments in sec. 5.2.12). Growing and quiescent cells were transiently transfected with respective siRNAs as described in sec. 5.2.10. Cells were then fixed with PFA, permeabilised and immunolabelled for α-adaptin as marker for AP2 KD, for Dynamin 1 and Dynamin 2 as markers for Dyn DKD and for Endophilin A2 as marker for EndoA TKD. Cell nuclei were stained with DAPI. Plates were imaged on a high-content widefield fluorescence microscope and images quantified by automated image analysis. Knockdown efficiencies in growing cells ranged from 92 ± 4 % reduction of α-adaptin for AP2 KD, 88 ± 1 % decrease of Dynamin 1 and 86 ± 3 % of Dynamin 2 for Dyn DKD, and 99 ± 1 % reduction of Endophilin A2 for EndophA TKD (Fig. 5.2.17). In quiescent cells, α-adaptin was reduced by 89 ± 6 % for AP2 KD, Dynamin 1 and 2 were reduced by 58 ± 2 % and 39 ± 2 %, respectively, for Dyn DKD, and Endophilin A2 was reduced by 65 ± 2 % for EndoA TKD. Interestingly, the shape of quiescent RPE1 cells changed depending on the proteins knocked down and was elongated and spindle-like for AP2 KD and EndoA TKD, but cuboid and disorganised for Dyn DKD (Fig. 5.2.17A).

Cell surface levels and uptake of α3-integrin upon EndoA TKD and Dyn DKD were assessed for growing and quiescent cells as described in sec. 5.2.10. Cells treated with scrambled siRNA were used as controls. Cell surface levels of α3-integrin were significantly reduced by 75 ± 1 % in quiescent control cells compared to growing control

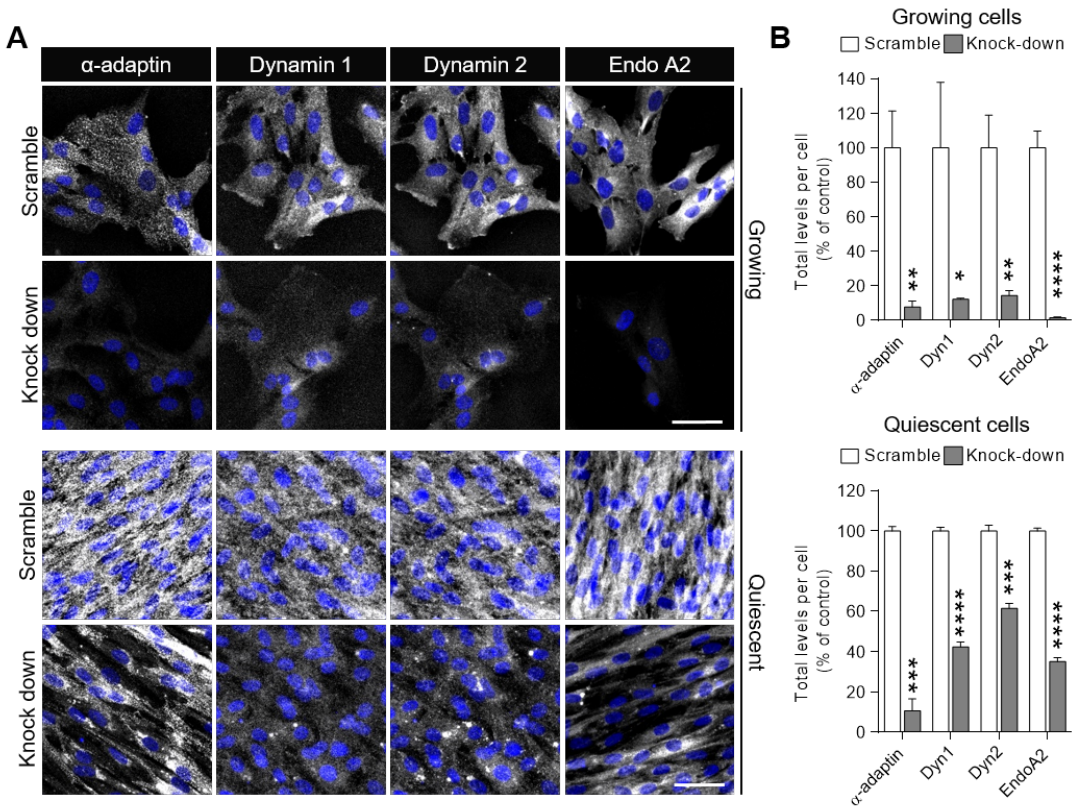


**Figure 5.2.17:** AP2, dynamin and endophilin knockdown efficiency in growing and quiescent RPE1 cells Knockdown (KD) protocols differ between cell populations: Growing cells were treated with siRNA on the day of seeding, 24 hours later and were used for experiments 72 hours after seeding. Quiescent cells were treated with siRNA 5 and 7 days after seeding. Medium exchange to serum-free occured 10 days after seeding. Quiescent cells were used for experiments 17 days after seeding. **A:** Representative epifluorescence microscopy images growing and quiescent cells treated with scrambled, µ2-adaptin (AP2 KD), Dynamin1 and 2 (Dyn DKD) or Endophilin A1, 2 and 3 (EndoA TKD) siRNA counterstained for α-adaptin, Dynamin1/Dynamin2 or Endophilin A2 to assess knock down efficiency. Scale bars: 50 µm. **B:** Quantification of epifluorescence microscopy images from **A** in growing (upper graph) and quiescent (lower graph) cells. Total fluorescence intensity per cell was normalised to scrambled control. Bar graphs represent mean +SEM from n=6 (growing cells) or 3 (quiescent cells) biological replicates equivalent to a minimum of 4,000 growing or 9,000 quiescent cells per sample; ****P < 0.0001, ***P < 0.001, **P < 0.01, *P < 0.05; Student's unpaired two-tailed t-test comparing knockdown to respective scrambled control.

cells, but did not differ between growing and quiescent cells upon EndoA TKD or Dyn DKD (Fig. 5.2.18A and B top). Similarly, α3-integrin uptake was reduced by 75 ± 2 % in quiescent control cells but did not differ upon EndoA TKD or Dyn DKD (Fig. 5.2.18A and B bottom). In scrambled control cells and upon EndoA TKD, uptake of α3-integrin normalised to cell surface levels did not differ between quiescent and growing cells (Fig. 5.2.18C). When Dynamin 1 and 2 were knocked down, however, α3-integrin endocytosis was significantly reduced by 79 ± 8 % in growing cells compared to only 42 ± 3 % in quiescent cells, and was therefore almost 2.7-fold increased in quiescent cells. This effect however, could have been caused by the partial Dyn DKD in quiescent cells (Fig. 5.2.17). Increase or decrease of α3-integrin uptake, surface-normalised uptake and surface levels in quiescent cells were then compared to scrambled siRNA-treated quiescent cells. Although quiescent cells internalised 36 ± 8 % more α3-integrin than control upon EndoA TKD, surface-normalised uptake was decreased by 34 ± 2 % because of the 2-fold increased α3-integrin cell surface levels (Fig. 5.2.18D). Dyn DKD resulted in a nonsignificant decrease of α3-integrin uptake by 29 ± 3 % and nonsignificant increase of cell surface levels by 22 ± 9 %. When internalised α3-integrin was normalised to cell surface levels, its endocytosis was significantly reduced by 41 ± 7 %. This shows that both EndophilinA and Dynamin, are involved in α3-integrin endocytosis in quiescent cells. The effect of Dynamin DKD on cell surface levels of α3-integrin was only modest, but might have been more pronounced upon better knockdown efficiency. EndoA TKD resulted in accumulation of cell surface-α3-integrin and reduction of its endocytosis when normalised to cell surface levels. Endophilin is required for CCV uncoating in neurons (Milosevic *et al.*, 2011; Watanabe *et al.*, 2018b), but has a redundant function with SNX9 and Bin1 in non-neuronal cells, so that its knockdown did not affect transferrin uptake or AP2 dynamics (Meinecke *et al.*, 2013; Boucrot *et al.*, 2015). This suggests that α3-integrin might be internalised by either FEME or another Clathrin-independent pathway in addition to CME. AP2 KD resulted in a residual α3-integrin endocytosis of about 20 %, which could be explained by incomplete knockdown or might imply that the residual uptake indeed occured by a Clathrin-independent and Endophilin or/and Dynamin-dependent pathway.

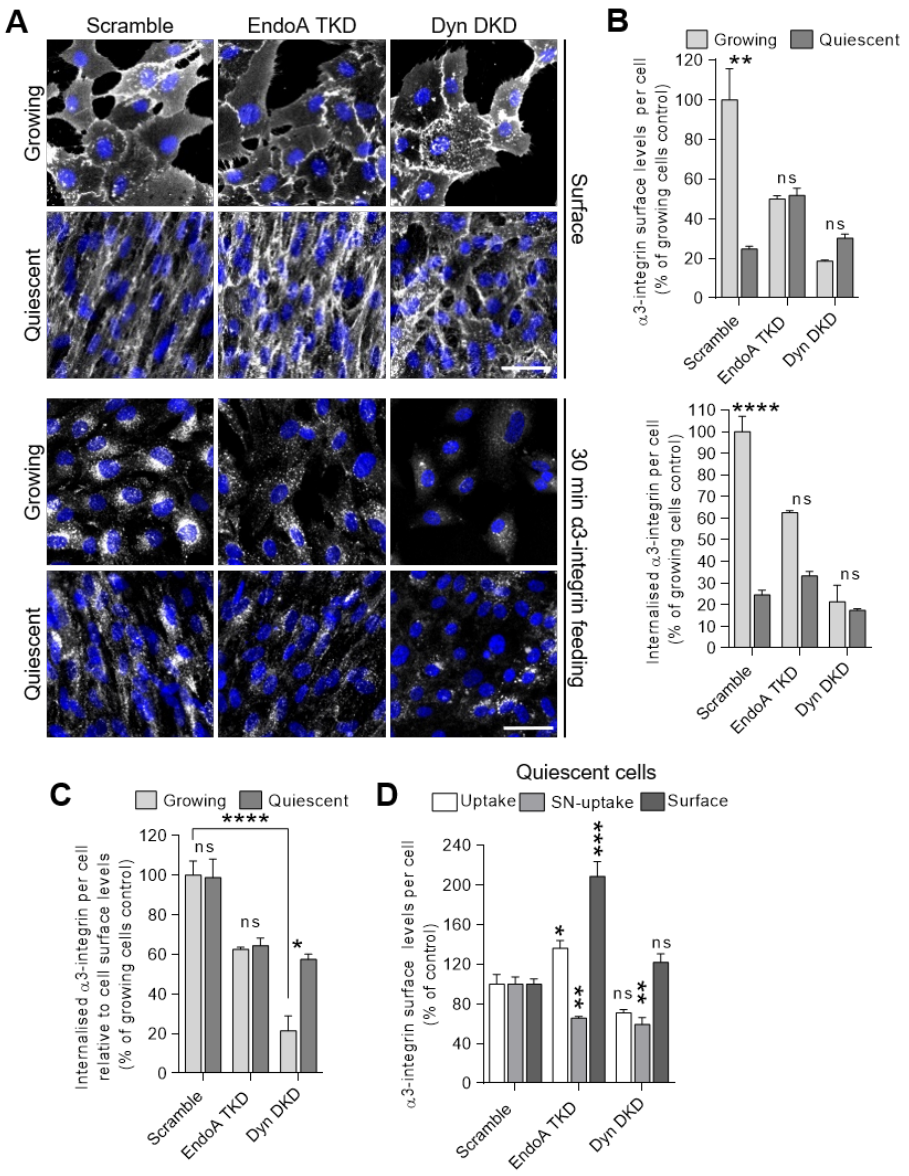


**Figure 5.2.18:** Cell surface levels and uptake of α3-integrin with reduced Dynamin or Endophilin expression

Endophilin and Dynamin expression knockdown was performed as described in Fig. 5.2.17. **A:** Representative epifluorescence microscopy images of α3-integrin cell surface immunolabelling (upper panel) and 30 min α3-integrin antibody feeding (lower panel) in growing and quiescent RPE1 cells treated with scrambled, Endophilin A1, 2 and 3 (EndoA TKD) or Dynamin 1 and 2 (Dyn DKD) siRNA. For surface labelling, cells were placed on ice and incubated with anti-α3-integrin antibody for 90 min before washing and fixing with 4 % PFA. Following antibody feeding, surface-bound antibody was removed by washes with acidic buffer. After fixation with 4 % PFA, cells were permeabilised and stained with secondary antibody and DAPI (blue pseudocolour). Scale bars: 50 µm. **B:** Quantification of epifluorescence microscopy images from **A:** Total fluorescence intensity of surface-bound (upper graph) or internalised (lower graph) α3-integrin per cell was normalised to growSiing cells scrambled control. Bar graphs represent mean + SEM from n=6 (growing cells) or n=3 (quiescent cells) biological replicates equivalent to a minimum of 4,000 growing or 9,000 quiescent cells per sample; ***P < 0.001, ns, not significant, two-way ANOVA with Tukey's multiple comparisons test comparing quiescent to growing cells for each condition. **C:** Internalised α3-integrin antibody was normalised to cell surface levels (data from **B**). Bar graphs represent mean + SEM; *P < 0.05, ns, not significant, two-way ANOVA with Tukey's multiple comparisons test comparing quiescent to growing cells for each condition. **D:** Internalised, surface-normalised internalised (SN-uptake) and surface-bound α3-integrin in quiescent cells quantified in B and C was normalised to scrambled control. Bar graphs represent mean + SEM; ****P < 0.0001, **P < 0.01, *P < 0.05, ns, not significant, one-way ANOVA with Dunett's multiple comparisons test comparing uptake, SN-uptake or surface levels in siRNA-treated condition to scrambled control

### 5.2.12 Quiescence survival signalling depends on Dynamin and Endophilin

With a method at hand that has a significant effect on α3-integrin endocytosis, it was then tested whether impaired α3-integrin would be reflected in reduced quiescence survival signalling. Growing and quiescent RPE1 cells, in which μ-adaptin (AP2 KD), Dynamin 1 and 2 (Dyn DKD) or EndophilinA1-3 (EndoA TKD) were knocked down (see Fig. 5.2.18 for knockdown efficiency), were fixed with PFA, permeabilised and immunolabelled for pAKT or p4E-BP1, which are down-regulated in quiescence, for quiescence survival-mediating pERK and pBAD (see sec. 5.2.7 for more details). Nuclei were stained with DAPI. Plates were imaged on a high-content widefield fluorescence microscope and images analysed by automated image analysis. First, total protein levels per cell were compared between growing and quiescent cells to find out whether AP2 KD, Dyn DKD or EndoA TKD might reverse signalling in quiescent cells to that observed in growing cells. Levels of pAKT were significantly lower (47 ± 4 %) in quiescent than in growing control cells (Fig. 5.2.19A and B top). After AP2 KD, Dyn DKD and EndoA TKD, pAKT levels in quiescent cells were 1.7-fold, 2.9-fold and 1.75-fold higher, respectively, than in respective growing cells, but only AP2 KD and EndoA TKD increased pAKT levels to those in growing control cells. Levels of p4E-BP1 were 50 ± 0.3 % lower in quiescent than in growing control cells and remained significantly lower for all knockdowns in quiescent cells when compared to growing contol cells (Fig. 5.2.19A and B bottom). Similarly, p4E-BP1 levels were significantly lower in quiescent than in growing cells after AP2 KD and EndoA TKD. P4E-BP1 levels did not differ between growing and quiescent cells after Dyn DKD, but that was because because of 2.4 fold reduced levels in growing cells.

Levels of pERK did not significantly differ between growing and quiescent control cells, but were significantly increased 2.2-fold and 1.7-fold in quiescent cells upon AP2 KD and EndoA TKD, respectively, when compared to growing control (Fig. 5.2.20A and B top). Phospho-ERK levels did not differ between growing control cells and quiescent Dyn KD cells, but all three knockdowns resulted in higher pERK levels in quiescent than in growing cells for the respective condition. Levels of pBAD did not differ between growing and quiescent cells in this experiment (Fig. 5.2.20A and B bottom). This conflicts with elevated pBAD in quiescent cells in Fig. 5.2.14. The reduction of relative pBAD levels

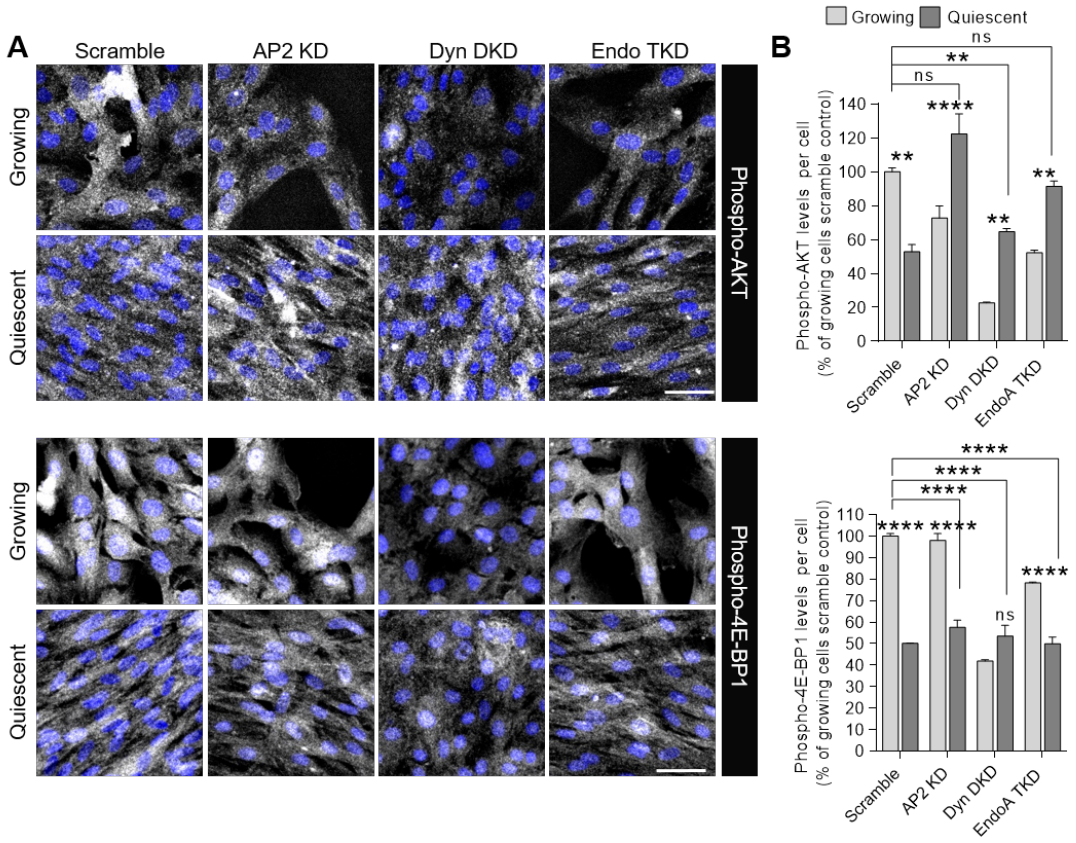


**Figure 5.2.19:** Effect of AP2, Dynamin and Endophilin knockdown on growth signalling in growing and quiescent RPE1 cells

AP2, Endophilin and Dynamin expression knockdown was performed as described in Fig. 5.2.17. **A:** Representative epifluorescence microscopy images of growing and quiescent RPE1 cells treated with scrambled, µ2-adaptin (AP2 KD), Dynamin 1 and 2 (Dyn DKD) or Endophilin A1, 2 and 3 (EndoA TKD) siRNA. Cells were fixed with 4 % PFA, permeabilised and immunolabelled with anti-phospho-4E-BP1 (T37/46) or anti-phospho-AKT (S473) antibody. DNA was stained with DAPI (blue pseudocolour). Scale bars: 50 µm. **B:** Quantification of epifluorescence microscopy images from **A**. Total fluorescence intensity of phospho-4E-BP1 (upper graph) and phospho-AKT (lower graph) per cell was normalised to growing cells scrambled control. Bar graphs represent mean + SEM from n=6 (growing cells scrambled and AP2 KD) or n=3 (all others) biological replicates equivalent to a minimum of 4,000 growing or 9,000 quiescent cells per sample; two-way ANOVA with Tukey's multiple comparisons test comparing quiescent and growing cells of each knockdown condition and pairs as indicated; ****P < 0.0001, **P < 0.01, ns, not significant.

in quiescent cells in this experiment is not severe (109 ± 1 % compared to 130 ± 2 % in Fig. 5.2.14 relative to growing control) and could have been caused by transfection with scrambled siRNA and the high concentration of lipids required for transfecting quiescent cells or as a result of scrambled siRNA transfection in growing cells. Interestingly, pBAD levels were significantly higher than growing control cells after AP2 KD (by 61 ± 7 %), Dyn DKD (by 41 ± 12 %) and EndoA TKD (by 69 ± 7 %), as well as higher than in growing cells subjected to the respective knockdowns.

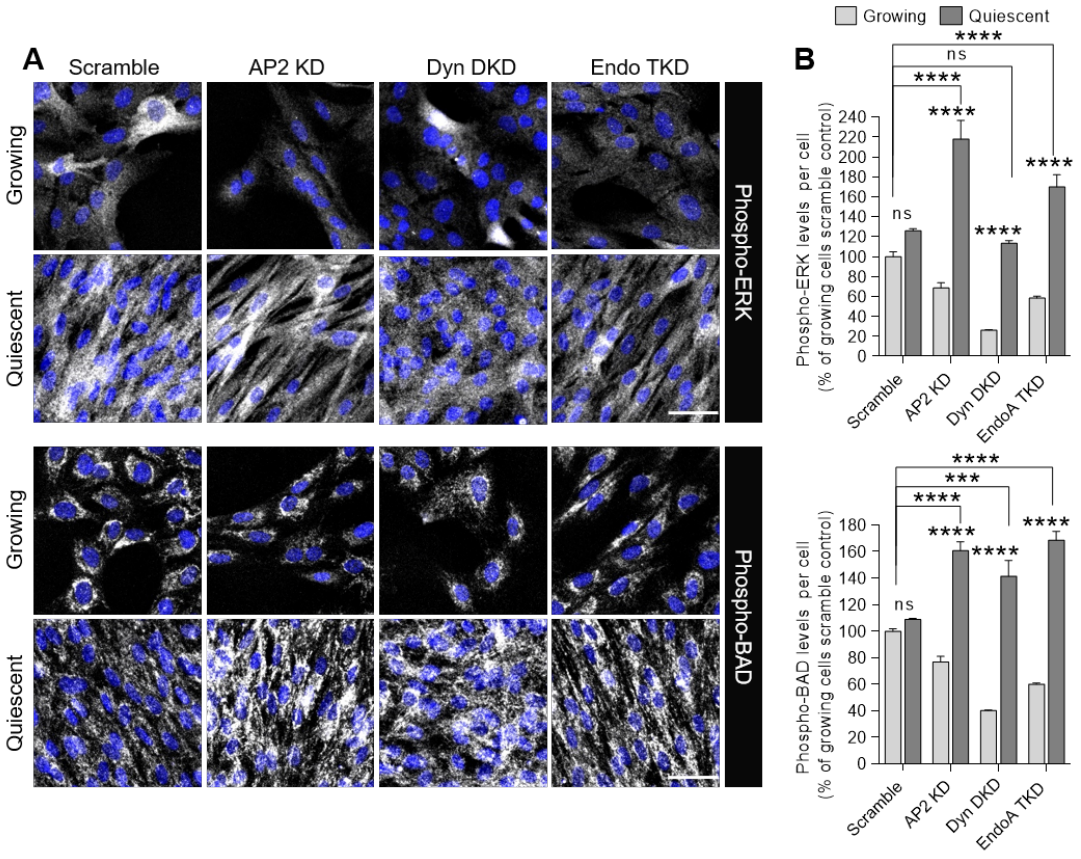


**Figure 5.2.20:** Effect of AP2, Dynamin and Endophilin knockdown on quiescence survival signalling in growing and quiescent RPE1 cells
AP2, Endophilin and Dynamin expression knockdown was performed as described in Fig. 5.2.17. **A:** Representative epifluorescence microscopy images of growing and quiescent RPE1 cells treated with scrambled, µ2-adaptin (AP2 KD), Dynamin 1 and 2 (Dyn DKD) or Endophilin A1, 2 and 3 (EndoA TKD) siRNA. Cells were fixed with 4 % PFA, permeabilised and immunolabelled with anti-phospho-ERK (T202/Y204) or anti-phospho-BAD (S112) antibody. DNA was stained with DAPI (blue pseudocolour). Scale bars: 50 µm. **B:** Quantification of epifluorescence microscopy images from **A**. Total fluorescence intensity of phospho-ERK (upper graph) and phospho-BAD (lower graph) per cell was normalised to growing cells scrambled control. Bar graphs represent mean + SEM from n=6 (growing cells scrambled and AP2 KD) or n=3 (all others) biological replicates equivalent to a minimum of 4,000 growing or 9,000 quiescent cells per sample; two-way ANOVA with Tukey's multiple comparisons test comparing quiescent and growing cells of each knockdown condition and pairs as indicated; ****P < 0.0001, ns, not significant.

When comparing the effect of AP2 KD to quiescent siRNA-transfected quiescent cells, pAKT levels were 2.3-fold, pERK levels 1.7-fold and pBAD levels were 1.5-fold increased (Fig. 5.2.21). Dyn DKD, which was only partial, had a minor effect on pBAD levels, increasing them 1.3-fold. EndoA TKD elevated pAKT levels 1.7-fold and pBAD levels 1.5-fold. Levels of p4E-BP1, implying mTORC activity, were not changed by any knockdown. This suggests that AP2 KD has the strongest effect on quiescence survival signalling and points out an important role for CME in quiescence maintenance. Dynamin had a marginal effect exclusively on pBAD signalling. Although the altered morphology of quiescent cells implies an effect of Dyn DKD, the low knockdown efficiency might have allowed for sufficient residual Dynamin levels to not alter the observed signalling events significantly. EndoA TKD had similar results to AP2 KD with respect to pAKT and pBAD upregulation, but failed to significantly increase ERK signalling.

Summarised, knockdown of AP2 and EndoA elevated activated AKT in quiescent cells to levels similar in control growing cells, while mTORC1 activity, monitored by phosphorylation of 4E-BP1, was not changed. AP2 and EndoA knockdown further elevated levels of pERK higher than they were in growing control cells, while only AP2 KD significantly increased pERK levels with respect to quiescent control cells. This might be explained by the differing endocytic pathways AP2 and Endophilin are involved in, or by lower EndoA TKD efficiency. Finally, knockdown of AP2, Dynamin and EndophilinA all resulted in increased BAD phosphorylation, both relative to growing and quiescent control cells.

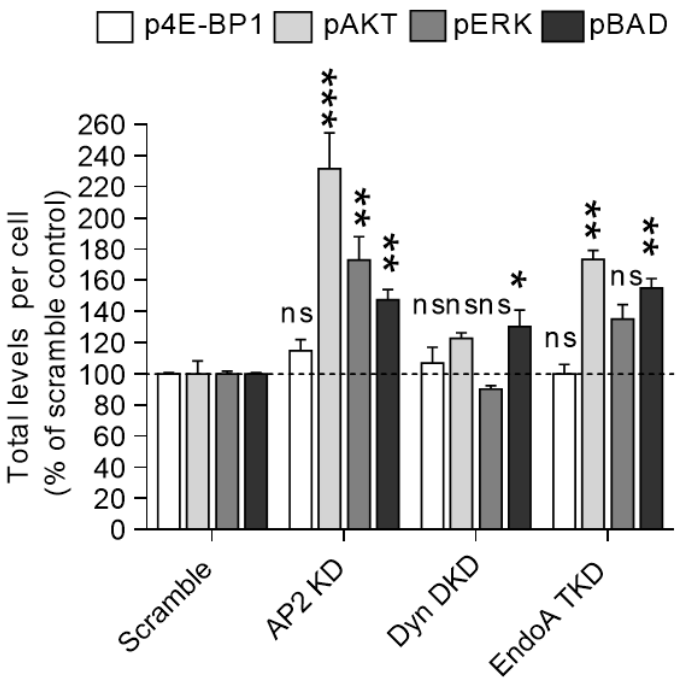


**Figure 5.2.21:** Quiescence signalling upon AP2, Dynamin and Endophilin knockdown
Data from quiescent cells in the previous two figures were normalised to quiescent cells scrambled control to demonstrate relative changes in the quiescent cell population. Bar graphs represent mean + SEM from n=3 biological replicates equivalent to a minimum 9,000 cells per sample; one-way ANOVA with Dunnett's multiple comparisons test comparing each knockdown with respective scrambled control; ***P < 0.001, **P < 0.01, *P < 0.05, ns, not significant.

### 5.2.13 AP2 and Dynamin knockdown increase cell cycle progression marker expression in quiescent cells

Lastly, it was tested whether AP2, Dynamin or Endophilin were required for quiescence maintenance. This was approached by immunolabelling for the expression of the cell cycle progression markers Cyclin D1, phosphorylated Rb (pRb) and Ki67. Nuclear Cyclin D1 promotes cell cycle progression from G1 to S phase (Baldin *et al.*, 1993; Ruiz-Miró *et al.*, 2011). Rb is a substrate of Cyclin D1 and promotes cell cycle progression when fully phosphorylated (Connell-Crowley *et al.*, 1997). Ki67 is a proliferation marker, which is present throughout all cell cycle phases but absent in quiescent cells (Takasaki *et al.*, 1981).

AP2, Dynamin 1 and 2 and EndophilinA1-3 were knocked down in growing and quiescent RPE1 cells as described sec. 5.2.10 (see Fig. 5.2.18 for knockdown efficiency). Cells were fixed with PFA, permeabilised and immunolabelled for cell cycle progression markers. Plates were imaged on a high-content widefield fluorescence microscope and images quantified by automated image analysis. Because active Cyclin D1 as well as pRb and and Ki67 are nuclear, nuclei positive for each markers were identified and expressed as percentage of all identified nuclei. Cyclin D1 labelling was very weak in this experiment, so that the threshold for maximal pixel intensity had to be decreased, which reduced the signal-to-noise-ratio and resulted in visible autofluorescence in quiescent cells (secondary antibody was conjugated to AlexaFluor488 which emits in similar wavelengths as yellow cell-intrinsic autofluorescence, mentioned in Cho & Hwang, 2012) (Fig. 5.2.22A top). The signal detected in quiescent cells was, however, mostly cytoplasmic. Active Cyclin D1 resides in the nucleus, as shown for 59 ± 9 % growing control cells with Cyclin D1-positive nuclei (Fig. 5.2.22B top) and is just below the 68 % G0/G1 cells with 2n DNA content identified by flow cytometry in Fig. 3.2.1. 9.6 ± 0.4 % quiescent cells with Cyclin D1-positive nuclei were identified under control conditions, which might be an exaggerated number because of autofluorescence colocalising with nuclei, as nuclei in microscopy images look devoid of Cyclin D1. Nonetheless, significantly less quiescent control cells had Cyclin D1-positive nuclei than growing control cells for scrambled control, AP2 KD and Dyn DKD. No significant difference was observed upon EndoA TKD, but that was due to a reduction of the fraction of Cyclin D1-positive nuclei to 14 ± 6 %. Phospho-Rb was present in 86 ± 1 % of growing control cells, which confirms

the 86 % pRb-positive cells identified by flow cytometry in sec. 3.2.3 (Fig. 5.2.22A and B middle). The pRb-positive population in quiescent control cells was negligibly small with 0.5 ± 0.1 %. Significantly less nuclei were pRb-positive in quiescent cells compared to growing cells after AP2 KD and Dyn DKD, but similar to Cyclin D1, no difference between growing and quiescent cells was observed for EndoA TKD, because the population of pRb-positive growing cells was reduced to 1.1 ± 0.3 %. Nuclear expression of Ki67 was similar to pRb in growing and quiescent control cells with 85 ± 1 % and 0.8 ± 0.2 % Ki67-positive nuclei, respectively. Significantly less nuclei were Ki-positive in quiescent cells compared to growing cells after AP2 KD and Dyn DKD, but similar to Cyclin D1, no difference between growing and quiescent cells was observed for EndoA TKD, because the population of Ki-positive growing cells was reduced to 6.3 ± 0.5 %.

Although percentages of pRb- and Ki67-positive quiescent cells were significantly smaller than those in growing cells after AP2 KD and Dyn DKD, changes relative to quiescent control cells were more pronounced. The number of pRb- and Ki67-positive nuclei increased 20-fold relative to quiescent control cells (Fig. 5.2.23), resulting in 9 ± 2 % pRb- and 17 ± 1 % Ki67-positive nuclei. AP2 KD increased the pRB-positive fraction 4.5-fold and the Ki67-positive fraction 6.7-fold, although the increase of pRb-positive nuclei was not considered significant using a one-way ANOVA (Student's unpaired two-sided t-test p-value=0.0019) because of the large difference upon Dyn DKD. 2.0 ± 0.2 % and 5.4 ± 0.5 % nuclei were positive for pRb and Ki67, respectively, upon AP2 KD. Interestingly, the number of Ki67-positive nuclei significantly increased 7.8-fold to 6.3 ± 0.5 % upon EndoA TKD, despite EndoA TKD resulting in significant decrease of cell cycle progression marker expression in growing cells (Fig. 5.2.22). Numbers of Cyclin D1-positive nuclei did not change (AP2 KD) or were slightly decreased (Dyn DKD and EndoA TKD), but with a low signal-to-noise ratio and high background of autofluorescence, these results are not robust.

Concluding, AP2 and Dynamin knockdown increased levels of cell cycle progression markers in a subpopulation of nuclei in quiescent cells. It is, however, not clear whether these cells entered a deep quiescent state, because knockdowns were performed before cells were 100 % confluent and before mitogen withdrawal. It is thus most likely to conclude that AP2 and Dynamin are required for quiescence entry. Loss of Endophilin, conversely, appeared to mediate cell cycle exit of growing cells, but increased Ki67 expression in a number of quiescent cells.

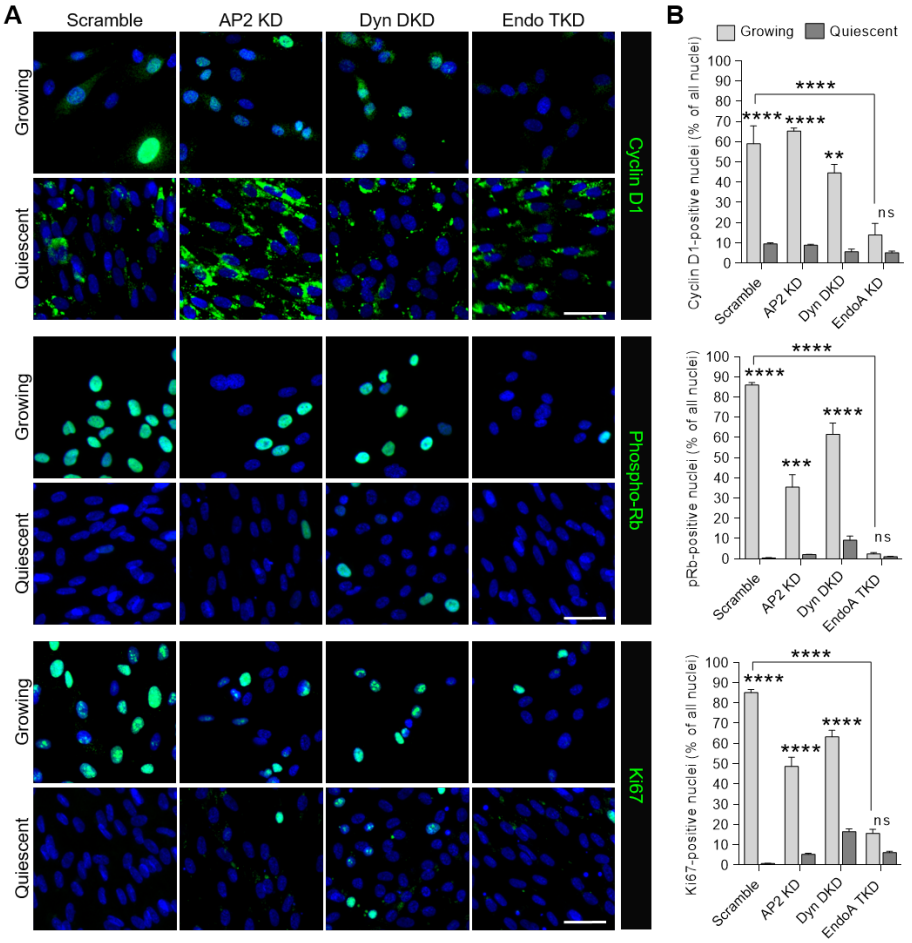


**Figure 5.2.22:** Effect of AP2, Dynamin and Endophilin knockdown on expression of cell cycle progression markers in growing and quiescent RPE1 cells

AP2, Endophilin and Dynamin expression knockdown was performed as described in Fig. 5.2.17. **A:** Representative epifluorescence microscopy images of growing and quiescent RPE1 cells treated with scrambled, µ2-adaptin (AP2 KD), Dynamin 1 and 2 (Dyn DKD) or Endophilin A1, 2 and 3 (EndoA TKD) siRNA. Cells were fixed with 4 % PFA, permeabilised and immunolabelled with anti-Cyclin D1, anti-phospho-Rb (S807/811) or anti-Ki67 antibody. DNA was stained with DAPI (blue pseudocolour). Scale bars: 50 µm. **B:** Quantification of epifluorescence microscopy images from **A**. The number of nuclei positive for Cyclin D1, (upper graph) phospho-Rb (middle) and Ki67 (lower graph) fluorescence was quantified and expressed as percentage of the total number of nuclei. Bar graphs represent mean + SEM from n=6 (growing cells scrambled and AP2 KD) or n=3 (all others) biological replicates equivalent to a minimum of 4,000 growing or 9,000 quiescent cells per sample; two-way ANOVA with Tukey's multiple comparisons test comparing quiescent and growing cells of each knockdown condition and pairs as indicated; ****P < 0.0001, ***P < 0.001, **P < 0.01, ns, not significant.

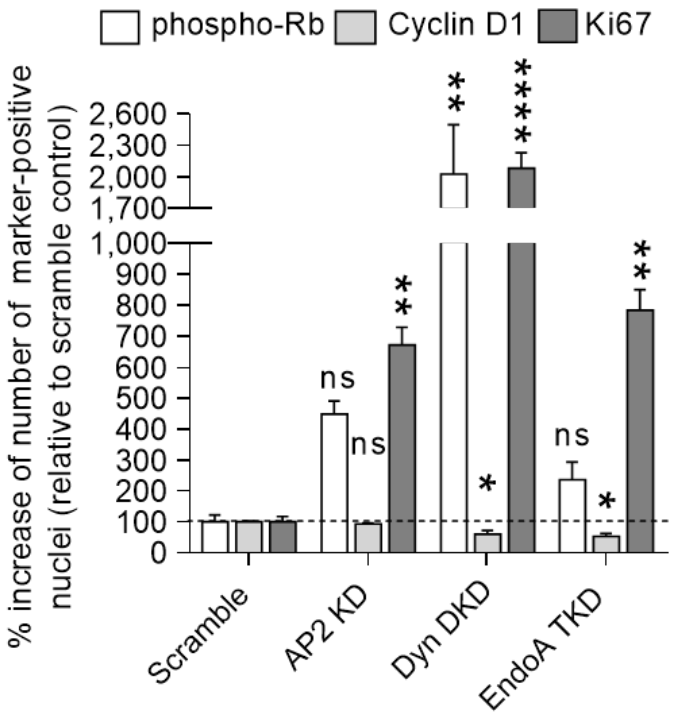


**Figure 5.2.23:** Cell cycle progression markers in quiescent cells after AP2, Dynamin and Endophilin knockdown

Data from quiescent cells in the previous two figures were normalised to quiescent cells scrambled control to demonstrate relative changes in the quiescent cell population. Bar graphs represent mean + SEM from n=3 biological replicates equivalent to a minimum 9,000 cells per sample; one-way ANOVA with Dunnett's multiple comparisons test comparing each knockdown with respective scrambled control; ****P < 0.0001, **P < 0.01, *P < 0.05, ns, not significant.

## 5.3 Discussion

Integrins form a connection between the cell and its environment, mediating vital cellular processes ranging from cell adhesion to differentiation, proliferation and survival (Streuli, 2016). The specific function of integrins depends on ther β- and α-subunit composition and interaction with cognate ECM ligands (Hynes, 2002; Humphries, 2006). Many integrin signalling events occur at the plasma membrane upon ECM ligand binding, however alternative integrin signalling has been observed, such as adhesion-independent endosomal signalling (Alanko *et al.*, 2015). In this chapter, endocytosis and endocytic recycling of α3β1-integrin, a putative regulator of proliferative quiescence, and the effect of endocytosis and recycling inhibition, was studied.

### 5.3.1 α3β1-integrin endocytosis and recycling in growing and quiescent cells

Integrins are highly endocytic molecules and their endocytosis and trafficking was reported in multiple studies (De Franceschi *et al.*, 2015). Integrin endocytosis can serve translocation of inactive integrins from dorsal plasma membrane areas via recycling to leading edges in migration (Bretscher, 1992; Arjonen *et al.*, 2012; Teckchandani *et al.*, 2012), to supply mitogen-starved cells with ECM proteins for amino acid supply and mTORC1 signalling to mediate survival (Rainero *et al.*, 2015; Muranen *et al.*, 2017) or to mediate adhesion-independent FAK-survival signalling from endosomes (Alanko *et al.*, 2015). While most studies on integrin trafficking were performed in cancer cells and are related to migration (De Franceschi *et al.*, 2015), the aim in this chapter was to discover a role for integrin trafficking in quiescent cells.

The conformational state of an integrin can be assessed by its recognition by monoclonal antibodies. These antibodies bind to extracellular regions of integrins, which are either blocked or exposed when the integrin is collapsed and non-ligandbound or in an extended conformation when bound to ligands (Byron *et al.*, 2009). When α3-integrin dimerises with β1-integrin, it is recognised by the mAbP1B5 (Nicolaou *et al.*, 2012), which was used for α3-integrin detection throughout this study. A general reduction in endocytosis of ligandbound (detected by mAb13) relative to non-ligandbound β1-integrin (detected by mAb9EG7) distinguished both growing and quiescent RPE1 cells

from cancer cells, in which endocytosis of ligand-bound β1-integrin dominates and might serve amino acid supply or ECM remodelling (Arjonen *et al.*, 2012). In colocalisation studies, α3-integrin endocytosed mainly dimerised with non-ligandbound β1-integrin, in both growing and quiescent RPE1 cells and endocytosis of α3-integrin with ligand-bound β1-integrin was even less prevalent in quiescent than in growing cells (Fig. 5.2.1), suggesting a pivotal role for endocytosis of non-ligandbound α3β1-integrin during quiescence. However, mAb9EG7 was questioned as a suitable antibody for β1-integrin detection, because it did not precipitate mature, glycosylated β1-integrin and did not label surface-β1-integrin on podocytes (Nicolaou *et al.*, 2012). MAb9EG7 did bind to cell surface-β1-integrin on RPE1 cells, particularly on quiescent cells (data not shown), but it might be beneficial to verify results with another monoclonal antibody against active β1-integrin, such as mAb12G10 (Humphries *et al.*, 2005; Arjonen *et al.*, 2012).

Uptake and cell surface levels of α3-integrin were lower in quiescent than in growing cells, as was endocytosis for 10 min when the lower cell surface levels were considered, but internalised α3-integrin remained in quiescent cells longer than in growing cells before being degraded or recycled (Fig. 5.2.2). The subcellular localisation of α3-integrin was then studied by colocalisation with endosomal markers and identified VPS35-positive endosomal compartments as major site of α3-integrin residence within quiescent cells, whereas it was mainly found in EEA1- and APPL1-positive compartments in growing cells (Fig. 5.2.6). This, together with reduced localisation of phosphorylated FAK, suggested that endosomal signalling mediated by α3-integrin does not occur to an extended amount in quiescent cells (Fig. 5.2.4). Instead, α3-integrin is retained in a recycling compartment associated with Retromer, which was shown to mediate α3-integrin recycling (McNally *et al.*, 2017). Retromer is involved in multiple endosomal sorting routes, ranging from fast SNX27-mediated early endosomal recycling to SNX3- or SNX-BAR-domain-mediated retrograde transport to the *trans*-Golgi network (TGN) and presumably direct transport from late endosomes to the TGN (Gallon & Cullen, 2015). Riggs *et al.* proposed a novel Syntaxin 6- and VAMP3-dependent recycling mechanism for α3β1-integrin via the TGN in cancer cells overexpressing Syntaxin 6 (Riggs *et al.*, 2012). Slow recycling via the TGN would explain the retention of internalised α3β1-integrin in quiescent cells and the observed potentially slower kinetics of α3-integrin recycling in a functional recycling assay, although this experiment should be repeated with controls accounting for incomplete surface-bound antibody blocking

(Fig. 5.2.7). It would be interesting to find out whether the STX6- recycling pathway is related to the Retromer pathway or whether Retromer-mediated recycling via the TGN is the preferred route in quiescent cells.

### 5.3.2 Pharmacological inhibition of α3β1-integrin recycling and effect on quiescence survival signalling

Recycling of integrins is important to regulate their many functions, such as adhesion turnover during migration and ECM remodelling (Caswell *et al.*, 2009; Frittoli *et al.*, 2014; Riggs *et al.*, 2012). While migration and concomitant relocation of focal adhesions play an important role in cancer cells, migration of confluent quiescent cells is limited and integrin recycling might not be associated with it. Monensin and Primaquine were shown to inhibiting integrin recycling (Woods *et al.*, 2004; Marre *et al.*, 2010) and were employed in this study to test the effects of recycling inhibition on α3-integrin recycling and whether it would affect quiescence survival signalling. Inhibition of recycling with Monensin or Primaquine resulted in higher relative accumulation of α3-integrin during steady-state labelling of fixed cells and for functional endocytosis assays (Fig. 5.2.8). With lower endocytosis and potentially slower recycling in quiescent cells, this could be explained by a higher pool cycling through quiescent cells becoming trapped and accumulating in vesicles upon recycling inhibition. The amount of accumulated α3-integrin in intracellular vesicles upon Monensin or Primaquine inhibition was not as high as observed at steady state, but still higher than in growing cells (Fig. 5.2.9). Interestingly, cell surface levels of α3-integrin did not change in quiescent cells upon recycling inhibition, which might indicate an increased α3-integrin synthesis rate during quiescence to replenish the plasma membrane surface pool. This would support a hypothesis of α3-integrin exocytosis via exosomes from quiescent cells. α3-integrin was discovered together with its interaction partner CD151 in exosomes required for ECM remodeling (Yue *et al.*, 2015). The activity of α3-integrin in ECM remodeling and maintenance is well known (Conti *et al.*, 2003; DiPersio *et al.*, 1997). α3-integrin-containing exosomes from quiescent cells might thus contribute to Laminin processing. Another possibility is information exchange via exosomes, as has been reported for the induction of vascularisation in cancers (Nazarenko *et al.*, 2010). How these signals would be processed in quiescent cells, however, is not known.

Pharmacological inhibition of recycling had a modest effect on, but did not revert down-regulated AKT- and mTORC1-signalling to the activity they have in growing cells and expression of the cell cycle exit marker p27 was not affected (Fig. 5.2.11 and Fig. 5.2.10). Quiescence survival signaling mediated by ERK and BAD, however, was slightly decreased. With pleiotropic inhibitors such as Monensin, which inhibits vesicle fusion and trafficking by neutralising endosomal pH (Wileman *et al.*, 1984), it is likely that induction of a standstill in endosomal trafficking results in a variety of nonspecific effects. Knockdown or overexpression of dominant-negative mutants of specific recycling pathway components such as SNX27 or SNX3 to assess Retromer-dependent recycling, or of Retromer subunits might be better suited to study signalling events and will link them at the same time to a mechanism. Furthermore, it will be interesting to address the role of Retriever in recycling of α3-integrin. The SNX17 subunit of Retriever was suggested to play a role in recycling of both α3-integrin and β1-integrin (McNally *et al.*, 2017), but it has not yet been functionally studied in α3-integrin recycling. It was also shown that VPS3 and VPS8 play a role in recycling of integrins in Rab4-positive endosomes (Jonker *et al.*, 2018). Screening markers of integrin recycling pathways via knockdown or, preferentially, overexpression of dominant-negative mutants will be the way forward to dissect the recycling mechanism of α3-integrin and its role in quiescence signalling.

### 5.3.3 Inhibition of α3β1-integrin endocytosis

Clathrin-mediated endocytosis plays a pivotal role in integrin endocytosis. β1-integrin can interact with the adaptor proteins Numb and Dab2 via its membrane-proximal NPXY motif. Numb and Dab2, in turn, recruit endocytic adaptor proteins, such as AP2 (Nishimura & Kaibuchi, 2007; Calderwood *et al.*, 2003; Teckchandani *et al.*, 2012; Mishra *et al.*, 2004). Some of the β1-integrin dimerisation partners, including α3-integrin, are internalised in a Dab2-dependent manner from dorsal surfaces of migrating cells (Teckchandani *et al.*, 2012). In addition, α3-integrin itself contains two YXXΦ AP2 binding motifs (De Franceschi *et al.*, 2016). Indeed, knockdown of AP2 decreased α3-integrin endocytosis in both growing and quiescent cells by about 80 % (Fig. 5.2.16). The residual 20 % might have been due to partial knockdown and residual active AP2, but they might also be the result of Clathrin-independent endocytic pathways internalising α3-integrin. Galectin-3 was reported to cluster β1-integrin

and regulate its endocytosis (Lakshminarayan *et al.*, 2014; Yang *et al.*, 2017). In fact, Lakshminarayan *et al.* could show dependency of β1-integrin internalisation on both Clathrin- and Galectin-3-dependent endocytosis. Galectin-3 induces endocytic carrier formation by extracellular clustering of glycosylated lipids or proteins in the exoplasmic membrane leaflet, whose scission is dynamin-independent, relies on actin polymerisation and might involve BAR-domain protein-mediated membrane friction (Lakshminarayan *et al.*, 2014; Renard *et al.*, 2015; Simunovic *et al.*, 2017). One of these BAR-domain proteins is EndophilinA2, which also mediates FEME, a fast endocytic process dependent on dynamin for endocytic vesicle scission (Renard *et al.*, 2015; Boucrot *et al.*, 2015). Both Dynamin and Endophilin knockdown decreased α3-integrin endocytosis by about 40 % and 30 % in quiescent RPE1 cells (Fig. 5.2.18). With the dependency of CME on dynamin scission, a more profound decrease, correlating with AP2 knockdown, would have been expected. However, Dynamin knockdown efficiency was only about 50 % in quiescent cells, so that enough residual Dynamin might have been present for vesicle scission (Fig. 5.2.17). Although a role was reported for Endophilin in CME, it appears to have a major function only in neuronal and is redundant in non-neuronal cells (Meinecke *et al.*, 2013; Boucrot *et al.*, 2015). Hence, the partial dependency of α3-integrin on Endophilin suggests a potential reliance on FEME or Clathrin-independent pathways relying on Endophilin for vesicle scission. It will be interesting to investigate whether combined knockdown of AP2 and Endophilin completely abrogates α3-integrin endocytosis and whether β1-integrin is internalised together with α3-integrin by Galectin-3-mediated CLIC/GEEC. This will not only describe the endocytic mechanism of α3-integrin uptake, but might also highlight differences in endocytic pathways for integrin internalisation in growing and quiescent cells. However, knockdown experiments in quiescent cells should be interpreted with caution, because siRNA treatments are performed before cells enter quiescence. It can therefore not be confirmed whether the results here are caused as a consequence of knockdown during quiescence or whether they are observed because cells could not enter a deep quiescent state because the (partially) inhibited endocytic pathways were required for quiescence entry. Confirmation by overexpression of dominant-negative mutants, which can be performed on quiescent cells in serum-free medium allow for quiescence entry under normal condition and inhibit endocytic pathways for a shorter time period (24-48 hours, as opposed to 10 days for knockdown). With this method,

dominant-negative mutants of integrin adaptor proteins, such as Numb and Dab2, can be tested (Santolini *et al.*, 2000). Inhibitor treatments might not always be suitable, because of differing cell densities and exposed cell surface area, which might result in a different concentration of inhibitor acting on its target. Specific inhibitors such as Dyngo, which were highly potent in growing cells, showed only small effects in quiescent cells (Fig. 5.2.12). To observe an effect in quiescent cells, doses might have to be adjusted, but this would compromise the comparability of experiments because of potential off-target effects.

### 5.3.4 Changes in quiescence survival signalling and cell cycle progression marker expression upon inhibition of endocytocytic pathways

Integrin endocytosis is linked to uptake of extracellular matrix for nutrient supply and survival, endosomal signalling or ECM remodelling and removal of inactive integrins from the dorsal cell surface to relocate it via recycling to focal adhesion sites during migration (Muranen *et al.*, 2017; Gopalakrishna *et al.*, 2018; Alanko *et al.*, 2015; Caswell *et al.*, 2009). A potential role for endocytosis in the regulation of quiescence survival signalling was investigated in this chapter. While inhibitors of dynamin (Dyngo; McCluskey *et al.*, 2013) and CME (Ikarugamycin; Elkin *et al.*, 2016) did not alter quiescence survival signalling (concomitant with no or minimal effect on $\alpha$3-integrin endocytosis, Fig. 5.2.12), macropinocytosis inhibitors Monensin and Rottlerin elevated active pERK, but had no or the opposite effect on survival signalling mediated by BAD phosphorylation at Serine 112 (Fig. 5.2.13 and Fig. 5.2.14; Scheid *et al.*, 1999). It is difficult to draw conclusions on the mechanism by which both macropinocytosis inhibitors elevated pERK levels. Importantly, they do not act on a specific molecule, but rather increase submembraneous pH (EIPA; Koivusalo *et al.*, 2010) or act by an unknown mechanism (Rottlerin). Therefore, pleiotropic effects cannot be ruled out, as it was reported that EIPA inhibits other Clathrin-independent pathways, such as FEME (Boucrot *et al.*, 2015). A recently discovered macropinocytosis inhibitor, imipramine, specifically inhibits macropinocytosis by preventing membrane ruffling and does not affect Ras/MEK/ERK signalling nor PI3K activity (Buyya & Pandey, 2018). It might be a promising drug to test macropinocytosis effects on signalling while no specific macropinocytosis-specific marker is known.

Knockdown of AP2, Dynamin and Endophilin all significantly affected α3-integrin endocytosis, thereby proving more efficient than treatmemt with pharmacological inhibitors. However, as discussed above, it is not sure whether the change in endocytosis was because of impaired quiescence entry because knockdown occured before that. AKT was activated in quiescent cells in all three knockdowns, reverting pAKT levels to those in growing cells (Fig. 5.2.19). This is a sign for proliferation (Segrelles *et al.*, 2014; Gude *et al.*, 2006), but mTORC1 activity, which is a substrate of AKT and regulates cell growth (Laplante & Sabatini, 2012), was not elevated upon either knockdown (Fig. 5.2.21). The quiescence survival model proposed by K. McGourty (E. Boucrot lab) suggests activation of ERK, which is retained in the cytosol, followed by survival-mediating phosphorylation of Serine 112 on BAD (Fig. 5.2.3). ERK activation was only significantly increased upon AP2 KD, but BAD phosphorylation at Serine 112, which is mediated by ERK (Scheid *et al.*, 1999), was elevated for all knockdowns (Fig. 5.2.20 and Fig. 5.2.21). However, total levels of proteins were not assessed, so increased BAD phosphorylation might have been a result of elevated BAD expression and thus more substrate for phosphorylation by ERK. Furthermore, multiple cargoes are endocytosed by each pathway and the sum of decreased endcytosis and signalling, or increased cell surface signalling, might result in a phenotype which is not easy to explain. The data imply, however, that reduction of CME via AP2 KD as well as reduction of Clathrin-independent pathways by Endophilin KD disrupts the signalling signature in quiescent RPE1 cells. The effect of Dynamin KD was not as pronounced. Considering its requirement for CME as well as Clathrin-independent pathways, which might affect signalling homeostasis even more severely, this might have been a result of inefficient knockdown.

A more robust assessment of the quiescent state upon endocytosis disruption is to assess cell cycle progression markers. Cell cycle exit is characterised by Cyclin D1 absence from the nucleus (Baldin *et al.*, 1993; Ruiz-Miró *et al.*, 2011), hypophosphorylated pRb (Connell-Crowley *et al.*, 1997) and absence of Ki67 (Takasaki *et al.*, 1981). The increased proportion of nuclei expressing pRb and Ki67 among quiescent cells upon AP2 (only Ki67), Dynamin and Endophilin knock down suggests that multiple endocytic pathways cooperate to induce or maintain quiescence. Problems with Cyclin D1 labelling in Fig. 5.2.22 did not encourage conclusions, but as it is required for Rb phosphorylation (Connell-Crowley *et al.*, 1997), it is likely that its nuclear expression might be increased. Although these findings imply that multiple endocytic pathways are required for quies-

cence, it is not clear whether they are required for quiescence induction, maintenance or both. As mentioned in sec. 5.3.3, knockdowns were performed before cells entered quiescence. Because integrin signalling is required for quiescence entry, it is likely that quiescence signalling homeostasis could never be established by down-regulation of endocytosis (Lampe *et al.*, 1998; Da Silva *et al.*, 2010; Spencer *et al.*, 2011).

## 5.4 Conclusions

In this chapter, an attempt was made to link integrin trafficking to survival signalling in quiescence. Using an *in vitro* model of quiescent RPE1 cells, it could be shown that $\alpha 3\beta 1$-integrin, which is a receptor for laminins prevalent in the matrisome of quiescent cells (K. McGourty), is endocytosed in quiescent cells primarily in a Clathrin-dependent manner, but Clathrin-independent pathways relying on Dynamin and/or Endophilin might be involved in its internalisation as well. Clathrin-dependent and independent pathways are required for quiescence survival signalling and complete down-regulation of cell cycle expression markers. $\alpha 3$-integrin recycling might differ between fast recycling in growing cells and slow, Retromer-mediated recycling in quiescent cells. Further studies are required to define the precise recycling pathway of $\alpha 3\beta 1$-integrin during quiescence and the purpose of changes in recycling kinetics. While the importance of continuous endocytosis and recycling was mostly emphasised for relocating integrins to new focal adhesion sites in migrating cells or to separate integrins from their ECM ligands in late endosomal compartments, quiescent RPE1 cells used in this study form a tightly packed monolayer, in which migration is hardly possible. Additionally, adhesion sites were not as pronounced as in proliferating cells. Furthermore, endocytosis of ECM-ligands does not maintain survival in quiescent cells, as they rely on extracellular amino acids. A direct connection between $\alpha 3\beta 1$-integrin endocytosis or recycling could not be shown in this chapter. However $\alpha 3\beta 1$-integrin is actively turned over during quiescence, which suggests a signalling mechanism relying on trafficking instead of plasma-membrane based signalling.

# 6 General discussion and future work

## 6.1 Summary and conclusions

### 6.1.1 Induction of quiescence in an *in vitro* cell line model

Mammalian cells can enter proliferative quiescence in culture upon contact inhibition, mitogen starvation or loss of adhesion to substrate (only adherent cells, while remaining attached to each other; Coller *et al.* 2006; Ruiz-Miró *et al.* 2011; Neurauter *et al.* 2012). To date, studies in quiescent cells have been limited to cells residing in a natural quiescent state (Cheng *et al.*, 2000a; Orford & Scadden, 2008; Malumbres & Barbacid, 2001) or to primary cell cultures, such as fibroblasts (Lemons *et al.*, 2010).

In Chapter 3, a combinational approach of contact inhibition and mitogen starvation was employed to induce quiescence in hTERT-immortalised RPE1 cells. Quiescent RPE1 cells did not replicate DNA and featured down-regulated cell cycle progression markers, in agreement with the literature (Baldin *et al.*, 1993; Ruiz-Miró *et al.*, 2011; Takasaki *et al.*, 1981; Stevaux & Dyson, 2002; Lemons *et al.*, 2010). Quiescent cells are furthermore characterised by low transcriptional activity (Shapiro, 1981). DNA/RNA staining identified a larger cell population with 2n DNA content and low RNA content in quiescent than in proliferating RPE1 cells. A similar observation was demonstrated for contact-inhibited and serum-starved quiescent fibroblasts (Lemons *et al.*, 2010), but for both experiments, the low-RNA population was smaller than observed in cells residing in a natural quiescent state, such as naive lymphocytes, dormant hematopoietic stem cells or musle satellite cells (Shapiro, 1981; Hüttmann *et al.*, 2001; Sharma *et al.*, 2012). Furthermore, the phosphorylation status of Rb did not correlate with low or high RNA level-containing quiescent RPE1 cells. Hypophosphorylated Rb blocks cell cycle progression and mediates cell cycle exit (Lundberg & Weinberg, 1998; Ren & Rollins, 2004; Stein *et al.*, 2013). Thus, DNA/RNA staining might not be a bona fide quiescence

marker and should be validated by other cell cycle progression markers such as decreased Cyclin D1 or Ki67 and elevated p27 (Chapter 5). In fact, it is often used in combination with counterstaining of proliferation markers (Hüttmann *et al.*, 2001; Sharma *et al.*, 2012). However, the lack of a specific positive marker for quiescent cells poses a problem when evaluating proliferative quiescence.

A caveat of hTERT-immortalised cell lines as quiescence model is the potential transcriptional activity of TERT, which might influence the expression of independent genes, among which are growth-controlling (Smith *et al.*, 2003) and apoptosis-regulating genes (Smith *et al.*, 2003; Rahman *et al.*, 2005; Lee *et al.*, 2008). The non-telomeric activities of TERT are diverse, ranging from survival enhancement to supporting cancer cell proliferation (Majerska *et al.*, 2011). Interestingly, mTERT is naturally expressed in slowly-cycling mouse intestinal stem cells, conveying resistance to senescence, which might display a quiescence-intrinsic feature (Montgomery *et al.*, 2011). As long as the direct effect of hTERT overexpression on a cell line is not defined, caution should be taken when interpreting results solely based on this cell line. On the other hand, many advantages support the use of hTERT-immortalised RPE1 cells, such as a stable diploid genome and sensitivity to contact inhibition. Additionally, experiments are highly reproducible and large quantities of cells can be used. Quiescent RPE1 cells survive for weeks in serum-free medium without losing the capacity to resume proliferation. Their likeness to primary cells makes them an adequate model to study physiological conditions such as proliferative quiescence, as opposed to cancer cell lines, which continuously divide. Naturally, key results should be verified in primary cells to exclude independent effects of hTERT.

### 6.1.2 Changes in endocytosis during proliferative quiescence

Establishment of an *in vitro* cell line model of proliferative quiescence paved the way to assess functional regulations during quiescence and directly compare them to proliferating cells of the same cell type. In Chapter 4, it was studied whether endocytic pathways were still active during quiescence and if so, how their activity related to proliferating cells. CME activity for the classical cargoes Tf, EGF and LDL, as well as their total and cell survace receptor levels, were strongly decreased during quiescence. Endocytosis of Tf, EGF and LDL serves nutrient acquisition and growth-stimulatory sig-

nalling for proliferation. A decrease of these pathways in quiescent RPE1 cells confirms *in vivo* observations of down-regulated VEGF uptake in mature blood vessels (Nakayama *et al.*, 2013) and reduction of RTK or Wnt-signalling cell surface receptor levels (Cruse *et al.*, 2015; Koo *et al.*, 2012). Differing activity of CME in two different cell cycle states of the same cell type provided a practical system to investigate CME regulation. A SILAC mass spectrometry screen identified that phosphorylation sites of the early-arriving CME protein FCHo2 in G1, which were hypophosphorylated during G0. However, a non-phosphorylable as well as a phosphomimetic FCHo2 mutant increased Tf uptake, which implies that sustained phosphorylation or dephosphorylation do not regulate FCHo2 function in CME. Moreover, phosphomimetics are not exact surrogates of phosphorylation, which should be considered when interpreting the results for phosphomimetic FCHo2. It is possible that hierarchical phosphorylation of FCHo2 may play a role in conjunction with Eps15, with whom FCHo2 was shown to interact, or with other CME-specific adaptor proteins (Ma *et al.*, 2016). The latter would explain that CME in quiescent RPE1 cells is active for dedicated cargoes, such as Lamp1.

CLIC endocytosis might occur in quiescent RPE1 cells, which was shown by β1-integrin (Chapter 5) and Cholera toxin uptake (which enters cells in a dynamin-dependent manner as opposed to classical CLIC) (Lakshminarayan *et al.*, 2014). However, uptake of some of the main CLIC cargoes, such as CD44, could not be functionally assessed in antibody feeding assays because antibodies clustered at the cell surface. Finally, macropinocytosis was highly elevated in quiescent RPE1 cells. Interestingly, uptake of low molecular weight macropinocytosis cargoes such as 10 kDa dextran and BSA strongly depended on AP2. Clathrin-dependence of low molecular weight dextran is consistent with observations by Li *et al.* (2015) and Cao *et al.* (2007) and the fact that it can bind to cell surface receptors (Kato *et al.*, 2000). BSA binding to several cell surface reptors and uptake by CME in addition to macropinocytosis has also been reported (Buchäckert *et al.*, 2012; Yumoto *et al.*, 2012; Koral & Erkan, 2012; Larsen *et al.*, 2016). It remains to be established which receptors mediate CME of small Dextran and BSA in quiescent cells, as well as why these pathways are upregulated. BSA did not promote survival upon amino acid starvation, indicating that extracellular protein did not replace the need for extracellular free amino acids and that ECM components are not internalised to initiate mTORC1-mediated survival signalling in quiescent RPE1 cells (Commisso *et al.*, 2013; Muranen *et al.*, 2017).

While a number of endocytic pathways, including CME, CLIC and Macropinocytosis, were investigated in this study, Clathrin-indepedent pathways such as FEME and Caveolar endocytosis were not assessed. Identification of FEME carriers in fixed quiescent cells did not lead to conclusive results, because Endophilin-positive vesicles were distributed across the whole cell area and stimulation of receptors did not induce their colocalisation with FEME carriers (Boucrot *et al.*, 2015). In collaboration with R. G. Parton, quiescent cells will be visualised by electron microcopy, which may provide information on the abundance of Cavelolae, as well as macropinosomes and CCPs.

### 6.1.3 Endocytosis and recycling during quiescence

A complementary project by K. McGourty identified a subset of Laminins in the ECM of quiescent RPE1 cells as inducers of quiescence in multiple cell types, concomitant with a quiescence survival signalling pathway. Among the integrin receptors for these Laminins was $\alpha$3-integrin. $\alpha$3-integrin mediates cell adhesion as well as quiescence and survival signalling (Pazzagli *et al.*, 2017; Nguyen *et al.*, 2000; Manohar *et al.*, 2004; Tesfay *et al.*, 2016). $\alpha$3$\beta$1-integrin trafficking is known to be required in cancer migration, but little is known about its trafficking in quiescent cells.

In Chapter 5, $\alpha$3$\beta$1-integrin was shown to be internalised into quiescent cells in an AP2-, Dynamin- and Endophilin-dependent manner, suggesting that it is internalised by CME as well as clathrin-independent pathways. $\alpha$3$\beta$1-integrin was primarily internalised in the non-ligandbound, inactive form, in both growing and quiescent RPE1 cells. This is different from cancer cells, where primarily ligand-bound $\beta$1-integrins are endocytosed to remodel the ECM or acquire nutrients (Arjonen *et al.*, 2012). $\alpha$3-integrin endocytosis was lower in quiescent than in growing RPE1 cells, but internalised $\alpha$3-integrin was retained in VPS35-positive endosomal compartments. An important role for $\alpha$3-integrin recycling pathways during quiescence was confirmed by pharmacologically inhibiting recycling, which accumulated more internalised $\alpha$3-integrin in quiescent than in growing cells. Retention of $\alpha$3-integrin in endosomal vesicles could serve a similar purpose as reported by Pellinen (2006), who showed that Rab21 keeps integrins in an early-endosomal pool close to the plasma membrane. Pharmacological recycling inhibition perturbed quiescence survival signalling, but did not trigger cell cycle progression. This could be due to the time frame of inhibitor treatment being too short to observe

changes such as upregulation of cell cycle-promoting genes. Pharmalogical inhibition of endocytosis neither had a strong effect on α3-integrin endocytosis in quiescent cells nor on quiescence signalling. However, quiescence signalling was strongly perturbed when endocytic pathways were knocked down, but resulted in up-regulation of both AKT-activity, which regulates growth, as well as quiescence-specific survival signalling. Knockdown of an endocytic pathway inhibits endocytosis of a variety of other cargoes that might contribute to quiescence signalling homeostasis. α3β1-integrin was shown to have overlapping ligand specificities with α6β1-integrin (Delwel *et al.*, 1994; Margadant *et al.*, 2009) and both can act in a co-stimulatory manner (Chang *et al.*, 1995). In addition, knockdowns in quiescent cells were performed over a long time period, and initiated while the cells were not yet quiescent. This proposes two caveats: First, cells might be devoid of proteins they need for quiescence entry. Second, the signalling pathway balance might shift during the period following knockdown while cells are cultured in serum-free medium. Pharmacological inhibitors, in turn, have rapid effects, but can have off target effects and are often less effective in quiescent than in growing cells. Hydrophobic inhibitors, such as Dynamine or Dyngo, adhere to culture vessel walls or plasma membrane before reaching their target. This results in a lower effective concentration and becomes apparent in quiescent RPE1 cells, which are a confluent monolayer providing a large membrane reservoir inhibitors can unspecifically bind to. Additionally, the available cell surface area for inhibitors to penetrate is smaller than in subconfluent, stretched out cells. It might therefore be worth considering not to use the same dose for both cell states, as was done in this study, but to adjust inhibitor concentrations for quiescent cells. Lastly, integrin uptake was measured by antibody feeding, which bears the risk of inducing endocytosis, particularly CME, by antibody-mediated receptor clustering at the plasma membrane (Liu *et al.*, 2010). Monoclonal antibodies have been widely employed to study integrin endocytosis and trafficking, but using ecto-tagged integrins, allowing for a variety of modifications to assess endocytosis and recycling, would eliminates the risk of endocytosis artefacts (Huet-Calderwood *et al.*, 2017).

## 6.2 Conclusions

Chapter 3 describes hTERT-immortalised RPE1 cells as an *in vitro* model for proliferative quiescence. Although non-specific side effects of hTERT immortalisation cannot be

excluded, RPE1 cells proved a suitable quiescence model for the development and optimisation of cell biological assays. They are advantageous to cancer cell lines, which are continuously proliferating. HTERT-immortalised cell lines, which contain a stable diploid genome and are not transformed, are a suitable quiescence model system to set up and optimise experimental procedures before testing hypotheses in primary cells, which are limited by phenotypic differences between donors as well as changes upon long culturing periods. However, because of the uncertainty whether quiescence in hTERT-immortalised cells truly mimicks that *in vivo*, key findings should be confirmed in primary cells.

In Chapter 4, a comparison of endocytic pathways in growing and quiescent RPE1 cells identified a cargo-dedicated function for CME during quiescence, adapted to the requirements of the quiescent state. While an approach to identify a mechanism regulating CME based on FCHo2 phosphorylation did not lead to conclusive results, this does not mean that such a regulation might not exist. Further proteins arriving at early sites of CME showed differences in phosphorylation, and regulation of CME might be achieved by hierarchical phosphorylation. The cargo-specific activity of CME during quiescence furthermore implies underlying regulation of adaptor proteins, the CME machinery or both. Additionally, CME plays an important role in quiescent RPE1 cells in the uptake of non-typical clathrin cargoes, such as BSA or small molecular weight dextran. The purpose for these upregulated pathways, however, does not appear to serve nutrient supply and remains to be elucidated.

Clathrin-independent pathways such as the CLIC pathway, Cholera Toxin uptake or macropinocytosis were all active during quiescence. Pathways such as FEME or Caveolae endocytosis as well as uptake of further CLIC cargoes were not assessed and remain to be investigated. In summary, multiple endocytic pathways are active in quiescent RPE1 cells, and might be actively regulated to maintain the quiescent state. This is the first time that endocytosis in quiescent cells was directly compared to that in proliferating cells and sheds light on the existing differences and the so far limited knowledge in this field.

Chapter 5 proposes that endocytic pathways including CME, Dynamin- and Endophilin-dependent pathways are required in proliferative quiescence. Due to the limitations of a long-term knockdown protocol and reduced efficiency of pharmacological inhibitors in

quiescent RPE1 cells, it cannot be determined whether these pathways are required for quiescence entry, quiescence maintenance or both. Chapter 5 furthermore suggests a role for integrin recycling in quiescent cells. Integrin recycling and endocytosis in confluent quiescent, and thus not migrating cells are peculiar and might be involved in quiescence signalling, as they were mainly reported to serve (cancer) cell migration or nutrient supply. Manipulations of trafficking pathways during quiescence are still in their early stages, and further investigations and optimisations will be required to directly link integrin trafficking to quiescence signalling.

## 6.3 Future work

This study presented hTERT-immortalised RPE1 cells as a suitable quiescence model. Quiescent cells in the adult human body, however, perform tissue-specific functions in addition to residing in a quiescent state. Testing the relevance of changes in endocytosis and recycling in quiescent RPE1 cells in primary cells will not only validate them in a physiological context, but might eventually lead to a common quiescence signature of endocytic trafficking. The list of endocytic pathways measured in this study was not exhaustive. Further routes, such as FEME, Caveolae or GPI-anchored protein endocytosis remain to be assessed for a complete understanding of endocytosis during quiescence. Furthermore, studying differential regulation of endocytic pathways in two different cell cycle states will contribute to our understanding of their mechanisms. In this study, the effect of FCHo2 phosphorylation on CME activity was tested. The dedicated CME of quiescent cells suggests even more possible regulations of this pathway, ranging from interactions and hierarchical phosphorylation of proteins of the clathrin machinery to the regulation of endocytic adaptor proteins.

Precise and efficient manipulation of endocytic pathways during quiescence poses a challenge when quiescence is induced by contact inhibition and mitogen withdrawal. Higher cell numbers can result in lower efficiency of pharmacological treatments and knockdown efficiency is reduced because proteins are not diluted during cell division. A knockdown protocol targeting cells before they enter quiescence does not allow for conclusions on whether cells were actually able to enter a deep quiescent state. Additionally, cells are deprived of a potentially vital protein for the long period of mitogen withdrawal. Alternative methods for the specific manipulation of trafficking pathways

should be considered in the future. These include transient overexpression of dominant-negative mutants, allowing for shorter manipulation periods of 24 to 48 hours, establishment of cell lines with inducible overexpression of dominant-negative mutants, or an inducible 'knock sideways' approach, which does not rely on protein turnover or cell division to decrease levels of functioning protein (Robinson *et al.*, 2010). Since the latter two approaches are time-consuminig, knockdown screens combined with transient overexpression of dominant-negative mutants and pharmacological inhibition tailored to inhibitory concentrations in quiescent cells might identify target candidates. Establishment of these methods will pave the way for identification of a function of endocytic and recycling pathways in quiescent cells and establish a relationship between ECM composition, integrin signalling and integrin trafficking regulating proliferative quiescence.

Our understanding of how quiescence is maintained is still limited and this study has scratched merely the surface of the complex regulations underlying this cellular state. The work in this study proposes an cell line model to study proliferative quiescence and sheds light on the role of trafficking during this state, which has not yet received enough attention.

# Bibliography


Abelson, H T, Johnson, L F, Penman, S., & Green, H. 1974. Changes in Rna in Relation to Growth of Fibroblast .2. Lifetime of Messenger-Rna, Ribosomal-Rna, and Transfer-Rna in Resting and Growing Cells. *Cell*, **1**(4), 161–165.

Abravanel, Daniel L, Belka, George K, Pan, Tien-chi, Pant, Dhruv K, Collins, Meredith A, Sterner, Christopher J, & Chodosh, Lewis A. 2015. Notch promotes recurrence of dormant tumor cells following HER2/neu-targeted therapy. *The Journal of clinical investigation*, **125**(6), 2484–96.

Acton, S L, Wong, D H, Parham, P, Brodsky, F M, & Jackson, A P. 1993. Alteration of clathrin light chain expression by transfection and gene disruption. *Molecular biology of the cell*, **4**(6), 647–60.

Adams, Ralf H, & Alitalo, Kari. 2007. Molecular regulation of angiogenesis and lymphangiogenesis. *Nature reviews. Molecular cell biology*, **8**(6), 464–78.

Adhikari, Deepak, Zheng, Wenjing, Shen, Yan, Gorre, Nagaraju, Hämäläinen, Tuula, Cooney, Austin J, Huhtaniemi, Ilpo, Lan, Zi-Jian, & Liu, Kui. 2010. Tsc/mTORC1 signaling in oocytes governs the quiescence and activation of primordial follicles. *Human molecular genetics*, **19**(3), 397–410.

Aguet, François, Antonescu, Costin N, Mettlen, Marcel, Schmid, Sandra L, & Danuser, Gaudenz. 2013. Advances in analysis of low signal-to-noise images link dynamin and AP2 to the functions of an endocytic checkpoint. *Developmental cell*, **26**(3), 279–91.

Alanko, Jonna, & Ivaska, Johanna. 2016. Endosomes: Emerging Platforms for Integrin-Mediated FAK Signalling. *Trends in Cell Biology*, **26**(6), 391–398.

Alanko, Jonna, Mai, Anja, Jacquemet, Guillaume, Schauer, Kristine, Kaukonen, Riina, Saari, Markku, Goud, Bruno, & Ivaska, Johanna. 2015. Integrin endosomal signalling suppresses anoikis. *Nature Cell Biology*, **17**(11), 1412–1421.

Alvarez-Cubero, Maria J., Vázquez-Alonso, Fernando, Puche-Sanz, Ignacio, Ortega, F. Gabriel, Martin-Prieto, M., Garcia-Puche, José L., Pascual-Geler, Manrique, Lorente, José A., Cozar-Olmo, José M., & Serrano, Maria J. 2016. Dormant Circulating Tumor Cells in Prostate Cancer: Therapeutic, Clinical and Biological Implications. *Current Drug Targets*, **17**(6), 693–701.

Amyere, Mustapha, Payrastre, Bernard, Krause, Ulrike, Smissen, Patrick Van Der, Veithen, Alex, & Courtoy, Pierre J. 2000. Constitutive Macropinocytosis in Oncogene-transformed Fibroblasts Depends on Sequential Permanent Activation of Phosphoinositide 3-Kinase and Phospholipase C. *Molecular Biology of the Cell*, **11**(10), 3453–3467.

Anderson, R G W, Brown, Michael S, & Goldstein, J L. 1977. Role of the coated endocytic vesicle in the uptake of receptor-bound low density lipoprotein in human fibroblasts. *Cell*, **10**(3), 351–364.

Antonny, Bruno, Burd, Christopher, De Camilli, Pietro, Chen, Elizabeth, Daumke, Oliver, Faelber, Katja, Ford, Marijn, Frolov, Vadim A, Frost, Adam, Hinshaw, Jenny E, Kirchhausen, Tom, Kozlov, Michael M, Lenz, Martin, Low, Harry H, McMahon, Harvey, Merrifield, Christien, Pollard, Thomas D, Robinson, Phillip J, Roux, Aurélien, & Schmid, Sandra. 2016. Membrane fission by dynamin: what we know and what we need to know. *The EMBO Journal*, **35**(21), 2270–2284.

Aponte, Pedro M., & Caicedo, Andrés. 2017. Stemness in cancer: Stem cells, cancer stem cells, and their microenvironment. *Stem Cells International*, **2017**(5619472), 1–17.

Arai, Fumio, Hirao, Atsushi, Ohmura, Masako, Sato, Hidetaka, Matsuoka, Sahoko, Takubo, Keiyo, Ito, Keisuke, Koh, Gou Young, & Suda, Toshio. 2004. Tie2/Angiopoietin-1 Signaling Regulates Hematopoietic Stem Cell Quiescence in the Bone Marrow Niche. *Cell*, **118**(2), 149–161.

Ariotti, Nicholas, Rae, James, Leneva, Natalya, Ferguson, Charles, Loo, Dorothy, Okano, Satomi, Hill, Michelle M, Walser, Piers, Collins, Brett M, & Parton, Robert G. 2015. Molecular characterization of caveolin-induced membrane curvature. *Journal of Biological Chemistry*, **290**(41), 24875–24890.

Arjonen, Antti, Alanko, Jonna, Veltel, Stefan, & Ivaska, Johanna. 2012. Distinct Recycling of Active and Inactive $\beta$1 Integrins. *Traffic*, **13**(4), 610–625.

Arndt-Jovin, D J, & Jovin, T M. 1977. Analysis and sorting of living cells according to deoxyribonucleic acid content. *Journal of Histochemistry and Cytochemistry*, **25**(7), 585–9.

Askari, Janet A, Tynan, Christopher J, Webb, Stephen E.D., Martin-Fernandez, Marisa L, Ballestrem, Christoph, & Humphries, Martin J. 2010. Focal adhesions are sites of integrin extension. *Journal of Cell Biology*, **188**(6), 891–903.

Aspuria, Paul-Joseph, Sato, Tatsuhiro, & Tamanoi, Fuyuhiko. 2007. The TSC/Rheb/TOR signaling pathway in fission yeast and mammalian cells: temperature sensitive and constitutive active mutants of TOR. *Cell Cycle*, **6**(14), 1692–5.

Augustin, Hellmut G, Koh, Gou Young, Thurston, Gavin, & Alitalo, Kari. 2009. Control of vascular morphogenesis and homeostasis through the angiopoietin-Tie system. *Nature Reviews. Molecular Cell Biology*, **10**(March), 165–177.

Aumailley, Monique, Bruckner-Tuderman, Leena, Carter, William G., Deutzmann, Rainer, Edgar, David, Ekblom, Peter, Engel, Jürgen, Engvall, Eva, Hohenester, Erhard, Jones, Jonathan C R, Kleinman, Hynda K., Marinkovich, M. Peter, Martin, George R., Mayer, Ulrike, Meneguzzi, Guerrino, Miner, Jeffrey H., Miyazaki, Kaoru, Patarroyo, Manuel, Paulsson, Mats, Quaranta, Vito, Sanes, Joshua R., Sasaki, Takako, Sekiguchi, Kiyotoshi, Sorokin, Lydia M., Talts, Jan F., Tryggvason, Karl, Uitto,

Jouni, Virtanen, Ismo, Von Der Mark, Klaus, Wewer, Ulla M., Yamada, Yoshihiko, & Yurchenco, Peter D. 2005 (aug). *A simplified laminin nomenclature*.

Avinoam, O., Schorb, M., Beese, C. J., Briggs, J. A. G., & Kaksonen, M. 2015. Endocytic sites mature by continuous bending and remodeling of the clathrin coat. *Science*, **348**(6241), 1369–1372.

Avrov, K O, Aksenov, N D, Melikova, M S, Nikol'skiÄ, N N, & Kornilova, E S. 1999. [Endocytosis of EGF-receptor complexes at various cell cycle stages]. *Tsitologiia*, **41**(12), 1007–13.

Bacia, Kirsten, Schwille, Petra, & Kurzchalia, Teymuras. 2005. Sterol structure determines the separation of phases and the curvature of the liquid-ordered phase in model membranes. *Proceedings of the National Academy of Sciences of the United States of America*, **102**(9), 3272–7.

Bain, Jenny, Plater, Lorna, Elliott, Matt, Shpiro, Natalia, Hastie, C. James, Mclauchlan, Hilary, Klevernic, Iva, Arthur, J. Simon C., Alessi, Dario R., & Cohen, Philip. 2007. The selectivity of protein kinase inhibitors: a further update. *Biochemical Journal*, **408**(3), 297–315.

Baldin, V, Lukas, J, Marcote, M J, Pagano, M, & Draetta, G. 1993. Cyclin D1 is a nuclear protein required for cell cycle progression in G1. *Genes & development*, **7**(5), 812–21.

Barbieri, Elisa, Di Fiore, Pier Paolo, & Sigismund, Sara. 2016. Endocytic control of signaling at the plasma membrane. *Current Opinion in Cell Biology*, **39**(April), 21–27.

Bazinet, C, Katzen, A L, Morgan, M, Mahowald, A P, & Lemmon, S K. 1993. The Drosophila clathrin heavy chain gene: clathrin function is essential in a multicellular organism. *Genetics*, **134**(4), 1119–34.

Bazzoni, G, Shih, D T, Buck, C A, & Hemler, M E. 1995. Monoclonal antibody 9EG7 defines a novel beta 1 integrin epitope induced by soluble ligand and manganese, but inhibited by calcium. *Journal of Biological Chemistry*, **270**(43), 25570–25577.

Beck, K A, & Keen, J H. 1991. Interaction of phosphoinositide cycle intermediates with the plasma membrane-associated clathrin assembly protein AP-2. *The Journal of biological chemistry*, **266**(7), 4442–7.

Benecke, B J, Ben-Ze'ev, A, & Penman, S. 1978. The control of mRNA production, translation and turnover in suspended and reattached anchorage-dependent fibroblasts. *Cell*, **14**(4), 931–9.

Berditchevski, Fedor, Gilbert, Elizabeth, Griffiths, Meryn R, Fitter, Steven, Ashman, Leonie, & Jenner, Sonya J. 2001. Analysis of the CD151·$\alpha$3$\beta$1 Integrin and CD151·Tetraspanin Interactions by Mutagenesis. *Journal of Biological Chemistry*, **276**(44), 41165–41174.

Berger, Dustin R, Ware, Brenton R, Davidson, Matthew D, Allsup, Samuel R, & Khetani, Salman R. 2015. Enhancing the functional maturity of induced pluripotent stem cell-derived human hepatocytes by controlled presentation of cell-cell interactions in vitro. *Hepatology*, **61**(4), 1370–81.

Bergman, Lawrence W. 2001. Growth and Maintenance of Yeast. *Chap. 2, pages 9–14 of:* MacDonald, Paul N. (ed), *Two-Hybrid Systems. Methods in Molecular Biology.*, vol. 177. Totowa, NJ: Humana Press Inc.

Bern, Malin, Sand, Kine Marita Knudsen, Nilsen, Jeannette, Sandlie, Inger, & Andersen, Jan Terje. 2015. The role of albumin receptors in regulation of albumin homeostasis: Implications for drug delivery. *Journal of Controlled Release*, **211**(Aug 10), 144–162.

Bhanot, Haymanti, Young, Ashley M, Overmeyer, Jean H, & Maltese, William A. 2010. Induction of nonapoptotic cell death by activated Ras requires inverse regulation of Rac1 and Arf6. *Molecular Cancer Research*, **8**(10), 1358–74.

Bitsikas, Vassilis, Corrêa, Ivan R, & Nichols, Benjamin J. 2014. Clathrin-independent pathways do not contribute significantly to endocytic flux. *eLife*, **3**(sep), e03970.

Blanpain, Cédric, & Fuchs, Elaine. 2006. Epidermal stem cells of the skin. *Annual review of cell and developmental biology*, **22**(jan), 339–73.

Bodnar, a. G. 1998. Extension of Life-Span by Introduction of Telomerase into Normal Human Cells. *Science*, **279**(5349), 349–352.

Boettner, Douglas R, Friesen, Helena, Andrews, Brenda, & Lemmon, Sandra K. 2011. Clathrin light chain directs endocytosis by influencing the binding of the yeast Hip1R homologue, Sla2, to F-actin. *Molecular Biology of the Cell*, **22**(19), 3699–3714.

Boettner, Douglas R, Chi, Richard J, & Lemmon, Sandra K. 2012. Lessons from yeast for clathrin-mediated endocytosis. *Nature cell biology*, **14**(1), 2–10.

Bonazzi, Matteo, Vasudevan, Lavanya, Mallet, Adeline, Sachse, Martin, Sartori, Anna, Prevost, Marie Christine, Roberts, Allison, Taner, Sabrina B., Wilbur, Jeremy D., Brodsky, Frances M., & Cossart, Pascale. 2011. Clathrin phosphorylation is required for actin recruitment at sites of bacterial adhesion and internalization. *Journal of Cell Biology*, **195**(3), 525–536.

Böttcher, Ralph Thomas, Stremmel, Christopher, Meves, Alexander, Meyer, Hannelore, Widmaier, Moritz, Tseng, Hui Yuan, & Fässler, Reinhard. 2012. Sorting nexin 17 prevents lysosomal degradation of $\beta$1 integrins by binding to the $\beta$ 1-integrin tail. *Nature Cell Biology*, **14**(6), 584–592.

Boucrot, E., Howes, M. T., Kirchhausen, T., & Parton, R. G. 2011. Redistribution of caveolae during mitosis. *Journal of Cell Science*, **124**(12), 1965–1972.

Boucrot, Emmanuel, & Kirchhausen, Tomas. 2007. Endosomal recycling controls plasma membrane area during mitosis. *Proceedings of the National Academy of Sciences of the United States of America*, **104**(19), 7939–44.

Boucrot, Emmanuel, Saffarian, Saveez, Zhang, Rongying, & Kirchhausen, Tomas. 2010. Roles of AP-2 in clathrin-mediated endocytosis. *PLoS ONE*, **5**(5), e10597.

Boucrot, Emmanuel, Ferreira, Antonio P A, Almeida-Souza, Leonardo, Debard, Sylvain, Vallis, Yvonne, Howard, Gillian, Bertot, Laetitia, Sauvonnet, Nathalie, & McMahon, Harvey T. 2015. Endophilin marks and controls a clathrin-independent endocytic pathway. *Nature*, **517**(1), 460–465.

Boulant, Steeve, Kural, Comert, Zeeh, Jean-Christophe, Ubelmann, Florent, & Kirchhausen, Tomas. 2011. Actin dynamics counteract membrane tension during clathrin-mediated endocytosis. *Nature Cell Biology*, **13**(9), 1124–1131.

Bouma, M E, Pessah, M, Renaud, G, Amit, N, Catala, D, & Infante, R. 1988. Synthesis and secretion of lipoproteins by human hepatocytes in culture. *In vitro cellular & developmental biology : journal of the Tissue Culture Association*, **24**(2), 85–90.

Boya, Patricia, González-Polo, Rosa-Ana, Casares, Noelia, Perfettini, Jean-Luc, Dessen, Philippe, Larochette, Nathanael, Métivier, Didier, Meley, Daniel, Souquere, Sylvie, Yoshimori, Tamotsu, Pierron, Gérard, Codogno, Patrice, & Kroemer, Guido. 2005. Inhibition of macroautophagy triggers apoptosis. *Molecular and cellular biology*, **25**(3), 1025–40.

Boyd, Nolan L, Park, Heonyong, Yi, Hong, Boo, Yong Chool, Sorescu, George P, Sykes, Michelle, & Jo, Hanjoong. 2003. Chronic shear induces caveolae formation and alters ERK and Akt responses in endothelial cells. *American journal of physiology. Heart and circulatory physiology*, **285**(3), H1113–22.

Bradford, G B, Williams, B, Rossi, R, & Bertoncello, I. 1997. Quiescence, cycling, and turnover in the primitive hematopoietic stem cell compartment. *Experimental hematology*, **25**(5), 445–53.

Brady, Rebecca J, Damer, Cynthia K, Heuser, John E, & O'Halloran, Theresa J. 2010. Regulation of Hip1r by epsin controls the temporal and spatial coupling of actin filaments to clathrin-coated pits. *Journal of Cell Science*, **123**(21), 3652–3661.

Brand, K. 1985. Glutamine and glucose metabolism during thymocyte proliferation. Pathways of glutamine and glutamate metabolism. *The Biochemical journal*, **228**, 353–361.

Branza-Nichita, Norica, Macovei, Alina, & Lazar, Catalin. 2012. Caveolae-Dependent Endocytosis in Viral Infection. *Pages 1–32 of:* Ceresa, Brian (ed), *Molecular Regulation of Endocytosis*.

Bretou, Marine, Sáez, Pablo J, Sanséau, Doriane, Maurin, Mathieu, Lankar, Danielle, Chabaud, Melanie, Spampanato, Carmine, Malbec, Odile, Barbier, Lucie, Muallem, Shmuel, Maiuri, Paolo, Ballabio, Andrea, Helft, Julie, Piel, Matthieu, Vargas, Pablo, & Lennon-Duménil, Ana-Maria. 2017. Lysosome signaling controls the migration of dendritic cells. *Science Immunology*, **2**(16), eaak9573.

Bretscher, Mark S. 1992. Circulating integrins: $\alpha 5\beta 1$, $\alpha 6\beta 4$ and Mac-1, but not $\alpha 3\beta 1$, $\alpha 4\beta 1$ or LFA-1. *EMBO Journal*, **11**(2), 405–410.

Brett, Tom J., Traub, Linton M., & Fremont, Daved H. 2002. Accessory Protein Recruitment Motifs in Clathrin-Mediated Endocytosis. *Structure*, **10**(6), 797–809.

Briand, Nolwenn, Prado, Cécilia, Mabilleau, Guillaume, Lasnier, FrancÂžoise, Le Lièpvre, Xavier, Covington, Jeffrey D, Ravussin, Eric, Le Lay, Soazig, & Dugail, Isabelle. 2014. Caveolin-1 expression and cavin stability regulate caveolae dynamics in adipocyte lipid store fluctuation. *Diabetes*, **63**(12), 4032–4044.

Bridgewater, R. E., Norman, J. C., & Caswell, P. T. 2012. Integrin trafficking at a glance. *Journal of Cell Science*, **125**(16), 3695–3701.

Brown, M S, & Goldstein, J L. 1975. Regulation of the activity of the low density lipoprotein receptor in human fibroblasts. *Cell*, **6**(3), 307–16.

Bryant, David M, Kerr, Markus C, Hammond, Luke A, Joseph, Shannon R, Mostov, Keith E, Teasdale, Rohan D, & Stow, Jennifer L. 2007. EGF induces macropinocytosis and SNX1-modulated recycling of E-cadherin. *Journal of Cell Science*, **120**(10), 1818–1828.

Bucci, Cecilia, Parton, Robert G, Mather, Ian H, Stunnenberg, Henk, Simons, Kai, Hoflack, Bernard, & Zerial, Marino. 1992. The small GTPase rab5 function as a regulatory factor in the early endocytic pathway. *Cell*, **70**, 715–728.

Buchäckert, Yasmin, Rummel, Sebastian, Vohwinkel, Christine U., Gabrielli, Nieves M., Grzesik, Benno A., Mayer, Konstantin, Herold, Susanne, Morty, Rory E., Seeger, Werner, & Vadász, István. 2012. Megalin mediates transepithelial albumin clearance from the alveolar space of intact rabbit lungs. *Journal of Physiology*, **590**(20), 5167–5181.

Bucher, Delia, Frey, Felix, Sochacki, Kem A., Kummer, Susann, Bergeest, Jan Philip, Godinez, William J., Kräusslich, Hans Georg, Rohr, Karl, Taraska, Justin W., Schwarz, Ulrich S., & Boulant, Steeve. 2018. Clathrin-Adaptor ratio and membrane tension regulate the flat-to-curved transition of the clathrin coat during endocytosis. *Nature Communications*, **9**(1), 1109.

Buckley, Catherine M., & King, Jason S. 2017. Drinking problems: mechanisms of macropinosome formation and maturation. *FEBS Journal*, **284**(22), 3778–3790.

Buyya, Rajkumar, & Pandey, Suraj. 2018. Identification of novel macropinocytosis inhibitors using a rational screen of Food and Drug Administration-approved drugs. *British Journal of Pharmacology*, **275**(8), 3640–3655.

Byron, Adam, Humphries, J. D., Askari, Janet A, Craig, Sue E, Mould, A Paul, & Humphries, Martin J. 2009. Anti-integrin monoclonal antibodies. *Journal of Cell Science*, **122**(22), 4009–4011.

Calderwood, David A, Fujioka, Yosuke, de Pereda, Jose M, Garcia-Alvarez, B., Nakamoto, Tetsuya, Margolis, Ben, McGlade, C Jane, Liddington, Robert C, & Ginsberg, Mark H. 2003. Integrin $\beta$ cytoplasmic domain interactions with phosphotyrosine-binding domains: A structural prototype for diversity in integrin signaling. *Proceedings of the National Academy of Sciences*, **100**(5), 2272–2277.

Calvi, L M, Adams, G B, Weibrecht, K W, Weber, J M, Olson, D P, Knight, M C, Martin, R P, Schipani, E, Divieti, P, Bringhurst, F R, Milner, L A, Kronenberg, H M, & Scadden, D T. 2003. Osteoblastic cells regulate the haematopoietic stem cell niche. *Nature*, **425**(6960), 841–6.

Cambi, Alessandra, Joosten, Ben, Koopman, Marjolein, de Lange, Frank, Beeren, Inge, Torensma, Ruurd, Fransen, Jack A., Garcia-Parajó, Maria, van Leeuwen, Frank N., &

Figdor, Carl G. 2006. Organization of the integrin LFA-1 in nanoclusters regulates its activity. *Molecular biology of the cell*, **17**(10), 4270–81.

Canton, Johnathan, Schlam, Daniel, Breuer, Christian, Gütschow, Michael, Glogauer, Michael, & Grinstein, Sergio. 2016. Calcium-sensing receptors signal constitutive macropinocytosis and facilitate the uptake of NOD2 ligands in macrophages. *Nature Communications*, **7**(apr), 11284.

Cao, Hong, Chen, Jing, Awoniyi, Muyiwa, Henley, John R., & McNiven, Mark A. 2007. Dynamin 2 mediates fluid-phase micropinocytosis in epithelial cells. *Journal of Cell Science*, **120**(23), 4167–4177.

Carmeliet, Peter, & Jain, Rakesh K. 2011. Molecular mechanisms and clinical applications of angiogenesis. *Nature*, **473**(7347), 298–307.

Carpenter, Anne E, Jones, Thouis R, Lamprecht, Michael R, Clarke, Colin, Kang, In, Friman, Ola, Guertin, David A, Chang, Joo, Lindquist, Robert A, Moffat, Jason, Golland, Polina, & Sabatini, David M. 2006. CellProfiler: image analysis software for identifying and quantifying cell phenotypes. *Genome Biology*, **7**(10), R100.

Cascio, S M. 2001. Novel strategies for immortalization of human hepatocytes. *Artificial organs*, **25**(7), 529–38.

Caswell, Patrick T., Spence, Heather J., Parsons, Maddy, White, Dominic P., Clark, Katherine, Cheng, Kwai Wa, Mills, Gordon B., Humphries, Martin J., Messent, Anthea J., Anderson, Kurt I., McCaffrey, Mary W., Ozanne, Bradford W., & Norman, Jim C. 2007. Rab25 Associates with $\alpha 5\beta 1$ Integrin to Promote Invasive Migration in 3D Microenvironments. *Developmental Cell*, **13**(4), 496–510.

Caswell, Patrick T., Vadrevu, Suryakiran, & Norman, Jim C. 2009. Integrins: Masters and slaves of endocytic transport. *Nature Reviews Molecular Cell Biology*, **10**(12), 843–853.

Chakkalakal, Joe V, Jones, Kieran M, Basson, M Albert, & Brack, Andrew S. 2012. The aged niche disrupts muscle stem cell quiescence. *Nature*, **490**(7420), 355–60.

Chakkalakal, Joe V, Christensen, Josef, Xiang, Wanyi, Tierney, Mathew T, Boscolo, Francesca S, Sacco, Alessandra, & Brack, Andrew S. 2014. Early forming label-retaining muscle stem cells require p27kip1 for maintenance of the primitive state. *Development*, **141**(8), 1649–59.

Chan Wah Hak, Laura, Khan, Shaheen, Meglio, Ilaria Di, Law, Ah-Lai, Lucken-Ardjomande Häsler, Safa, Quintaneiro, Leonor M., Ferreira, Antonio P. A., Krause, Matthias, McMahon, Harvey T., & Boucrot, Emmanuel. 2018. FBP17 and CIP4 recruit SHIP2 and lamellipodin to prime the plasma membrane for fast endophilinmediated endocytosis. *Nature Cell Biology*, **20**(9), 1023–1031.

Chang, A C, Salomon, D R, Wadsworth, S, Hong, M J, Mojcik, C F, Otto, S, Shevach, E M, & Coligan, J E. 1995. Alpha 3 beta 1 and alpha 6 beta 1 integrins mediate laminin/merosin binding and function as costimulatory molecules for human thymocyte proliferation. *Journal of immunology*, **154**(2), 500–510.

Chapman-Andresen, Cicily. 1984. The Early Days of Pinocytosis. *Carlsberg Res. Commun*, **49**, 179–186.

Chappie, Joshua S, Mears, Jason A, Fang, Shunming, Leonard, Marilyn, Schmid, Sandra L, Milligan, Ronald A, Hinshaw, Jenny E, & Dyda, Fred. 2011. A pseudoatomic model of the dynamin polymer identifies a hydrolysis-dependent powerstroke. *Cell*, **147**(1), 209–22.

Chen, Chih Ying, & Brodsky, Frances M. 2005. Huntingtin-interacting protein 1 (Hip1) and Hip1-related protein (Hip1R) bind the conserved sequence of clathrin light chains and thereby influence clathrin assembly in vitro and actin distribution in vivo. *Journal of Biological Chemistry*, **280**(7), 6109–6117.

Cheng, T, Rodrigues, N, Shen, H, Yang, Y, Dombkowski, D, Sykes, M, & Scadden, D T. 2000a. Hematopoietic stem cell quiescence maintained by p21cip1/waf1. *Science*, **287**(5459), 1804–8.

Cheng, T, Rodrigues, N, Dombkowski, D, Stier, S, & Scadden, D T. 2000b. Stem cell repopulation efficiency but not pool size is governed by p27(kip1). *Nature medicine*, **6**(11), 1235–40.

Cheng, Zhi-Jie, Singh, Raman Deep, Marks, David L, & Pagano, Richard E. 2006. Membrane microdomains, caveolae, and caveolar endocytosis of sphingolipids. *Molecular membrane biology*, **23**(1), 101–10.

Cheung, Tom H., & Rando, Thomas A. 2013. Molecular regulation of stem cell quiescence. *Nature Reviews Molecular Cell Biology*, **14**(6), 329–340.

Cho, Sohee, & Hwang, Eun Seong. 2012. Status of mTOR activity may phenotypically differentiate senescence and quiescence. *Molecules and Cells*, **33**(6), 597–604.

Clairfeuille, Thomas, Mas, Caroline, Chan, Audrey S.M., Yang, Zhe, Tello-Lafoz, Maria, Chandra, Mintu, Widagdo, Jocelyn, Kerr, Markus C, Paul, Blessy, Mérida, Isabel, Teasdale, Rohan D, Pavlos, Nathan J, Anggono, Victor, & Collins, Brett M. 2016. A molecular code for endosomal recycling of phosphorylated cargos by the SNX27-retromer complex. *Nature Structural and Molecular Biology*, **23**(10), 921–932.

Cocucci, Emanuele, Aguet, François, Boulant, Steeve, & Kirchhausen, Tom. 2012. The first five seconds in the life of a clathrin-coated pit. *Cell*, **150**(3), 495–507.

Coller, Hilary a, Sang, Liyun, & Roberts, James M. 2006. A new description of cellular quiescence. *PLoS biology*, **4**(3), e83.

Collins, Agnieszka, Warrington, Anthony, Taylor, Kenneth A., & Svitkina, Tatyana. 2011. Structural organization of the actin cytoskeleton at sites of clathrin-mediated endocytosis. *Current Biology*, **21**(14), 1167–1175.

Collins, Brett M., McCoy, Airlie J., Kent, Helen M., Evans, Philip R., & Owen, David J. 2002. Molecular Architecture and Functional Model of the Endocytic AP2 Complex. *Cell*, **109**(4), 523–535.

Collins, Richard F, Touret, Nicolas, Kuwata, Hirotaka, Tandon, Narendra N, Grinstein, Sergio, & Trimble, William S. 2009. Uptake of oxidized low density lipoprotein by

CD36 occurs by an actin-dependent pathway distinct from macropinocytosis. *Journal of Biological Chemistry*, **284**(44), 30288–30297.

Commisso, Cosimo, Davidson, Shawn M, Soydaner-Azeloglu, Rengin G, Parker, Seth J, Kamphorst, Jurre J, Hackett, Sean, Grabocka, Elda, Nofal, Michel, Drebin, Jeffrey A, Thompson, Craig B, Rabinowitz, Joshua D, Metallo, Christian M, Vander Heiden, Matthew G, & Bar-Sagi, Dafna. 2013. Macropinocytosis of protein is an amino acid supply route in Ras-transformed cells. *Nature*, **497**(7451), 633–7.

Cong, Xin, Zhang, Y., Li, Jing, Mei, Mei, Ding, Chong, Xiang, R.-L., Zhang, L.-W., Wang, Yun, Wu, L.-L., & Yu, G.-Y. 2015. Claudin-4 is required for modulation of paracellular permeability by muscarinic acetylcholine receptor in epithelial cells. *Journal of Cell Science*, **128**(12), 2271–2286.

Connell-Crowley, L, Harper, J W, & Goodrich, D W. 1997. Cyclin D1/Cdk4 regulates retinoblastoma protein-mediated cell cycle arrest by site-specific phosphorylation. *Molecular biology of the cell*, **8**(2), 287–301.

Conner, Sean D., Schröter, Thomas, & Schmid, Sandra L. 2003. AAK1-mediated $\mu$2 phosphorylation is stimulated by assembled clathrin. *Traffic*, **4**(12), 885–890.

Conti, Francesco J A, Rudling, Robert J, Robson, Alistair, & Hodivala-Dilke, Kairbaan M. 2003. $\alpha 3\beta 1$-Integrin Regulates Hair Follicle But Not Interfollicular Morphogenesis in Adult Epidermis. *Journal of cell science*, **116**(Pt 13), 2737–2747.

Crissman, HA, Darzynkiewicz, Z, Tobey, RA, & Steinkamp, JA. 1985. Correlated measurements of DNA, RNA, and protein in individual cells by flow cytometry. *Science*, **228**(4705), 1321–1324.

Crowther, R A, Finch, J T, & Pearse, B M. 1976. On the structure of coated vesicles. *Journal of molecular biology*, **103**(4), 785–98.

Cruse, Glenn, Beaven, Michael A., Music, Stephen C., Bradding, Peter, Gilfillan, Alasdair M., & Metcalfe, Dean D. 2015. The CD20 homologue MS4A4 directs trafficking of KIT toward clathrin-independent endocytosis pathways and thus regulates receptor signaling and recycling. *Molecular Biology of the Cell*, **26**(9), 1711–1727.

Cupers, P, Jadhav, A P, & Kirchhausen, T. 1998. Assembly of clathrin coats disrupts the association between Eps15 and AP-2 adaptors. *The Journal of biological chemistry*, **273**(4), 1847–50.

Da Silva, Rita Graça, Tavora, Bernardo, Robinson, Stephen D, Reynolds, Louise E., Szekeres, Charles, Lamar, John, Batista, Sílvia, Kostourou, Vassiliki, Germain, Mitchel A, Reynolds, Andrew R, Jones, Dylan T., Watson, Alan R, Jones, Janet L, Harris, Adrian, Hart, Ian R, Iruela-Arispe, M. Luisa, DiPersio, C. Michael, Kreidberg, Jordan A, & Hodivala-Dilke, Kairbaan M. 2010. Endothelial $\alpha 3\beta 1$-integrin represses pathological angiogenesis and sustains endothelial-VEGF. *American Journal of Pathology*, **177**(3), 1534–1548.

Dacks, Joel B, & Robinson, Margaret S. 2017. Outerwear through the ages: evolutionary cell biology of vesicle coats. *Current Opinion in Cell Biology*, **47**(aug), 108–116.

D'Amore, Patricia A. 1992. Mechanisms of Endothelial Growth Control. *American Journal of Respiratory Cell and Molecular Biology*, **6**(1), 1–8.

D'Andrea, V, Guarino, S, Di Matteo, F M, Maugeri Saccà, M, & De Maria, R. 2014. Cancer stem cells in surgery. *Il Giornale di chirurgia*, **35**(11-12), 257–9.

Dangi, Anil, Huang, Chao, Tandon, Ashish, Stolz, Donna, Wu, Tong, & Gandhi, Chandrashekhar R. 2016. Endotoxin-stimulated Rat Hepatic Stellate Cells Induce Autophagy in Hepatocytes as a Survival Mechanism. *Journal of cellular physiology*, **231**(1), 94–105.

Dannhauser, Philip N, Platen, Mitja, Böning, Heike, Ungewickell, Huberta, Schaap, Iwan A T, & Ungewickell, Ernst J. 2015. Effect of clathrin light chains on the stiffness of clathrin lattices and membrane budding. *Traffic (Copenhagen, Denmark)*, **16**(5), 519–33.

Darzynkiewicz, Z, Sharpless, T, Staiano-Coico, L, & Melamed, M R. 1980. Subcompartments of the G1 phase of cell cycle detected by flow cytometry. *Proceedings of the National Academy of Sciences of the United States of America*, **77**(11), 6696–9.

Das, Lipsa, Anderson, Todd A., Gard, Jaime M.C., Sroka, Isis C., Strautman, Stephanie R., Nagle, Raymond B., Morrissey, Colm, Knudsen, Beatrice S., & Cress, Anne E. 2017. Characterization of Laminin Binding Integrin Internalization in Prostate Cancer Cells. *Journal of Cellular Biochemistry*, **118**(5), 1038–1049.

Davies, Peter F., & Ross, Russell. 1980. Growth-mediated, density-dependent inhibition of endocytosis in cultured arterial smooth muscle cells. *Experimental Cell Research*, **129**(2), 329–336.

Day, Charles A., Baetz, Nicholas W., Copeland, Courtney A., Kraft, Lewis J., Han, Bing, Tiwari, Ajit, Drake, Kimberly R., De Luca, Heidi, Chinnapen, Daniel J.-F., Davidson, Michael W., Holmes, Randall K., Jobling, Michael G., Schroer, Trina A., Lencer, Wayne I., & Kenworthy, Anne K. 2015. Microtubule Motors Power Plasma Membrane Tubulation in Clathrin-Independent Endocytosis. *Traffic*, **16**(6), 572–590.

de Beco, Simon, Gueudry, Charles, Amblard, François, & Coscoy, Sylvie. 2009. Endocytosis is required for E-cadherin redistribution at mature adherens junctions. *Proceedings of the National Academy of Sciences*, **106**(17), 7010–7015.

De Franceschi, N., Hamidi, H., Alanko, J., Sahgal, P., & Ivaska, J. 2015. Integrin traffic - the update. *Journal of Cell Science*, **128**(5), 839–852.

De Franceschi, Nicola, Arjonen, Antti, Elkhatib, Nadia, Denessiouk, Konstantin, Wrobel, Antoni G, Wilson, Thomas A, Pouwels, Jeroen, Montagnac, Guillaume, Owen, David J, & Ivaska, Johanna. 2016. Selective integrin endocytosis is driven by interactions between the integrin $\alpha$-chain and AP2. *Nature Structural and Molecular Biology*, **23**(2), 172–179.

De Virgilio, Claudio. 2012. The essence of yeast quiescence. *FEMS microbiology reviews*, **36**(2), 306–39.

Delwel, Gepke O, de Melker, a a, Hogervorst, Frans, Jaspars, Lies H, Fles, D L, Kuikman, Ingrid, Lindblom, Anders, Paulsson, Mats, Timpl, Rupert, & Sonnenberg, Arnoud. 1994. Distinct and overlapping ligand specificities of the alpha 3 beta 1 and alpha 6 beta 1 integrins: recognition of laminin isoforms. *Molecular biology of the cell*, **5**, 203–215.

Diggins, Nicole L, Kang, Hakmook, Weaver, Alissa, & Webb, Donna J. 2018. $\alpha 5\beta 1$ integrin trafficking and Rac activation are regulated by APPL1 in a Rab5-dependent manner to inhibit cell migration. *Journal of Cell Science*, **131**(5), jcs207019.

Dimri, G P, Lee, X, Basile, G, Acosta, M, Scott, G, Roskelley, C, Medrano, E E, Linskens, M, Rubelj, I, & Pereira-Smith, O. 1995. A biomarker that identifies senescent human cells in culture and in aging skin in vivo. *Proceedings of the National Academy of Sciences*, **92**(20), 9363–9367.

DiPersio, C Michael, Hodivala-Dilke, Kairbaan M, Jaenisch, Rudolf, Kreidberg, Jordan A, & Hynes, Richard O. 1997. $\alpha 3\beta 1$ integrin is required for normal development of the epidermal basement membrane. *Journal of Cell Biology*, **137**(3), 729–742.

Disanza, Andrea, Frittoli, Emanuela, Palamidessi, Andrea, & Scita, Giorgio. 2009. Endocytosis and spatial restriction of cell signaling. *Molecular oncology*, **3**(4), 280–96.

Dittman, Jeremy S, & Kaplan, Joshua M. 2006. Factors regulating the abundance and localization of synaptobrevin in the plasma membrane. *Proceedings of the National Academy of Sciences of the United States of America*, **103**(30), 11399–404.

Doherty, Gary J, & McMahon, Harvey T. 2009. Mechanisms of endocytosis. *Annual review of biochemistry*, **78**(jan), 857–902.

Dozynkiewicz, Marta A., Jamieson, Nigel B., MacPherson, Iain, Grindlay, Joan, Vanden-Berghe, Peter V.E., VonThun, Anne, Morton, Jennifer P., Gourley, Charlie, Timpson, Paul, Nixon, Colin, McKay, Colin J., Carter, Ross, Strachan, David, Anderson, Kurt, Sansom, Owen J., Caswell, Patrick T., & Norman, Jim C. 2012. Rab25 and CLIC3 Collaborate to Promote Integrin Recycling from Late Endosomes/Lysosomes and Drive Cancer Progression. *Developmental Cell*, **22**(1), 131–145.

Drake, M T, Downs, M A, & Traub, L M. 2000. Epsin binds to clathrin by associating directly with the clathrin-terminal domain. Evidence for cooperative binding through two discrete sites. *The Journal of biological chemistry*, **275**(9), 6479–89.

Druso, Joseph E, Endo, Makoto, Joy Lin, Miao Chong, Peng, Xu, Antonyak, Marc A, Meller, Stephanie, & Cerione, Richard A. 2016. An essential role for Cdc42 in the functioning of the adult mammary gland. *Journal of Biological Chemistry*, **291**(17), 8886–8895.

Dukes, Joseph D., Fish, Laura, Richardson, Judith D., Blaikley, Elizabeth, Burns, Samir, Caunt, Christopher J., Chalmers, Andrew D., & Whitley, Paul. 2011. Functional ESCRT machinery is required for constitutive recycling of claudin-1 and maintenance of polarity in vertebrate epithelial cells. *Molecular Biology of the Cell*, **22**(17), 3192–3205.

Echarri, Asier, & Del Pozo, Miguel A. 2015. Caveolae - mechanosensitive membrane invaginations linked to actin filaments. *Journal of Cell Science*, **128**(15), 2747–58.

Eddaoudi, Ayad, Canning, Stephanie Louise, & Kato, Itaru. 2018. Flow cytometric detection of g0 in live cells by Hoechst 33342 and Pyronin Y staining. *Pages 49–57 of:* Walker, John M. (ed), *Methods in Molecular Biology*, vol. 1686. New York, N: Humana Press.

Edick, Mathew J., Tesfay, Lia, Lamb, Laura E., Knudsen, Beatrice S., & Miranti, Cindy K. 2007. Inhibition of integrin-mediated crosstalk with epidermal growth factor receptor/Erk or src signaling pathways in autophagic prostate epithelial cells induces caspase-independent death. *Molecular Biology of the Cell*, **18**(7), 2481–2490.

Ehrlich, Marcelo, Boll, Werner, Van Oijen, Antoine, Hariharan, Ramesh, Chandran, Kartik, Nibert, Max L, & Kirchhausen, Tomas. 2004. Endocytosis by random initiation and stabilization of clathrin-coated pits. *Cell*, **118**(5), 591–605.

Elkin, Sarah R., Oswald, Nathaniel W., Reed, Dana K., Mettlen, Marcel, MacMillan, John B., & Schmid, Sandra L. 2016. Ikarugamycin: A Natural Product Inhibitor of Clathrin-Mediated Endocytosis. *Traffic*, **17**(10), 1139–1149.

Engqvist-Goldstein, Åsa E. Y., Zhang, Claire X., Carreno, Sebastien, Barroso, Consuelo, Heuser, John E., & G.Drubin, David. 2004. RNAi-mediated Hip1R Silencing Results in Stable Association between the Endocytic Machinery and the Actin Assembly Machinery. *Molecular Biology of the Cell*, **15**(4), 1666–1679.

Ewers, Helge, Römer, Winfried, Smith, Alicia E., Bacia, Kirsten, Dmitrieff, Serge, Chai, Wengang, Mancini, Roberta, Kartenbeck, Jürgen, Chambon, Valérie, Berland, Ludwig, Oppenheim, Ariella, Schwarzmann, Günter, Feizi, Ten, Schwille, Petra, Sens, Pierre, Helenius, Ari, & Johannes, Ludger. 2010. GM1 structure determines SV40-induced membrane invagination and infection. *Nature Cell Biology*, **12**(1), 11–18.

Fenyvesi, Ferenc, Réti-Nagy, Katalin, Bacsó, Zsolt, Gutay-Tóth, Zsuzsanna, Malanga, Milo, Fenyvesi, Éva, Szente, Lajos, Váradi, Judit, Ujhelyi, Zoltán, Fehér, Pálma, Szabó, Gábor, Vecsernyés, Miklós, & Bácskay, Ildikó. 2014. Fluorescently labeled methyl-beta-cyclodextrin enters intestinal epithelial Caco-2 cells by fluid-phase endocytosis. *PLoS ONE*, **9**(1), e84856.

Ferguson, S S, Downey, W E, Colapietro, A M, Barak, L S, Ménard, L, & Caron, M G. 1996. Role of beta-arrestin in mediating agonist-promoted G protein-coupled receptor internalization. *Science*, **271**(5247), 363–6.

Ferguson, Shawn M, & De Camilli, Pietro. 2012. Dynamin, a membrane-remodelling GTPase. *Nature reviews. Molecular cell biology*, **13**(2), 75–88.

Ferguson, Shawn M, Raimondi, Andrea, Paradise, Summer, Shen, Hongying, Mesaki, Kumi, Ferguson, Agnes, Destaing, Olivier, Ko, Genevieve, Takasaki, Junko, Cremona, Ottavio, O' Toole, Eileen, De Camilli, Pietro, Ferguson, Shawn M, Raimondi, Andrea, Paradise, Summer, Shen, Hongying, Mesaki, Kumi, Ferguson, Agnes, Destaing, Olivier, Ko, Genevieve, Takasaki, Junko, Cremona, Ottavio, O' Toole, Eileen, & De

Camilli, Pietro. 2009. Coordinated Actions of Actin and BAR Proteins Upstream of Dynamin at Endocytic Clathrin-Coated Pits. *Developmental Cell*, **17**(6), 811–822.

Ferreira, Antonio P.A., & Boucrot, Emmanuel. 2018. Mechanisms of Carrier Formation during Clathrin-Independent Endocytosis. *Trends in Cell Biology*, **28**(3), 188–200.

Ferrini, J B, Pichard, L, Domergue, J, & Maurel, P. 1997. Long-term primary cultures of adult human hepatocytes. *Chemico-biological interactions*, **107**(1-2), 31–45.

Fiedler, Ulrike, & Augustin, Hellmut G. 2006. Angiopoietins: a link between angiogenesis and inflammation. *Trends in immunology*, **27**(12), 552–8.

Fiore, Ana Paula Zen Petisco, Spencer, Virginia A., Mori, Hidetoshi, Carvalho, Hernandes F., Bissell, Mina J., & Bruni-Cardoso, Alexandre. 2017. Laminin-111 and the Level of Nuclear Actin Regulate Epithelial Quiescence via Exportin-6. *Cell Reports*, **19**(10), 2102–2115.

Fleming, Heather E, Janzen, Viktor, Lo Celso, Cristina, Guo, Jun, Leahy, Kathleen M, Kronenberg, Henry M, & Scadden, David T. 2008. Wnt signaling in the niche enforces hematopoietic stem cell quiescence and is necessary to preserve self-renewal in vivo. *Cell stem cell*, **2**(3), 274–83.

Fong, John T., Nimlamool, Wutigri, & Falk, Matthias M. 2014. EGF induces efficient Cx43 gap junction endocytosis in mouse embryonic stem cell colonies via phosphorylation of Ser262, Ser279/282, and Ser368. *FEBS Letters*, **588**(5), 836–844.

Ford, M G, Pearse, B M, Higgins, M K, Vallis, Y, Owen, D J, Gibson, A, Hopkins, C R, Evans, P R, & McMahon, H T. 2001. Simultaneous binding of PtdIns(4,5)P2 and clathrin by AP180 in the nucleation of clathrin lattices on membranes. *Science*, **291**(5506), 1051–5.

Ford, Marijn G. J., Mills, Ian G., Peter, Brian J., Vallis, Yvonne, Praefcke, Gerrit J. K., Evans, Philip R., & McMahon, Harvey T. 2002. Curvature of clathrin-coated pits driven by epsin. *Nature*, **419**(6905), 361–366.

Foudi, Adlen, Hochedlinger, Konrad, Van Buren, Denille, Schindler, Jeffrey W, Jaenisch, Rudolf, Carey, Vincent, & Hock, Hanno. 2009. Analysis of histone 2B-GFP retention reveals slowly cycling hematopoietic stem cells. *Nature biotechnology*, **27**(1), 84–90.

Frittoli, Emanuela, Palamidessi, Andrea, Marighetti, Paola, Confalonieri, Stefano, Bianchi, Fabrizio, Malinverno, Chiara, Mazzaro, Giovanni, Viale, Giuseppe, Martin-Padura, Giuseppe, Garré, Massimilliano, Parazzoli, Dario, Mattei, Valentina, Cortellino, Salvatore, Bertalot, Giovanni, Di Fiore, Pier Paolo, & Scita, Giorgio. 2014. A RAB5/RAB4 recycling circuitry induces a proteolytic invasive program and promotes tumor dissemination. *Journal of Cell Biology*, **206**(2), 307–328.

Fujiwara, Hironobu, Kikkawa, Yamato, Sanzen, Noriko, & Sekiguchi, Kiyotoshi. 2001. Purification and Characterization of Human Laminin-8. Laminin-8 stimulates cell adhesion and migration through alpha3beta1 and alpha6beta1 integrins. *Journal of Biological Chemistry*, **276**(20), 17550–17558.

Fukada, So-ichiro, Uezumi, Akiyoshi, Ikemoto, Madoka, Masuda, Satoru, Segawa, Masashi, Tanimura, Naoki, Yamamoto, Hiroshi, Miyagoe-Suzuki, Yuko, & Takeda, Shin'ichi. 2007. Molecular Signature of Quiescent Satellite Cells in Adult Skeletal Muscle. *Stem Cells*, **25**(10), 2448–2459.

Fung, Karen Y., Wang, Changsen, Nyegaard, Steffen, Heit, Bryan, Fairn, Gregory D., & Lee, Warren L. 2017. SR-BI mediated transcytosis of HDL in brain microvascular endothelial cells is independent of caveolin, clathrin, and PDZK1. *Frontiers in Physiology*, **8**(Oct), 841.

Gaengel, Konstantin, Genové, Guillem, Armulik, Annika, & Betsholtz, Christer. 2009. Endothelial-mural cell signaling in vascular development and angiogenesis. *Arteriosclerosis, thrombosis, and vascular biology*, **29**(5), 630–8.

Gaidarov, I, Chen, Q, Falck, J R, Reddy, K K, & Keen, J H. 1996. A functional phosphatidylinositol 3,4,5-trisphosphate/phosphoinositide binding domain in the clathrin adaptor AP-2 alpha subunit. Implications for the endocytic pathway. *The Journal of biological chemistry*, **271**(34), 20922–9.

Gallon, Matthew, & Cullen, Peter J. 2015. Retromer and sorting nexins in endosomal sorting. *Biochemical Society Transactions*, **43**(1), 33–47.

Gallop, Jennifer L, Walrant, Astrid, Cantley, Lewis C, & Kirschner, Marc W. 2013. Phosphoinositides and membrane curvature switch the mode of actin polymerization via selective recruitment of toca-1 and Snx9. *Proceedings of the National Academy of Sciences*, **110**(18), 7193–7198.

Gan, Boyi, & DePinho, Ronald A. 2009. mTORC1 signaling governs hematopoietic stem cell quiescence. *Cell Cycle*, **8**(7), 1003–1006.

García-Pérez, Blanca Estela, Hernández-González, Juan Carlos, García-Nieto, Samuel, & Luna-Herrera, Julieta. 2008. Internalization of a non-pathogenic mycobacteria by macropinocytosis in human alveolar epithelial A549 cells. *Microbial pathogenesis*, **45**(1), 1–6.

Gehne, Nora, Lamik, Agathe, Lehmann, Martin, Haseloff, Reiner F., Andjelkovic, Anuska V., & Blasig, Ingolf E. 2017. Cross-over endocytosis of claudins is mediated by interactions via their extracellular loops. *PLoS ONE*, **12**(8), e0182106.

Geiger, Benjamin, Bershadsky, Alexander, Pankov, Roumen, & Yamada, Kenneth M. 2001. Transmembrane extracellular matrix-cytoskeleton crosstalk. *Nature Reviews Molecular Cell Biology*, **2**(11), 793–805.

Georgiou, Marios, Marinari, Eliana, Burden, Jemima, & Baum, Buzz. 2008. Cdc42, Par6, and aPKC Regulate Arp2/3-Mediated Endocytosis to Control Local Adherens Junction Stability. *Current Biology*, **18**(21), 1631–1638.

Gerdes, J, Schwab, U, Lemke, H, & Stein, H. 1983. Production of a mouse monoclonal antibody reactive with a human nuclear antigen associated with cell proliferation. *International journal of cancer. Journal international du cancer*, **31**(1), 13–20.

Gerdes, J, Li, L, Schlueter, C, Duchrow, M, Wohlenberg, C, Gerlach, C, Stahmer, I, Kloth, S, Brandt, E, & Flad, H D. 1991. Immunobiochemical and molecular biologic characterization of the cell proliferation-associated nuclear antigen that is defined by monoclonal antibody Ki-67. *The American journal of pathology*, **138**(4), 867–73.

Gerhardt, Holger, Golding, Matthew, Fruttiger, Marcus, Ruhrberg, Christiana, Lundkvist, Andrea, Abramsson, Alexandra, Jeltsch, Michael, Mitchell, Christopher, Alitalo, Kari, Shima, David, & Betsholtz, Christer. 2003. VEGF guides angiogenic sprouting utilizing endothelial tip cell filopodia. *The Journal of cell biology*, **161**(6), 1163–77.

Ghossoub, Rania, Lindbæk, Louise, Molla-Herman, Anahi, Schmitt, Alain, Christensen, Søren Tvorup, & Benmerah, Alexandre. 2016. Morphological and Functional Characterization of the Ciliary Pocket by Electron and Fluorescence Microscopy. *Pages 35–51 of:* Satir P., Christensen S. (ed), *Cilia. Methods in Molecular Biology*, vol. 1454. Humana Press, New York, NY.

Gibson, Daniel G, Young, Lei, Chuang, Ray-Yuan, Venter, J Craig, Hutchison, Clyde a, & Smith, Hamilton O. 2009. Enzymatic assembly of DNA molecules up to several hundred kilobases. *Nature methods*, **6**(5), 343–345.

Gingras, Anne Claude, Raught, Brian, Gygi, Steven P, Niedzwiecka, Anna, Miron, Mathieu, Burley, Stephen K, Polakiewicz, Roberto D, Wyslouch-Cieszynska, Aleksandra, Aebersold, Ruedi, & Sonenberg, Nahum. 2001. Hierarchical phosphorylation of the translation inhibitor 4E-BP1. *Genes and Development*, **15**(21), 2852–2864.

Giuliani, Chiara, Troglio, Flavia, Bai, Zhiyong, Patel, Falshruti B., Zucconi, Adriana, Malabarba, Maria Grazia, Disanza, Andrea, Stradal, Theresia B., Cassata, Giuseppe, Confalonieri, Stefano, Hardin, Jeffrey D., Soto, Martha C., Grant, Barth D., & Scita, Giorgio. 2009. Requirements for F-BAR proteins TOCA-1 and TOCA-2 in actin dynamics and membrane trafficking during Caenorhabditis elegans oocyte growth and embryonic epidermal morphogenesis. *PLoS Genetics*, **5**(10), e1000675.

Glynne, R, Ghandour, G, Rayner, J, Mack, D H, & Goodnow, C C. 2000. B-lymphocyte quiescence, tolerance and activation as viewed by global gene expression profiling on microarrays. *Immunological reviews*, **176**(1), 216–46.

Goldstein, J L, Anderson, R G, & Brown, M S. 1979. Coated pits, coated vesicles, and receptor-mediated endocytosis. *Nature*, **279**(5715), 679–85.

Goldstein, J L, Brown, M S, Anderson, R G, Russell, D W, & Schneider, W J. 1985. Receptor-mediated endocytosis: concepts emerging from the LDL receptor system. *Annual review of cell biology*, **1**(jan), 1–39.

Goode, Bruce L, Eskin, Julian A, & Wendland, Beverly. 2014. Actin and endocytosis in budding yeast. *Genetics*, **199**(2), 315–358.

Goodman, Oscar B., Krupnick, Jason G., Santini, Francesca, Gurevich, Vsevolod V., Penn, Raymond B., Gagnon, Alison W., Keen, James H., & Benovic, Jeffrey L. 1996. $\beta$-Arrestin acts as a clathrin adaptor in endocytosis of the $\beta$2-adrenergic receptor. *Nature*, **383**(6599), 447–450.

Gookin, Sara, Min, Mingwei, Phadke, Harsha, Chung, Mingyu, Moser, Justin, Miller, Iain, Carter, Dylan, & Spencer, Sabrina L. 2017. A map of protein dynamics during cell-cycle progression and cell-cycle exit. *PLoS Biology*, **15**(9), e2003268.

Gopalakrishna, Rayudu, Gundimeda, Usha, Zhou, Sarah, Bui, Helena, Davis, Andrew, McNeill, Thomas, & Mack, William. 2018. Laminin-1 induces endocytosis of 67KDa laminin receptor and protects Neuroscreen-1 cells against death induced by serum withdrawal. *Biochemical and Biophysical Research Communications*, **495**(1), 230–237.

Goto, Hidemasa, Inaba, Hironori, & Inagaki, Masaki. 2017. Mechanisms of ciliogenesis suppression in dividing cells. *Cellular and Molecular Life Sciences*, **74**(5), 881–890.

Govaere, Olivier, Wouters, Jasper, Petz, Michaela, Vandewynckel, Yves Paul, Van Den Eynde, Kathleen, Van Den Broeck, Anke, Verhulst, Stefaan, Dollé, Laurent, Gremeaux, Lies, Ceulemans, An, Nevens, Frederik, Van Grunsven, Leo A., Topal, Baki, Vankelecom, Hugo, Giannelli, Gianluigi, Van Vlierberghe, Hans, Mikulits, Wolfgang, Komuta, Mina, & Roskams, Tania. 2016. Laminin-332 sustains chemoresistance and quiescence as part of the human hepatic cancer stem cell niche. *Journal of Hepatology*, **64**(3), 609–617.

Grassart, Alexandre, Cheng, Aaron T, Hong, Sun Hae, Zhang, Fan, Zenzer, Nathan, Feng, Yongmei, Briner, David M, Davis, Gregory D, Malkov, Dmitry, & Drubin, David G. 2014. Actin and dynamin2 dynamics and interplay during clathrin-mediated endocytosis. *Journal of Cell Biology*, **205**(5), 721–735.

Gray, Joseph V, Petsko, Gregory A, Johnston, Gerald C, Ringe, Dagmar, Singer, Richard A, & Werner-washburne, Margaret. 2004. " Sleeping Beauty ": Quiescence in Saccharomyces cerevisiae. *Microbiology and Molecular Biology Reviews*, **68**(2), 187–206.

Greener, T, Zhao, X, Nojima, H, Eisenberg, E, & Greene, L E. 2000. Role of cyclin G-associated kinase in uncoating clathrin-coated vesicles from non-neuronal cells. *The Journal of biological chemistry*, **275**(2), 1365–70.

Grove, Joe, Metcalf, Daniel J, Knight, Alex E, Wavre-Shapton, Silène T, Sun, Tony, Protonotarios, Emmanouil D, Griffin, Lewis D, Lippincott-Schwartz, Jennifer, & Marsh, Mark. 2014. Flat clathrin lattices: stable features of the plasma membrane. *Molecular biology of the cell*, **25**(22), 3581–94.

Gruenberg, Jean, & Van Der Goot, F. Gisou. 2006. Mechanisms of pathogen entry through the endosomal compartments. *Nature Reviews Molecular Cell Biology*, **7**(7), 495–504.

Gu, Changkyu, Yaddanapudi, Suma, Weins, Astrid, Osborn, Teresia, Reiser, Jochen, Pollak, Martin, Hartwig, John, & Sever, Sanja. 2010. Direct dynaming-actin interactions regulate the actin cytoskeleton. *EMBO Journal*, **29**(21), 3593–3606.

Gu, Changkyu, Chang, Joann, Shchedrina, Valentina A., Pham, Vincent A., Hartwig, John H., Suphamungmee, Worawit, Lehman, William, Hyman, Bradley T., Bacskai,

Brian J., & Sever, Sanja. 2014. Regulation of dynamin oligomerization in cells: The role of dynamin-actin interactions and its GTPase activity. *Traffic*, **15**(8), 819–838.

Gu, Zhizhan, Noss, Erika H, Hsu, Victor W, & Brenner, Michael B. 2011. Integrins traffic rapidly via circular dorsal ruffles and macropinocytosis during stimulated cell migration. *Journal of Cell Biology*, **193**(1), 61–70.

Gude, Natalie, Muraski, John, Rubio, Marta, Kajstura, Jan, Schaefer, Erik, Anversa, Piero, & Sussman, Mark A. 2006. Akt promotes increased cardiomyocyte cycling and expansion of the cardiac progenitor cell population. *Circulation Research*, **99**(4), 381–388.

Habermann, Bianca. 2004. The BAR-domain family of proteins: a case of bending and binding? *EMBO reports*, **5**(3), 250–5.

Haffner, C, Di Paolo, G, Rosenthal, J A, & de Camilli, P. 2000. Direct interaction of the 170 kDa isoform of synaptojanin 1 with clathrin and with the clathrin adaptor AP-2. *Current biology*, **10**(8), 471–4.

Hanover, John A, Willingham, Mark C, & Pastan, Ira. 1984. Kinetics of transit of transferrin and epidermal growth factor through clathrin-coated membranes. *Cell*, **39**(Pt 1), 283–293.

Hao, W, Luo, Z, Zheng, L, Prasad, K, & Lafer, E M. 1999. AP180 and AP-2 interact directly in a complex that cooperatively assembles clathrin. *The Journal of biological chemistry*, **274**(32), 22785–94.

Haraga, Andrea, Ohlson, Maikke B, & Miller, Samuel I. 2008. Salmonellae interplay with host cells. *Nature reviews. Microbiology*, **6**(1), 53–66.

Hartwell, L H, Mortimer, R K, Culotti, J, & Culotti, M. 1973. Genetic Control of the Cell Division Cycle in Yeast: V. Genetic Analysis of cdc Mutants. *Genetics*, **74**(2), 267–86.

Hasumi, Keiji, Shinohara, Chikara, Naganumaa, Shin, & Endo, Akira. 1992. Inhibition of the uptake of oxidized low-density lipoprotein in macrophage J774 by the antibiotic ikarugamycin. *European Journal of Biochemistry*, **205**(2), 841–846.

Haucke, Volker, Neher, Erwin, & Sigrist, Stephan J. 2011. Protein scaffolds in the coupling of synaptic exocytosis and endocytosis. *Nature reviews. Neuroscience*, **12**(3), 127–38.

Hayashi, Yukiko K, Matsuda, Chie, Ogawa, Megumu, Goto, Kanako, Tominaga, Kayo, Mitsuhashi, Satomi, Park, Young-eun, Nonaka, Ikuya, Hino-fukuyo, Naomi, & Haginoya, Kazuhiro. 2009. Human PTRF mutations cause secondary deficiency of caveolins resulting in muscular dystrophy with generalized lipodystrophy. *The Journal of Clinical Investigation*, **119**(9), 2623–2633.

He, Kangmin, Marsland, Robert, Upadhyayula, Srigokul, Song, Eli, Dang, Song, Capraro, Benjamin R., Wang, Weiming, Skillern, Wesley, Gaudin, Raphael, Ma, Minghe, & Kirchhausen, Tom. 2017. Dynamics of phosphoinositide conversion in clathrin-mediated endocytic traffic. *Nature*, **552**(7685), 410–414.

Hegde, Manjunath, Jindal, Rohit, Bhushan, Abhinav, Bale, Shyam Sundhar, McCarty, William J, Golberg, Inna, Usta, O Berk, & Yarmush, Martin L. 2014. Dynamic interplay of flow and collagen stabilizes primary hepatocytes culture in a microfluidic platform. *Lab on a chip*, **14**(12), 2033–9.

Henne, William Mike, Kent, Helen M, Ford, Marijn G J, Hegde, Balachandra G, Daumke, Oliver, Butler, P Jonathan G, Mittal, Rohit, Langen, Ralf, Evans, Philip R, & McMahon, Harvey T. 2007. Structure and analysis of FCHo2 F-BAR domain: a dimerizing and membrane recruitment module that effects membrane curvature. *Structure*, **15**(7), 839–52.

Henne, William Mike, Boucrot, Emmanuel, Meinecke, Michael, Evergren, Emma, Vallis, Yvonne, Mittal, Rohit, & McMahon, Harvey T. 2010. FCHo proteins are nucleators of clathrin-mediated endocytosis. *Science*, **328**(5983), 1281–4.

Henry, Kenneth R. 2002. Scd5p and Clathrin Function Are Important for Cortical Actin Organization, Endocytosis, and Localization of Sla2p in Yeast. *Molecular Biology of the Cell*, **13**(8), 2607–2625.

Herbert, Shane P., & Stainier, Didier Y. R. 2011. Molecular control of endothelial cell behaviour during blood vessel morphogenesis. *Nature Reviews Molecular Cell Biology*, **12**(9), 551–564.

Heuser, J. 1980. Three-dimensional visualization of coated vesicle formation in fibroblasts. *The Journal of cell biology*, **84**(3), 560–83.

Heuser, J E, & Reese, T S. 1973. Evidence for recycling of synaptic vesicle membrane during transmitter release at the frog neuromuscular junction. *The Journal of cell biology*, **57**(2), 315–44.

Hewlett, L J, Prescott, A R, & Watts, C. 1994. The coated pit and macropinocytic pathways serve distinct endosome populations. *The Journal of cell biology*, **124**(5), 689–703.

Hill, Michelle M, Bastiani, Michele, Luetterforst, Robert, Kirkham, Matthew, Kirkham, Annika, Nixon, Susan J, Walser, Piers, Abankwa, Daniel, Oorschot, Viola M J, Martin, Sally, Hancock, John F, & Parton, Robert G. 2008. PTRF-Cavin, a conserved cytoplasmic protein required for caveola formation and function. *Cell*, **132**(1), 113–24.

Hinshaw, J E, & Schmid, S L. 1995. Dynamin self-assembles into rings suggesting a mechanism for coated vesicle budding. *Nature*, **374**(6518), 190–2.

Hinze, Claudia, & Boucrot, Emmanuel. 2018. Local actin polymerization during endocytic carrier formation. *Biochemical Society transactions*, **46**(3), 565–576.

Hiromura, K, Pippin, J W, Fero, M L, Roberts, J M, & Shankland, S J. 1999. Modulation of apoptosis by the cyclin-dependent kinase inhibitor p27(Kip1). *The Journal of clinical investigation*, **103**(5), 597–604.

Hirst, Jennifer, Sahlender, Daniela A., Li, Sam, Lubben, Nienke B., Borner, Georg H.H., & Robinson, Margaret S. 2008. Auxilin depletion causes self-assembly of clathrin into membraneless cages In Vivo. *Traffic*, **9**(8), 1354–1371.

Hogan, DA. 2006. Talking to themselves: Autoregulation and quorum sensing in fungi. *Eukaryotic cell*, **5**(4), 613–619.

Hollopeter, Gunther, Lange, Jeffrey J, Zhang, Ying, Vu, Thien N, Gu, Mingyu, Ailion, Michael, Lambie, Eric J, Slaughter, Brian D, Unruh, Jay R, Florens, Laurence, & Jorgensen, Erik M. 2014. The membrane-associated proteins FCHo and SGIP are allosteric activators of the AP2 clathrin adaptor complex. *eLife*, **3**(Oct), e03648.

Holvoet, P. 2006. Analytical Performance and Diagnostic Accuracy of Immunometric Assays for the Measurement of Circulating Oxidized LDL. *Clinical Chemistry*, **52**(4), 760–764.

Honegger, A M, Kris, R M, Ullrich, A, & Schlessinger, J. 1989. Evidence that autophosphorylation of solubilized receptors for epidermal growth factor is mediated by intermolecular cross-phosphorylation. *Proceedings of the National Academy of Sciences of the United States of America*, **86**(3), 925–9.

Honegger, A M, Schmidt, A, Ullrich, A, & Schlessinger, J. 1990. Evidence for epidermal growth factor (EGF)-induced intermolecular autophosphorylation of the EGF receptors in living cells. *Molecular and cellular biology*, **10**(8), 4035–44.

Hongu, Tsunaki, Funakoshi, Yuji, Fukuhara, Shigetomo, Suzuki, Teruhiko, Sakimoto, Susumu, Takakura, Nobuyuki, Ema, Masatsugu, Takahashi, Satoru, Itoh, Susumu, Kato, Mitsuyasu, Hasegawa, Hiroshi, Mochizuki, Naoki, & Kanaho, Yasunori. 2015. Arf6 regulates tumour angiogenesis and growth through HGF-induced endothelial $\beta$1 integrin recycling. *Nature Communications*, **6**(1), 7925.

Horton, Edward R., Byron, Adam, Askari, Janet A., Ng, Daniel H.J., Millon-Frémillon, Angélique, Robertson, Joseph, Koper, Ewa J., Paul, Nikki R., Warwood, Stacey, Knight, David, Humphries, Jonathan D., & Humphries, Martin J. 2015. Definition of a consensus integrin adhesome and its dynamics during adhesion complex assembly and disassembly. *Nature Cell Biology*, **17**(12), 1577–1587.

Howes, Mark T, Kirkham, Matthew, Riches, James, Cortese, Katia, Walser, Piers J, Simpson, Fiona, Hill, Michelle M, Jones, Alun, Lundmark, Richard, Lindsay, Margaret R, Hernandez-Deviez, Delia J, Hadzic, Gordana, McCluskey, Adam, Bashir, Rumasia, Liu, Libin, Pilch, Paul, McMahon, Harvey, Robinson, Phillip J, Hancock, John F, Mayor, Satyajit, & Parton, Robert G. 2010. Clathrin-independent carriers form a high capacity endocytic sorting system at the leading edge of migrating cells. *Journal of Cell Biology*, **190**(4), 675–691.

Hsu, Peggy P., Kang, Seong A., Rameseder, Jonathan, Zhang, Yi, Ottina, Kathleen A., Lim, Daniel, Peterson, Timothy R., Choi, Yongmun, Gray, Nathanael S., Yaffe, Michael B., Marto, Jarrod A., & Sabatini, David M. 2011. The mTOR-regulated phosphoproteome reveals a mechanism of mTORC1-mediated inhibition of growth factor signaling. *Science*, **332**(6035), 1317–1322.

Huang, Fangtian, Khvorova, Anastasia, Marshall, William, & Sorkin, Alexander. 2004. Analysis of clathrin-mediated endocytosis of epidermal growth factor receptor by RNA interference. *The Journal of biological chemistry*, **279**(16), 16657–61.

Huang, Haixia, Bae, Chilman, Sachs, Frederick, & Suchyna, Thomas M. 2013. Caveolae Regulation of Mechanosensitive Channel Function in Myotubes. *PLoS ONE*, **8**(8), e72894.

Huet-Calderwood, Clotilde, Rivera-Molina, Felix, Iwamoto, Daniel V., Kromann, Emil B., Toomre, Derek, & Calderwood, David A. 2017. Novel ecto-tagged integrins reveal their trafficking in live cells. *Nature Communications*, **8**(1), 570.

Hughes, P E, O'Toole, T E, Ylanne, J., Shattil, S J, & Ginsberg, M H. 1995. The conserved membrane-proximal region of an integrin cytoplasmic domain specifies ligand binding affinity. *Journal of Biological Chemistry*, **270**(21), 12411–12417.

Humphries, J. D. 2006. Integrin ligands at a glance. *Journal of Cell Science*, **119**(19), 3901–3903.

Humphries, Jonathan D., Schofield, Neil R, Mostafavi-Pour, Zohreh, Green, Linda J, Garratt, Alistair N, Mould, A Paul, & Humphries, Martin J. 2005. Dual functionality of the anti-$\beta$1 integrin antibody, 12G10, exemplifies agonistic signalling from the ligand binding pocket of integrin adhesion receptors. *Journal of Biological Chemistry*, **280**(11), 10234–10243.

Huotari, Jatta, & Helenius, Ari. 2011. Endosome maturation. *EMBO Journal*, **30**(17), 3481–3500.

Hurst, Robert E, Hauser, Paul J, You, Youngjae, Bailey-Downs, Lora C, Bastian, Anja, Matthews, Stephen M, Thorpe, Jessica, Earle, Christine, Bourguignon, Lilly Y W, & Ihnat, Michael A. 2015. Identification of novel drugs to target dormant micrometastases. *BMC cancer*, **15**(jan), 404.

Hussain, Natasha K., Jenna, Sarah, Glogauer, Michael, Quinn, Christopher C., Wasiak, Sylwia, Guipponi, Michel, Antonarakis, Stylianos E., Kay, Brian K., Stossel, Thomas P., Lamarche-Vane, Nathalie, & McPherson, Peter S. 2001. Endocytic protein intersectin-l regulates actin assembly via Cdc42 and N-WASP. *Nature Cell Biology*, **3**(10), 927–932.

Hüttmann, Andreas, Liu, Shan L, Boyd, Andrew W, & Li, Chung L. 2001. Functional heterogeneity within rhodamine123(lo) Hoechst33342(lo/sp) primitive hemopoietic stem cells revealed by pyronin Y. *Experimental hematology*, **29**(9), 1109–16.

Hynes, Richard O. 2002. Integrins: Bidirectional, allosteric signaling machines. *Cell*, **110**(6), 673–687.

Ikari, Akira, Takiguchi, Ayumi, Atomi, Kosuke, & Sugatani, Junko. 2011. Epidermal growth factor increases clathrin-dependent endocytosis and degradation of claudin-2 protein in MDCK II cells. *Journal of Cellular Physiology*, **226**(9), 2448–2456.

Illinger, Dominique, Italiano, Liliane, Beck, Jean Paul, Waltzinger, Caroline, & Kuhry, Jean Georges. 1993. Comparative evolution of endocytosis levels and of the cell surface area during the L929 cell cycle: a fluorescence study with TMA-DPH. *Biology of the Cell*, **79**(3), 265–268.

Ingber, Donald. 1991. Extracellular matrix and cell shape: Potential control points for inhibition of angiogenesis. *Journal of Cellular Biochemistry*, **47**(3), 236–241.

Ishii, Kana, Sakurai, Hidetoshi, Suzuki, Nobuharu, Mabuchi, Yo, Sekiya, Ichiro, Sekiguchi, Kiyotoshi, & Akazawa, Chihiro. 2018. Recapitulation of Extracellular LAMININ Environment Maintains Stemness of Satellite Cells In Vitro. *Stem Cell Reports*, **10**(2), 568–582.

Itoh, T. 2001. Role of the ENTH Domain in Phosphatidylinositol-4,5-Bisphosphate Binding and Endocytosis. *Science*, **291**(5506), 1047–1051.

Itoh, Toshiki, Erdmann, Kai S, Roux, Aurelien, Habermann, Bianca, Werner, Hauke, & De Camilli, Pietro. 2005. Dynamin and the actin cytoskeleton cooperatively regulate plasma membrane invagination by BAR and F-BAR proteins. *Developmental cell*, **9**(6), 791–804.

Ivanov, Andrei I. 2008. Pharmacological inhibition of endocytic pathways: Is it specific enough to be useful? *Pages 15–33 of:* Ivanov, A.I. (ed), *Exocytosis and Endocytosis. Methods in Molecular Biology*, vol. 440. Humana Press.

Iyer, Vishwanath R, Eisen, Michael B, Ross, Douglas T, Schuler, Greg, Moore, Troy, Lee, Jeffrey C F, Trent, Jeffrey M, Staudt, Louis M, Hudson, James Jr, Boguski, Mark S, Lashkari, Deval, Shalon, Dari, Botstein, David, & Brown, Patrick O. 1999. The Transcriptional Program in the Response of Human Fibroblasts to Serum. *Science*, **283**(Jan), 83–87.

Jain, Rajul K, Hong, David S, Naing, Aung, Wheler, Jennifer, Helgason, Thorunn, Shi, Nai-Yi, Gad, Yash, & Kurzrock, Razelle. 2015. Novel Phase I Study Combining G1 Phase, S Phase, and G2/M Phase Cell Cycle Inhibitors in Patients with Advanced Malignancies. *Cell Cycle*, **14**(21), 3434–40.

Jain, Rakesh K. 2003. Molecular regulation of vessel maturation. *Nature medicine*, **9**(6), 685–93.

Janvier, K., & Bonifacino, Juan S. 2005. Role of the Endocytic Machinery in the Sorting of Lysosome-associated Membrane Proteins. *Molecular Biology of the Cell*, **16**(9), 4231–4242.

Jensen, Kim B, & Watt, Fiona M. 2006. Single-cell expression profiling of human epidermal stem and transit-amplifying cells: Lrig1 is a regulator of stem cell quiescence. *Proceedings of the National Academy of Sciences*, **103**(32), 11958–11963.

Jensen, Kim B, Collins, Charlotte a, Nascimento, Elisabete, Tan, David W, Frye, Michaela, Itami, Satoshi, & Watt, Fiona M. 2009. Lrig1 expression defines a distinct multipotent stem cell population in mammalian epidermis. *Cell stem cell*, **4**(5), 427–39.

Jing, S Q, Spencer, T, Miller, K, Hopkins, C, & Trowbridge, I S. 1990. Role of the human transferrin receptor cytoplasmic domain in endocytosis: localization of a specific signal sequence for internalization. *The Journal of cell biology*, **110**(2), 283–94.

Johannes, Ludger. 2017. Shiga toxin - a model for glycolipid-dependent and lectin-driven endocytosis. *Toxins*, **9**(11), 340.

Johannes, Ludger, Parton, Robert G, Bassereau, Patricia, & Mayor, Satyajit. 2015. Building endocytic pits without clathrin. *Nature reviews. Molecular cell biology*, **16**(5), 311–321.

Johannes, Ludger, Wunder, Christian, & Shafaq-Zadah, Massiullah. 2016. Glycolipids and Lectins in Endocytic Uptake Processes. *Journal of Molecular Biology*, **428**(24), 4792–4818.

Jonker, C. T.H., Galmes, R., Veenendaal, T., Ten Brink, C., Van Der Welle, R. E.N., Liv, N., De Rooij, J., Peden, A. A., Van Der Sluijs, P., Margadant, C., & Klumperman, J. 2018. Vps3 and Vps8 control integrin trafficking from early to recycling endosomes and regulate integrin-dependent functions. *Nature Communications*, **9**(1), 792.

Jost, M, Simpson, F, Kavran, J M, Lemmon, M A, & Schmid, S L. 1998. Phosphatidylinositol-4,5-bisphosphate is required for endocytic coated vesicle formation. *Current biology*, **8**(25), 1399–402.

Kabbani, Abir M., & Kelly, Christopher V. 2017. Nanoscale Membrane Budding Induced by CTxB and Detected via Polarized Localization Microscopy. *Biophysical Journal*, **113**(8), 1795–1806.

Kadlecova, Zuzana, Spielman, Stephanie J, Loerke, Dinah, Mohanakrishnan, Aparna, Reed, Dana Kim, & Schmid, Sandra L. 2016. Regulation of clathrin-mediated endocytosis by hierarchical allosteric activation of AP2. *Journal of Cell Biology*, **216**(1), 167–179.

Kaksonen, Marko, & Roux, Aurelien. 2018. Mechanisms of clathrin-mediated endocytosis. *Nature Reviews Molecular Cell Biology*, **19**(5), 313–326.

Kaksonen, Marko, Sun, Yidi, & Drubin, David G. 2003. A pathway for association of receptors, adaptors, and actin during endocytic internalization. *Cell*, **115**(4), 475–487.

Kaksonen, Marko, Toret, Christopher P., & Drubin, David G. 2005. A modular design for the clathrin- and actin-mediated endocytosis machinery. *Cell*, **123**(2), 305–320.

Kalaidzidis, Inna, Miaczynska, Marta, Brewinska-Olchowik, Marta, Hupalowska, Anna, Ferguson, Charles, Parton, Robert G, Kalaidzidis, Yannis, Zerial, Marino, Brewińska-Olchowik, Marta, Hupalowska, Anna, Ferguson, Charles, Parton, Robert G, Kalaidzidis, Yannis, & Zerial, Marino. 2015. APPL endosomes are not obligatory endocytic intermediates but act as stable cargo-sorting compartments. *Journal of Cell Biology*, **211**(1), 123–144.

Kalthoff, Christoph, Alves, Jürgen, Urbanke, Claus, Knorr, Ruth, & Ungewickell, Ernst J. 2002. Unusual structural organization of the endocytic proteins AP180 and epsin 1. *The Journal of biological chemistry*, **277**(10), 8209–16.

Kanai, Yoshimitsu, Wang, Daliang, & Hirokawa, Nobutaka. 2014. KIF13B enhances the endocytosis of LRP1 by recruiting LRP1 to caveolae. *Journal of Cell Biology*, **204**(3), 395–408.

Kanaseki, T, & Kadota, K. 1969. The "vesicle in a basket". A morphological study of the coated vesicle isolated from the nerve endings of the guinea pig brain, with special reference to the mechanism of membrane movements. *The Journal of cell biology*, **42**(1), 202–20.

Kapuscinski, Jan, & Darzynkiewicz, Zbigniew. 1987. Interctions of pyronin Y(G) with nucleic acids. *Cytometry*, **8**(2), 129–137.

Kato, Masato, Nell, Teresa K., Fearnley, David B., McLellan, Alexander D., Vuckovic, Slavica, & Hart, Derek N.J. 2000. Expression of multilectin receptors and comparative FITC-dextran uptake by human dendritic cells. *International Immunology*, **12**(11), 1511–1519.

Katoh, Masuko, & Katoh, Masaru. 2004. Identification and characterization of human FCHO2 and mouse Fcho2 genes in silico. *International journal of molecular medicine*, **14**(2), 327–31.

Kaur, Satdip, Fielding, Andrew B, Gassner, Gisela, Carter, Nicholas J, & Royle, Stephen J. 2014. An unmet actin requirement explains the mitotic inhibition of clathrin-mediated endocytosis. *eLife*, **3**(feb), e00829.

Kelly, Bernard T., McCoy, Airlie J., Späte, Kira, Miller, Sharon E., Evans, Philip R., Höning, Stefan, & Owen, David J. 2008. A structural explanation for the binding of endocytic dileucine motifs by the AP2 complex. *Nature*, **456**(7224), 976–979.

Kelly, Bernard T., Graham, Stephen C., Liska, Nicole, Dannhauser, Philip N., Höning, Stefan, Ungewickell, Ernst J., & Owen, David J. 2014. Clathrin adaptors. AP2 controls clathrin polymerization with a membrane-activated switch. *Science*, **345**(6195), 459–63.

Kerr, Markus C., Lindsay, Margaret R., Luetterforst, Robert, Hamilton, Nicholas, Simpson, Fiona, Parton, Robert G., Gleeson, Paul A., & Teasdale, Rohan D. 2006. Visualisation of macropinosome maturation by the recruitment of sorting nexins. *Journal of Cell Science*, **119**(Pt 19), 3967–3980.

Keyel, P. A. 2006. A Single Common Portal for Clathrin-mediated Endocytosis of Distinct Cargo Governed by Cargo-selective Adaptors. *Molecular Biology of the Cell*, **17**(10), 4300–4317.

Kirchhausen, T, Nathanson, K L, Matsui, W, Vaisberg, A, Chow, E P, Burne, C, Keen, J H, & Davis, A E. 1989. Structural and functional division into two domains of the large (100- to 115-kDa) chains of the clathrin-associated protein complex AP-2. *Proceedings of the National Academy of Sciences of the United States of America*, **86**(8), 2612–6.

Kirchhausen, Tom. 2009. Imaging endocytic clathrin structures in living cells. *Trends in cell biology*, **19**(11), 596–605.

Kirkham, Matthew, & Parton, Robert G. 2005. Clathrin-independent endocytosis: new insights into caveolae and non-caveolar lipid raft carriers. *Biochimica et biophysica acta*, **1746**(3), 349–63.

Kitagawa, M, Higashi, H, Jung, H K, Suzuki-Takahashi, I, Ikeda, M, Tamai, K, Kato, J, Segawa, K, Yoshida, E, Nishimura, S, & Taya, Y. 1996. The consensus motif for phosphorylation by cyclin D1-Cdk4 is different from that for phosphorylation by cyclin A/E-Cdk2. *The EMBO journal*, **15**(24), 7060–9.

Knezevic, Ivana, Predescu, Dan, Bardita, Cristina, Wang, Minhua, Sharma, Tiffany, Keith, Barbara, Neamu, Radu, Malik, Asrar B, & Predescu, Sanda. 2011. Regulation of dynamin-2 assembly-disassembly and function through the SH3A domain of intersectin-1s. *Journal of cellular and molecular medicine*, **15**(11), 2364–76.

Knudsen, Erik S, & Wang, Jean Y.J. 1996. Differential regulation of retinoblastoma protein function by specific Cdk phosphorylation sites. *Journal of Biological Chemistry*, **271**(14), 8313–8320.

Koivusalo, Mirkka, Welch, Christopher, Hayashi, Hisayoshi, Scott, Cameron C, Kim, Moshe, Alexander, Todd, Touret, Nicolas, Hahn, Klaus M, & Grinstein, Sergio. 2010. Amiloride inhibits macropinocytosis by lowering submembranous pH and preventing Rac1 and Cdc42 signaling. *Journal of Cell Biology*, **188**(4), 547–563.

Koo, Bon Kyoung, Spit, Maureen, Jordens, Ingrid, Low, Teck Y., Stange, Daniel E., Van De Wetering, Marc, Van Es, Johan H., Mohammed, Shabaz, Heck, Albert J. R., Maurice, Madelon M., & Clevers, Hans. 2012. Tumour suppressor RNF43 is a stem-cell E3 ligase that induces endocytosis of Wnt receptors. *Nature*, **488**(7413), 665–669.

Koral, Kelly, & Erkan, Elif. 2012. PKB/Akt partners with Dab2 in albumin endocytosis. *American Journal of Physiology-Renal Physiology*, **302**(8), F1013–F1024.

Kozer, Noga, Barua, Dipak, Henderson, Christine, Nice, Edouard C, Burgess, Antony W, Hlavacek, William S, & Clayton, Andrew H A. 2014. Recruitment of the adaptor protein Grb2 to EGFR tetramers. *Biochemistry*, **53**(16), 2594–604.

Kozera, Lukasz, White, Ed, & Calaghan, Sarah. 2009. Caveolae act as membrane reserves which limit mechanosensitive I(Cl,swell) channel activation during swelling in the rat ventricular myocyte. *PLoS ONE*, **4**(12), e8312.

Kreso, Antonija, & Dick, John E. 2014. Evolution of the cancer stem cell model. *Cell stem cell*, **14**(3), 275–91.

Kübler, E, & Riezman, H. 1993. Actin and fimbrin are required for the internalization step of endocytosis in yeast. *The EMBO journal*, **12**(7), 2855–62.

Kzhyshkowska, Julia, Neyen, Claudine, & Gordon, Siamon. 2012. Role of macrophage scavenger receptors in atherosclerosis. *Immunobiology*, **217**(5), 492–502.

Ladha, M H, Lee, K Y, Upton, T M, Reed, M F, & Ewen, M E. 1998. Regulation of exit from quiescence by p27 and cyclin D1-CDK4. *Molecular and cellular biology*, **18**(11), 6605–15.

Lajoie, Patrick, Kojic, Liliana D., Nim, Satra, Li, Lei, Dennis, James W., & Nabi, Ivan R. 2009. Caveolin-1 regulation of dynamin-dependent, raft-mediated endocytosis of cholera toxin-B sub-unit occurs independently of caveolae. *Journal of Cellular and Molecular Medicine*, **13**(9 B), 3218–3225.

Lakshminarayan, Ramya, Wunder, Christian, Becken, Ulrike, Howes, Mark T., Benzing, Carola, Arumugam, Senthil, Sales, Susanne, Ariotti, Nicholas, Chambon, Valérie, Lamaze, Christophe, Loew, Damarys, Shevchenko, Andrej, Gaus, Katharina, Parton, Robert G., & Johannes, Ludger. 2014. Galectin-3 drives glycosphingolipid-dependent biogenesis of clathrin-independent carriers. *Nature Cell Biology*, **16**(6), 592–603.

Lampe, Paul D, Nguyen, Beth P, Gil, Susana, Usui, Marcia, Olerud, John, Takada, Yoshikazu, & Carter, William G. 1998. Cellular interaction of integrin $\alpha 3 \beta 1$ with laminin 5 promotes gap junctional communication. *Journal of Cell Biology*, **143**(6), 1735–1747.

Lamprecht, Michael R, Sabatini, David M, & Carpenter, Anne E. 2007. CellProfiler: free, versatile software for automated biological image analysis. *BioTechniques*, **42**(1), 71–5.

Laplante, Mathieu, & Sabatini, David M. 2012. MTOR signaling in growth control and disease. *Cell*, **149**(2), 274–293.

Laporte, Damien, Lebaudy, Anne, Sahin, Annelise, Pinson, Benoît, Ceschin, Johanna, Daignan-Fornier, Bertrand, & Sagot, Isabelle. 2011. Metabolic status rather than cell cycle signals control quiescence entry and exit. *Journal of Cell Biology*, **192**(6), 949–957.

Larsen, Maja Thim, Kuhlmann, Matthias, Hvam, Michael Lykke, & Howard, Kenneth A. 2016. Albumin-based drug delivery: harnessing nature to cure disease. *Molecular and Cellular Therapies*, **4**(1), 3.

Lau, Alan W, & Chou, Margaret M. 2008. The adaptor complex AP-2 regulates post-endocytic trafficking through the non-clathrin Arf6-dependent endocytic pathway. *Journal of cell science*, **121**(Pt 24), 4008–4017.

Le Clainche, Christophe, Pauly, Barbara S, Zhang, Claire X, Sa, Å, Engqvist-Goldstein, Ey, Cunningham, Kimberley, & Drubin, David G. 2007. A Hip1R-cortactin complex negatively regulates actin assembly associated with endocytosis. *The EMBO Journal*, **26**, 1199–1210.

Lee, Dong-Won, Wu, Xufeng, Eisenberg, Evan, & Greene, Lois E. 2006. Recruitment dynamics of GAK and auxilin to clathrin-coated pits during endocytosis. *Journal of cell science*, **119**(Pt 17), 3502–12.

Lee, J., Sung, Y H, Cheong, C, Choi, Y S, Jeon, H K, Sun, W, Hahn, W C, Ishikawa, F, & Lee, H. W. 2008. TERT promotes cellular and organismal survival independently of telomerase activity. *Oncogene*, **27**(26), 3754–3760.

Lee, Jessica L, & Streuli, Charles H. 2014. Integrins and epithelial cell polarity. *Journal of Cell Science*, **127**(15), 3217–3225.

Legesse-Miller, Aster, Raitman, Irene, Haley, Erin M., Liao, Albert, Sun, Lova L., Wang, David J., Krishnan, Nithya, Lemons, Johanna M. S., Suh, Eric J., Johnson, Elizabeth L., Lund, Benjamin A., & Coller, Hilary A. 2012. Quiescent fibroblasts are protected from proteasome inhibition-mediated toxicity. *Molecular Biology of the Cell*, **23**(18), 3566–3581.

Leibfried, Andrea, Fricke, Robert, Morgan, Matthew J., Bogdan, Sven, & Bellaiche, Yohanns. 2008. Drosophila Cip4 and WASp Define a Branch of the Cdc42-Par6-aPKC Pathway Regulating E-Cadherin Endocytosis. *Current Biology*, **18**(21), 1639–1648.

Leibundgut, Kurt, Schmitz, Nicole M.R., & Hirt, Andreas. 2005. Catalytic Activities of G 1 Cyclin-Dependent Kinases and Phosphorylation of Retinoblastoma Protein in Mobilized Peripheral Blood CD34 + Hematopoietic Progenitor Cells. *Stem Cells*, **23**(7), 1002–1011.

Lemons, Johanna M S, Feng, Xiao-Jiang, Bennett, Bryson D, Legesse-Miller, Aster, Johnson, Elizabeth L, Raitman, Irene, Pollina, Elizabeth a, Rabitz, Herschel a, Rabinowitz, Joshua D, & Coller, Hilary a. 2010. Quiescent fibroblasts exhibit high metabolic activity. *PLoS biology*, **8**(10), e1000514.

Lewis, WH. 1931. Pinocytosis. *Bulletins of the Johns Hopkins Hospital*, **49**(1-6), 17–27.

Li, June. 2011. Quiescence regulators for hematopoietic stem cell. *Experimental hematology*, **39**(5), 511–20.

Li, Lei, Wan, Tao, Wan, Min, Liu, Bei, Cheng, Ran, & Zhang, Rongying. 2015. The effect of the size of fluorescent dextran on its endocytic pathway. *Cell Biology International*, **39**(5), 531–539.

Liao, Hung-Fu, Chen, Wendy S C, Chen, Yu-Hsiang, Kao, Tzu-Hao, Tseng, Yen-Tzu, Lee, Chien-Yueh, Chiu, Yu-Chiao, Lee, Pei-Lung, Lin, Qian-Jia, Ching, Yung-Hao, Hata, Kenichiro, Cheng, Winston T K, Tsai, Mong-Hsun, Sasaki, Hiroyuki, Ho, Hong-Nerng, Wu, Shinn-Chih, Huang, Yen-Hua, Yen, Pauline, & Lin, Shau-Ping. 2014. DNMT3L promotes quiescence in postnatal spermatogonial progenitor cells. *Development*, **141**(12), 2402–13.

Libera, Jeanette, Pomorski, Thomas, Müller, Peter, & Herrmann, Andreas. 1997. Influence of pH on Phospholipid Redistribution in Human Erythrocyte Membrane. *Blood*, **90**(4), 1684–1693.

Lillie, S H, & Pringle, J R. 1980. Reserve carbohydrate metabolism in Saccharomyces cerevisiae: responses to nutrient limitation. *Journal of bacteriology*, **143**(3), 1384–94.

Lim, Jet Phey, Wang, Jack T H, Kerr, Markus C, Teasdale, Rohan D, & Gleeson, Paul A. 2008. A role for SNX5 in the regulation of macropinocytosis. *BMC cell biology*, **9**(jan), 58.

Lin, Y.-H., Currinn, Heather, Pocha, Shirin Meher, Rothnie, Alice, Wassmer, Thomas, & Knust, Elisabeth. 2015. AP-2-complex-mediated endocytosis of Drosophila Crumbs regulates polarity by antagonizing Stardust. *Journal of Cell Science*, **128**(24), 4538–4549.

Lindberg, Aa, Brown, J E, Strömberg, N, Westling-Ryd, M, Schultz, J E, & Karlsson, K a. 1987. Identification of the carbohydrate receptor for Shiga toxin produced by Shigella dysenteriae type 1. *The Journal of biological Chemistry*, **262**(4), 1779–85.

Lindner, R, & Ungewickell, E. 1991. Light-chain-independent binding of adaptors, AP180, and auxilin to clathrin. *Biochemistry*, **30**(37), 9097–101.

Ling, Ji, Lewis, Jamie, Douglas, Donna, Kneteman, Norman M, & Vance, Dennis E. 2013. Characterization of lipid and lipoprotein metabolism in primary human hepatocytes. *Biochimica et biophysica acta*, **1831**(2), 387–97.

Lipps, Christoph, May, Tobias, Hauser, Hansjörg, & Wirth, Dagmar. 2013. Eternity and functionality - rational access to physiologically relevant cell lines. *Biological chemistry*, **394**(12), 1637–48.

Littlewood, B S. 1975. Methods for selecting auxotrophic and temperature-sensitive mutants in yeasts. *Methods in cell biology*, **11**(jan), 273–85.

Liu, Allen P, Aguet, François, Danuser, Gaudenz, & Schmid, Sandra L. 2010. Local clustering of transferrin receptors promotes clathrin-coated pit initiation. *Journal of Cell Biology*, **191**(7), 1381–1393.

Liu, Li, He, Bo, Liu, Wei M, Zhou, Dongming, Cox, John V, & Zhang, Xin A. 2007. Tetraspanin CD151 promotes cell migration by regulating integrin trafficking. *Journal of Biological Chemistry*, **282**(43), 31631–31642.

Liu, Shu-Hui, Wong, Mei Lie, Craik, Charles S., & Brodsky, Frances M. 1995. Regulation of clathrin assembly and trimerization defined using recombinant triskelion hubs. *Cell*, **83**(2), 257–267.

Liu, Ya-Wen, Mattila, Juha-Pekka, & Schmid, Sandra L. 2013. Dynamin-catalyzed membrane fission requires coordinated GTP hydrolysis. *PloS one*, **8**(1), e55691.

Liu, Zhenzhen, & Roche, Paul A. 2015. Macropinocytosis in phagocytes: regulation of MHC class-II-restricted antigen presentation in dendritic cells. *Frontiers in physiology*, **6**(jan), 1.

Lo, Harriet P, Nixon, Susan J, Hall, Thomas E, Cowling, Belinda S, Ferguson, Charles, Morgan, Garry P, Schieber, Nicole L, Fernandez-Rojo, Manuel A, Bastiani, Michele, Floetenmeyer, Matthias, Martel, Nick, Laporte, Jocelyn, Pilch, Paul F, & Parton, Robert G. 2015. The caveolin-Cavin system plays a conserved and critical role in mechanoprotection of skeletal muscle. *Journal of Cell Biology*, **210**(5), 833–849.

Löber, Günter. 1981. The fluorescence of dye-nucleic acid complexes. *Journal of Luminescence*, **22**(3), 221–265.

Loerke, Dinah, Mettlen, Marcel, Yarar, Defne, Jaqaman, Khuloud, Jaqaman, Henry, Danuser, Gaudenz, & Schmid, Sandra L. 2009. Cargo and Dynamin Regulate Clathrin-Coated Pit Maturation. *PLoS Biology*, **7**(3), e1000057.

López-Ceballos, Pablo, Herrera-Reyes, Alejandra Donají, Coombs, Daniel, & Tanentzapf, Guy. 2016. In vivo regulation of integrin turnover by outside-in activation. *Journal of Cell Science*, **129**(15), 2912–2924.

Lowenstein, E J, Daly, R J, Batzer, A G, Li, W, Margolis, B, Lammers, R, Ullrich, A, Skolnik, E Y, Bar-Sagi, D, & Schlessinger, J. 1992. The SH2 and SH3 domain-containing protein GRB2 links receptor tyrosine kinases to ras signaling. *Cell*, **70**(3), 431–42.

Lucas, María, Gershlick, David C., Vidaurrazaga, Ander, Rojas, Adriana L., Bonifacino, Juan S., & Hierro, Aitor. 2016. Structural Mechanism for Cargo Recognition by the Retromer Complex. *Cell*, **167**(6), 1623–1635.e14.

Lundberg, A S, & Weinberg, R A. 1998. Functional inactivation of the retinoblastoma protein requires sequential modification by at least two distinct cyclin-cdk complexes. *Molecular and cellular biology*, **18**(2), 753–61.

Lundmark, Richard, & Carlsson, Sven R. 2003. Sorting nexin 9 participates in clathrin-mediated endocytosis through interactions with the core components. *The Journal of biological chemistry*, **278**(47), 46772–81.

Lundmark, Richard, & Carlsson, Sven R. 2004. Regulated membrane recruitment of dynamin-2 mediated by sorting nexin 9. *The Journal of biological chemistry*, **279**(41), 42694–702.

Lundmark, Richard, Doherty, Gary J., Howes, Mark T., Cortese, Katia, Vallis, Yvonne, Parton, Robert G., & McMahon, Harvey T. 2008. The GTPase-Activating Protein GRAF1 Regulates the CLIC/GEEC Endocytic Pathway. *Current Biology*, **18**(22), 1802–1808.

Luzio, J Paul, Parkinson, Michael D J, Gray, Sally R, & Bright, Nicholas A. 2009. The delivery of endocytosed cargo to lysosomes. *Biochemical Society transactions*, **37**(Pt 5), 1019–21.

Ma, Li, Umasankar, Perunthottathu K., Wrobel, Antoni G., Lymar, Anastasia, McCoy, Airlie J., Holkar, Sachin S., Jha, Anupma, Pradhan-Sundd, Tirthadipa, Watkins, Simon C., Owen, David J., & Traub, Linton M. 2016. Transient Fcho1/2-Eps15/R-AP-2 Nanoclusters Prime the AP-2 Clathrin Adaptor for Cargo Binding. *Developmental Cell*, **37**(5), 428–443.

Macia, Eric, Ehrlich, Marcelo, Massol, Ramiro, Boucrot, Emmanuel, Brunner, Christian, & Kirchhausen, Tomas. 2006. Dynasore, a cell-permeable inhibitor of dynamin. *Developmental cell*, **10**(6), 839–50.

Mai, Anja, Veltel, Stefan, Pellinen, Teijo, Padzik, Artur, Coffey, Eleanor, Marjomäki, Varpu, & Ivaska, Johanna. 2011. Competitive binding of Rab21 and p120RasGAP to integrins regulates receptor traffic and migration. *Journal of Cell Biology*, **194**(2), 291–306.

Majeed, Sophia R., Vasudevan, Lavanya, Chen, Chih Ying, Luo, Yi, Torres, Jorge A., Evans, Timothy M., Sharkey, Andrew, Foraker, Amy B., Wong, Nicole M.L., Esk, Christopher, Freeman, Theresa A., Moffett, Ashley, Keen, James H., & Brodsky, Frances M. 2014. Clathrin light chains are required for the gyrating-clathrin recycling pathway and thereby promote cell migration. *Nature Communications*, **5**(1), 3891.

Majerska, Jana, Sykorova, Eva, & Fajkus, Jiri. 2011. Non-telomeric activities of telomerase. *Molecular BioSystems*, **7**(4), 1013–1023.

Majoul, Irina, Schmidt, Tobias, Pomasanova, Maria, Boutkevich, Evgenia, Kozlov, Yuri, & Söling, Hans-Dieter. 2002. Differential expression of receptors for Shiga and Cholera toxin is regulated by the cell cycle. *Journal of cell science*, **115**(Pt 4), 817–26.

Malavolta, Marco, Bracci, Massimo, Santarelli, Lory, Sayeed, Md Abu, Pierpaoli, Elisa, Giacconi, Robertina, Costarelli, Laura, Piacenza, Francesco, Basso, Andrea, Cardelli,

Maurizio, & Provinciali, Mauro. 2018. Inducers of Senescence, Toxic Compounds, and Senolytics: The Multiple Faces of Nrf2-Activating Phytochemicals in Cancer Adjuvant Therapy. *Mediators of Inflammation*, **2018**(4159013), 1–32.

Malumbres, Marcos, & Barbacid, Mariano. 2001. To cycle or not to cycle: a critical decision in cancer. *Nature Reviews Cancer*, **1**(3), 222–231.

Mann, Matthias, & Kelleher, Neil L. 2008. Precision proteomics: The case for high resolution and high mass accuracy. *Proceedings of the National Academy of Sciences*, **105**(47), 18132–18138.

Manna, Paul T, Smith, Andrew J, Taneja, Tarvinder K, Howell, Gareth J, Lippiat, Jonathan D, & Sivaprasadarao, Asipu. 2010. Constitutive Endocytic Recycling and Protein Kinase C-mediated Lysosomal Degradation Control K ATP Channel Surface Density. *Journal of Biological Chemistry*, **285**(8), 5963–5973.

Manohar, Asha, Shome, Swati Ghosh, John Lamar, Lee Stirling, Vandana Iyer, Kevin Pumiglia, & DiPersio, C. Michael. 2004. $\alpha 3\beta 1$ integrin promotes keratinocyte cell survival through activation of a MEK/ERK signaling pathway. *Journal of Cell Science*, **117**(18), 4043–4054.

Mao, Y, Chen, J, Maynard, J A, Zhang, B, & Quiocho, F A. 2001. A novel all helix fold of the AP180 amino-terminal domain for phosphoinositide binding and clathrin assembly in synaptic vesicle endocytosis. *Cell*, **104**(3), 433–40.

Margadant, Coert, Raymond, Karine, Kreft, Maaike, Sachs, Norman, Janssen, Hans, & Sonnenberg, Arnoud. 2009. Integrin 3 1 inhibits directional migration and wound re-epithelialization in the skin. *Journal of Cell Science*, **122**(2), 278–288.

Marguerat, Samuel, Schmidt, Alexander, Codlin, Sandra, Chen, Wei, Aebersold, Ruedi, & Bähler, Jürg. 2012. Quantitative analysis of fission yeast transcriptomes and proteomes in proliferating and quiescent cells. *Cell*, **151**(3), 671–683.

Maritzen, Tanja, & Haucke, Volker. 2017. Coupling of exocytosis and endocytosis at the presynaptic active zone. *Neuroscience Research*, **127**(feb), 45–52.

Marrack, P, Mitchell, T, Hildeman, D, Kedl, R, Teague, T K, Bender, J, Rees, W, Schaefer, B C, & Kappler, J. 2000. Genomic-scale analysis of gene expression in resting and activated T cells. *Current opinion in immunology*, **12**(2), 206–9.

Marre, Meghan L, Petnicki-Ocwieja, Tanja, Defrancesco, Alicia S., Darcy, Courtney T, & Hu, Linden T. 2010. Human integrin $\alpha 3\beta 1$ regulates TLR2 recognition of lipopeptides from endosomal compartments. *PLoS ONE*, **5**(9), 1–14.

Marsh, Mark. 1993. Biochemical and Morphological Assays of Virus Entry. *Methods in Enzymology*, **220**(C), 249–261.

Massol, Ramiro H., Larsen, Jakob E., Fujinaga, Yukako, Lencer, Wayne I., & Kirchhausen, Tomas. 2004. Cholera Toxin Toxicity Does Not Require Functional Arf6- and Dynamin-dependent Endocytic Pathways. *Molecular biology of the cell*, **15**(8), 3631–3641.

Massol, Ramiro H, Boll, Werner, Griffin, April M, & Kirchhausen, Tomas. 2006. A burst of auxilin recruitment determines the onset of clathrin-coated vesicle uncoating. *Proceedings of the National Academy of Sciences of the United States of America*, **103**(27), 10265–70.

Matter, Karl, Aijaz, Saima, Tsapara, Anna, & Balda, Maria S. 2005. Mammalian tight junctions in the regulation of epithelial differentiation and proliferation. *Current Opinion in Cell Biology*, **17**(5), 453–458.

Maurer, Meghan E, & Cooper, Jonathan A. 2006. The adaptor protein Dab2 sorts LDL receptors into coated pits independently of AP-2 and ARH. *Journal of cell science*, **119**(Pt 20), 4235–46.

Mazzone, Massimiliano, Dettori, Daniela, Leite de Oliveira, Rodrigo, Loges, Sonja, Schmidt, Thomas, Jonckx, Bart, Tian, Ya-Min, Lanahan, Anthony A, Pollard, Patrick, Ruiz de Almodovar, Carmen, De Smet, Frederik, Vinckier, Stefan, Aragonés, Julián, Debackere, Koen, Luttun, Aernout, Wyns, Sabine, Jordan, Benedicte, Pisacane, Alberto, Gallez, Bernard, Lampugnani, Maria Grazia, Dejana, Elisabetta, Simons, Michael, Ratcliffe, Peter, Maxwell, Patrick, & Carmeliet, Peter. 2009. Heterozygous deficiency of PHD2 restores tumor oxygenation and inhibits metastasis via endothelial normalization. *Cell*, **136**(5), 839–51.

McCluskey, Adam, Daniel, James A., Hadzic, Gordana, Chau, Ngoc, Clayton, Emma L., Mariana, Anna, Whiting, Ainslie, Gorgani, Nick N., Lloyd, Jonathan, Quan, Annie, Moshkanbaryans, Lia, Krishnan, Sai, Perera, Swetha, Chircop, Megan, von Kleist, Lisa, Mcgeachie, Andrew B., Howes, Mark T., Parton, Robert G., Campbell, Michael, Sakoff, Jennette A., Wang, Xuefeng, Sun, Jian Yuan, Robertson, Mark J., Deane, Fiona M., Nguyen, Tam H., Meunier, Frederic A., Cousin, Michael A., & Robinson, Phillip J. 2013. Building a better dynasore: The dyngo compounds potently inhibit dynamin and endocytosis. *Traffic*, **14**(12), 1272–1289.

McGowan, J A, Strain, A J, & Bucher, N L. 1981. DNA synthesis in primary cultures of adult rat hepatocytes in a defined medium: effects of epidermal growth factor, insulin, glucagon, and cyclic-AMP. *Journal of cellular physiology*, **108**(3), 353–63.

McMahon, Harvey T, & Boucrot, Emmanuel. 2011. Molecular mechanism and physiological functions of clathrin-mediated endocytosis. *Nature reviews. Molecular cell biology*, **12**(8), 517–33.

McNally, Kerrie E., Faulkner, Rebecca, Steinberg, Florian, Gallon, Matthew, Ghai, Rajesh, Pim, David, Langton, Paul, Pearson, Neil, Danson, Chris M., Nägele, Heike, Morris, Lindsey L., Singla, Amika, Overlee, Brittany L., Heesom, Kate J., Sessions, Richard, Banks, Lawrence, Collins, Brett M., Berger, Imre, Billadeau, Daniel D., Burstein, Ezra, & Cullen, Peter J. 2017. Retriever is a multiprotein complex for retromer-independent endosomal cargo recycling. *Nature Cell Biology*, **19**(10), 1214–1225.

Meinecke, Michael, Boucrot, Emmanuel, Camdere, Gamze, Hon, Wai-Ching, Mittal, Rohit, & McMahon, Harvey T. 2013. Cooperative recruitment of dynamin and

BIN/amphiphysin/Rvs (BAR) domain-containing proteins leads to GTP-dependent membrane scission. *The Journal of biological chemistry*, **288**(9), 6651–61.

Meredith, J, Takada, Y, Fornaro, M, Languino, L R, & Schwartz, M A. 1995. Inhibition of cell cycle progression by the alternatively spliced integrin beta 1C. *Science*, **269**(5230), 1570–1572.

Merrifield, Christien J., Perrais, David, & Zenisek, David. 2005. Coupling between clathrin-coated-pit invagination, cortactin recruitment, and membrane scission observed in live cells. *Cell*, **121**(4), 593–606.

Messa, Mirko, Fernández-Busnadiego, Rubén, en Sun, Elizabeth W, Chen, Hong, Czapla, Heather, Wrasman, Kristie, Wu, Yumei, Ko, Genevieve, Ross, Theodora, Wendland, Beverly, & De Camilli, Pietro. 2014. Epsin deficiency impairs endocytosis by stalling the actin-dependent invagination of endocytic clathrin-coated pits. *eLife*, **3**, e03311.

Mettlen, Marcel, Chen, Ping-Hung, Srinivasan, Saipraveen, Danuser, Gaudenz, & Schmid, Sandra L. 2018. Regulation of Clathrin-Mediated Endocytosis. *Annual Review of Biochemistry*, **87**, 871–896.

Miele, Adriana E, Watson, Peter J, Evans, Philip R, Traub, Linton M, & Owen, David J. 2004. Two distinct interaction motifs in amphiphysin bind two independent sites on the clathrin terminal domain beta-propeller. *Nature structural & molecular biology*, **11**(3), 242–8.

Mills, Ian G, Praefcke, Gerrit J K, Vallis, Yvonne, Peter, Brian J, Olesen, Lene E, Gallop, Jennifer L, Butler, P Jonathan G, Evans, Philip R, & McMahon, Harvey T. 2003. EpsinR: an AP1/clathrin interacting protein involved in vesicle trafficking. *The Journal of cell biology*, **160**(2), 213–22.

Milosevic, Ira, Giovedi, Silvia, Lou, Xuelin, Raimondi, Andrea, Collesi, Chiara, Shen, Hongying, Paradise, Summer, O'Toole, Eileen, Ferguson, Shawn, Cremona, Ottavio, & De Camilli, Pietro. 2011. Recruitment of endophilin to clathrin-coated pit necks is required for efficient vesicle uncoating after fission. *Neuron*, **72**(4), 587–601.

Mira, Helena, Andreu, Zoraida, Suh, Hoonkyo, Chichung Lie, D., Jessberger, Sebastian, Consiglio, Antonella, Emeterio, Juana San, Hortigüela, Rafael, Marqués-Torrejón, María Ángeles, Nakashima, Kinichi, Colak, Dilek, Götz, Magdalena, Fariñas, Isabel, & Gage, Fred H. 2010. Signaling through BMPR-IA regulates quiescence and long-term activity of neural stem cells in the adult hippocampus. *Cell Stem Cell*, **7**, 78–89.

Mishra, Sanjay K, Hawryluk, Matthew J, Brett, Tom J, Keyel, Peter A, Dupin, Amie L, Jha, Anupma, Heuser, John E, Fremont, Daved H, & Traub, Linton M. 2004. Dual engagement regulation of protein interactions with the AP-2 adaptor $\alpha$ appendage. *Journal of Biological Chemistry*, **279**(44), 46191–46203.

Mitra, Mithun, Ho, Linda D., & Coller, Hilary A. 2018. An In Vitro Model of Cellular Quiescence in Primary Human Dermal Fibroblasts. *Pages 27–47 of:* Walker, John M. (ed), *Methods in Molecular Biology*. New York, N: Humana Press.

Miyashita, Yayoi, & Ozawa, Masayuki. 2007. Increased internalization of p120-uncoupled E-cadherin and a requirement for a dileucine motif in the cytoplasmic domain for endocytosis of the protein. *The Journal of biological chemistry*, **282**(15), 11540–8.

Mohrin, Mary, Bourke, Emer, Alexander, David, Warr, Matthew R, Barry-Holson, Keegan, Le Beau, Michelle M, Morrison, Ciaran G, & Passegué, Emmanuelle. 2010. Hematopoietic stem cell quiescence promotes error-prone DNA repair and mutagenesis. *Cell stem cell*, **7**(2), 174–85.

Molla-Herman, Anahi, Ghossoub, Rania, Blisnick, Thierry, Meunier, Alice, Serres, Catherine, Silbermann, Flora, Emmerson, Chris, Romeo, Kelly, Bourdoncle, Pierre, Schmitt, Alain, Saunier, Sophie, Spassky, Nathalie, Bastin, Philippe, & Benmerah, Alexandre. 2010. The ciliary pocket: an endocytic membrane domain at the base of primary and motile cilia. *Journal of Cell Science*, **123**(10), 1785–1795.

Montgomery, Robert K, Carlone, Diana L, Richmond, Camilla A, Farilla, Loredana, Kranendonk, Mariette E G, Henderson, Daniel E, Baffour-Awuah, Nana Yaa, Ambruzs, Dana M, Fogli, Laura K, Algra, Selma, & Breault, David T. 2011. Mouse telomerase reverse transcriptase (mTert) expression marks slowly cycling intestinal stem cells. *Proceedings of the National Academy of Sciences*, **108**(1), 179–184.

Mooren, Olivia L, Kotova, Tatyana I, Moore, Andrew J, & Schafer, Dorothy A. 2009. Dynamin2 GTPase and cortactin remodel actin filaments. *Journal of Biological Chemistry*, **284**(36), 23995–24005.

Moreno-Layseca, Paulina, & Streuli, Charles H. 2014. Signalling pathways linking integrins with cell cycle progression. *Matrix Biology*, **34**(feb), 144–153.

Morgner, Jessica, Ghatak, Sushmita, Jakobi, Tobias, Dieterich, Christoph, Aumailley, Monique, & Wickström, Sara A. 2015. Integrin-linked kinase regulates the niche of quiescent epidermal stem cells. *Nature Communications*, **6**(1), 8198.

Morris, S A, Mann, A, & Ungewickell, E. 1990. Analysis of 100-180-kDa phosphoproteins in clathrin-coated vesicles from bovine brain. *The Journal of biological chemistry*, **265**(6), 3354–7.

Motley, Alison, Bright, Nicholas A, Seaman, Matthew N.J. J, & Robinson, Margaret S. 2003. Clathrin-mediated endocytosis in AP-2-depleted cells. *Journal of Cell Biology*, **162**(5), 909–18.

Motley, Alison M., Berg, Nicola, Taylor, Marcus J., Sahlender, Daniela A., Hirst, Jennifer, Owen, David J., & Robinson, Margaret S. 2006. Functional Analysis of AP-2 $\alpha$ and $\mu$2 Subunits. *Molecular Biology of the Cell*, **17**(12), 5298–5308.

Mukadam, Aamir S., & Seaman, Matthew N.J. 2015. Retromer-mediated endosomal protein sorting: The role of unstructured domains. *FEBS Letters*, **589**(19), 2620–2626.

Mulkearns, E. E., & Cooper, J. A. 2012. FCH domain only-2 organizes clathrin-coated structures and interacts with Disabled-2 for low-density lipoprotein receptor endocytosis. *Molecular Biology of the Cell*, **23**(7), 1330–1342.

Mull, Jesse L, & Asakura, Atsushi. 2012. A New Look at an Immortal DNA Hypothesis for Stem Cell Self-Renewal. *Journal of stem cell research & therapy*, **2**(1), e105.

Multhaupt, Hinke A.B., Leitinger, Birgit, Gullberg, Donald, & Couchman, John R. 2016. Extracellular matrix component signaling in cancer. *Advanced Drug Delivery Reviews*, **97**(feb), 28–40.

Muranen, Taru, Iwanicki, Marcin P., Curry, Natasha L., Hwang, Julie, DuBois, Cory D., Coloff, Jonathan L., Hitchcock, Daniel S., Clish, Clary B., Brugge, Joan S., & Kalaany, Nada Y. 2017. Starved epithelial cells uptake extracellular matrix for survival. *Nature Communications*, **8**(jan), 13989.

Murata, M, Peränen, J, Schreiner, R, Wieland, F, Kurzchalia, T V, & Simons, K. 1995. VIP21/caveolin is a cholesterol-binding protein. *Proceedings of the National Academy of Sciences of the United States of America*, **92**(22), 10339–43.

Murphy, J E, & Keen, J H. 1992. Recognition sites for clathrin-associated proteins AP-2 and AP-3 on clathrin triskelia. *The Journal of biological chemistry*, **267**(15), 10850–5.

Murphy, Jane E, Vohra, Ravinder S, Dunn, Sarah, Holloway, Zoe G, Monaco, Anthony P, Homer-Vanniasinkam, Shervanthi, Walker, John H, & Ponnambalam, Sreenivasan. 2008. Oxidised LDL internalisation by the LOX-1 scavenger receptor is dependent on a novel cytoplasmic motif and is regulated by dynamin-2. *Journal of Cell Science*, **121**(13), 2136–2147.

Naci, Dalila, & Aoudjit, Fawzi. 2014. Alpha2beta1 integrin promotes T cell survival and migration through the concomitant activation of ERK/Mcl-1 and p38 MAPK pathways. *Cellular Signalling*, **26**(9), 2008–2015.

Nader, Guilherme P.F., Ezratty, Ellen J., & Gundersen, Gregg G. 2016. FAK, talin and PIPKI 3 regulate endocytosed integrin activation to polarize focal adhesion assembly. *Nature Cell Biology*, **18**(5), 491–503.

Nagai, J, Christensen, E I, Morris, S M, Willnow, T E, Cooper, J A, & Nielsen, R. 2005. Mutually dependent localization of megalin and Dab2 in the renal proximal tubule. *American journal of physiology. Renal physiology*, **289**(3), F569–76.

Nagy, Péter, Kovács, Laura, Sándor, Gyöngyvér O, & Juhász, Gábor. 2016. Stem-cell-specific endocytic degradation defects lead to intestinal dysplasia in Drosophila. *Disease Models & Mechanisms*, **9**(5), 501–512.

Nakada, M, Nambu, E, Furuyama, N, Yoshida, Y, Takino, T, Hayashi, Y, Sato, H, Sai, Y, Tsuji, T, Miyamoto, K. I., Hirao, A, & Hamada, J. I. 2013. Integrin $\alpha$3 is overexpressed in glioma stem-like cells and promotes invasion. *British Journal of Cancer*, **108**(12), 2516–2524.

Nakamura, Katsuyuki, Yamanouchi, Keitaro, & Nishihara, Masugi. 2014. Secreted protein acidic and rich in cysteine internalization and its age-related alterations in skeletal muscle progenitor cells. *Aging Cell*, **13**(1), 175–184.

Nakamura, T, Nawa, K, & Ichihara, A. 1984. Partial purification and characterization of hepatocyte growth factor from serum of hepatectomized rats. *Biochemical and biophysical research communications*, **122**(3), 1450–9.

Nakamura, T, Nishizawa, T, Hagiya, M, Seki, T, Shimonishi, M, Sugimura, A, Tashiro, K, & Shimizu, S. 1989. Molecular cloning and expression of human hepatocyte growth factor. *Nature*, **342**(6248), 440–3.

Nakase, Ikuhiko, Kobayashi, Nahoko Bailey, Takatani-Nakase, Tomoka, & Yoshida, Tetsuhiko. 2015. Active macropinocytosis induction by stimulation of epidermal growth factor receptor and oncogenic Ras expression potentiates cellular uptake efficacy of exosomes. *Scientific Reports*, **5**(1), 10300.

Nakayama, Masanori, Nakayama, Akiko, Van Lessen, Max, Yamamoto, Hiroyuki, Hoffmann, Sarah, Drexler, Hannes C.A., Itoh, Norimichi, Hirose, Tomonori, Breier, Georg, Vestweber, Dietmar, Cooper, Jonathan A., Ohno, Shigeo, Kaibuchi, Kozo, & Adams, Ralf H. 2013. Spatial regulation of VEGF receptor endocytosis in angiogenesis. *Nature Cell Biology*, **15**(3), 249–260.

Nanes, Benjamin A, Chiasson-MacKenzie, Christine, Lowery, Anthony M, Ishiyama, Noboru, Faundez, Victor, Ikura, Mitsuhiko, Vincent, Peter A, & Kowalczyk, Andrew P. 2012. p120-catenin binding masks an endocytic signal conserved in classical cadherins. *Journal of Cell Biology*, **199**(2), 365–380.

Naslavsky, Naava, & Caplan, Steve. 2018. The enigmatic endosome - sorting the ins and outs of endocytic trafficking. *Journal of Cell Science*, **131**(13), jcs216499.

Nassoy, Pierre, & Lamaze, Christophe. 2012. Stressing caveolae new role in cell mechanics. *Trends in cell biology*, **22**(7), 381–9.

Nazarenko, Irina, Rana, Sanyukta, Baumann, Alexandra, McAlear, Jessica, Hellwig, Andrea, Trendelenburg, Michael, Lochnit, Günter, Preissner, Klaus T, & Zöller, Margot. 2010. Cell surface tetraspanin Tspan8 contributes to molecular pathways of exosome-induced endothelial cell activation. *Cancer Research*, **70**(4), 1668–1678.

Nemetschke, Linda, & Knust, Elisabeth. 2016. Drosophila Crumbs prevents ectopic Notch activation in developing wings by inhibiting ligand-independent endocytosis. *Development*, **143**(23), 4543–4553.

Nesterov, A, Carter, R E, Sorkina, T, Gill, G N, & Sorkin, A. 1999. Inhibition of the receptor-binding function of clathrin adaptor protein AP-2 by dominant-negative mutant mu2 subunit and its effects on endocytosis. *The EMBO journal*, **18**(9), 2489–99.

Neumann, Sylvia, & Schmid, Sandra L. 2013. Dual role of BAR domain-containing proteins in regulating vesicle release catalyzed by the GTPase, dynamin-2. *The Journal of biological chemistry*, **288**(35), 25119–28.

Neurauter, Christine Gran, Luna, Luisa, & Bjørås, Magnar. 2012. Release from quiescence stimulates the expression of human NEIL3 under the control of the Ras dependent ERK-MAP kinase pathway. *DNA repair*, **11**(4), 401–9.

Newmyer, Sherri L, Christensen, Arne, & Sever, Sanja. 2003. Auxilin-Dynamin Interactions Link the Uncoating ATPase Chaperone Machinery with Vesicle Formation. *Developmental Cell*, **4**(6), 929–940.

Nguyen, Beth P, Ryan, Maureen C, Gil, Susana G, & Carter, William G. 2000. Deposition of laminin 5 in epidermal wounds regulates integrin signaling and adhesion. *Current Opinion in Cell Biology*, **12**(5), 554–562.

Nguyen, Phong Dang, Gurevich, David Baruch, Sonntag, Carmen, Hersey, Lucy, Alaei, Sara, Nim, Hieu Tri, Siegel, Ashley, Hall, Thomas Edward, Rossello, Fernando Jaime, Boyd, Sarah Elizabeth, Polo, Jose Maria, & Currie, Peter David. 2017. Muscle Stem Cells Undergo Extensive Clonal Drift during Tissue Growth via Meox1-Mediated Induction of G2 Cell-Cycle Arrest. *Cell Stem Cell*, **21**(1), 107–119.e6.

Nicolaou, Nayia, Margadant, Coert, Kevelam, Sietske H, Lilien, Marc R, Oosterveld, Michiel J.S. S, Kreft, Maaike, van Eerde, Albertien M., Pfundt, Rolph, Terhal, Paulien A, van der Zwaag, Bert, Nikkels, Peter G.J. J, Sachs, Norman, Goldschmeding, Roel, Knoers, Nine V.A.M. A M, Renkema, Kirsten Y, & Sonnenberg, Arnoud. 2012. Gain of glycosylation in integrin $\alpha$3 causes lung disease and nephrotic syndrome. *Journal of Clinical Investigation*, **122**(12), 4375–4387.

Nieland, Thomas J.F., Ehrlich, Marcelo, Krieger, Monty, & Kirchhausen, Tomas. 2005. Endocytosis is not required for the selective lipid uptake mediated by murine SR-BI. *Biochimica et Biophysica Acta*, **1734**(1), 44–51.

Nimlamool, Wutigri, Andrews, Rachael M. Kells, & Falk, Matthias M. 2015. Connexin43 phosphorylation by PKC and MAPK signals VEGF-mediated gap junction internalization. *Molecular Biology of the Cell*, **26**(15), 2755–2768.

Nishimura, Takashi, & Kaibuchi, Kozo. 2007. Numb Controls Integrin Endocytosis for Directional Cell Migration with aPKC and PAR-3. *Developmental Cell*, **13**(1), 15–28.

Nishiuchi, Ryoko, Takagi, Junichi, Hayashi, Maria, Ido, Hiroyuki, Yagi, Yoshiko, Sanzen, Noriko, Tsuji, Tsutomu, Yamada, Masashi, & Sekiguchi, Kiyotoshi. 2006. Ligand-binding specificities of laminin-binding integrins: A comprehensive survey of laminin-integrin interactions using recombinant $\alpha$3$\beta$1, $\alpha$6$\beta$1, $\alpha$7$\beta$1 and $\alpha$6$\beta$4 integrins. *Matrix Biology*, **25**(3), 189–197.

Nonet, M L, Holgado, A M, Brewer, F, Serpe, C J, Norbeck, B A, Holleran, J, Wei, L, Hartwieg, E, Jorgensen, E M, & Alfonso, A. 1999. UNC-11, a Caenorhabditis elegans AP180 homologue, regulates the size and protein composition of synaptic vesicles. *Molecular biology of the cell*, **10**(7), 2343–60.

Norbury, Christopher C. 2006. Drinking a lot is good for dendritic cells. *Immunology*, **117**(4), 443–51.

Nourse, J, Firpo, E, Flanagan, W M, Coats, S, Polyak, K, Lee, M H, Massague, J, Crabtree, G R, & Roberts, J M. 1994. Interleukin-2-mediated elimination of the p27Kip1 cyclin-dependent kinase inhibitor prevented by rapamycin. *Nature*, **372**(6506), 570–3.

Novokhatska, Olga, Dergai, Mykola, Houssin, Nathalie, Tsyba, Liudmyla, Moreau, Jacques, & Rynditch, Alla. 2011. Intersectin 2 nucleotide exchange factor regulates Cdc42 activity during Xenopus early development. *Biochemical and Biophysical Research Communications*, **408**(4), 663–668.

Nunez, Daniel, Antonescu, Costin, Mettlen, Marcel, Liu, Allen, Schmid, Sandra L., Loerke, Dinah, & Danuser, Gaudenz. 2011. Hotspots Organize Clathrin-Mediated Endocytosis by Efficient Recruitment and Retention of Nucleating Resources. *Traffic*, **12**(12), 1868–1878.

Nurse, P. 1975. Genetic control of cell size at cell division in yeast. *Nature*, **256**(5518), 547–51.

Obermüller, Stefanie, Kiecke, Christina, von Figura, Kurt, & Höning, Stefan. 2002. The tyrosine motifs of Lamp 1 and LAP determine their direct and indirect targetting to lysosomes. *Journal of cell science*, **115**(Pt 1), 185–94.

Oesterle, Elizabeth C, Chien, Wei-Ming, Campbell, Sean, Nellimarla, Praveena, & Fero, Matthew L. 2011. p27(Kip1) is required to maintain proliferative quiescence in the adult cochlea and pituitary. *Cell cycle*, **10**(8), 1237–48.

Oh, Ju Eun, Jang, Da Hyun, Kim, Hyunsoo, Kang, Hyun Ki, Chung, Chong Pyoung, Park, Won Ho, & Min, Byung Moo. 2009. $\alpha 3\beta 1$ integrin promotes cell survival via multiple interactions between 14-3-3 isoforms and proapoptotic proteins. *Experimental Cell Research*, **315**(18), 3187–3200.

Ohno, H, Stewart, J, Fournier, M C, Bosshart, H, Rhee, I, Miyatake, S, Saito, T, Gallusser, A, Kirchhausen, T, & Bonifacino, J S. 1995. Interaction of tyrosine-based sorting signals with clathrin-associated proteins. *Science*, **269**(5232), 1872–5.

Oka, Kiyomasa, Ohya-Shimada, Wakana, Mizuno, Shinya, & Nakamura, Toshikazu. 2013. Up-regulation of cyclin-E1 via proline-mTOR pathway is responsible for HGF-mediated G1/S progression in the primary culture of rat hepatocytes. *Biochemical and Biophysical Research Communications*, **435**(1), 120–125.

Olusanya, Oyinkan, Andrews, Paul D., Swedlow, Jason R., & Smythe, Elizabeth. 2001. Phosphorylation of threonine 156 of the $\mu 2$ subunit of the AP2 complex is essential for endocytosis in vitro and in vivo. *Current Biology*, **11**(11), 896–900.

Onodera, Jun, & Ohsumi, Yoshinori. 2005. Autophagy is required for maintenance of amino acid levels and protein synthesis under nitrogen starvation. *Journal of Biological Chemistry*, **280**(36), 31582–31586.

Orford, Keith W., & Scadden, David T. 2008. Deconstructing stem cell self-renewal: genetic insights into cell-cycle regulation. *Nature Reviews Genetics*, **9**(2), 115–128.

Osborn, Michael J, & Miller, J Ross. 2007. Rescuing yeast mutants with human genes. *Briefings in functional genomics & proteomics*, **6**(2), 104–11.

Oshiro, Noriko, Takahashi, Rinako, Yoshino, Ken Ichi, Tanimura, Keiko, Nakashima, Akio, Eguchi, Satoshi, Miyamoto, Takafumi, Hara, Kenta, Takehana, Kenji, Avruch, Joseph, Kikkawa, Ushio, & Yonezawa, Kazuyoshi. 2007. The proline-rich Akt substrate of 40 kDa (PRAS40) is a physiological substrate of mammalian target of rapamycin complex 1. *Journal of Biological Chemistry*, **282**(28), 20329–20339.

Otsuki, L, & Brand, A H. 2018. Cell cycle heterogeneity directs the timing of neural stem cell activation from quiescence. *Science*, **360**(6384), 99–102.

Ottewell, Penelope D, Wang, Ning, Brown, Hannah K, Fowles, C Anne, Croucher, Peter I, Eaton, Colby L, & Holen, Ingunn. 2015. OPG-Fc inhibits ovariectomy-induced growth of disseminated breast cancer cells in bone. *International journal of cancer*, **137**(4), 968–77.

Overmeyer, Jean H, Kaul, Aparna, Johnson, Erin E, & Maltese, William A. 2008. Active ras triggers death in glioblastoma cells through hyperstimulation of macropinocytosis. *Molecular cancer research*, **6**(6), 965–77.

Overmeyer, Jean H, Young, Ashley M, Bhanot, Haymanti, & Maltese, William A. 2011. A chalcone-related small molecule that induces methuosis, a novel form of non-apoptotic cell death, in glioblastoma cells. *Molecular cancer*, **10**(jan), 69.

Owen, D J, & Evans, P R. 1998. A structural explanation for the recognition of tyrosine-based endocytotic signals. *Science*, **282**(5392), 1327–32.

Owen, D J, Vallis, Y, Pearse, B M, McMahon, H T, & Evans, P R. 2000. The structure and function of the beta 2-adaptin appendage domain. *The EMBO journal*, **19**(16), 4216–27.

Owen, David J., Vallis, Yvonne, Noble, Martin E.M., Hunter, Jack B., Dafforn, Tim R., Evans, Philip R., & McMahon, Harvey T. 1999. A Structural Explanation for the Binding of Multiple Ligands by the $\alpha$-Adaptin Appendage Domain. *Cell*, **97**(6), 805–815.

Palacios, Felipe, Schweitzer, Jill K., Boshans, Rita L., & D'Souza-Schorey, Crislyn. 2002. ARF6-GTP recruits Nm23-H1 to facilitate dynamin-mediated endocytosis during adherens junctions disassembly. *Nature Cell Biology*, **4**(12), 929–936.

Pallafacchina, Giorgia, François, Stéphanie, Regnault, Béatrice, Czarny, Bertrand, Dive, Vincent, Cumano, Ana, Montarras, Didier, & Buckingham, Margaret. 2010. An adult tissue-specific stem cell in its niche: a gene profiling analysis of in vivo quiescent and activated muscle satellite cells. *Stem cell research*, **4**(2), 77–91.

Palm, Wilhelm, Park, Youngkyu, Wright, Kevin, Pavlova, Natalya N., Tuveson, David A., & Thompson, Craig B. 2015. The Utilization of Extracellular Proteins as Nutrients Is Suppressed by mTORC1. *Cell*, **162**(2), 259–270.

Pardee, A B. 1974. A restriction point for control of normal animal cell proliferation. *Proceedings of the National Academy of Sciences of the United States of America*, **71**(4), 1286–90.

Pardee, A B. 1989. G1 events and regulation of cell proliferation. *Science*, **246**(4930), 603–8.

Parent, Romain, Durantel, David, Lahlali, Thomas, Sallé, Aurélie, Plissonnier, Marie-Laure, DaCosta, Daniel, Lesca, Gaëtan, Zoulim, Fabien, Marion, Marie-Jeanne, & Bartosch, Birke. 2014. An immortalized human liver endothelial sinusoidal cell line for the study of the pathobiology of the liver endothelium. *Biochemical and biophysical research communications*, **450**(1), 7–12.

Park, Ryan J, Shen, Hongying, Liu, L., Liu, Xinran, Ferguson, Shawn M, & De Camilli, Pietro. 2013. Dynamin triple knockout cells reveal off target effects of commonly used dynamin inhibitors. *Journal of Cell Science*, **126**(22), 5305–5312.

Parthasarathy, S, Fong, L G, Otero, D, & Steinberg, D. 1987. Recognition of solubilized apoproteins from delipidated, oxidized low density lipoprotein (LDL) by the acetyl-LDL receptor. *Proceedings of the National Academy of Sciences of the United States of America*, **84**(2), 537–40.

Parton, Robert G, & del Pozo, Miguel A. 2013. Caveolae as plasma membrane sensors, protectors and organizers. *Nature reviews. Molecular cell biology*, **14**(2), 98–112.

Parton, Robert G, & Simons, Kai. 2007. The multiple faces of caveolae. *Nature reviews. Molecular cell biology*, **8**(3), 185–94.

Pattaramalai, Sugit, Skubitz, K M, & Skubitz, A P. 1996. A novel recognition site on laminin for the $\alpha 3\beta 1$ integrin. *Experimental Cell Research*, **222**(2), 281–290.

Paul, Nikki R., Jacquemet, Guillaume, & Caswell, Patrick T. 2015. Endocytic Trafficking of Integrins in Cell Migration. *Current Biology*, **25**(22), R1092–R1105.

Paul Mould, A., Akiyama, Steven K, & Humphries, Martin J. 1996. The inhibitory anti-$\beta 1$ integrin monoclonal antibody 13 recognizes an epitope that is attenuated by ligand occupancy. Evidence for allosteric inhibition of integrin function. *Journal of Biological Chemistry*, **271**(34), 20365–20374.

Payne, G S. 1990. Genetic analysis of clathrin function in yeast. *The Journal of membrane biology*, **116**(2), 93–105.

Pazzagli, Chiara, He, Yinghong, Busch, Hauke, Esser, Philipp, Kiritsi, Dimitra, Gache, Yannick, Bruckner-Tuderman, Leena, Boerries, Melanie, & Has, Cristina. 2017. Absence of the Integrin $\alpha 3$ Subunit Induces an Activated Phenotype in Human Keratinocytes. *Journal of Investigative Dermatology*, **137**(6), 1387–1391.

Pearse, B M. 1976. Clathrin: a unique protein associated with intracellular transfer of membrane by coated vesicles. *Proceedings of the National Academy of Sciences of the United States of America*, **73**(4), 1255–9.

Pearse, BM M. 1982. Coated vesicles from human placenta carry ferritin, transferrin, and immunoglobulin G. *Proceedings of the National Academy of Sciences of the United States of America*, **79**(2), 451–455.

Peart, Teresa, Ramos Valdes, Yudith, Correa, Rohann J M, Fazio, Elena, Bertrand, Monique, McGee, Jacob, Préfontaine, Michel, Sugimoto, Akira, DiMattia, Gabriel E, & Shepherd, Trevor G. 2015. Intact LKB1 activity is required for survival of dormant ovarian cancer spheroids. *Oncotarget*, **6**(26), 22424–38.

Pedersen, Lotte B., Mogensen, Johanne B., & Christensen, Søren T. 2016. Endocytic Control of Cellular Signaling at the Primary Cilium. *Trends in Biochemical Sciences*, **41**(9), 784–797.

Pedersen, Torbjorn O, Blois, Anna L, Xue, Ying, Xing, Zhe, Sun, Yang, Finne-Wistrand, Anna, Lorens, James B, Fristad, Inge, Leknes, Knut N, & Mustafa, Kamal. 2014. Mesenchymal stem cells induce endothelial cell quiescence and promote capillary formation. *Stem cell research & therapy*, **5**(1), 23.

Pedraza-Alva, Gustavo, Koulnis, Miroslav, Charland, Colette, Thornton, Tina, Clements, James L, Schlissel, Mark S, & Rincón, Mercedes. 2006. Activation of p38 MAP kinase by DNA double-strand breaks in V(D)J recombination induces a G2/M cell cycle checkpoint. *EMBO Journal*, **25**(4), 763–773.

Pelkmans, Lucas, & Zerial, Marino. 2005. Kinase-regulated quantal assemblies and kiss-and-run recycling of caveolae. *Nature*, **436**(7047), 128–33.

Pellinen, Teijo. 2006. Integrin traffic. *Journal of Cell Science*, **119**(18), 3723–3731.

Pellinen, Teijo, Arjonen, Antti, Vuoriluoto, Karoliina, Kallio, Katja, Fransen, Jack A.M., & Ivaska, Johanna. 2006. Small GTPase Rab21 regulates cell adhesion and controls endosomal traffic of $\beta$1-integrins. *Journal of Cell Biology*, **173**(5), 767–780.

Peng, Yutian, Grassart, Alexandre, Barnes, Georjana, & Drubin, David G. 2014. Casein Kinase 1 Promotes Initiation of Clathrin- Mediated Endocytosis. *Developmental Cell*, **32**(2), 231–240.

Persad, Sujata, Attwell, Sarah, Gray, Virginia, Mawji, Nasrin, Deng, Jing Ti, Leung, Dan, Yan, Jun, Sanghera, Jasbinder, Walsh, Michael P, & Dedhar, Shoukat. 2001. Regulation of protein kinase B/Akt-serine 473 phosphorylation by integrin-linked kinase: Critical roles for kinase activity and amino acids arginine 211 and serine 343. *Journal of Biological Chemistry*, **276**(29), 27462–27469.

Peter, Brian J, Kent, Helen M, Mills, Ian G, Vallis, Yvonne, Butler, P Jonathan G, Evans, Philip R, & McMahon, Harvey T. 2004. BAR domains as sensors of membrane curvature: the amphiphysin BAR structure. *Science*, **303**(5657), 495–9.

Pol, Albert, Calvo, Maria, & Enrich, Carlos. 1998. Isolated endosomes from quiescent rat liver contain the signal transduction machinery: Differential distribution of activated Raf-1 and Mek in the endocytic compartment. *FEBS Letters*, **441**, 34–38.

Posor, York, Eichhorn-Grünig, Marielle, & Haucke, Volker. 2015. Phosphoinositides in endocytosis. *Biochimica et biophysica acta*, **1851**(6), 794–804.

Potente, Michael, Gerhardt, Holger, & Carmeliet, Peter. 2011. Basic and therapeutic aspects of angiogenesis. *Cell*, **146**(6), 873–87.

Potten, C S, Hume, W J, Reid, P, & Cairns, J. 1978. The segregation of DNA in epithelial stem cells. *Cell*, **15**(3), 899–906.

Poupon, Viviane, Girard, Martine, Legendre-Guillemin, Valerie, Thomas, Sebastien, Bourbonniere, Lyne, Philie, Jacynthe, Bright, Nicholas A, & McPherson, Peter S. 2008. Clathrin light chains function in mannose phosphate receptor trafficking via regulation of actin assembly. *Proceedings of the National Academy of Sciences of the United States of America*, **105**(1), 168–73.

Powelka, Aimee M., Sun, Jianlan, Li, Jian, Gao, Minggeng, Shaw, Leslie M., Sonnenberg, Arnoud, & Hsu, Victor W. 2004. Stimulation-dependent recycling of integrin $\beta$1 regulated by ARF6 and Rab11. *Traffic*, **5**(1), 20–36.

PrabhuDas, Mercy R, Baldwin, Cynthia L, Bollyky, Paul L, Bowdish, Dawn M E, Drickamer, Kurt, Febbraio, Maria, Herz, Joachim, Kobzik, Lester, Krieger, Monty, Loike,

John, McVicker, Benita, Means, Terry K, Moestrup, Soren K, Post, Steven R, Sawamura, Tatsuya, Silverstein, Samuel, Speth, Robert C, Telfer, Janice C, Thiele, Geoffrey M, Wang, Xiang-Yang, Wright, Samuel D, & El Khoury, Joseph. 2017. A Consensus Definitive Classification of Scavenger Receptors and Their Roles in Health and Disease. *The Journal of Immunology*, **198**(10), 3775–3789.

Praefcke, Gerrit J K, Ford, Marijn G J, Schmid, Eva M, Olesen, Lene E, Gallop, Jennifer L, Peak-Chew, Sew-Yeu, Vallis, Yvonne, Babu, M Madan, Mills, Ian G, & McMahon, Harvey T. 2004. Evolving nature of the AP2 alpha-appendage hub during clathrin-coated vesicle endocytosis. *The EMBO journal*, **23**(22), 4371–83.

Primeau, Martin, Ouadda, Ali Ben Djoudi, & Lamarche-Vane, Nathalie. 2011. Cdc42 GTPase-activating protein (CdGAP) interacts with the SH3D domain of Intersectin through a novel basic-rich motif. *FEBS Letters*, **585**(6), 847–853.

Prunier, Céline, & Howe, Philip H. 2005. Disabled-2 (Dab2) is required for transforming growth factor $\beta$-induced epithelial to mesenchymal transition (EMT). *Journal of Biological Chemistry*, **280**(17), 17540–17548.

Pryor, Paul R, Jackson, Lauren, Gray, Sally R, Edeling, Melissa A, Thompson, Amanda, Sanderson, Christopher M, Evans, Philip R, Owen, David J, & Luzio, J Paul. 2008. Molecular basis for the sorting of the SNARE VAMP7 into endocytic clathrin-coated vesicles by the ArfGAP Hrb. *Cell*, **134**(5), 817–27.

Qu, Fangfei, Lorenzo, Damaris N, King, Samantha J, Brooks, Rebecca, Bear, James E, & Bennett, Vann. 2016. Ankyrin-B is a PI3P effector that promotes polarized $\alpha 5\beta 1$-integrin recycling via recruiting RabGAP1L to early endosomes. *eLife*, **5**(Oct), e20417.

Quinlan, Dennis C., & Hochstadt, Joy. 1977. The regulation by fibroblast growth factor of early transport changes in quiescent 3T3 cells. *Journal of Cellular Physiology*, **93**(2), 237–246.

Quiñones-Hinojosa, Alfredo, Sanai, Nader, Soriano-Navarro, Mario, Gonzalez-Perez, Oscar, Mirzadeh, Zaman, Gil-Perotin, Sara, Romero-Rodriguez, Richard, Berger, Mitchell S, Garcia-Verdugo, Jose Manuel, & Alvarez-Buylla, Arturo. 2006. Cellular composition and cytoarchitecture of the adult human subventricular zone: a niche of neural stem cells. *The Journal of comparative neurology*, **494**(3), 415–34.

Rabouille, Catherine. 2017. Retriever fetches integrins from endosomes. *Nature Cell Biology*, **19**(10), 1144–1146.

Racoosin, E L, & Swanson, J A. 1993. Macropinosome maturation and fusion with tubular lysosomes in macrophages. *The Journal of cell biology*, **121**(5), 1011–20.

Radel, C, & Rizzo, V. 2005. Integrin mechanotransduction stimulates caveolin-1 phosphorylation and recruitment of Csk to mediate actin reorganization. *American journal of physiology. Heart and circulatory physiology*, **288**(2), H936–45.

Radeva, M. Y., & Waschke, J. 2018. Mind the gap: mechanisms regulating the endothelial barrier. *Acta Physiologica*, **222**(1), e12860.

Rahman, Rubaiyat, Latonen, Leena, & Wiman, Klas G. 2005. hTERT antagonizes p53-induced apoptosis independently of telomerase activity. *Oncogene*, **24**(8), 1320–1327.

Rainero, Elena, Howe, Jonathan D., Caswell, Patrick T., Jamieson, Nigel B., Anderson, Kurt, Critchley, David R., Machesky, Laura, & Norman, Jim C. 2015. Ligand-Occupied Integrin Internalization Links Nutrient Signaling to Invasive Migration. *Cell Reports*, **10**(3), 398–413.

Rajab, Anna, Straub, Volker, McCann, Liza J, Seelow, Dominik, Varon, Raymonda, Barresi, Rita, Schulze, Anne, Lucke, Barbara, Lützkendorf, Susanne, Karbasiyan, Mohsen, Bachmann, Sebastian, Spuler, Simone, & Schuelke, Markus. 2010. Fatal cardiac arrhythmia and long-QT syndrome in a new form of congenital generalized lipodystrophy with muscle rippling (CGL4) due to PTRF-CAVIN mutations. *PLoS genetics*, **6**(3), e1000874.

Ramsay, Alan G, Keppler, Melanie D, Jazayeri, Mona, Thomas, Gareth J, Parsons, Maddy, Violette, Shelia, Weinreb, Paul, Hart, Ian R, & Marshall, John F. 2007. HS1-associated protein X-1 regulates carcinoma cell migration and invasion via clathrin-mediated endocytosis of integrin $\alpha$v$\beta$6. *Cancer Research*, **67**(11), 5275–5284.

Reddy, Pradeep, Liu, Lian, Adhikari, Deepak, Jagarlamudi, Krishna, Rajareddy, Sangareddy, Shen, Yan, Du, Chun, Tang, Wenli, Hämäläinen, Tuula, Peng, Stanford L, Lan, Zi-Jian, Cooney, Austin J, Huhtaniemi, Ilpo, & Liu, Kui. 2008. Oocyte-specific deletion of Pten causes premature activation of the primordial follicle pool. *Science*, **319**(5863), 611–3.

Reider, Amanda, Barker, Sarah L, Mishra, Sanjay K, Im, Young Jun, Maldonado-Báez, Lymarie, Hurley, James H, Traub, Linton M, & Wendland, Beverly. 2009. Syp1 is a conserved endocytic adaptor that contains domains involved in cargo selection and membrane tubulation. *The EMBO Journal*, **28**(20), 3103–3116.

Reis, Carlos R, Chen, Ping-Hung, Srinivasan, Saipraveen, Aguet, François, Mettlen, Marcel, & Schmid, Sandra L. 2015. Crosstalk between Akt/GSK3$\beta$ signaling and dynamin-1 regulates clathrin-mediated endocytosis. *The EMBO journal*, **34**(16), 2132–46.

Ren, Shengjun, & Rollins, Barrett J. 2004. Cyclin C/Cdk3 promotes Rb-dependent G0 exit. *Cell*, **117**(2), 239–251.

Renard, Henri François, Simunovic, Mijo, Lemiere, Joel, Boucrot, Emmanuel, Garcia-Castillo, Maria Daniela, Arumugam, Senthil, Chambon, Valérie, Lamaze, Christophe, Wunder, Christian, Kenworthy, Anne K., Schmidt, Anne A., McMahon, Harvey T., Sykes, Cécile, Bassereau, Patricia, & Johannes, Ludger. 2015. Endophilin-A2 functions in membrane scission in clathrin-independent endocytosis. *Nature*, **517**(7535), 493–496.

Reynolds, Gary D, & St. Clair, R W. 1985. A comparative microscopic and biochemical study of the uptake of fluorescent and 125I-labeled lipoproteins by skin fibroblasts, smooth muscle cells, and peritoneal macrophages in culture. *American Journal of Pathology*, **121**(2), 200.

Rhee, Won Jong, & Bao, Gang. 2009. Simultaneous detection of mRNA and protein stem cell markers in live cells. *BMC biotechnology*, **9**(jan), 30.

Rich, Tyvin A, Shepard, Robert C, & Mosley, Stephen T. 2004. Four decades of continuing innovation with fluorouracil: current and future approaches to fluorouracil chemoradiation therapy. *Journal of Clinical Oncology*, **22**(11), 2214–32.

Ricotta, Doris, Conner, Sean D, Schmid, Sandra L, Von Figura, Kurt, & Höning, Stefan. 2002. Phosphorylation of the AP2 $\mu$ subunit by AAK1 mediates high affinity binding to membrane protein sorting signals. *Journal of Cell Biology*, **156**(5), 791–795.

Riggs, Krista A, Hasan, Nazarul, Humphrey, David, Raleigh, Christy, Nevitt, Chris, Corbin, Deborah, & Hu, Chuan. 2012. Regulation of integrin endocytic recycling and chemotactic cell migration by syntaxin 6 and VAMP3 interaction. *Journal of Cell Science*, **125**(16), 3827–3839.

Rigotti, Attilio, Miettinen, Helena E., & Krieger, Monty. 2003. The Role of the High-Density Lipoprotein Receptor SR-BI in the Lipid Metabolism of Endocrine and Other Tissues. *Endocrine Reviews*, **24**(3), 357–387.

Roberts, Marnie S, Woods, Alison J, Dale, Trevor C, van der Sluijs, P., & Norman, Jim C. 2004. Protein Kinase B/Akt Acts via Glycogen Synthase Kinase 3 To Regulate Recycling of alpha v beta 3 and alpha5 beta1 Integrins. *Molecular and Cellular Biology*, **24**(4), 1505–1515.

Robinson, Margaret S. 2004. Adaptable adaptors for coated vesicles. *Trends in Cell Biology*, **14**(4), 167–174.

Robinson, Margaret S. 2015. Forty Years of Clathrin-coated Vesicles. *Traffic*, **16**(12), 1210–1238.

Robinson, Margaret S, Sahlender, Daniela A, & Foster, Samuel D. 2010. Rapid Inactivation of Proteins by Rapamycin-Induced Rerouting to Mitochondria. *Developmental Cell*, **18**(2), 324–331.

Robinson, Michael W., Overmeyer, Jean H., Young, Ashley M., Erhardt, Paul W., & Maltese, William A. 2012. Synthesis and Evaluation of Indole-Based Chalcones as Inducers of Methuosis, a Novel Type of Nonapoptotic Cell Death. *Journal of Medicinal Chemistry*, **55**(5), 1940–1956.

Rodriguez-Boulan, Enrique, Kreitzer, Geri, & Müsch, Anne. 2005. Organization of vesicular trafficking in epithelia. *Nature Reviews Molecular Cell Biology*, **6**(3), 233–247.

Rohde, Gundula, Wenzel, Dirk, & Haucke, Volker. 2002. A phosphatidylinositol (4,5)-bisphosphate binding site within $\mu$2-adaptin regulates clathrin-mediated endocytosis. *Journal of Cell Biology*, **158**(2), 209–214.

Rohn, Friederike, Kordes, Claus, Castoldi, Mirco, Götze, Silke, Poschmann, Gereon, Stühler, Kai, Herebian, Diran, Benk, Amelie S., Geiger, Fania, Zhang, Tingyu, Spatz, Joachim P., & Häussinger, Dieter. 2018. Laminin-521 promotes quiescence in isolated stellate cells from rat liver. *Biomaterials*, **180**(oct), 36–51.

Röhrl, Clemens, & Stangl, Herbert. 2013. HDL endocytosis and resecretion. *Biochimica et Biophysica Acta - Molecular and Cell Biology of Lipids*, **1831**(11), 1626–1633.

Roskoski, Robert. 2012. ERK1/2 MAP kinases: Structure, function, and regulation. *Pharmacological Research*, **66**(2), 105–143.

Roth, T F, & Porter, K R. 1964. Yolk protein uptake in the oocyte of the mosquito Aedes aegypti. L. *The Journal of cell biology*, **20**(2), 313–332.

Rothberg, K G, Heuser, J E, Donzell, W C, Ying, Y S, Glenney, J R, & Anderson, R G. 1992. Caveolin, a protein component of caveolae membrane coats. *Cell*, **68**(4), 673–82.

Rotty, Jeremy D., Wu, Congying, & Bear, James E. 2013. New insights into the regulation and cellular functions of the ARP2/3 complex. *Nature Reviews Molecular Cell Biology*, **14**(1), 7–12.

Roux, Aurélien, Uyhazi, Katherine, Frost, Adam, & De Camilli, Pietro. 2006. GTP-dependent twisting of dynamin implicates constriction and tension in membrane fission. *Nature*, **441**(7092), 528–31.

Ruiz-Miró, Maria, Colomina, Neus, Fernández, Rita M.H., Garí, Eloi, Gallego, Carme, & Aldea, Martí. 2011. Translokin (Cep57) Interacts with Cyclin D1 and Prevents Its Nuclear Accumulation in Quiescent Fibroblasts. *Traffic*, **12**(5), 549–562.

Rumman, Mohammad, Dhawan, Jyotsna, & Kassem, Moustapha. 2015. Concise Review: Quiescence in Adult Stem Cells: Biological Significance and Relevance to Tissue Regeneration. *Stem cells*, **33**(10), 2903–12.

Saffarian, Saveez, Cocucci, Emanuele, & Kirchhausen, Tomas. 2009. Distinct dynamics of endocytic clathrin-coated pits and coated plaques. *PLoS biology*, **7**(9), e1000191.

Sage, H, Johnson, C, & Bornstein, P. 1984. Characterization of a novel serum albumin-binding glycoprotein secreted by endothelial cells in culture. *Journal of Biological Chemistry*, **259**(6), 3993–4007.

Sager, Polly R., Brown, Paul A., & Berlin, Richard D. 1984. Analysis of transferrin recycling in mitotic and interphase hela cells by quantitative fluorescence microscopy. *Cell*, **39**(Pt 1), 275–282.

Salzer, Ulrich, Kostan, Julius, & Djinović-Carugo, Kristina. 2017. Deciphering the BAR code of membrane modulators. *Cellular and Molecular Life Sciences*, **74**(13), 2413–2438.

Sandvig, K. 1987. Acidification of the cytosol inhibits endocytosis from coated pits. *The Journal of Cell Biology*, **105**(2), 679–689.

Sang, Liyun, Coller, Hilary a, & Roberts, James M. 2008. Control of the reversibility of cellular quiescence by the transcriptional repressor HES1. *Science*, **321**(5892), 1095–100.

Sangiorgi, Eugenio, & Capecchi, Mario R. 2008. Bmi1 is expressed in vivo in intestinal stem cells. *Nature genetics*, **40**(7), 915–20.

Santolini, Elisa, Puri, Claudia, Salcini, Anna Elisabetta, Gagliani, Maria Cristina, Pelicci, Pier Giuseppe, Tacchetti, Carlo, & Di Fiore, Pier Paolo. 2000. Numb is an endocytic protein. *Journal of Cell Biology*, **151**(6), 1345–1351.

Sarkar, Kakali, Kruhlak, Michael J., Erlandsen, Stanley L., & Shaw, Stephen. 2005. Selective inhibition by rottlerin of macropinocytosis in monocyte-derived dendritic cells. *Immunology*, **116**(4), 513–524.

Sarper, Muge, Cortes, Ernesto, Lieberthal, Tyler J., & Del Río Hernández, Armando. 2016. ATRA modulates mechanical activation of TGF-$\beta$ by pancreatic stellate cells. *Scientific Reports*, **6**(1), 27639.

Scheid, Michael P, Schubert, Kathryn M, & Duronio, Vincent. 1999. Regulation of bad phosphorylation and association with Bcl-x(L) by the MAPK/Erk kinase. *Journal of Biological Chemistry*, **274**(43), 31108–31113.

Scherer, P. E. 1996. Molecular Cloning of Caveolin-3, a Novel Member of the Caveolin Gene Family Expressed Predominantly in Muscle. *Journal of Biological Chemistry*, **271**(4), 2255–2261.

Schink, Kay Oliver, Tan, Kia Wee, Martorana, Domenica, Campsteijn, Coen, Raiborg, Camilla, & Stenmark, Harald. 2017. The PtdIns3P-binding protein Phafin2 escorts macropinosomes through the cortical actin cytoskeleton. *bioRxiv*, aug, 180760.

Schlörmann, Wiebke, Steiniger, Frank, Richter, Walter, Kaufmann, Roland, Hause, Gerd, Lemke, Cornelius, & Westermann, Martin. 2010. The shape of caveolae is omega-like after glutaraldehyde fixation and cup-like after cryofixation. *Histochemistry and cell biology*, **133**(2), 223–8.

Schlossman, D M, Schmid, S L, Braell, W A, & Rothman, J E. 1984. An enzyme that removes clathrin coats: purification of an uncoating ATPase. *The Journal of cell biology*, **99**(2), 723–33.

Schmid, Eva M, & McMahon, Harvey T. 2007. Integrating molecular and network biology to decode endocytosis. *Nature*, **448**(7156), 883–8.

Schmid, Eva M, Ford, Marijn G J, Burtey, Anne, Praefcke, Gerrit J K, Peak-Chew, Sew-Yeu, Mills, Ian G, Benmerah, Alexandre, & McMahon, Harvey T. 2006. Role of the AP2 beta-appendage hub in recruiting partners for clathrin-coated vesicle assembly. *PLoS biology*, **4**(9), e262.

Schmid, Sandra L. 1997. Clathrin-Coated Vesicle Formation and Protein Sorting: An Integrated Process. *Annual Review of Biochemistry*, **66**(1), 511–548.

Schnatwinkel, Carsten, Christoforidis, Savvas, Lindsay, Margaret R, Uttenweiler-Joseph, Sandrine, Wilm, Matthias, Parton, Robert G, & Zerial, Marino. 2004. The Rab5 effector Rabankyrin-5 regulates and coordinates different endocytic mechanisms. *PLoS biology*, **2**(9), E261.

Schöneberg, Johannes, Lehmann, Martin, Ullrich, Alexander, Posor, York, Lo, Wen-Ting, Lichtner, Gregor, Schmoranzer, Jan, Haucke, Volker, & Noé, Frank. 2017. Lipid-mediated PX-BAR domain recruitment couples local membrane constriction to endocytic vesicle fission. *Nature Communications*, **8**(jun), 15873.

Schroeder, Gunnar N, & Hilbi, Hubert. 2008. Molecular pathogenesis of Shigella spp.: controlling host cell signaling, invasion, and death by type III secretion. *Clinical microbiology reviews*, **21**(1), 134–56.

Schultz, E, Gibson, M C, & Champion, T. 1978. Satellite cells are mitotically quiescent in mature mouse muscle: an EM and radioautographic study. *The Journal of experimental zoology*, **206**(3), 451–6.

Schwartz, A L, Strous, G J, Slot, J W, & Geuze, H J. 1985. Immunoelectron microscopic localization of acidic intracellular compartments in hepatoma cells. *The EMBO journal*, **4**(4), 899–904.

Scita, Giorgio, & Di Fiore, Pier Paolo. 2010. The endocytic matrix. *Nature*, **463**(7280), 464–73.

Sears, Rosalie C, & Nevins, Joseph R. 2002. Signaling networks that link cell proliferation and cell fate. *The Journal of biological chemistry*, **277**(14), 11617–20.

Seetharaman, Shailaja, & Etienne-Manneville, Sandrine. 2018. Integrin diversity brings specificity in mechanotransduction. *Biology of the Cell*, **110**(3), 49–64.

Segrelles, Carmen, García-Escudero, Ramõn, Garín, Maria I., Aranda, Juan F., Hernández, Pilar, Ariza, José M., Santos, Mirentxu, Paramio, Jesús M., & Lorz, Corina. 2014. Akt signaling leads to stem cell activation and promotes tumor development in epidermis. *Stem Cells*, **32**(7), 1917–1928.

Shapiro, H M. 1981. Flow cytometric estimation of DNA and RNA content in intact cells stained with Hoechst 33342 and pyronin Y. *Cytometry*, **2**(3), 143–50.

Sharma, Monika B, Limaye, Lalita S, & Kale, Vaijayanti P. 2012. Mimicking the functional hematopoietic stem cell niche in vitro: Recapitulation of marrow physiology by hydrogel-based three-dimensional cultures of mesenchymal stromal cells. *Haematologica*, **97**(5), 651–660.

Shea, Kelly L, Xiang, Wanyi, LaPorta, Vincent S, Licht, Jonathan D, Keller, Charles, Basson, M Albert, & Brack, Andrew S. 2010. Sprouty1 regulates reversible quiescence of a self-renewing adult muscle stem cell pool during regeneration. *Cell stem cell*, **6**(2), 117–29.

Sherlock, Gavine, & Rosamond, John. 1993. Starting to cycle: G1 controls regulating cell division in budding yeast. *Journal of General Microbiology*, **139**(11), 2531–41.

Shih, Susan C, Katzmann, David J, Schnell, Joshua D, Sutanto, Myra, Emr, Scott D, & Hicke, Linda. 2002. Epsins and Vps27p/Hrs contain ubiquitin-binding domains that function in receptor endocytosis. *Nature cell biology*, **4**(5), 389–93.

Shimizu, Hideyuki, Wilkin, Marian B, Woodcock, Simon A, Bonfini, Alessandro, Hung, Yvonne, Mazaleyrat, Sabine, & Baron, Martin. 2017. The Drosophila ZO-1 protein Polychaetoid suppresses Deltex-regulated Notch activity to modulate germline stem cell niche formation. *Open Biology*, **7**(4), 160322.

Shin, Sunny, & Roy, Craig R. 2008. Host cell processes that influence the intracellular survival of Legionella pneumophila. *Cellular microbiology*, **10**(6), 1209–20.

Shnyrova, A. V., Bashkirov, P. V., Akimov, S. A., Pucadyil, T. J., Zimmerberg, J., Schmid, S. L., & Frolov, V. A. 2013. Geometric Catalysis of Membrane Fission Driven by Flexible Dynamin Rings. *Science*, **339**(6126), 1433–1436.

Shulman, Maria, & Nahmias, Yaakov. 2013. Long-Term Culture and Coculture of Primary Rat and Human Hepatocytes. *Pages 287–302 of:* Randell, Scott H., & Fulcher, M. Leslie (eds), *Epithelial Cell Culture Protocols*, 2 edn. Methods in Molecular Biology, vol. 945. Totowa, NJ: Humana Press.

Shupliakov, O, Löw, P, Grabs, D, Gad, H, Chen, H, David, C, Takei, K, De Camilli, P, & Brodin, L. 1997. Synaptic vesicle endocytosis impaired by disruption of dynamin-SH3 domain interactions. *Science*, **276**(5310), 259–63.

Sigismund, Sara, Confalonieri, Stefano, Ciliberto, Andrea, Polo, Simona, Scita, Giorgio, & Di Fiore, Pier Paolo. 2012. Endocytosis and signaling: cell logistics shape the eukaryotic cell plan. *Physiological reviews*, **92**(1), 273–366.

Simonsen, Anne, Roger, Lippe, Christoforidis, Savvas, Gaullier, Jean-Michael, Brech, Andreas, Callaghan, Judy, Toh, Ban-Hock, Murphy, Carol, Zerial, Marino, & Stenmark, Harald. 1998. EEA1 links PI(3)K function to Rab5 regulation of endosome fusion. *Nature*, **394**(6692), 494–498.

Simunovic, Mijo, Manneville, Jean Baptiste, Renard, Henri François, Evergren, Emma, Raghunathan, Krishnan, Bhatia, Dhiraj, Kenworthy, Anne K., Voth, Gregory A., Prost, Jacques, McMahon, Harvey T., Johannes, Ludger, Bassereau, Patricia, & Callan-Jones, Andrew. 2017. Friction Mediates Scission of Tubular Membranes Scaffolded by BAR Proteins. *Cell*, **170**(1), 172–184.

Smith, C J, Grigorieff, N, & Pearse, B M. 1998. Clathrin coats at 21 A resolution: a cellular assembly designed to recycle multiple membrane receptors. *The EMBO journal*, **17**(17), 4943–53.

Smith, Laura L., Coller, Hilary A., & Roberts, James M. 2003. Telomerase modulates expression of growth-controlling genes and enhances cell proliferation. *Nature Cell Biology*, **5**(5), 474–479.

Snow, Christopher. 2004. Flow cytometer electronics. *Cytometry. Part A*, **57**(2), 63–69.

Snyder, Joshua C, Rochelle, Lauren K, Ray, Caroline, Pack, Thomas F, Bock, Cheryl B, Lubkov, Veronica, Lyerly, H Kim, Waggoner, Alan S, Barak, Larry S, & Caron, Marc G. 2017. Inhibiting clathrin-mediated endocytosis of the leucine-rich G protein-coupled receptor-5 diminishes cell fitness. *Journal of Biological Chemistry*, **292**(17), 7208–7222.

Sochacki, Kem A., Dickey, Andrea M., Strub, Marie-Paule, & Taraska, Justin W. 2017. Endocytic proteins are partitioned at the edge of the clathrin lattice in mammalian cells. *Nature Cell Biology*, **19**(4), 352–361.

Song, Yu-Jiao, Zhang, Shan-Shan, Guo, Xian-Ling, Sun, Kai, Han, Zhi-Peng, Li, Rong, Zhao, Qiu-Dong, Deng, Wei-Jie, Xie, Xu-Qin, Zhang, Jian-Wei, Wu, Meng-Chao, & Wei, Li-Xin. 2013. Autophagy contributes to the survival of CD133+ liver cancer stem

cells in the hypoxic and nutrient-deprived tumor microenvironment. *Cancer letters*, **339**(1), 70–81.

Sorkin, Alexander, & von Zastrow, Mark. 2009. Endocytosis and signalling: intertwining molecular networks. *Nature reviews. Molecular cell biology*, **10**(9), 609–22.

Sorkina, Tatiana, Miranda, Manuel, Dionne, Kalen R, Hoover, Brian R, Zahniser, Nancy R, & Sorkin, Alexander. 2006. RNA interference screen reveals an essential role of Nedd4-2 in dopamine transporter ubiquitination and endocytosis. *The Journal of Neuroscience*, **26**(31), 8195–205.

Spencer, Sabrina L., Cappell, Steven D., Tsai, Feng Chiao, Overton, K. Wesley, Wang, Clifford L., & Meyer, Tobias. 2013. The proliferation-quiescence decision is controlled by a bifurcation in CDK2 activity at mitotic exit. *Cell*, **155**(2), 369–383.

Spencer, Virginia A, Costes, Sylvain, Inman, Jamie L, Xu, Ren, Chen, James, Hendzel, Michael J, & Bissell, Mina J. 2011. Depletion of nuclear actin is a key mediator of quiescence in epithelial cells. *Journal of Cell Science*, **124**(1), 123–132.

Spudich, Giulietta, Chibalina, Margarita V., Au, Josephine Sui Yan, Arden, Susan D., Buss, Folma, & Kendrick-Jones, John. 2007. Myosin VI targeting to clathrin-coated structures and dimerization is mediated by binding to Disabled-2 and PtdIns(4,5)P2. *Nature Cell Biology*, **9**(2), 176–183.

Srour, Edward F, & Jordan, Craig T. 2002. Isolation and characterization of primitive hematopoietic cells based on their position in the cell cycle. *Pages 93–111 of:* Klug, C.T., & Jordan, C.A. (eds), *Hematopoietic Stem Cell Protocols. Methods in Molecular Medicine*, vol. 63. Totowa, NJ: Humana Press.

Stamatovic, Svetlana M., Johnson, Allison M., Sladojevic, Nikola, Keep, Richard F., & Andjelkovic, Anuska V. 2017. Endocytosis of tight junction proteins and the regulation of degradation and recycling. *Annals of the New York Academy of Sciences*, **1397**(1), 54–65.

Stan, Radu V. 2005. Structure of caveolae. *Biochimica et Biophysica Acta*, **1746**(3), 334–348.

Steer, Clifford J., & Klausner, Richard D. 1983. Clathrin-Coated Pits and Coated Vesicles: Functional and Structural Studies. *Hepatology*, **3**(3), 437–454.

Stein, Jeffrey, Milewski, Wieslawa M, & Dey, Arunangsu. 2013. The negative cell cycle regulators, p27(Kip1), p18(Ink4c), and GSK-3, play critical role in maintaining quiescence of adult human pancreatic $\beta$-cells and restrict their ability to proliferate. *Islets*, **5**(4), 156–69.

Sterk, Lotus M. T., Geuijen, Cecile A. W., van den Berg, José G., Claessen, Nike, Weening, Jan J., & Sonnenberg, Arnoud. 2002. Association of the tetraspanin CD151 with the laminin-binding integrins $\alpha3\beta1$, $\alpha6\beta1$, $\alpha6\beta4$ and $\alpha7\beta1$ in cells in culture and in vivo. *Journal of Cell Science*, **115**(Pt 6), 1161–73.

Stevaux, Olivier, & Dyson, Nicholas J. 2002. A revised picture of the E2F transcriptional network and RB function. *Current opinion in cell biology*, **14**(6), 684–91.

Stimpson, Helen E M, Toret, Christopher P, Cheng, Aaron T, Pauly, Barbara S, & Drubin, David G. 2009. Early-arriving Syp1p and Ede1p function in endocytic site placement and formation in budding yeast. *Molecular biology of the cell*, **20**(22), 4640–51.

Stowell, M H, Marks, B, Wigge, P, & McMahon, H T. 1999. Nucleotide-dependent conformational changes in dynamin: evidence for a mechanochemical molecular spring. *Nature cell biology*, **1**(1), 27–32.

Streuli, Charles H. 2016. Integrins as architects of cell behavior. *Molecular Biology of the Cell*, **27**(19), 2885–2888.

Strochlic, Todd I, Setty, Thanuja Gangi, Sitaram, Anand, & Burd, Christopher G. 2007. Grd19/Snx3p functions as a cargo-specific adapter for retromer-dependent endocytic recycling. *Journal of Cell Biology*, **177**(1), 115–125.

Su, Yang, Xia, Wei, Li, Jing, Walz, Thomas, Humphries, Martin J, Vestweber, Dietmar, Cabañas, Carlos, Lu, Chafen, & Springer, Timothy A. 2016. Relating conformation to function in integrin $\alpha 5\beta$ 1. *Proceedings of the National Academy of Sciences*, **113**(27), E3872–E3881.

Sundborger, Anna, Soderblom, Cynthia, Vorontsova, Olga, Evergren, Emma, Hinshaw, Jenny E, & Shupliakov, Oleg. 2011. An endophilin-dynamin complex promotes budding of clathrin-coated vesicles during synaptic vesicle recycling. *Journal of cell science*, **124**(Pt 1), 133–43.

Susek, Katharina Helene, Korpos, Eva, Huppert, Jula, Wu, Chuan, Savelyeva, Irina, Rosenbauer, Frank, Müller-Tidow, Carsten, Koschmieder, Steffen, & Sorokin, Lydia. 2018. Bone marrow laminins influence hematopoietic stem and progenitor cell cycling and homing to the bone marrow. *Matrix Biology*, **67**(apr), 47–62.

Swanson, J A. 1989. Phorbol esters stimulate macropinocytosis and solute flow through macrophages. *Journal of Cell Science*, **94**(1), 135–142.

Sweitzer, S M, & Hinshaw, J E. 1998. Dynamin undergoes a GTP-dependent conformational change causing vesiculation. *Cell*, **93**(6), 1021–9.

Swirski, Filip K., Hilgendorf, Ingo, & Robbins, Clinton S. 2014. From proliferation to proliferation: monocyte lineage comes full circle. *Seminars in Immunopathology*, **36**(2), 137–148.

Tacheva-Grigorova, Silvia K, Santos, António J M, Boucrot, Emmanuel, & Kirchhausen, Tom. 2013. Clathrin-mediated endocytosis persists during unperturbed mitosis. *Cell reports*, **4**(4), 659–68.

Takasaki, Y, Deng, J S, & Tan, E M. 1981. A nuclear antigen associated with cell proliferation and blast transformation. *The Journal of experimental medicine*, **154**(6), 1899–909.

Takenawa, Tadaomi, & Suetsugu, Shiro. 2007. The WASP-WAVE protein network: connecting the membrane to the cytoskeleton. *Nature Reviews Molecular Cell Biology*, **8**(1), 37–48.

Takubo, Keiyo, Goda, Nobuhito, Yamada, Wakako, Iriuchishima, Hirono, Ikeda, Eiji, Kubota, Yoshiaki, Shima, Haruko, Johnson, Randall S, Hirao, Atsushi, Suematsu, Makoto, & Suda, Toshio. 2010. Regulation of the HIF-1alpha level is essential for hematopoietic stem cells. *Cell stem cell*, **7**(3), 391–402.

Tanaka, Tomohiro, Zhou, Yue, Ozawa, Tatsuhiko, Okizono, Ryuya, Banba, Ayako, Yamamura, Tomohiro, Oga, Eiji, Muraguchi, Atsushi, & Sakurai, Hiroaki. 2018. Ligand-activated epidermal growth factor receptor (EGFR) signaling governs endocytic trafficking of unliganded receptor monomers by non-canonical phosphorylation. *Journal of Biological Chemistry*, **293**(7), 2288–2301.

Tang, Ann H, & Rando, Thomas A. 2014. Induction of autophagy supports the bioenergetic demands of quiescent muscle stem cell activation. *The EMBO Journal*, **33**(23), 2782–2797.

Taylor, Marcus J., Perrais, David, & Merrifield, Christien J. 2011. A high precision survey of the molecular dynamics of mammalian clathrin-mediated endocytosis. *PLoS Biology*, **9**(3), e1000604.

Taylor, Marcus J., Lampe, Marko, & Merrifield, Christien J. 2012. A feedback loop between dynamin and actin recruitment during clathrin-mediated endocytosis. *PLoS Biology*, **10**(4), e1001302.

Tebar, F, Sorkina, T, Sorkin, A, Ericsson, M, & Kirchhausen, T. 1996. Eps15 is a component of clathrin-coated pits and vesicles and is located at the rim of coated pits. *The Journal of biological chemistry*, **271**(46), 28727–30.

Teckchandani, Anjali, Mulkearns, Erin E., Randolph, Timothy W., Toida, Natalie, & Cooper, Jonathan A. 2012. The clathrin adaptor Dab2 recruits EH domain scaffold proteins to regulate integrin 1 endocytosis. *Molecular Biology of the Cell*, **23**(15), 2905–2916.

Temkin, Paul, Lauffer, Ben, Jäger, Stefanie, Cimermancic, Peter, Krogan, Nevan J., & Von Zastrow, Mark. 2011. SNX27 mediates retromer tubule entry and endosome-to-plasma membrane trafficking of signalling receptors. *Nature Cell Biology*, **13**(6), 715–723.

Tesfay, Lia, Schulz, Veronique V., Frank, Sander B., Lamb, Laura E., & Miranti, Cindy K. 2016. Receptor tyrosine kinase Met promotes cell survival via kinase-independent maintenance of integrin $\alpha 3\beta 1$. *Molecular Biology of the Cell*, **27**(15), 2493–2504.

Theret, Louis, Jeanne, Albin, Langlois, Benoit, Hachet, Cathy, David, Marion, Khrestchatisky, Michel, Devy, Jérôme, Hervé, Emonard, Almagro, Sébastien, & Dedieu, Stéphane. 2017. Identification of LRP-1 as an endocytosis and recycling receptor for $\beta 1$-integrin in thyroid cancer cells. *Oncotarget*, **8**(45), 78614–78632.

Thoreen, Carson C, Kang, Seong A, Chang, Jae Won, Liu, Qingsong, Zhang, Jianming, Gao, Yi, Reichling, Laurie J, Sim, Taebo, Sabatini, David M, & Gray, Nathaniel S. 2009. An ATP-competitive mammalian target of rapamycin inhibitor reveals rapamycin-resistant functions of mTORC1. *Journal of Biological Chemistry*, **284**(12), 8023–8032.

Tomasetti, Cristian, & Bozic, Ivana. 2015. The (not so) immortal strand hypothesis. *Stem cell research*, **14**(2), 238–41.

Toné, Shigenobu, Sugimoto, Kenji, Tanda, Kazue, Suda, Taiji, Uehira, Kenzo, Kanouchi, Hiroaki, Samejima, Kumiko, Minatogawa, Yohsuke, & Earnshaw, William C. 2007. Three distinct stages of apoptotic nuclear condensation revealed by time-lapse imaging, biochemical and electron microscopy analysis of cell-free apoptosis. *Experimental Cell Research*, **313**(16), 3635–3644.

Torgersen, Maria L., Skretting, Grethe, van Deurs, Bo, & Sandvig, Kirsten. 2001. Internalization of cholera toxin by different endocytic mechanisms. *Journal of cell science*, **114**(Pt 20), 3737–47.

Totsugawa, Toshinori, Yong, Chen, Rivas-Carrillo, Jorge David, Soto-Gutierrez, Alejandro, Navarro-Alvarez, Nalú, Noguchi, Hirofumi, Okitsu, Teru, Westerman, Karen A, Kohara, Michinori, Reth, Michael, Tanaka, Noriaki, Leboulch, Philippe, & Kobayashi, Naoya. 2007. Survival of liver failure pigs by transplantation of reversibly immortalized human hepatocytes with Tamoxifen-mediated self-recombination. *Journal of hepatology*, **47**(1), 74–82.

Touil, Yasmine, Igoudjil, Wassila, Corvaisier, Matthieu, Dessein, Anne-Frédérique, Vandomme, Jérôme, Monté, Didier, Stechly, Laurence, Skrypek, Nicolas, Langlois, Carole, Grard, Georges, Millet, Guillaume, Leteurtre, Emmanuelle, Dumont, Patrick, Truant, Stéphanie, Pruvot, François-René, Hebbar, Mohamed, Fan, Fan, Ellis, Lee M, Formstecher, Pierre, Van Seuningen, Isabelle, Gespach, Christian, Polakowska, Renata, & Huet, Guillemette. 2014. Colon cancer cells escape 5FU chemotherapy-induced cell death by entering stemness and quiescence associated with the c-Yes/YAP axis. *Clinical Cancer Research*, **20**(4), 837–46.

Toyoshima, Hideo, & Hunter, Tony. 1994. p27, a novel inhibitor of G1 cyclin-Cdk protein kinase activity, is related to p21. *Cell*, **78**(1), 67–74.

Traub, L M, Downs, M A, Westrich, J L, & Fremont, D H. 1999. Crystal structure of the alpha appendage of AP-2 reveals a recruitment platform for clathrin-coat assembly. *Proceedings of the National Academy of Sciences of the United States of America*, **96**(16), 8907–12.

Tsujita, Kazuya, Suetsugu, Shiro, Sasaki, Nobunari, Furutani, Masahiro, Oikawa, Tsukasa, & Takenawa, Tadaomi. 2006. Coordination between the actin cytoskeleton and membrane deformation by a novel membrane tubulation domain of PCH proteins is involved in endocytosis. *The Journal of cell biology*, **172**(2), 269–79.

Tsukita, S, Yamazaki, Y, Katsuno, T, Tamura, A, & Tsukita, S. 2008. Tight junction-based epithelial microenvironment and cell proliferation. *Oncogene*, **27**(55), 6930–6938.

Uezu, Akiyoshi, Horiuchi, Ayaka, Kanda, Kousuke, Kikuchi, Naoya, Umeda, Kazuaki, Tsujita, Kazuya, Suetsugu, Shiro, Araki, Norie, Yamamoto, Hideyuki, Takenawa, Tadaomi, & Nakanishi, Hiroyuki. 2007. SGIP1alpha is an endocytic protein that directly interacts with phospholipids and Eps15. *The Journal of biological chemistry*, **282**(36), 26481–9.

Uezu, Akiyoshi, Umeda, Kazuaki, Tsujita, Kazuya, Suetsugu, Shiro, Takenawa, Tadaomi, & Nakanishi, Hiroyuki. 2011. Characterization of the EFC/F-BAR domain protein, FCHO2. *Genes to Cells*, **16**(8), 868–878.

Umasankar, P K, Sanker, Subramaniam, Thieman, James R, Chakraborty, Souvik, Wendland, Beverly, Tsang, Michael, & Traub, Linton M. 2012. Distinct and separable activities of the endocytic clathrin-coat components Fcho1/2 and AP-2 in developmental patterning. *Nature cell biology*, **14**(5), 488–501.

Umasankar, Perunthottathu K, Ma, Li, Thieman, James R, Jha, Anupma, Doray, Balraj, Watkins, Simon C, & Traub, Linton M. 2014. A clathrin coat assembly role for the muniscin protein central linker revealed by TALEN-mediated gene editing. *eLife*, **3**(oct), e04137.

Umeda, A, Meyerholz, A, & Ungewickell, E. 2000. Identification of the universal cofactor (auxilin 2) in clathrin coat dissociation. *European journal of cell biology*, **79**(5), 336–42.

Ungewickell, E, & Ungewickell, H. 1991. Bovine brain clathrin light chains impede heavy chain assembly in vitro. *The Journal of biological chemistry*, **266**(19), 12710–4.

Ungewickell, E, Ungewickell, H, Holstein, S E, Lindner, R, Prasad, K, Barouch, W, Martin, B, Greene, L E, & Eisenberg, E. 1995. Role of auxilin in uncoating clathrin-coated vesicles. *Nature*, **378**(6557), 632–5.

Uzarski, Joseph S, Scott, Edward W, & McFetridge, Peter S. 2013. Adaptation of endothelial cells to physiologically-modeled, variable shear stress. *PloS one*, **8**(2), e57004.

Valdembri, Donatella, Caswell, Patrick T, Anderson, Kurt I, Schwarz, Juliane P, König, Ireen, Astanina, Elena, Caccavari, Francesca, Norman, Jim C, Humphries, Martin J, Bussolino, Federico, & Serini, Guido. 2009. Neuropilin-1/GIPC1 signaling regulates $\alpha 5\beta 1$ integrin traffic and function in endothelial cells. *PLoS Biology*, **7**(1), e1000025.

Valentin, Mayda, & Yang, Elizabeth. 2008. Autophagy is activated, but is not required for the G0 function of BCL-2 or BCL-xL. *Cell Cycle*, **7**(17), 2762–2768.

van der Bliek, A M, Redelmeier, T E, Damke, H, Tisdale, E J, Meyerowitz, E M, & Schmid, S L. 1993. Mutations in human dynamin block an intermediate stage in coated vesicle formation. *The Journal of cell biology*, **122**(3), 553–63.

Van Heyningen, Simon. 1974. Cholera toxin: Interaction of subunits with ganglioside GM1. *Science*, **183**(4125), 656–657.

Van Weert, Anton W.M., Geuze, Hans J., Groothuis, Brigitte, & Stoorvogel, Willem. 2000. Primaquine interferes with membrane recycling from endosomes to the plasma membrane through a direct interaction with endosomes which does not involve neutralisation of endosomal pH nor osmotic swelling of endosomes. *European Journal of Cell Biology*, **79**(6), 394–399.

Van Zant, G. 1984. Studies of hematopoietic stem cells spared by 5-fluorouracil. *The Journal of experimental medicine*, **159**(3), 679–90.

Vanneste, Steffen, & Friml, Jirí. 2009. Auxin: a trigger for change in plant development. *Cell*, **136**(6), 1005–16.

Vaziri, Homayoun, & Benchimol, Samuel. 1998. Reconstitution of telomerase activity in normal human cells leads to elongation of telomeres and extended replicative life span. *Current Biology*, **8**(5), 279–282.

Veiga, Esteban, & Cossart, Pascale. 2005. Listeria hijacks the clathrin-dependent endocytic machinery to invade mammalian cells. *Nature Cell Biology*, **7**(9), 894–900.

Veiga, Esteban, Guttman, Julian A., Bonazzi, Matteo, Boucrot, Emmanuel, Toledo-Arana, Alejandro, Lin, Ann E., Enninga, Jost, Pizarro-Cerdá, Javier, Finlay, B. Brett, Kirchhausen, Tomas, & Cossart, Pascale. 2007. Invasive and Adherent Bacterial Pathogens Co-Opt Host Clathrin for Infection. *Cell Host and Microbe*, **2**(5), 340–351.

Vieira, Amandio V, Lamaze, Christophe, & Schmid, Sandra L. 1996. Control of EGF receptor signaling by clathrin-mediated endocytosis. *Science*, **274**(5295), 2086–2089.

Wang, Jia Huai. 2012. Pull and push: Talin activation for integrin signaling. *Cell Research*, **22**(11), 1512–1514.

Wang, Jing, Han, Fei, Wu, Juan, Lee, Szu Wei, Chan, Chia Hsin, Wu, Ching Yuan, Yang, Wei Lei, Gao, Yuan, Zhang, Xian, Jeong, Yun Seong, Moten, Asad, Samaniego, Felipe, Huang, Peng, Liu, Quentin, Zeng, Yi Xin, & Lin, Hui Kuan. 2011. The role of Skp2 in hematopoietic stem cell quiescence, pool size, and self-renewal. *Blood*, **118**(20), 5429–5438.

Watanabe, Shigeki, & Boucrot, Emmanuel. 2017. Fast and ultrafast endocytosis. *Current Opinion in Cell Biology*, **47**(aug), 64–71.

Watanabe, Shigeki, Morgan, Jennifer R, Perrais, David, Agrawal, Ashutosh, & Lou, Xuelin. 2018a. Sensing Exocytosis and Triggering Endocytosis at Synapses: Synaptic Vesicle Exocytosis-Endocytosis Coupling. *Frontiers in Cellular Neuroscience*, **12**(12), 663389–66.

Watanabe, Shigeki, Mamer, Lauren, Raychaudhuri, Sumana, Luvsanjav, Delgermaa, Eisen, Julia, Trimbuch, Thorsten, Sohl-Kielczynski, Berit, Fenske, Pascal, Milosevic, Ira, Rosenmund, Christien, & Jorgensen, Erik M. 2018b. Synaptojanin and Endophilin Mediate Neck Formation during Ultrafast Endocytosis. *Neuron*, **98**(6), 1184–1197.

Watson, Joanna R, Fox, Helen M, Nietlispach, Daniel, Gallop, Jennifer L, Owen, Darerca, & Mott, Helen R. 2016. Investigation of the interaction between Cdc42 and its effector TOCA1: Handover of Cdc42 to the actin regulator N-WASP is facilitated by differential binding affinities. *Journal of Biological Chemistry*, **291**(26), 13875–13890.

West, M A, Bretscher, M S, & Watts, C. 1989. Distinct endocytotic pathways in epidermal growth factor-stimulated human carcinoma A431 cells. *Journal of Cell Biology*, **109**(6 I), 2731–9.

West, M A, Bright, N A, & Robinson, M S. 1997. The role of ADP-ribosylation factor and phospholipase D in adaptor recruitment. *The Journal of cell biology*, **138**(6), 1239–54.

White, Andrew C, & Lowry, William E. 2015. Refining the role for adult stem cells as cancer cells of origin. *Trends in cell biology*, **25**(1), 11–20.

Wigge, P, Köhler, K, Vallis, Y, Doyle, C A, Owen, D, Hunt, S P, & McMahon, H T. 1997a. Amphiphysin heterodimers: potential role in clathrin-mediated endocytosis. *Molecular biology of the cell*, **8**(10), 2003–15.

Wigge, Patrick, Vallis, Yvonne, & McMahon, Harvey T. 1997b. Inhibition of receptor-mediated endocytosis by the amphiphysin SH3 domain. *Current Biology*, **7**(8), 554–560.

Wilbur, Jeremy D, Chen, Chih Ying, Manalo, Venus, Hwang, Peter K, Fletterick, Robert J, & Brodsky, Frances M. 2008. Actin binding by Hip1 (huntingtin-interacting protein 1) and Hip1R (Hip1-related protein) is regulated by clathrin light chain. *Journal of Biological Chemistry*, **283**(47), 32870–32879.

Wileman, Thomas, Boshans, Rita L, Schlesinger, Paul, & Stahl, Philip. 1984. Monensin inhibits recycling of macrophage mannose-glycoprotein receptors and ligand delivery to lysosomes. *The Biochemical journal*, **220**(3), 665–75.

Will, Britta, Vogler, Thomas O, Bartholdy, Boris, Garrett-Bakelman, Francine, Mayer, Jillian, Barreyro, Laura, Pandolfi, Ashley, Todorova, Tihomira I, Okoye-Okafor, Ujunwa C, Stanley, Robert F, Bhagat, Tushar D, Verma, Amit, Figueroa, Maria E, Melnick, Ari, Roth, Michael, & Steidl, Ulrich. 2013. Satb1 regulates the self-renewal of hematopoietic stem cells by promoting quiescence and repressing differentiation commitment. *Nature immunology*, **14**(5), 437–45.

Williams, M A, & Fukuda, M. 1990. Accumulation of membrane glycoproteins in lysosomes requires a tyrosine residue at a particular position in the cytoplasmic tail. *Journal of Cell Biology*, **111**(3), 955–966.

Wolf, Anne A, Jobling, Michael G, Saslowsky, David E, Kern, Eli, Drake, Kimberly R, Kenworthy, Anne K, Holmes, Randall K, & Lencer, Wayne I. 2008. Attenuated endocytosis and toxicity of a mutant cholera toxin with decreased ability to cluster ganglioside GM1 molecules. *Infection and Immunity*, **76**(4), 1476–1484.

Woodman, Philip G, & Futter, Clare E. 2008. Multivesicular bodies: co-ordinated progression to maturity. *Current Opinion in Cell Biology*, **20**(4), 408–414.

Woods, Alison J., White, Dominic P., Caswell, Patrick T., & Norman, Jim C. 2004. PKD1/PKC$\mu$ promotes $\alpha$v$\beta$3 integrin recycling and delivery to nascent focal adhesions. *EMBO Journal*, **23**(13), 2531–2543.

Wozniak, Michele A, Modzelewska, Katarzyna, Kwong, Lina, & Keely, Patricia J. 2004. Focal adhesion regulation of cell behavior. *Biochimica et Biophysica Acta*, **1692**(2), 103–119.

Wu, Shuang, Majeed, Sophia R, Evans, Timothy M, Camus, Marine D, Wong, Nicole M L, Schollmeier, Yvette, Park, Minjong, Muppidi, Jagan R, Reboldi, Andrea, Parham, Peter, Cyster, Jason G, & Brodsky, Frances M. 2016. Clathrin light chains' role in selective endocytosis influences antibody isotype switching. *Proceedings of the National Academy of Sciences*, **113**(35), 9816–9821.

Wullschleger, Stephan, Loewith, Robbie, & Hall, Michael N. 2006. TOR Signaling in Growth and Metabolism. *Cell*, **124**(3), 471–84.

Wuster, Arthur, & Babu, M Madan. 2010. Transcriptional control of the quorum sensing response in yeast. *Molecular bioSystems*, **6**(1), 134–41.

Wüstner, Daniel, Mondal, Mousumi, Huang, Amy, & Maxfield, Frederick R. 2004. Different transport routes for high density lipoprotein and its associated free sterol in polarized hepatic cells. *Journal of lipid research*, **45**(3), 427–37.

Xu, Xiaojin, Araki, Koichi, Li, Shuzhao, Han, Jin-Hwan, Ye, Lilin, Tan, Wendy G, Konieczny, Bogumila T, Bruinsma, Monique W, Martinez, Jennifer, Pearce, Erika L, Green, Douglas R, Jones, Dean P, Virgin, Herbert W, & Ahmed, Rafi. 2014. Autophagy is essential for effector CD8(+) T cell survival and memory formation. *Nature immunology*, **15**(12), 1152–61.

Yamaki, Tsutomu, Kamiya, Yusuke, Ohtake, Kazuo, Uchida, Masaki, Seki, Toshinobu, Ueda, Hideo, Kobayashi, Jun, Morimoto, Yasunori, & Natsume, Hideshi. 2014. A mechanism enhancing macromolecule transport through paracellular spaces induced by poly-L-arginine: Poly-L-arginine induces the internalization of tight junction proteins via clathrin-mediated endocytosis. *Pharmaceutical Research*, **31**(9), 2287–2296.

Yanagida, Mitsuhiro. 2009. Cellular quiescence: are controlling genes conserved? *Trends in cell biology*, **19**(12), 705–15.

Yang, Esther H., Rode, Julia, Howlader, Md. Amran, Eckermann, Marina, Santos, Jobette T., Hernandez Armada, Daniel, Zheng, Ruixiang, Zou, Chunxia, & Cairo, Christopher W. 2017. Galectin-3 alters the lateral mobility and clustering of $\beta$1-integrin receptors. *PLoS ONE*, **12**(10), e0184378.

Yao, Guang. 2014. Modelling mammalian cellular quiescence. *Interface Focus*, **4**(3), 20130074.

Yarden, Y, & Schlessinger, J. 1987a. Epidermal growth factor induces rapid, reversible aggregation of the purified epidermal growth factor receptor. *Biochemistry*, **26**(5), 1443–51.

Yarden, Y, & Schlessinger, J. 1987b. Self-phosphorylation of epidermal growth factor receptor: evidence for a model of intermolecular allosteric activation. *Biochemistry*, **26**(5), 1434–42.

Yoon, Sang O., Shin, Sejeong, & Mercurio, Arthur M. 2005. Hypoxia stimulates carcinoma invasion by stabilizing microtubules and promoting the Rab11 trafficking of the $\alpha$6$\beta$4 integrin. *Cancer Research*, **65**(7), 2761–2769.

Yoshida, Sei, Pacitto, Regina, Inoki, Ken, & Swanson, Joel. 2018. Macropinocytosis, mTORC1 and cellular growth control. *Cellular and Molecular Life Sciences*, **75**(7), 1227–1239.

Young, I S, & McEneny, J. 2001. Lipoprotein oxidation and atherosclerosis. *Biochemical Society transactions*, **29**(Pt 2), 358–62.

Yu, Anan, Rual, Jean-François, Tamai, Keiko, Harada, Yuko, Vidal, Marc, He, Xi, & Kirchhausen, Tomas. 2007. Association of Dishevelled with the Clathrin AP-2 Adaptor Is Required for Frizzled Endocytosis and Planar Cell Polarity Signaling. *Developmental Cell*, **12**(1), 129–141.

Yu, Cheng Han, Rafiq, Nisha Bte Mohd, Cao, Fakun, Zhou, Yuhuan, Krishnasamy, Anitha, Biswas, Kabir Hassan, Ravasio, Andrea, Chen, Zhongwen, Wang, Yu Hsiu, Kawauchi, Keiko, Jones, Gareth E., & Sheetz, Michael P. 2015. Integrin-beta3 clusters recruit clathrin-mediated endocytic machinery in the absence of traction force. *Nature Communications*, **6**(1), 8672.

Yu, Hang, & Schulten, Klaus. 2013. Membrane sculpting by F-BAR domains studied by molecular dynamics simulations. *PLoS computational biology*, **9**(1), e1002892.

Yu, Jun, Bergaya, Sonia, Murata, Takahisa, Alp, Ilkay F, Bauer, Michael P, Lin, Michelle I, Drab, Marek, Kurzchalia, Teymuras V, Stan, Radu V, & Sessa, William C. 2006. Direct evidence for the role of caveolin-1 and caveolae in mechanotransduction and remodeling of blood vessels. *Journal of Clinical Investigation*, **116**(5), 1284–1291.

Yu, Xiao-Hua, Fu, Yu-Chang, Zhang, Da-Wei, Yin, Kai, & Tang, Chao-Ke. 2013. Foam cells in atherosclerosis. *Clinica Chimica Acta*, **424**(sep), 245–252.

Yue, Shijing, Mu, Wei, Erb, Ulrike, & Zöller, Margot. 2015. The tetraspanins CD151 and Tspan8 are essential exosome components for the crosstalk between cancer initiating cells and their surrounding. *Oncotarget*, **6**(4), 2366–84.

Yumoto, Ryoko, Suzuka, Sayuri, Oda, Keisuke, Nagai, Junya, & Takano, Mikihisa. 2012. Endocytic Uptake of FITC-albumin by Human Alveolar Epithelial Cell Line A549. *Drug Metabolism and Pharmacokinetics*, **27**(3), 336–343.

Yusuf, Isharat, & Fruman, David A. 2003. Regulation of quiescence in lymphocytes. *Trends in Immunology*, **24**(7), 380–386.

Zanoni, Paolo, Velagapudi, Srividya, Yalcinkaya, Mustafa, Rohrer, Lucia, & von Eckardstein, Arnold. 2018. Endocytosis of lipoproteins. *Atherosclerosis*, **275**(Aug), 273–295.

Zaremba, S, & Keen, J H. 1985. Limited proteolytic digestion of coated vesicle assembly polypeptides abolishes reassembly activity. *Journal of cellular biochemistry*, **28**(1), 47–58.

Zeng, Ying, Hirano, Katsuya, Hirano, Mayumi, Nishimura, Junji, & Kanaide, Hideo. 2000. Minimal requirements for the nuclear localization of p27(Kip1), a cyclin-dependent kinase inhibitor. *Biochemical and Biophysical Research Communications*, **274**(1), 37–42.

Zeng, Youchun, Tao, Nengbing, Chung, Koong-Nah Nah, Heuser, John E, & Lublin, Douglas M. 2003. Endocytosis of Oxidized Low Density Lipoprotein through Scavenger Receptor CD36 Utilizes a Lipid Raft Pathway That Does Not Require Caveolin-1. *Journal of Biological Chemistry*, **278**(46), 45931–45936.

Zerial, Marino, & McBride, Heidi. 2001. Rab proteins as membrane organizers. *Nature Reviews Molecular Cell Biology*, **2**(2), 107–117.

Zetterberg, a, & Larsson, O. 1985. Kinetic analysis of regulatory events in G1 leading to proliferation or quiescence of Swiss 3T3 cells. *Proceedings of the National Academy of Sciences of the United States of America*, **82**(16), 5365–9.

Zhang, Jianghui, Fukuhara, Shigetomo, Sako, Keisuke, Takenouchi, Takato, Kitani, Hiroshi, Kume, Tsutomu, Koh, Gou Young, & Mochizuki, Naoki. 2011. Angiopoietin-1/Tie2 signal augments basal Notch signal controlling vascular quiescence by inducing delta-like 4 expression through AKT-mediated activation of beta-catenin. *The Journal of biological chemistry*, **286**(10), 8055–66.

Zhang, Jiwang, Niu, Chao, Ye, Ling, Huang, Haiyang, He, Xi, Tong, Wei-Gang, Ross, Jason, Haug, Jeff, Johnson, Teri, Feng, Jian Q, Harris, Stephen, Wiedemann, Leanne M, Mishina, Yuji, & Li, Linheng. 2003. Identification of the haematopoietic stem cell niche and control of the niche size. *Nature*, **425**(6960), 836–41.

Zhang, Tian, Wolfe, Clara, Pierle, Andrew, Welle, Kevin A, Hryhorenko, Jennifer R, & Ghaemmaghami, Sina. 2017. Proteome-wide modulation of degradation dynamics in response to growth arrest. *Proceedings of the National Academy of Sciences*, **114**(48), E10329–E10338.

Zhang, Tongli. 2013. Phase portraits of the proliferation-quiescence decision. *Science signaling*, **6**(305), pe37.

Zhao, Xuannv, Wang, Dongmei, Liu, Xing, Liu, Lifang, Song, Zhenwei, Zhu, Tongge, Adams, Gregory, Gao, Xinjiao, Tian, Ruijun, Huang, Yuejia, Chen, Runhua, Wang, Fengsong, Liu, Dong, Yu, Xue, Chen, Yong, Chen, Zhengjun, Teng, Maikun, Ding, Xia, & Yao, Xuebiao. 2013. Phosphorylation of the Bin, Amphiphysin, and RSV161/167 (BAR) domain of ACAP4 regulates membrane tubulation. *Proceedings of the National Academy of Sciences of the United States of America*, **110**(27), 11023–8.

Zhou, Yue, Tanaka, Tomohiro, Sugiyama, Naoyuki, Yokoyama, Satoru, Kawasaki, Yuki, Sakuma, Tsutomu, Ishihama, Yasushi, Saiki, Ikuo, & Sakurai, Hiroaki. 2014. P38-Mediated phosphorylation of Eps15 endocytic adaptor protein. *FEBS Letters*, **588**(1), 131–137.

Zhu, Qing, Xia, Haiyan, Xia, Cindy Q, Yang, Qian, Doshi, Utkarsh, Li, Albert P, & Liao, Mingxiang. 2014. Culture duration-, donor-, and medium-dependent changes in OATP1B3-mediated telmisartan uptake in human hepatocytes. *Drug metabolism letters*, **7**(2), 117–25.

Zimmermann, Arthur. 2004. Regulation of liver regeneration. *Nephrology, Dialysis, Transplantation*, **19**(Suppl 4), iv6–iv10.

Zoncu, Roberto, Bar-Peled, Liron, Efeyan, Alejo, Wang, Shuyu, Sancak, Yasemin, & Sabatini, David M. 2011. mTORC1 Senses Lysosomal Amino Acids Through an Inside-Out Mechanism That Requires the Vacuolar H+-ATPase. *Science*, **334**(6056), 678–683.